Syntheses and Characterizations Using Molybdenum and Tungsten Bound Diphosphorus and Cyclotriphosphorus Complexes

Dissertation zur Erlangung des
Doktorgrades der Naturwissenschaften (Dr. rer. nat.)
der Naturwissenschaftlichen Fakultät IV – Chemie und Pharmazie
der Universität Regensburg

vorgelegt von

Brian Keith Wegley

aus Williston, North Dakota, USA

Regensburg 2009

Diese Arbeit wurde angeleitet von Professor Doktor Manfred Scheer.

Promotionsgesuch eingereicht am: Januar 19, 2010
Tag der mündlichen Prüfung: Februar 17, 2010

Vorsitzer: Professor Doktor Albrecht Mannschreck

Prüfungsausschuss: Professor Doktor Manfred Scheer
Professor Doktor Henri Brunner
Professor Doktor Oliver Reiser

Die vorliegende Arbeit wurde in der Zeit von September 2005 bis Februar 2010 am Institut für Anorganische Chemie der Universität Regensburg angefertigt.

Eidesstattliche Erklärung
Ich erkläre hiermit an Eides statt, dass ich die vorliegende Arbeit ohne unzulässige Hilfe Dritter und ohne Benutzung anderer als der angegebenen Hilfsmittel angefertigt habe; die aus anderen Quellen direkt oder indirekt übernommenen Daten und Konzepte sind unter Angabe des Literaturzitats gekennzeichnet.

Brian K. Wegley

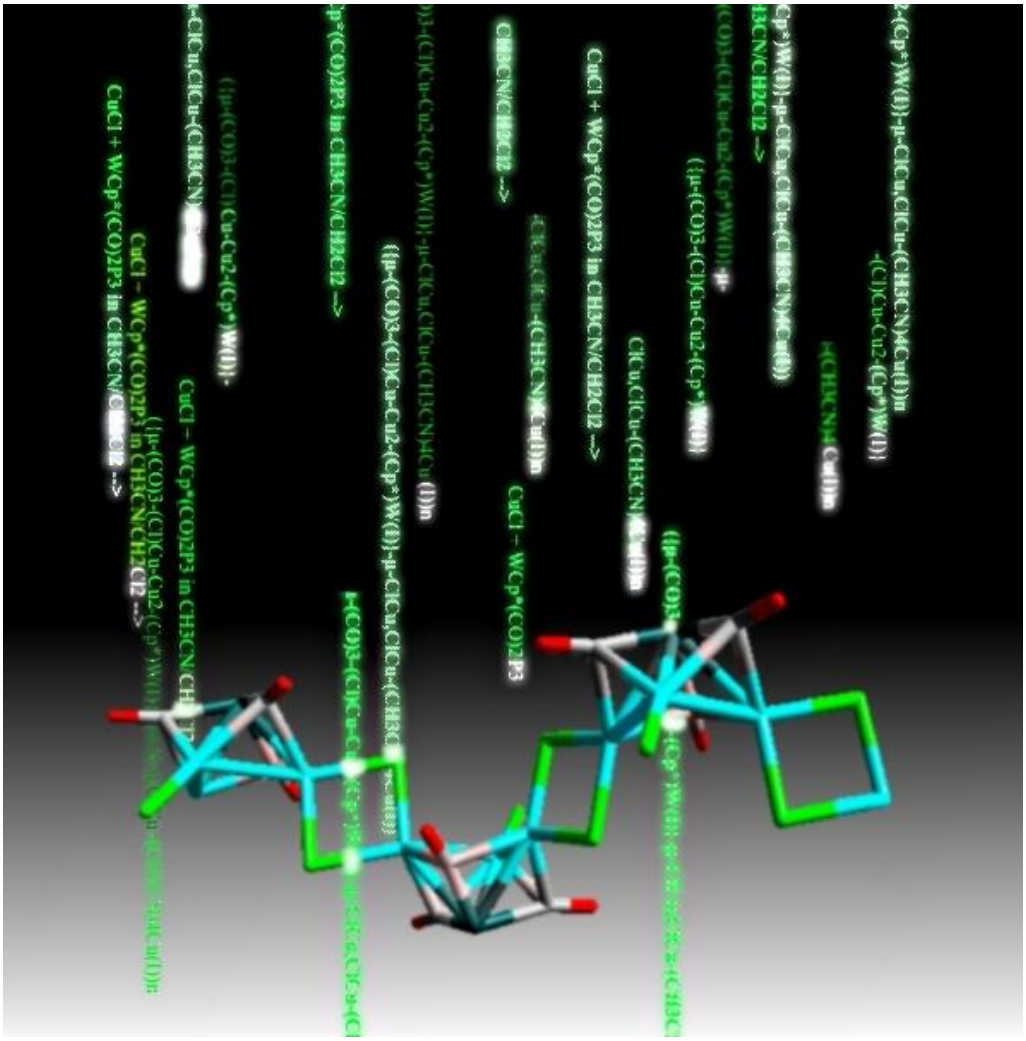

The Matrix is Broken. This is the first example of a phosphorus-free polymer produced from an organometallic P_n-ligand complex.

“It doesn’t matter how much time you put in. It only matters how many results you have.”

– *Manfred Scheer*

“Be courteous to all, but intimate with few, and let those few be well tried before you give them your confidence.”

– *George Washington*

Table of Contents

Abstract

24 previously unknown inorganic compounds are structurally characterized by single crystal X-ray diffraction. Of these complexes, 8 inorganic polymers (**21**–**24**, **26**, **29**, **30**, **32**) and 8 dimers (**1**, **2**, **10**, **12**, **14**–**16**, **31**) are synthesized from uncharacterized (**11**, **13**, **25**, **28**) and characterized molybdenum and tungsten containing species with electron rich di- and tri-phosphorus ligands by treatment with group 10 and 11 metal salts. These species are further characterized by low temperature solution- and solid-state ^{31}P NMR; ^{1}H, ^{13}C, and ^{19}F NMR; IR; positive and negative ESI-MS; EI-MS; EA; and M.P. where appropriate.

I. Introduction and Research Objectives

1.1. Historical Development

Since the discovery of the first reported organometallic compound of a transition metal in 1831[1] by W. C. Zeise, new avenues in syntheses were on the verge of creation allowing the incorporation of metals into the archive of traditional chemistry. It was and still is common for landmark examples to be the result of an unpredicted product and create entirely new complexes, many of which do not have a present application. Such was the case of ferrocene from an attempt to produce a fulvalene.[2]

Such is the case of substituent-free (naked) phosphorus containing complexes used in the continual discovery of artificially produced inorganic polymers born in unnatural environments. This is the pinnacle of forty years of applied research started in 1969 when it was discovered that group 15 elements other than nitrogen were able to form naked complexes. This discovery also led to the shortest As–As bond of its time.[3] Two years later (1971), the first naked phosphorus metal complex was synthesized by treating white phosphorus with $(Ph_3P)_3RhCl$ at low temperature (–78 °C) which proved to be unstable at room temperature.[4] In the following years other reactants such as PX_3 (X = Cl, Br) and red phosphorus were employed producing the first naked P_2 and P_6 complexes, respectively.[5, 6] Wichelhaus later produced the first P_7 and P_{11} complexes[7, 8] in the form of anions, and even though they may not have been the first naked phosphorus anions to be produced,[9] they were more significant in their uses as reactants than the others that were produced in later years.[10-23] Within the advent of the first naked P_3 complexes ever reported[24] Sacconi and coworkers also provided the first double sandwich complex containing the same P_3 configuration by treating white phosphorous with metal ions in the presence of what would become their signature ligand, triphos.[25] Size potential continued to grow as the Scherer group used rhenium metal carbonyls to bridge two naked diphosphorus complexes,[26] and then two years later provided the encore of simultaneously producing the first naked P_5 example in the form of the first naked P_5 sandwich complex.[27] The Scherer group continued exploring the reactivity of white phosphorus and successfully built cubane structures when they utilized nickel carbonyl derivatives.[28]

An important hint was provided when Stoppioni and his associates showed that a naked P_3 containing complex could be tethered by a group 11 transition metal, in this case gold.[29] The ramifications of this discovery will be more than clear as the readership will learn that the main reactant utilized in the primary research reported herein is CuX (X = Cl, Br, I). Meanwhile, a partially substituted naked P_{10} cluster was formed[30] and two years later Scherer presented a totally naked P_{10} complex.[31] Only one year before this he presented the first bicyclic P_6 complex coupled only with two equivalents of thalliumcyclopentadienyl.[32] Scherer also provided the first cage complex[33] with naked phosphorus and the first naked P_8 and P_{12} complexes[34] by reacting iron and cobalt carbonyl complexes, respectively, with P_4 in decalin. Then, in 1999 white phosphorus was successfully used to tether two rhenium triphos complexes[35] and only three years later the Scheer group provided the first polymer by treating pentaphosphaferrocene with CuX (X = Cl, Br, I).[36] This synthetic strategy was also used to form an inorganic ball consisting of 90 inorganic core atoms.[37] Later, for an encore to this fabulous discovery, a C_{60} ball was successfully trapped in this inorganic ball[38] a mere three years after Pfitzner used CuI as an aid in the crystallization of phosphorus nanorods.[39] Since the initiation of polymerization using naked phosphorus subunits, it has become the main goal of our research.

Landmark Developments in Naked Phosphorus Metal Complexes

1971 First example with naked Phosphorus bound (P_4)

1974 First naked P_6 example

1979 First naked and first P_3 double sandwich complex

1984 First naked phosphorus species bridged by a metal complex

1988 Cubanes containing naked phosphorus are introduced

1990 First example of a naked phosphorus cluster

1992 First naked P_{10} complex

1996 First naked P_8 and P_{12} complexes

2002 First example of a polymer synthesized from naked phosphorus subunits

2004 Phosphorus nanorods are assembled

1969 First example of a non nitrogen naked group 15 element in a complex, introduced by As

1973 First naked P_2 metal complex

1975 First naked P_7 and P_{11} complex

1981 First triple decker with naked P_3

1986 First naked P_5 example and first P_5 sandwich complex

1990 First example of a naked phosphorus complex tethered by a group 11 transistion metal (Au)

1991 First example of a bicyclic naked P_6 complex

1995 First cage complex with naked phosphorus

1999 First time white phosphorus bridged two complexes

2003 The first 3-D inorganic ball shaped complex is synthesized from a naked phosphorus complex

2007 The first ball in a ball is synthesized by trapping a C_{60} molecule in an inorganic sphere synthesized from a naked phosphorus subunit.

The examples of naked phosphorus complexes presented in the literature are conveniently divided into six categories based on the number of naked phosphorus atoms present: >6, 6, 5, 4, 3, and 2. One member units are not considered because, according to our research, at least two naked phosphorus atoms are needed to facilitate the binding for polymer formation and until now no evidence has shown that it is possible for a one member unit to perform in this manner.

1.2. More than 6 Phosphorus Atoms

Starting with the first cluster in 1990,[30] these phosphorus rich structures have commanded attention. Even in recent times infinite polymers in the form of nanorods have been reported after it was found that crystallization is aided with CuI.[39] Also of startling importance is the characterized structure of fibrous red phosphorus which is found to be very similar to the violet allotrope.[40] Aside from infinite polymers, the remainder of the significant examples in this category is clusters and cages.[41]

The complex $[CpCr(CO)_2]_5P_{10}$ (Figure 1) was one of four products produced from the co-thermolysis of $[CpCr(CO)_3]_2$ ($Cp = \eta^5\text{-}C_5H_5$) with P_4 (1.5 molar equivalents) in toluene at 80–85 °C for four hours. The average P–P bond lengths (2.21 Å) suggest that single bonds exist in the whole P_{10} core. The core is surrounded by five $CrCp(CO)_2$ units; each chromium atom is bound to a phosphorus atom located around the parameter through one formal bond and through one lone pair of electrons for a total electron count of 18 on each chromium atom.

Another successful, higher-temperature, co-thermolysis reaction is reported by treating $RhCp''(CO)_2$ ($Cp'' = 1,3\text{-}t\text{Bu}_2C_5H_3$) with P_4 in decalin and also produces a naked P_{10} complex (Figure 1).[31] In this structure the $RhCp''$ subunits are preserved and exhibits a centrosymmetric polycyclic structure. In this structure the apical rhodium atoms (2) covalently bound to four phosphorus atoms have an electron count of 18 and preside over the rich π-electrons shown from the double bond-like character of the P2–P3 and the P4–P5 (2.143(2) and 2.148(2) Å). The two interstitial rhodium atoms (1) bound to P1, P3, and P4 greatly disturb the electron density associated with the P3–P4 bond lengthening it to 2.624(2) Å, meanwhile, having little effect on the P–P bonds associated with P1. A cobalt analog is also produced using the same procedure.[42]

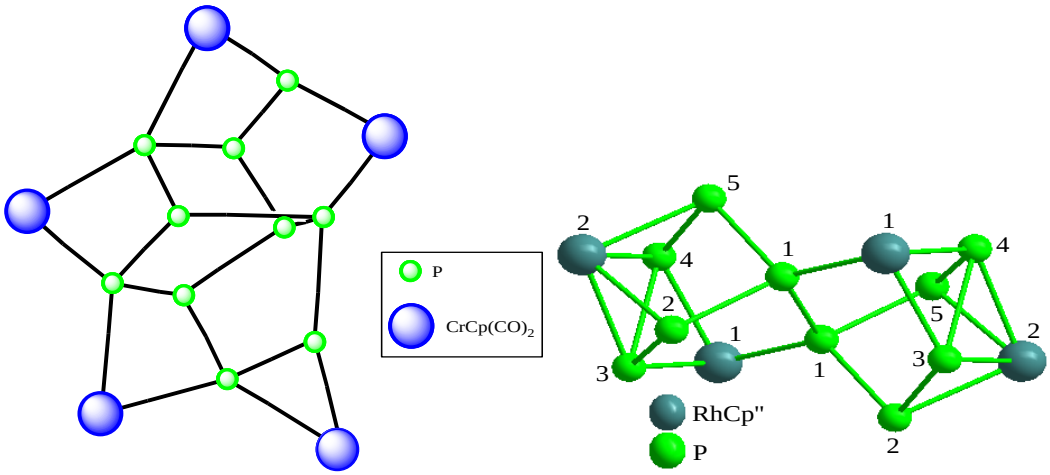

Figure 1. Left, structure of $[(Cp)Cr(CO)_2]_5P_{10}$.[30, 43] Right, structure of $[(Cp''Rh)_2(P_5\text{–}P_5)(RhCp'')_2]$, $Cp'' = 1,3\text{-}^t\text{Bu}_2C_5H_3$.[31]

Since the arrival of K_3P_7 and other naked phosphorus anions,[8, 13, 44-46] the possibility of treating nucleophically activated metal chlorides with this anion is explored. In one scenario iron(II) chloride is treated with LiCp and $P_7(SiMe_3)_3$.[47] The product (Figure 2), $[(Cp^*Fe)_3\{(\eta^3\text{-}P_3)Fe\}P_6]$, is composed of an Fe_4P_6 polyhedron with a P_3 ligand attached to one of the iron atoms. No notable abnormalities exist other than the slightly elongated P–P bond lengths (2.326–2.413 Å) of the cage caused from the electron withdrawing effects of the iron atoms and the shortened bond lengths (2.107–2.117 Å) contained in the P_3 portion from the π-bond electron density.

Another reactive source for phosphorus is the iron-containing butterfly complex, $[\{Cp^R(OC)_2Fe\}_2(\mu\text{-}\eta^1\text{:}\eta^1\text{-}P_4)]$, $Cp^R = i\text{Pr}_5C_5$. When treated with diphenylethylyne in boiling toluene the cluster shown in Figure 2 is formed along with an attractive sandwich complex containing a P_3 arrangement. Throughout the skeleton of the P11, the phophorus-phosphorus bonds are singly bonded (2.181–2.268 Å). The most striking feature of this molecule is the similarity to Hitorf's phosphorus as the phophorus atoms bind in a similar manner to the subunits of the polymer.[48]

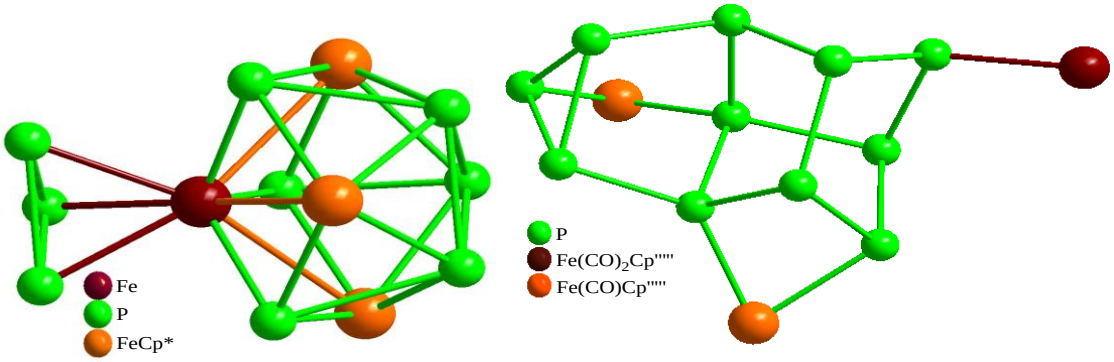

Figure 2. Left, $[(Cp^*Fe)_3\{(\eta^3\text{-}P_3)Fe\}P_6]$.[47] Right, $[\{Cp'''''_3(CO)_4Fe_3\}P_{11}]$, Cp''''' = $C_5(i\text{Pr})_5$.[48]

Direct methods treat a K_3P_7/2,2,2-crypt solution with $[(C_6H_3\text{-}(CH_3)_3]Cr(CO)_3$ in toluene also give a P_7^{3-} cage while preserving the original negative charge. The chromium affects the phosphorus-phosphorus bond lengths. The P6–P7 and P5–P4 bond lengths are slightly constrained (2.113(9)–2.129(9) Å) from the orbital binding accommodation of the Cr–P4, Cr–P5, Cr–P6, and Cr–P7 bonds. The π-bond character of P3–P6, P3–P5, P2–P7, and P2–P4 bonds is disrupted (2.211(9)–2.238(8) Å) in comparison to the preserved π-electron density of P1–P2 and P1–P3 (2.146(8)–2.125(10) Å). The tungsten analog is produced when the reactant $[(C_6H_3\text{-}(CH_3)_3]W(CO)_3$ is used.[49] Other studies show that when K_3P_7 is treated with $[(en)(CO)_3W(\eta^1, \eta^4\text{-}P_7Cr(CO)_3]^{3-}$ the same tungsten and chromium ions are isolated through crystallization.[50]

Just as in the chromium analog, the tungsten species has shortened P6–P7 and P4–P5 bonds from the binding orbital influence of tungsten (2.134(6)–2.136(5) Å). Surprisingly, the same is true for the P1–P2 and P1–P3 bond lengths (2.144(5)–2.150(4) Å) as they are not significantly affected by the $W(CO)_3$ fragment. This conservation is also observed for the P3–P6, P3–P5, P2–P7, and P2–P4 (2.215(6)–2.231(4) Å). An ethyl group has also been attached to P1 in related research by alkylation with excess R_4N^+.[51] Analogous seven member clusters with niobium,[52] nickel,[53] and platinum[53] attached are also reported.

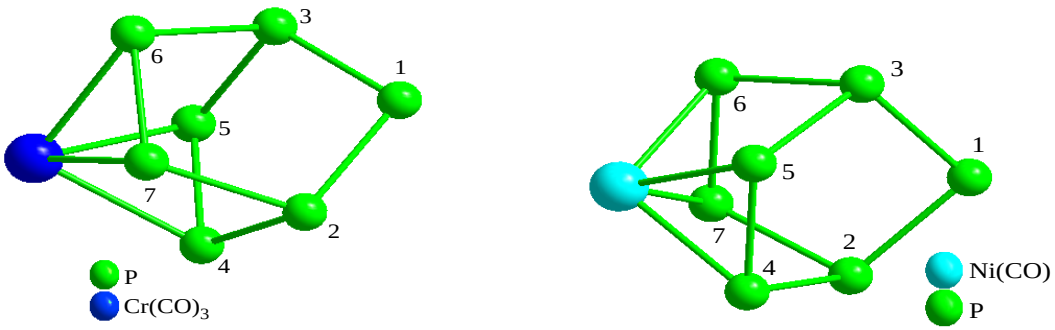

Figure 3. Figure on the left, $[P_7Cr(CO)_3]^{3-}$ ion, $[K(2,2,2\text{-crypt})]_3$ and ethylenediamine omitted for clarity.[49] Figure on the right, analogous $[P_7Ni(CO)]^{3-}$, $[K(2,2,2\text{-crypt})]_3$, and phosphines omitted for clarity.[53]

A method alternative to thermolysis is reported by substituting heat for ultraviolet light in the successful production of unsubstituted P_8 complexes.[54] Other synthetic aspects

remain similar, namely, a metal carbonyl as a reactant, in this case $[Cp'Fe(CO)_2]_2$ ($Cp' = \eta^5$-C_5H_5Me), the solvent (toluene) as well as treatment with white phosphorus. The resulting structure (Figure 13) contains a P_8 cage with two terminal and two chelating iron fragments. The chelating iron fragment is covalently bound to one phosphorus atom (5 and 6) and bound to the lone pair of the other (7 and 8), whereas the terminally bound iron fragment is covalently bound to one phosphorus (7 and 8) giving each iron atom a valence count of 18 electrons.

When this complex is further treated with additional $Fe(CO)_5$ in the presence of Me_3NO or alternatively with $Fe_2(CO)_9$ (both cases in THF) an even greater substituted species (Figure 4, right) is produced.[54] Given the increased complexity of this complex, every iron atom maintains an 18 electron count. Each of the bridging iron atoms provides a dative and a formal bond with the phosphorus atoms P7, P5 and P8, P6, respectively. The remaining iron ligands are covalently bound to P7 and P8 and datively bound to P5 and P6.

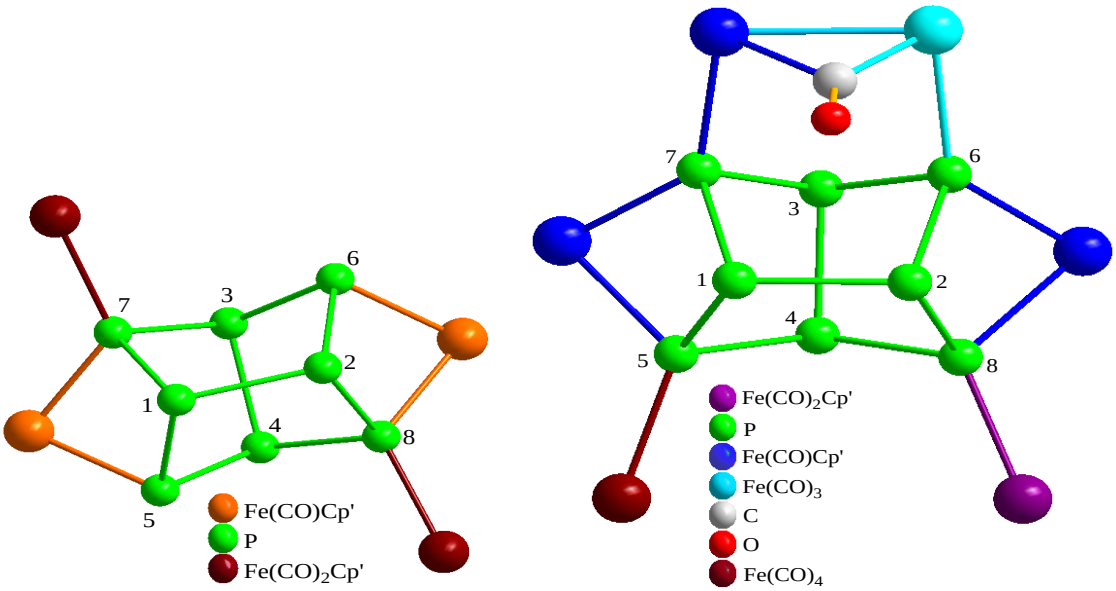

Figure 4. Left, $Cp'_4Fe_4(CO)_6P_8$ ($Cp' = \eta^5$-C_5H_5Me).[54] Right, $Cp'_4Fe_6(CO)_{13}P_8$ ($Cp' = \eta^5$-C_5H_5Me).[54]

1.3. 6 Phosphorus Atoms

Starting with the higher order structures, the employment of LiCp* in conjunction with $P_7(SiMe)_3$ and $FeCl_2$ at low temperatures yields the cage complex shown in Figure 5.[47] By strictest definition this complex is naked in the sense that the phosphorus atoms have no substituents outside of the cage, but the phosphorus atoms also lack lone pairs of electrons as demonstrated by the four and five coordinations exhibited so it should be of no surprise if the potential of forming a dative bond is limited. The P–P bonds lengths (2.268(2)–2.498(2) Å) suggest single bonding throughout the entire cage. The longest (connecting the two P_3 motifs) are likely strained from the iron bond.

An oblique square bipyramidal vanadium-phosphorus polyhedron (Figure 5) is obtained from a traditional thermal reaction with $V(CO)_4Cp$ and white phosphorus. This structure can be thought of as two $CpV(\mu,\eta^3$-$P_3)VCp$ units. As mentioned above, even though the phosphorus atoms are formally unsubstituted it is reasonable that all of the lone pairs from phosphorus participate in the interstitial bonds of the complex. The other remarkable side

product of this reaction is the hexaphosphorus-vanadium-cyclopentadienyl sandwich complex.[55]

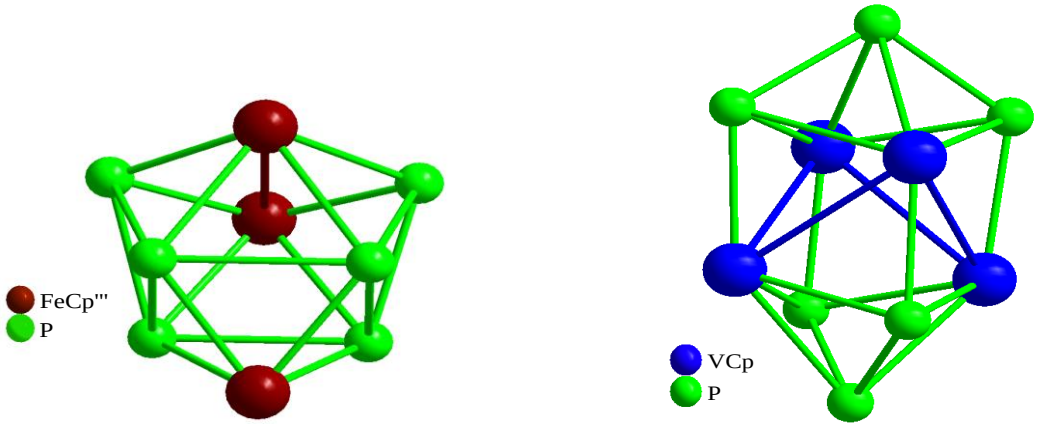

Figure 5. Left, $[(Cp'''Fe)_3P_6]^+$ ($Cp''' = C_5H_2Me_3$), $[FeCl_3(THF)]^-$ removed for clarity.[47] Right, $(VCp)_4(P_3)_2$ complex.[55]

Since its introduction in 1974, the flat P_6 ring has gained considerable attention because of its isolobalness to benzene.[6] It is important to note from all proven and theoretical examples of P_6 complexes presented in the literature,[6, 13, 55-64] that only if the symmetry properties, approximate energy, and shape of the frontier orbitals are similar and the number of electrons in them are equal, only then can the species be isolobal.[65] The phosphorus atoms in the niobium complex in Figure 6 exemplify isolobility to CH by their flat P_6 ring and the constricted phosphorus-phosphorus bonds (av. = 2.11 Å) with only slight distortion.[66] Other metal sandwich complexes containing flat P_6 rings include niobium,[67] tungsten,[68] molybdenum,[61] vanadium,[58, 68] and iron.[57]

Other examples have six membered rings attached, but are not isolobal to benzene because they are structurally different. The iron-molybdenum $Cp^*FeP_6MoCp^*$ example[69, 70] in Figure 6 show the deformity of the six membered ring. Even though the side view of the complex is distorted, the bond distances (Mo–P3/P6 = 2.44/2.44 Å, Mo–P4/P5 = 2.59/2.59 Å, Mo–P1/2 = 2.53/2.54 Å, Fe–P4/5 = 2.29/2.30 Å, and Fe–P3/P6 = 2.28/2.28 Å) reflect the high bilateral symmetry of the MoP_4FeP_2 skeleton. It is not clear whether the P1–P6 or the P2–P3 bonds (2.51 Å and 2.50 Å respectively) are real or not because they are longer than the longest reported P–P bonds in the literature at the time (2.46 Å).[71]

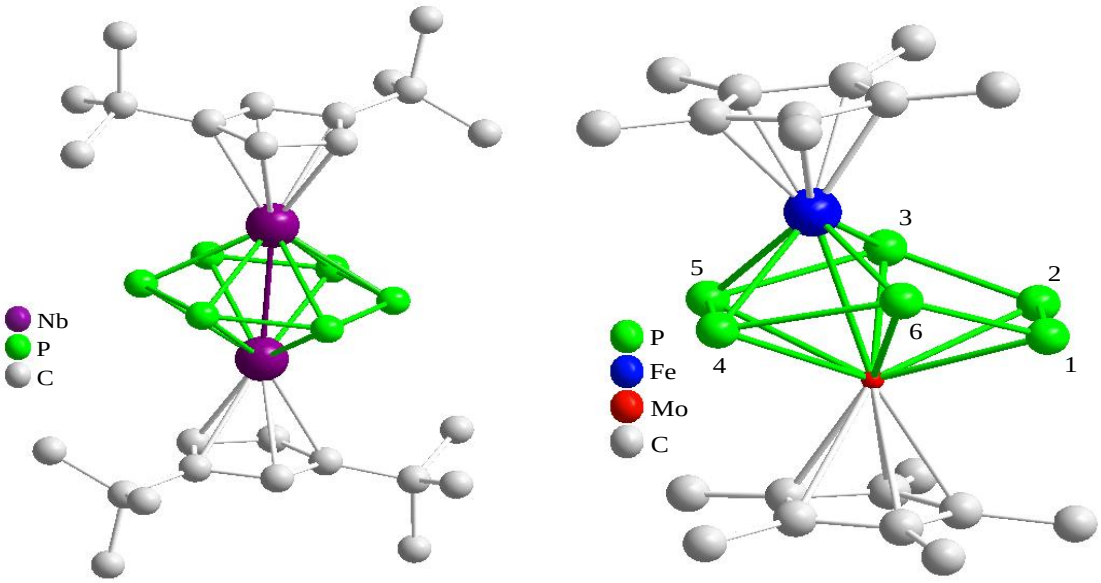

Figure 6. Left, $[(Cp''Nb)_2(\mu\text{-}\eta^6\text{:}\eta^6\text{-}P_6)]$, ($Cp'' = \eta^5\text{-}C_5H_5(^tBu)_2\text{-}1,3$), hydrogens removed for clarity.[66] Right, $[\eta^5\text{-}Cp^*FeP_6Mo\eta^5\text{-}Cp^*]$, hydrogens removed for clarity.[69, 70]

Finally, the titanium containing complex[62] (Figure 7) lacks hyperconjugation of electron density as demonstrated by the chair conformation and the slight elongation of P–P single bonds (2.23(2)–2.25(2) Å). The phosphorus atoms are all chemically equivalent in C_6D_6, δ (^{31}P NMR = 386.7 ppm). All three examples mentioned are undoubtedly different with respect to the naked P_6 ring, but all are synthesized using a combination of metal carbonyls and white phosphorus under the conditions of thermolysis. There is no special way of engineering a targeted structure; all structures characterized are completely accidental.

The thorium complex[32] in Figure 7 is the first bicyclic structure composed of naked phosphorus atoms. The four member butterfly shaped ring is bound to two phosphorus atoms (the handle) above and shouldered by two thorium atoms. While view shown in Figure 7 nearly possesses a σ plane of symmetry, the view perpendicular (bisecting the butterfly) is obviously not. All phosphorus-phosphorus bonds are singly bonded (2.18(2)–2.24(1) Å) and the shortest is positioned above the butterfly (the handle) from the orbital constriction of the thorium metals. It is possible to separate the "handle" as demonstrated by the cobalt connection of the iron shouldered analog.[72]

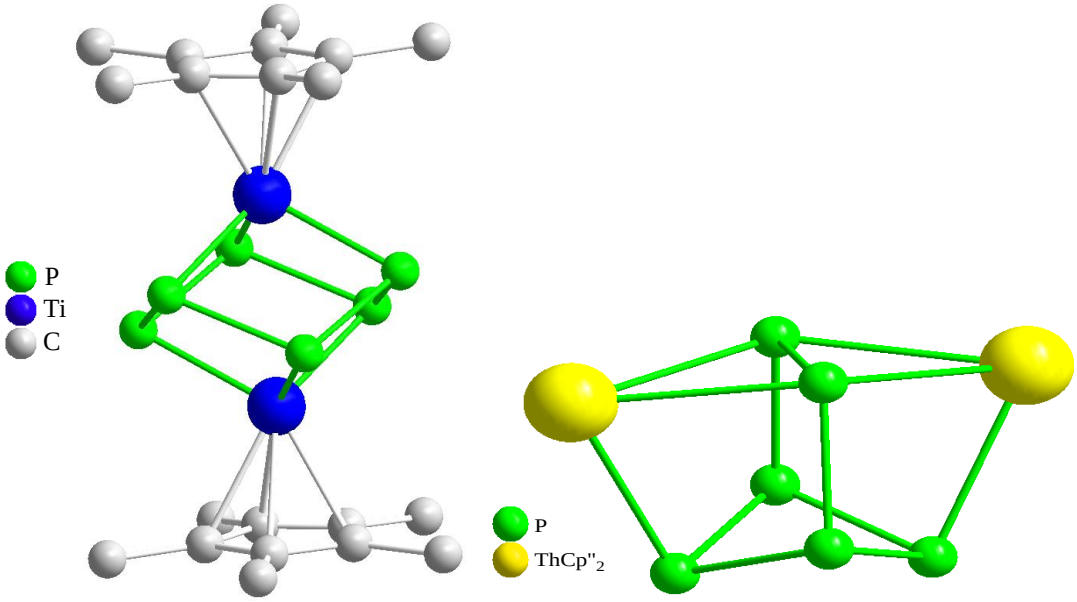

Figure 7. Left, $Cp^*TiP_6TiCp^*$, hydrogens removed for clarity.[62] Right, $Cp_2''ThP_6ThCp_2''$($Cp'' = \eta^5$-1,3-$^tBu_2C_5H_3$).[32]

1.4. 5 Phosphorus Atoms

Unsubstituted five membered rings dominate this field and the only exception listed in these examples is the double titanium complex with two sets of P_5 rings (Figure 8). By strict definition this complex has ten unsubstituted phosphorus atoms and is more appropriately placed in the category of '>6 naked phosphorus atoms', however, because of the significance of this discovery is it more rewarding to discuss it along with other unsubstituted P_5 rings. All the metals listed in the examples of Table 1 are group 6 or 8 transition metals with the exception of manganese (Entry **22**), and it is by no coincidence that all the ligands bound are either carbonyls or cyclopentadienyl derivatives. These ligands offer better stability through their π-electron acceptation, and they aid crystallization. Two P_5 complexes (GaP_5 and InP_5) are investigated to help understand GaP and InP semiconducting materials.[73]

Entry	R_1	M_1	M_2	R_2
1	η^5-Cp*	Fe	Cr	$(CO)_3$
2	η^5-Cp*	Fe	Mo	$(CO)_3$
3	η^5-Cp*	Cr	Cr	η^5-Cp*
4	η^5-Cp	Fe	Fe	η^5-Cp
5	η^5-Cp	Fe	Fe	η^5-$C_5(Me)_4Et$
6	η^5-Cp	Fe	Ru	η^5-Cp*
7	η^5-Cp	Fe	Fe	η^5-Cp*
8	η^5-Cp*	Fe	Ru	η^5-Cp
9	η^5-Cp*	Fe	Ru	η^5-Cp*
10	η^5-Cp	Ru	Ru	η^5-Cp
11	η^5-Cp*	Ru	Ru	η^5-Cp*
12	$(CO)_3$	W	Si	(Me)

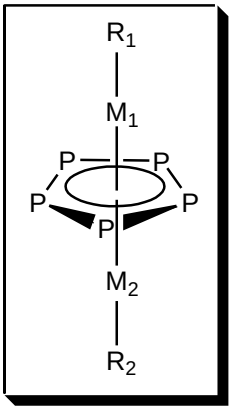

Entry	R_1	M_1
13	η^5-$C_5(^tBu)_3H_2$	Fe
14	η^5-Cp*	Fe
15	η^5-$C_5(^tBu)_2H_3$	Fe
16	η^5-$C_5(Et)(Me)_4$	Fe
17	η^5-Cp*	Ru
18	η^5-$C_5(Et)(Me)_4$	Ru
19	$(CO)_3$	Cr
20	$(CO)_3$	Mo
21	$(CO)_3$	W
22	$(CO)_3$	Mn

Table 1. Examples of naked P_5 ring containing complexes. Entries **1**–**2**,[74] **3**,[27] **4**,[30] **5**,[75, 76] **6**,[76, 77] **7**–**11**,[77] **12**,[78] illustrate the multimetal centered complexes. Entries **13**,[79, 80] **14**,[75, 81-84] **15**,[83, 85] **16**–**18**,[75] and **19**–**22**[78] are not.

Two examples shown in Figure 8 are the titanocene[86] and an iron/ruthenium tripledecker complex (Entry **6**).[76, 77] The most common synthetic procedure is to treat a metal carbonyl with white phosphorus or a phosphorus-rich metal by thermolysis, ultraviolet light, or ambient conditions. One notable reactant, $X^+P_5^-$ (X = Na, K), although not formally characterized, can be thought of as a P_5 example in itself,[87] and successful employment of this reactant has led to the formation of Entries **12**, **19**–**22**, **14**, and **15**.[78, 83, 84]

Normal phosphorus-phosphorus single bond lengths are about 2.20 Å and under electronic or steric influences can be elongated to about 2.50 Å, however, when the bonds are constricted to ≤ 2.18 Å the inspection must be made to determine if the multiplicity is increased. This is certainly the case with titanocene (bond lengths 2.147(1)–2.166(1) Å), and with its flat structure it provides a perfect example to the isolobility of P to CH units. The same can also be said about Entry **6** (2.155(1)–2.159(1) Å). The high degree of symmetry (D_{5h}) from titanocene is caused from the eclipsed η^5-P_5-metal bonds. This is also the case with Entry **6** where every η^5 bond is eclipsed yielding its C_{5v} symmetry only to a difference in substituents (also bound in an η^5 fashion). The titanocene orbitals are lower in energy when compared to those of Cp in ferrocene, and the P_5 ligand is a σ-bonded ligand whereas the Cp is a π-bonded ligand. In this respect carbon and nitrogen have the weakest metal-ligand bonds, while the bonds of titanocene with analogous As_5 and Sb_5 rings are only slightly weaker than the phosphorus analog.[88] Other theoretical studies for similar P_5–M_1–M_2–P_5 scenarios (M_1 = Cd, M_2 = Zn; M_1 = Cd, M_2 = Cd; M_1 = Zn, M_2 = Zn) show that the bonds are ionic and, in this instance, the metal-metal bond is free to rotate.[89]

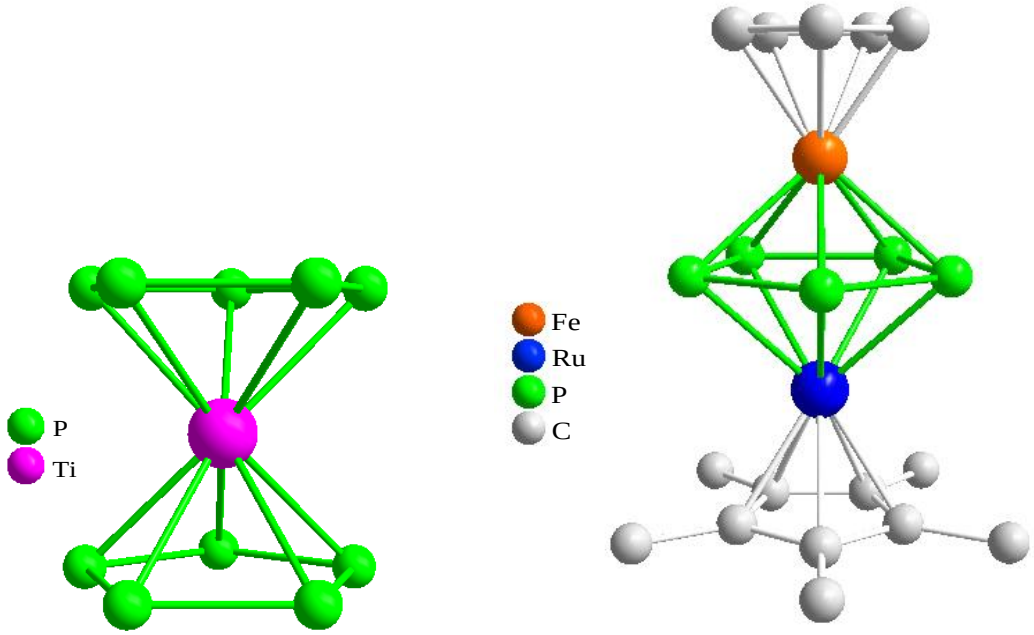

Figure 8. Left, $[Ti(\eta^5\text{-}P_5)_2]^{2-}$, Ph_4P^+ omitted for clarity.[86] Right, η^5-$CpFeP_5Ru$-η^5-Cp*, PF_6^- omitted for clarity (Entry **6**, Table 1).[76, 77]

It should also be stressed that five membered flat rings are not always the most stable species. The iron-molybdenum containing complex (Figure 9, left) possesses a P_5 motif that is structurally interrupted by a *tert*-butyl group and disconnected. A 1,2-insertion with ^{t}BuC≡P into $[(^tBu_3Cp)(OC)Mo(\mu\text{-}\eta^{2:2}\text{-}P_2)_2\text{-}Fe(Cp^*Et)]$ using thermolysis expands the phosphorus-phosphorus connectivity (P2–P3) providing a questionable bond (2.559(1) Å) while forming an additional adjacent phosphorus-phosphorus bond. The remaining unbound phosphorus atoms (P1 and P5) remain unbound just as they were in the starting material. The P4–P5, P4–C, and C–P3 bonds are considerably shorter (2.147(1), 1.760(3), and 1.775(3) Å) than would be expected for their singly bound counterparts. It is reasonable to assume that there is double bond character associated and that the lone pairs of electrons from phosphorus atoms 3, 4, and 5 are hyperconjugated.

Further treatment of a ring complex, $[Cp^*Fe(\eta^5\text{-}P_5)]$, with $[\{Cp''Ru(CO)_2\}_2]$ using thermolysis gives multiple cage complexes, one of which is featured in Figure 9 (right). Of course, the cage offers five naked phosphorus atoms, but all the lone pairs of all the phosphorus atoms are occupied. Such a variety of multiple phosphorus-phosphorus bonds are present in this structure from strained single bonds (P1–P3, 2.489(4) Å; P2–P3, 2.504(4) Å), single bonds (P4–P5; 2.207(4) Å) and constricted bonds (P3–P4, 2.129(5) Å; P1–P2, 2.174(4) Å). These differences are most likely produced from steric effects from the cage being that no pattern is noticeable for an electronic influence. Other cages are also produced using thermolysis[90, 91] including the $FeCo_2$ analog.[92]

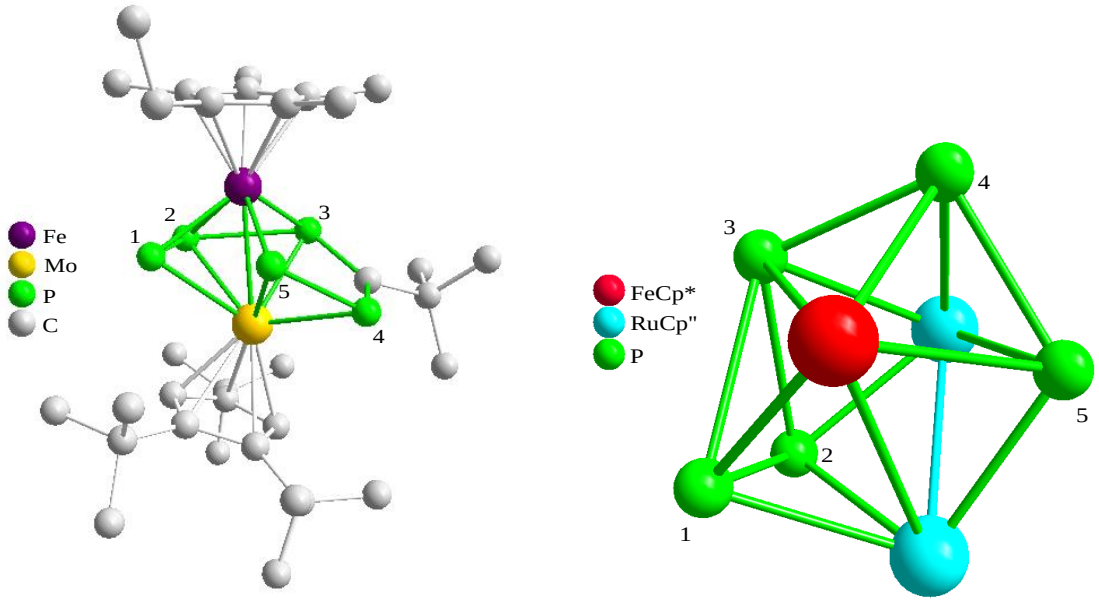

Figure 9. Left, η^5-Cp(Me$_4$Et)FeP$_5$(C-^{t}Bu)Moη^5-Cp(^{i}Pr)$_3$.[70] Right, η^5-Cp*FeP$_5$(Ru-η^5-Cp(^{t}Bu)$_2$)$_2$.[93]

The quasi cubic nickel-phosphorus cage[28, 94] (Figure 10) is a product of the thermolysis of [Cp*Ni(CO)]$_2$ and P$_4$. In this case the single phosphorus-phosphorus bonds are unperturbed from the influence of nickel. One would expect this complex to have greater potential for dative bond formation because each of the lone pairs of electrons on each phosphorus atom in this complex is retained.

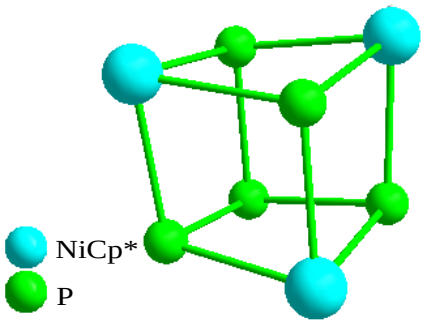

Figure 10. Structure of (NiCp*)$_3$P$_5$.[94]

1.5. 4 Phosphorus Atoms

Tetrahedral, white phosphorus can bind to a metal in an η^1 or an η^2 fashion. The iron complex[95] in Figure 11 shows one such example synthesized from the analogous chloride containing analog in THF. The chloride ligand is replaced by the η^1 bound tetrahedral P$_4$ ligand. As one would expect, the iron complex has two sets of similar phosphorus-phosphorus bonds. The P1–P2, P1–P3, and P1–P4 bonds are shorter (2.159(1) Å, 2.166(1) Å, and 2.162(1) Å, respectively) than the P2–P4, P3–P4, and P2–P3 (2.203(1) Å, (2.236(1) Å,

and 2.211(1) Å, respectively). With evidence of equatorial in-plane π overlap from the $4d_{yz}$ with a P_4 $2P\pi^*_{\parallel}$ in a related species,[71] it is tempting to say this phenomenon is a result of π-backbonding from the metal as is it seen in other examples as well,[96-98] however, it is not consistent with every metal complex of this type.[99, 100] Similar terminally bound tetrahedral P_4 ligands bridging two metals together have also shown a constriction in the P–P bond shared by the two metals and a lesser effect from the other less proximal P–P bonds.[101, 102] Other complexes are characterized by NMR.[35, 103-105]

Treating $RhCl(PPh_3)_3$ with white phosphorus under low temperature (–78 °C) in CH_2Cl_2 or Et_2O affords the rhodium complex in Figure 11 where the tetrahedral P_4 is bound in an η^2 fashion.[4, 71] This ligand has a large trans influence as seen from the enormous elongation of the Rh–Cl bond (2.4095 (14) Å). Aside from the other phosphorus-phosphorus bonds (2.188(3)–2.222(2) Å), the P1–P2 bond is significantly lengthened (2.461(2) Å) to accommodate the orbitals of the rhodium metal. Complexes with other terminal η^2-P_4 metal/substituent combinations,[106] totally naked silver bridging two η^2-P_4 substituents,[106-110] and totally naked copper bridging two η^2-P_4 substituents[109] show that this is not a result of the trans influence shown in the featured rhodium complex. As predicted by density functional calculations the M–P bond energies increase in the order Ag<Cu<Au. The anomaly occurs because the orbital interactions of the 6s and 5d orbitals cause stronger metal ligand interactions. Furthermore, the Ag–P and Ag–C interactions are nearly identical in the $Ag(C_2H_4)^+$ and $Ag(P_4)^+$ ions, and both shrink due to the π-backbonding from the phosphorus atoms and carbons back to the metal.[111]

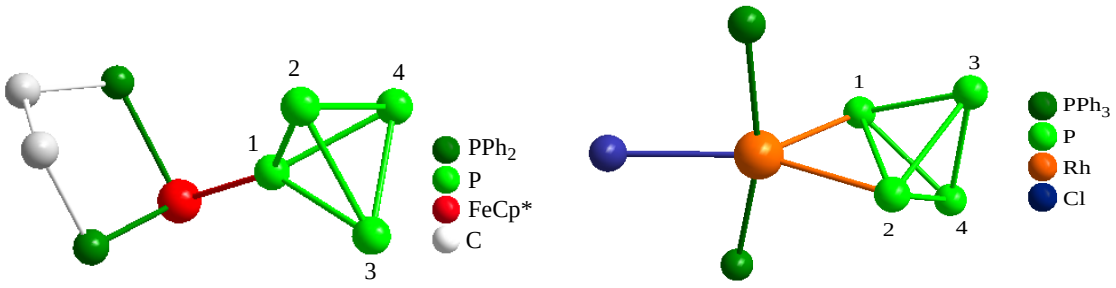

Figure 11. Left, $[(C_2H_4(PPh_2)_2)Cp^*Fe\eta^1\text{-}P_4]^+$, $[BPh_4]^-$ and hydrogens removed for clarity.[95] Right, $Cl(PPh_3)_2Rh\eta^2\text{-}P_4$, CH_2Cl_2 and hydrogens removed for clarity.[4, 71]

Four membered naked phosphorus atoms also exist in "butterfly" conformation as shown by the iron complex in Figure 12. The complex is rendered when iron carbonyl complex, $[\{C_5H_2{}^tBu_3(CO)_2Fe\}_2]$, is treated with white phosphorus by applying thermolysis.[80] The selective activation of the P1–P4 bond creates a widened angle between the P1–P3–P2/P1–P2–P4 planes (84.29(9)°). The P1–P2, P2–P4, P4–P3, and P3–P1 bonds around the parameter remain single (2.197(2)–2.218(2) Å), while constriction occurs in the middle P2–P3 bond (2.150(3) Å). Few butterfly complexes exist, and even as most contain a constricted center (P2–P3) bond,[112, 113] at least one example does not and the other is tethered by phosphorus.[114, 115] Other examples are characterized by NMR.[116]

The complex $[Co\eta^5\text{-}C_5H_3(SiMe)_2]_2\text{-}(\mu\text{-}P_2)_2$ has two sets of phosphorus atoms doubly bonded to each other (2.054(2) Å) and positioned parallel to each other in a near perfect equator. Analogs with Cp* and $C_5H_2{}^tBu_3$ also exist and the bond lengths and angles are similar to the featured complex.[117, 118] Although examples like this motif are few, the significance of the separation is great because if, in fact, the two sets were connected,

hyperconjugation of the lone pairs of elections would be permitted around a, then formed, ring. A similar planar P_4 motif is reported where only three phosphorus atoms are bound.[119]

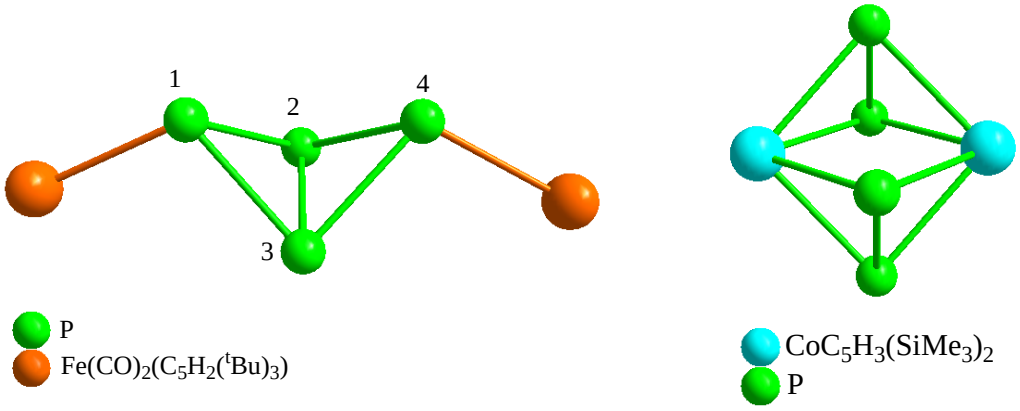

Figure 12. Right, $[Fe(CO)_2\eta^5\text{-}C_5H_2{}^tBu_3]_2\text{-}\mu\text{-}P_4$.[80] Left, $[Co\eta^5\text{-}C_5H_3(SiMe)_2]_2\text{-}(\mu\text{-}P_2)_2$.[42]

One such example of a closed four membered ring is shown by the niobium species in Figure 13. The molecule is synthesized under ultraviolet radiation by treating $Cp^*Nb(CO)_4$ with white phosphorus in the presence of hexane at room temperature, and is accompanied by a disubstituted $[\{Cp^*(CO)Nb\}_2(P_4)]$ and $[\{Cp^*Nb\}_2(P_6)]$. The shortened phosphorus-phosphorus bonds (2.136(3)–2.180(3) Å) imply that they are doubly bonded, and the cyclic connection deviates only slightly from a perfect square (~3°). By Hückel's rule, the featured planar, cyclic ring possessing 6 conjugated π electrons qualifies this as aromatic (4n+2).[120] The 2 additional π electrons are added from the *d* orbital of the niobium with the correct symmetry. If niobium is unbound the number of electrons is changed to 4; the species becomes antiaromatic (4n, n = 2). A tantalum[121] and vanadium[55, 58] analog as well as an unrelated Cs_2P_4 complex[122, 123] are the only other examples in the literature.

Five membered heterorings containing four naked phosphorus atoms certainly qualify. The featured iron centered ring in Figure 13[79] is, ironically enough, synthesized by treating the butterfly complex in Figure 12 with $P{\equiv}C^tBu$ using thermolysis in a toluene solution. The sandwich complex has close alignment with each of the C_5 and P_4C rings (~5° distortion), and the angles around the P_4C ring are not ideal (108°), distorting the C_5 symmetry. The P_4C ring is, however, flat and each of the P–P and C–P bonds lengths suggest they are double bond in character (P–P av. = 2.124(2) Å and C–P av. = 1.775(4) Å) meaning that the lone pairs of electrons are also hyperconjugated. The $SiMe_3$ substituent is also tunable and the ^tBu analog is reported.[124]

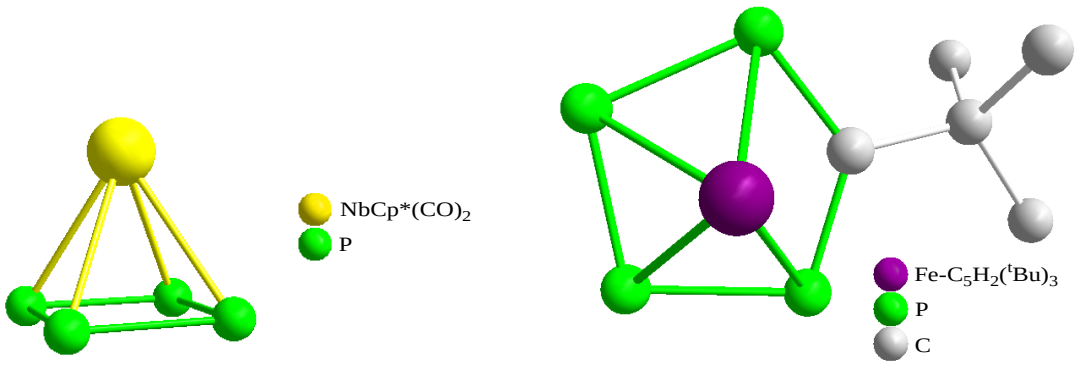

Figure 13. Left, NbCp*η^4-P_4.[67] Right, η^5-$P_4C(^tBu)Fe\eta^5$-$C_5H_2(^tBu)_3$.[79]

Using the direct method of treating $Li_3P_7(DME)_3$ with 3 equivalents of $[FeCp(CO)_2Br]$ while the synthesis is conducted at –78 °C in a THF solution and gently layered with heptane precipitates a red crystalline $[(Cp^*Fe)_3P_6][FeCl_3(THF)]$ cage (Figure 14) covalently bound to three equivalents of $Fe(CO)_2Cp$. In contrast to the previously mentioned example, a slight reduction in the P–P bond length (0.02 Å) is evident in comparison to the non-metal bonded phosphorus atoms. Other similar cages with four naked phosphorus atoms have also been reported.[125-129]

An iron-phosphorus heterocage is also reported where two sets of P–P bonds are situated perpendicular to each other.[33] The iron cluster (Figure 14, right) is afforded from the thermolysis of $[CpFe(CO)_2]_2$ with white phosphorus. Planes of symmetry included in this molecule are Fe1–P2–P1–Fe4 and Fe2–P3–P4–Fe3, and the average phosphorus-phosphorus bond distances are only slightly elongated (Av: 2.306(5) Å).

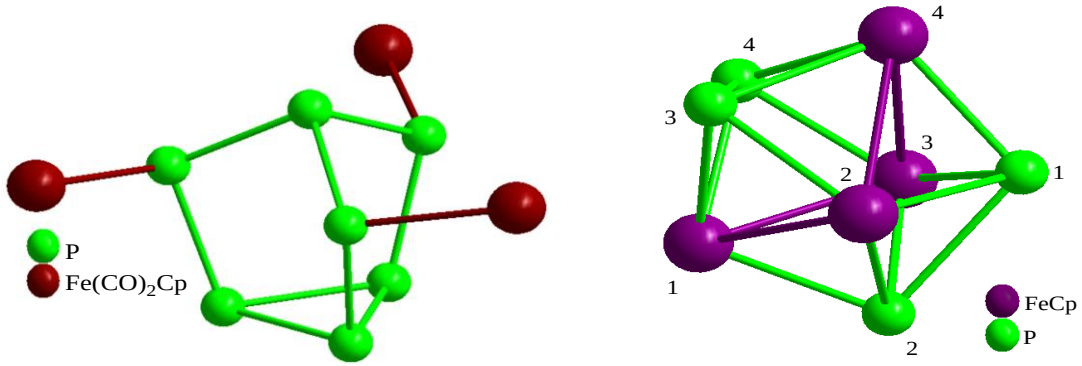

Figure 14. Left, $[(Cp^*Fe)_3P_6]$, $[FeCl_3(THF)]$ is excluded for clarity.[47] Right $(FeCp)_4P_4$.[33]

1.6. 3 Phosphorus Atoms

Stopponi and Sacooni heavily dominate (Table 2) in the number of complexes synthesized containing an unsubstituted P_3 substituent due to their signature triphos (1,1,1-tris((diphenylphosphino)methyl)ethane) ligand. Introduction is generally imposed by treating the triphos ligand in a polar solution (ie. THF, alcohol) with the appropriate carbonyl or aqua substituted metal. The anion is attached to the treated metal or separated from the metal using a carrier cation. The examples shown in Figure 15 show the mono- and disubstituted (Entries 27 and 11, Table 2) analogous palladium complexes. These P_3 rings are especially electron

rich as noted from their phosphorus-phosphorus bond distances where the monosubstituted species on the left (Av P–P: 2.115(6) Å) and the disubstituted species on the right (Av P–P: 2.136(1) Å) indicate that the phosphorus atoms are multiply bonded to each other. The phosphorus atoms in the triphos ligand are eclipsed in the mono- as well as in the disubstituted species.[130]

The multiple metals employed in the construction of many mono- and disubstituted triphos featured species are shown in Table 2. The next best ligand is cyclopentadienyl, which has also been consistently present in the previous categories.

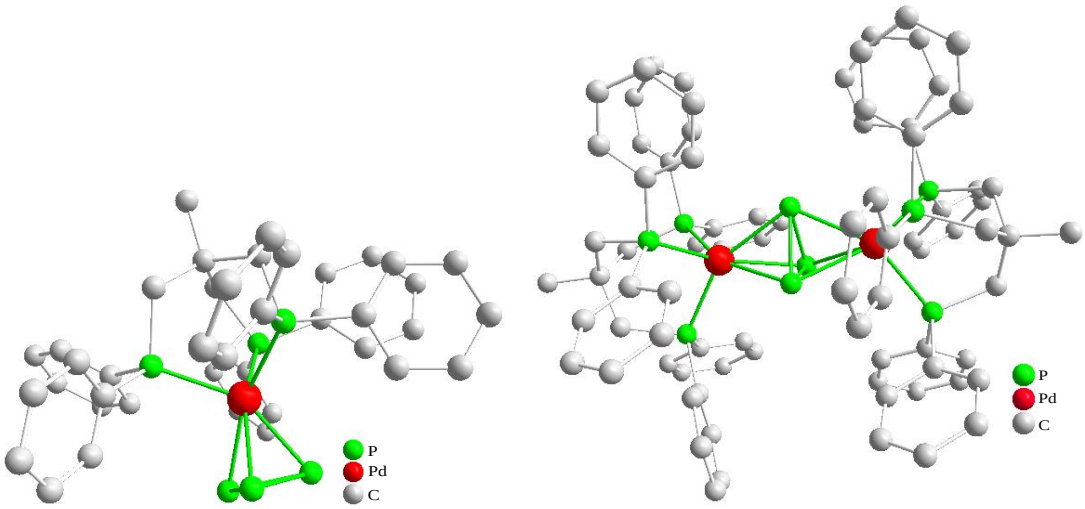

Figure 15. Left, $[(triphos)PdP_3]^+$, $[BF_4]^-$, and hydrogens removed for clarity.[130] Right, $[(triphos)PdP_3Pd(triphos)]^+$, $[BPh_4]^-$ and hydrogens removed for clarity.[130]

Entry	R_1	M_1	M_2	R_2
1	triphos	Co	Cu	triphos
2	triphos	Co	Ag	triphos
3	triphos	Rh	Ag	triphos
4	triphos	Ni	Pt	$(PPh_3)_2$
5	triphos	Co	Pt	(PPh_3)
6	triphos	Co	Rh	triphos
7	triphos	Ni	Rh	triphos
8	triphos	Co	Ir	triphos
9	triphos	Rh	Rh	triphos
10	triphos	Co	Ni	triphos
11	triphos	Pd	Pd	triphos
12	triphos	Co	Fe	triphos
13	triphos	Co	Co	triphos
14	triphos	Th	Th	triphos

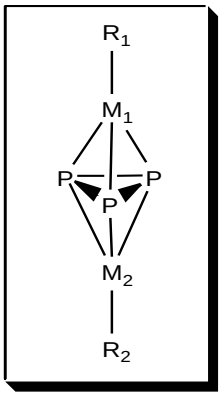

Entry	R_1	M_1
15	triphos	Ir
16	triphos	Rh
17	$Cp^*(CO)_2$	Mo
18	$C_5H_4{}^tBu$	Mo
19	$C_5H_3({}^tBu)_2$	Mo
20	$((Me_2C_6H_3)N({}^iPr))_3$	Mo
21	$((Me_2C_6H_3)N({}^iPr))_3$	W
22	$Cp(CO)_2$	W
23	$Cp(CO)_2$	Mo
24	$Cp(CO)_2$	Cr
25	triphos	Ni
26	triphos	Pt
27	triphos	Pt
28	triphos	Pd
29	triphos	Co
30	triphos	Ir
31	triphos	Rh
32	$(CO)_3$	Co
33	$(OCH_2{}^tBu)_3(CH_3NHCH_3)$	W
34	Cp^*	Ni
35	$(O\text{-cylcohexyl})_2$(O-cyclohexyl-NH(Ar))	Mo

Table 2. Summary of complexes containing a cyclo P_3 ligand. **1**–**3**,[131] **4**–**5**,[132] **6**–**9**,[24] **10**,[25] **11**,[130] **12**–**13**,[133] **14**,[32] **15**–**16**,[134] **17**,[85, 135-138] **18**,[85, 135] **19**,[85] **10**–**21**,[139] **22**,[135] **23**,[135, 140] **24**,[141-143] **25**–**26**,[144] **27**–**28**,[130] **29**,[145] **30**–**31**,[146] **32**,[147] **33**,[148] **34**,[94] **35**.[149] Triphos = (1,1,1-tris((R-phosphino)R)ethane) and R = various organic substituents. Counterions are removed for clarity.

The cyclopentadienyl ligand is also versatile at forming double- and triple-decker complexes. The thorium complex in Figure 15 is obtained by treating $[(\eta^5\text{-}1,3\text{-}{}^tBu_2C_5H_3)_2Th(\eta^4\text{-}C_4H_6)]$ with white phosphorus and $MgCl_2(OEt)_2$ during thermolysis. The labile alkene detaches and facilitates the formation of a P_3 centered triple-decker complex with a chlorine atom attached to one of the thorium atoms. Aside from the disruption of symmetry, the chlorine is eclipsed to the phosphorus atoms in the P_3 motif.[32] The nickel complex $[Cp^*Ni\eta^3\text{-}P_3]$ is the coproduct of a P_5 cage complex obtained by treating $[Cp^*Ni(CO)]_2$ with white phosphorus through thermolysis. The commonality of the constrained phosphorus-phosphorus bonds of the nickel (av. P–P: 2.100(4) Å) and the thorium (av. P–P: 2.185(9) Å) complex shows consistency between the different P_3 bearing complexes.[94]

Other cluster[143, 150] and ring[79, 151, 152] complexes with P_3 configurations are also noted. Entries **17**, **22**, and **23** are described in detail in the Results and Discussion section.

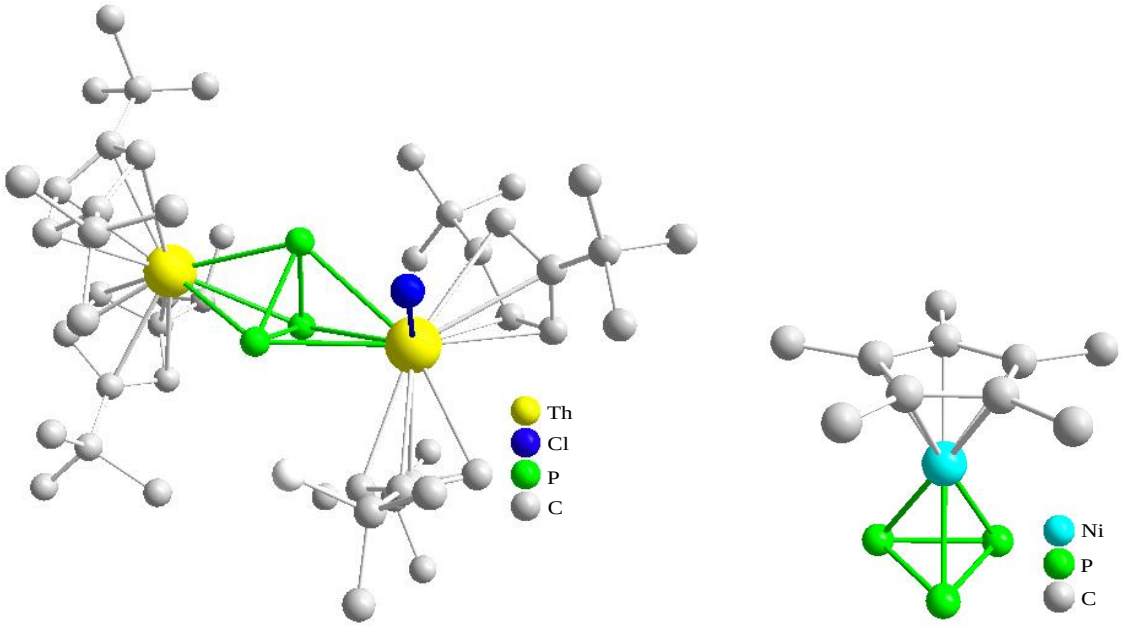

Figure 15. Left, $Th(Cp^tBu_2)_2\eta^3{:}\eta^3\text{-}P_3ThCl(Cp^tBu_2)_2$.[32] Right, $Cp^*Ni\eta^3\text{-}P_3$.[94]

1.7. 2 Phosphorus Atoms

The discussion of two naked phosphorus atoms can be trivial unless certain scenarios are addressed. The iron complex[153] in Figure 16 shows two sets of mono substituted cyclopentadienyl rings in a staggered conformation, each bearing the ability of the electron rich phosphorus atoms (av. C–P bond length: 1.778(1) Å) to datively bind to an electrophile. The disubstituted molybdenum complex[139] (right) contains both of its phosphorus atoms in the same three-membered heterocycle. Surprisingly, the C–P bonds are not shortened (1.804(2) Å), and most of the electron density seems to be localized at the P=P double bond (2.137(1) Å). Similarly, as in the iron complex, the nitrogen containing substituents are staggered with respect to the atoms of the heterocycle.

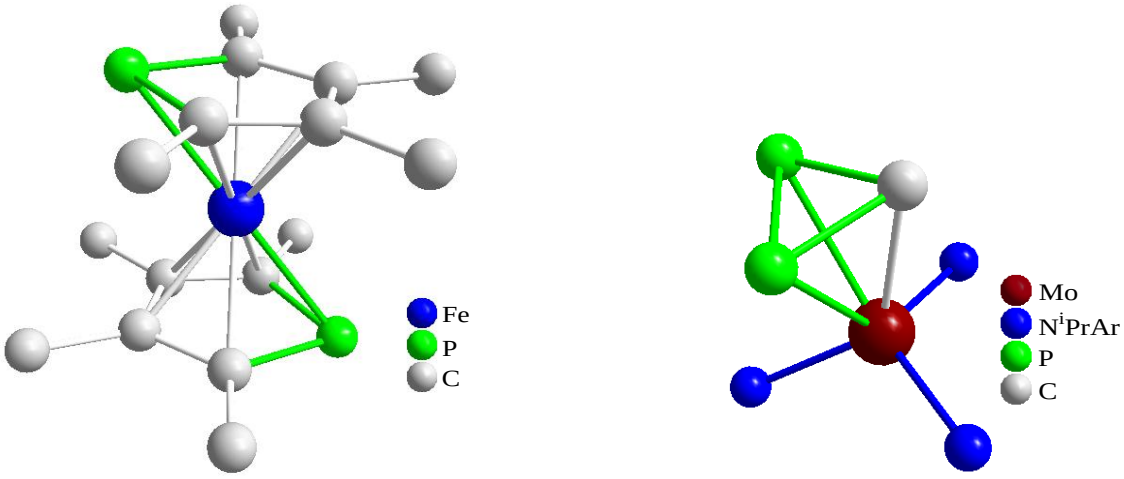

Figure 16. Left, $Fe(Me_4C_4P)_2$, hydrogens omitted for clarity.[153] Right, $\eta^3\text{-}P_2CMo(N(Ar)^iPr)_3$ and hydrogens omitted for clarity. Ar = 1-adamantyl, Ar = 3,5-$Me_2C_6H_3$.[139]

The Fe_2P_2 heterocycle dissected by an Fe–Fe bond in Figure 17 offers two lone pairs located trans from each other. In contrast to the previously mentioned cyclopentadienyl ligands in $Fe(Me_4C_4P)_2$, the Cp''' rings are eclipsed. This metal- phosphorus motif was first synthesized in 1973 with an analogous cobalt carbonyl[5, 117, 147] and is also present in chromium,[143] molybdenum,[85, 136-138, 140] and tungsten complexes.[154] The complexes containing group six elements have formal P–P bonds. The molybdenum and tungsten species are described in detail in the Results and Discussion section.

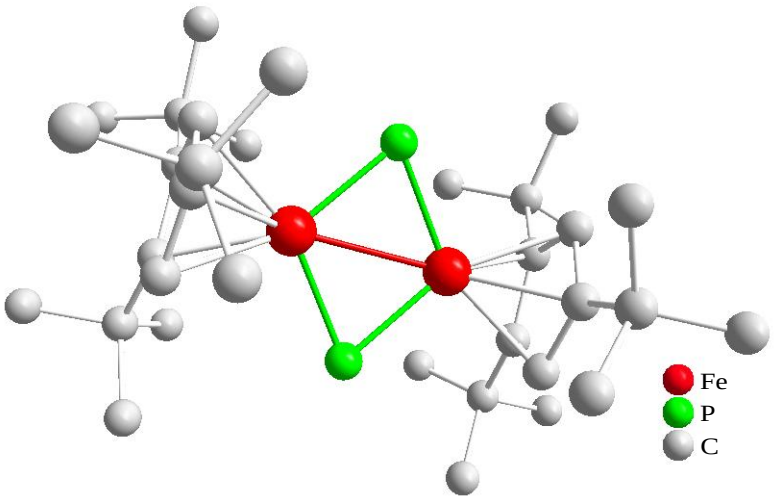

Figure 17. $(1,2,4\text{-}^tBu_3C_5H_2)Fe\mu\text{-}P_2Fe(1,2,4\text{-}^tBu_3C_5H_2)$, hydrogens omitted for clarity.[155]

Many reviews discussing complexes containing naked phosphorus atoms and the complexes' reaction abilities are published.[110, 156-159]

1.8. Research strategy

The chemistry presented in this thesis focuses on electron rich naked di- and triphosphorus-containing molybdenum and tungsten complexes and their reactivities toward selected group 10 and 11 metallic salts.[36-38, 79, 81, 151, 152, 160-173] The products are then characterized by single crystal X-ray diffraction, solid- and solution-state NMR (nuclear magnetic resonance), IR (infrared radiation), melting point, EA (elemental analysis), as well as EI-MS and ESI-MS (electron impact, electrospray ionization, mass spectrometry). The starting materials contain anywhere from 2–6 unsubstituted phosphorus atoms at the binding sites in the form of rings with the exception of the pure dimer. Inorganic two- and three-dimensional polymers are the most rewarding products obtained in these reactions, but the significant data obtained from clusters, dimers, and monomers offer valuable insight and are, many times, unprecedented. This strategy is not limited to phosphorus, however, the research conducted in this thesis is. Because of the usual lack of difference in shift between the ^1H, ^{13}C, and ^{31}P NMR of the reactants and products, ***every*** newly synthesized unknown compound presented in this thesis is accompanied by a solid-state projection generated from a single crystal X-ray measurement. For more examples involving arsenic- and sulfur- containing starting materials, the interested reader may wish to consider other articles.[174-176]

The greatest potential to produce polymers arises from the most phosphorus-rich complexes. Every naked phosphorus atom has the potential to datively bind to another metal and if multiple phosphors atoms are present then availability of binding sites is increased as well as the potential to bind in multiple instances to the same phosphorus containing ligand. Until this point only complexes containing four or greater phosphorus atoms in close proximity have shown the capacity of producing three-dimensional polymers (ie. spherical cages, and half cages) whereas, the research presented here; complexes with three and two phosphorus atoms have only produced linear polymers at best. The reactants for this research involve late transition metal carbonyls (ie. Cr, Mo, W), group 11 salts, and a new, successfully tested class of reactants involving ML_2Cl_2 (M = Pd and Pt) species. Other significant reactions exist that are beyond the scope of this research.

II. Results and Discussion

2.1. Reactants

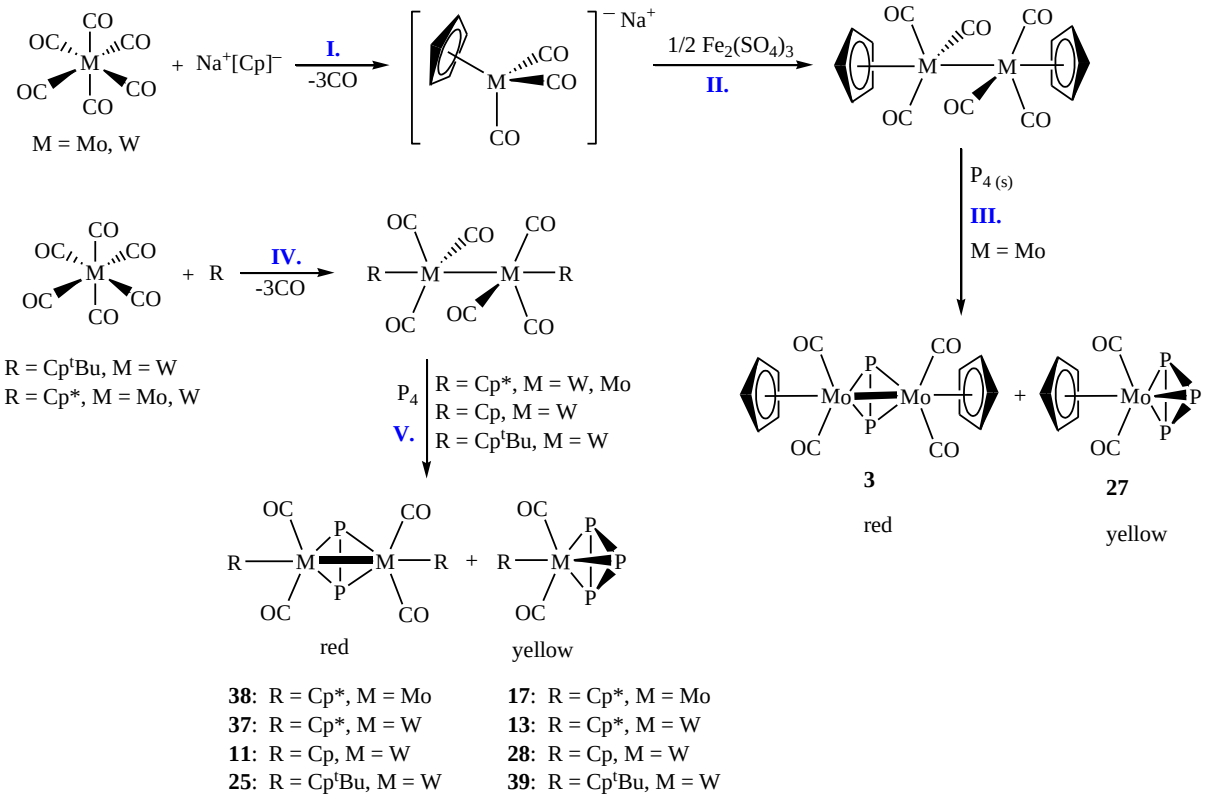

Scheme 1. **I.** Reflux for 40 min. in predried diglyme. **II.** A filtered solution of H_2O, acetic acid, and $Fe_2(SO_4)_3$ is added, and stirred approximately 15 minutes. Contents are filtered with a fritted filter and rinsed with H_2O, then cold methanol, and finally pentane. The material collected on the filter is dried under reduced pressure.[177] **III.** Refluxed in toluene for 24 h. Toluene is removed by reduced pressure. A small amount of SiO_2 and CH_2Cl_2 is used to soak up the product. This dust is then placed into a column (10" long) and flushed with a pentane/toluene gradient[178] solution. **IV.** For R = Cp^{t}Bu, M = W, Reflux 18h in decalin.[179] For R = Cp. Cp*; M = Mo,W, Reflux 50 h in xylene. **V.** Reflux 16 h in xylene; Reflux 16 h in decalin, for R = Cp^{t}Bu, M = W.[154]

The reactants used in this research contain 2 and 3 naked phosphorus atoms and are synthesized by different methods (Scheme 1). Complexes **3** and **27** are synthesized by the introduction of a cyclopentadienyl substituent to the featured hexacarbonyl followed by oxidation with $Fe_2(SO_4)_3$ and, finally, a treatment with white phosphorus. Even though the tungsten analog is capable of being produced though steps **I** and **II**, the final step **III** is not active enough to facilitate a reaction. Step **V** is, therefore, conducted in a solvent with a higher boiling point to achieve a successful reaction. Steps **I** and **II** are also possible for the introduction of Cp* to tungsten and molybdenum hexacarbonyl, but since the last step in the synthesis involves the treatment of white phosphorus in the presence of xylene, **IV** is more efficient rather than spending extra time for evacuation followed by a change in solvent. The method used for the preparation of **3** and **27** is new. Previous preparations used an indirect method.[136, 180]

2.2. Reactions with Group 10 Complexes and Tungstenpentacarbonyl

The planar hexagonal PtP_4Pt and PdP_4Pd motifs are unprecedented both by proposed and proven structures. The inherent configuration of this complex is the result of three reactants regardless of an initial cis, $(COD)PtCl_2$; cis and trans mixture, $Pt(SMe_2)_2Cl_2$; and trans $Pt(MeSPh)_2Cl_2$ configuration (Scheme 2). This phenomenon is also exhibited for the palladium analog. If the initial binding of the two species is trans, the possibility of forming a polymer could be realized by extending the array of repeating units. Previous examples of this have been synthesized using **3** and CuX (X = Cl, Br, I) species.[181] Any attempts to react these products further are foiled by the difficulty of producing tangible amounts of material and also the problem of solubility as the only workable solvent known is DMSO. Powder diffraction of amorphous precipitate from the reaction involving the trans platinum starting material showed no sign of polymer. The nickel analog was attempted using trans $NiCl_2(MeSPh)_2$ and crystallized using the same protocol. Repeated X-ray diffraction experimentation showed the crystal to be amorphous and immeasurable.

The synthesis of this compound is performed by layering a **3**/CH_2Cl_2 solution on a cold (0 °C) $PtCl_2L_X/CH_2Cl_2$ solution via cannula. The best results for both platinum (49.9% yield) and palladium (42.3% yield) analogs (Scheme 2) are obtained using the metal species with the defined sulfur bound ligands rather than the COD substituent, which often results in the formation of reduced platinum or palladium. The six membered ring unit is obtained regardless of the stoichiometric ratio used for the starting materials. It is also independent of the cis or trans configuration of the sulfur substituent of the platinum or palladium containing starting material. Single brown crystals are obtained for each of the platinum (**1**) and palladium (**2**) ring containing complexes.

Fluxional behavior, common in many Pt–P bound metallic complexes,[182-185] in solution or the solid-state is not detected, however, the freezing point of DMSO-d_6 (18.4 °C) does not allow NMR measurements at the low temperatures where this kind of activity is typically detected (about –110 °C). The solid-state X-ray structure is in agreement with the ^1H, ^{13}C, and ^{31}P NMR. The ^{31}P NMR (Figure 19) detects only one species in solution as well as the satellite peaks (approximating an AA'BB'X spin system) of the ^{195}Pt isomer (non, $^1J_{P',P''}$ = 253.2 Hz and $^1J_{P',Pt}$ = 2051.1 Hz; $^1J_{P'',P'}$ = 157.8 Hz and $^2J_{P'',Pt}$ = 1629.3 Hz). These coupling constants are in agreement with those reported in the literature for both J(P–P) and $J(^{195}Pt–P)$ bonds.[186-191]

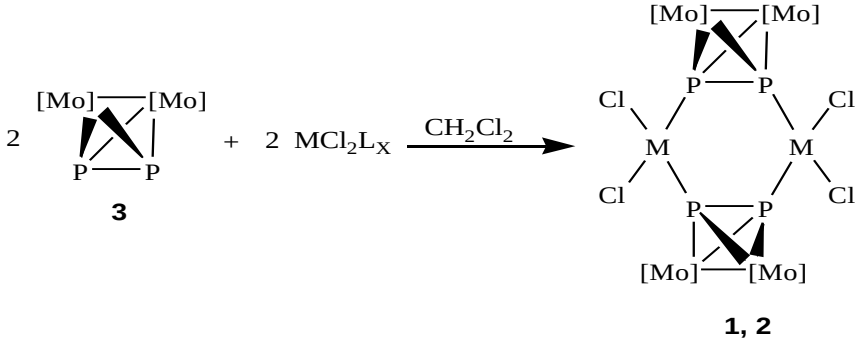

Scheme 2. Synthesis of **1** and **2**. MCl_2L_X = $(COD)PtCl_2$ (**4**, cis), $Pt(SMe_2)_2Cl_2$ (**5**, cis and trans mixture), $Pt(MeSPh)_2Cl_2$ (**6**, trans), $Pd(MeSPh)_2Cl_2$ (**7**, trans), and $Pd(SMe_2)_2Cl_2$ (**8**, cis and trans mixture). [Mo] = $MoCp(CO)_2$.

In the solid-state X-ray structure, the center $PtCl_2P_4PtCl_2$ motif is planar. The angle summation of the six membered Pt,P,P,Pt,P,P hexagonal ring deviates about 5° from the ideal 720° causing only a slight bend. Yet, the angle summation (360°) about the $PtCl_2P_2$ motif contributes no deviations from the plane. The Pt–P dative bond lengths (2.2241(18)–2.2405(20) Å; 2.2323 av.)[53, 182, 183, 192-199] are expected and are comparable to other examples in the literature. The Pd–P dative bonds are also comparable to those in the literature and are slightly constrained (0.1 Å) compared to those in the trans position.[200-205] The total angular summation of the six membered Pd,P,P,Pd,P,P ring is approximately 1.04° less than 720° contributing virtually no bending in the ring along with the angle summation about the $PdCl_2P_2$ motif (360°). Other comparisons of strictly datively bound Pt–P[206-210] and Pd–P[211-215] (Figure 18) reveal that the larger cone angles generally produce larger dative bonds by the influence of sterics. The average Pt–P (2.231(2) Å) and Pd–P (2.244(3) Å) are relatively small in comparison, however, the average Pd–Cl (2.343(4) Å) and Pt–Cl (2.347(2) Å) lengths do not deviate significantly. The P–P bond lengths remain very consistent in complexes **1** (2.078(3) and 2.074(2) Å) and **2** (2.076(5) Å) in comparision to the unbound starting material **3** (2.079(2) Å).

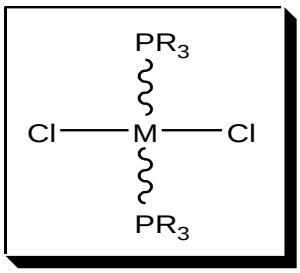

R	Pt–P	Pd–P	Pt–Cl	Pd–Cl
Cy	2.337(2)	2.363(1)	2.317(2)	2.301(1)
Ph	2.316(1)	2.337(1)	2.300(1)	2.290(1)
Ph_2CH_3	2.249(1)	2.265(2)	2.352(1)	2.341(2)
Et	2.263(2)	2.186(2)	2.369(2)	2.293(2)
Me	2.238(1)	2.258(2)	2.373(2)	2.369(3)

Figure 18. Motif used for the comparison of the average dative M–P and formal M–Cl bond lengths (Å). R (cone angle)[216] = Cy (170°), Ph (145°), Ph_2CH_3 (136°), Et (132°), Me (118°), M = Pt[206-210] and Pd.[211-215]

Both the platinum and palladium complexes (**1** and **2** respectively) possess an approximate D_{2h} symmetry down the middle when the $MoCp(CO)_2$ substituents are ignored. Complex **1** contains no center of inversion and in each of the four quadrants containing a cyclopentadienyl group, no pattern is noticed. Looking down the eclipse of the $PtCl_2P_4PtCl_2$ motif one sees that the both of the cyclopentadienyl groups on the upper and lower left quadrants protrude downward. The upper right protrudes upward and the lower right quadrant protrudes only slightly downward in comparison to the two on the right, however, all groups possess two carbonyl groups that are located in the opposite direction at an angle tetrahedral through the molybdenum center. Similarly, the palladium analog also possesses carbonyl groups pointed tetrahedrally in the opposite direction, but the orientation of the cyclopentadienyl groups is more ordered. Inspection across the analogous $PdCl_2P_4PdCl_2$ motif reveals that the upper and lower left quadrants protrude out of the plane by about the

same degree as the upper and lower right quadrants protrude into the plane. This contains an inversion center and thus, a higher degree of symmetry and is also apparent from the lack of deviation in the angular summation of the hexagonal (PdP_4Pd) ring and the square planar P_2PdCl_2 groups on either end. The two very close peaks in the IR spectrum of **1** show an antisymmetric (2014) and a symmetric (1977) stretch just as the IR spectrum of **2** exhibits one symmetric (1950) and one asymmetric (1908) peak.

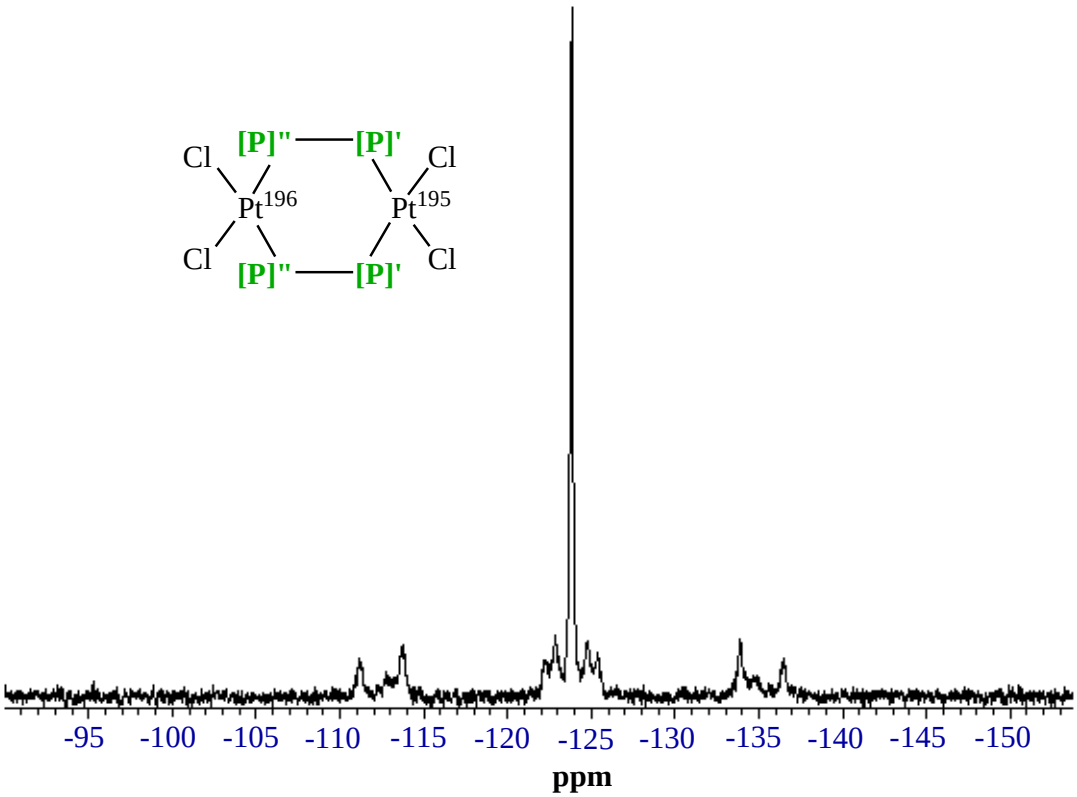

Figure 19. ^{31}P NMR spectrum of **1** with simplified isotope reference δ = –123.8 (non, $^{1}J_{P',P''}$ = 253.2 Hz and $^{1}J_{P',Pt}$ = 2051.1 Hz; $^{1}J_{P'',P'}$ = 157.8 Hz and $^{2}J_{P'',Pt}$ = 1629.3 Hz). $Mo(CO)_2Cp$ groups connected to the [P] are omitted for clarity.

The solid-state structure of the Pd analog is not in total agreement with the solution phase ^{31}P NMR. Of the three singlets reported, one is identified as **3** (–43.09 ppm) resulting from the decomposition of the datively bound phosphorus. The other two signals are significantly deshielded in comparison to the platinum analog, and given the relatively similar electronegativity of the two metals, it is thought that one or more equivalents of DMSO are asymmetrically bound to one or both of the palladium atoms in solution.

The electron impact mass spectrum (EI-MS) of **1** shows the presence of multiple species in an inert high voltage environment. The least abundant fragment is the uncoordinated $[PtCl_2]^+$ salt followed by the uncoordinated $[Cp_2Mo_2(CO)_4P_2]^+$ ligand. Progressive loss of carbonyl groups form the $[Cp_2Mo_2(CO)_2P_2]^+$ and the more abundant $[Cp_2Mo_2P_2]^+$ species, while an increase in carbonyl groups when bound to platinum(II)chloride form the more abundant $[Pt(CO)_2Cl_2]^+$ ion. The most abundant species detected is the $[Mo(CO)]^+$ ion formed from the decomposition of $[Cp_2Mo_2(CO)_4P_2]$.

The EI-MS of **2** also shows the presence of the same uncoordinated $[Cp_2Mo_2(CO)_4P_2]^+$ ligand and progressive loss of CO groups including the additional

presence of $[Cp_2Mo_2(CO)P_2]^+$. The most abundant species is the uncoordinated $[Mo(CO)]^+$ ion and it is accompanied by a greater variety of uncoordinated species ($[Pd(CO)Cl_2]^+$, $[Pd_2Cl_3]^+$, $[MoPd(CO)_2Cl_2]^+$, and $[Pd_2Cl_4]^+$) as it does with the platinum analog.

The positive ion electrospray mass spectrum (ESI-MS) reveals many species of **3** bound to $[Pd_X(CH_3CN)_X]^+$ followed by unbound species of $[Pd_X(CH_3CN)_X]^+$. Furthermore, the negative ESI-MS shows the presence of halide containing $[Pd_XCl_X(CH_3CN)_X]^-$ and $[Mo_XCl_X(CH_3CN)_X]^-$ species. These two experiments reveal the extreme binding affinity of palladium to nitrogen and show why electron impact is more suitable because it allows much smaller concentrations when performed in CH_2Cl_2. Unfortunately, no data can be collected from ESI-MS when **1** or **2** is dissolved in a pure CH_2Cl_2 solution.

Complementary syntheses involving the Cp* substituted Mo_2P_2* basal unit (**38**) was used in an attempt to produce analogous structures for species **1** and **2**. The obtained crystals were not of sufficient quality for diffraction and a known side product, $(CO)_2Cp^*Mo$-μ-H-μ-PH_2-$Mo(CO)_2Cp^*$, was obtained in the pursuit of the palladium analog. Further analysis by ESI-MS showed, however, one instance of an almost complete palladium complex, $[\{Cp^*_2Mo_2(CO)_2P_2\}_2PdCl_2]^+$.

Complex **10** is obtained by layering a **3**/THF solution with a solution of **9**/THF via cannula. Single maroon-brown crystals are obtained after the homogeneous solution is concentrated giving a product yield of 76%. The six membered ring complex of **10** is given regardless of the stoichiometric ratio of the starting materials. Complex **12** is obtained by an analogous procedure. Both **10** and **12** are somewhat soluable in THF and marginally soluable in CH_2Cl_2 but insoluable in CH_3CN, hexanes, and pentanes.

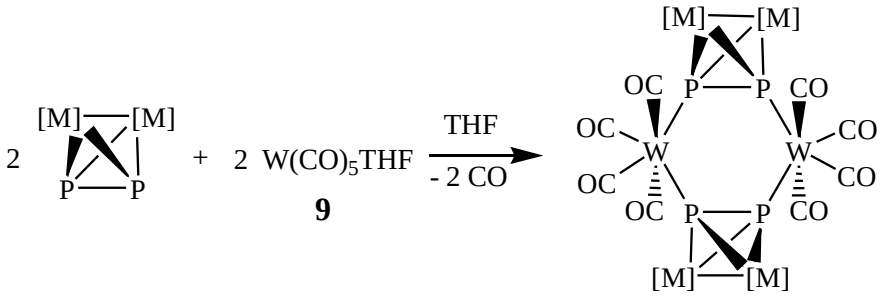

Scheme 3. Synthesis of **10** and **12**. [M] = $MoCp(CO)_2$ for **10** and $WCp(CO)_2$ for **12**.

The W,P,P,W,P,P ring solid-state structure of **10** is the second example in the literature,[217] however, it is the first example with a completely flat hexagonal (angle summation 720°) motif. The first example with a W,P,P,W,P,P ring contains a bent chair-like configuration and contains similar W–P (2.508(3) and 2.529(4) Å) and slightly longer P–P (2.130(5) Å) bond lengths. The two tungsten atoms on either side of the complex are square planar with respect to P1, P2, and the two equatorial CO ligands (angle summation 359.95°). This motif, along with the finely aligned axial and equatorial carbonyls, is almost perfectly octahedral. Further inspection along the flat plane of the six membered ring shows that the cyclopentadienyl groups in the upper left and right quadrants point into the plane whereas the lower left and right point out of the plane. In the absence of the $MoCp(CO)_2$ substituents the center of the molecule has an approximate D_{2h} symmetry.

The energy bands detected in the IR spectra (1944 cm^{-1} and 1983 cm^{-1}) are not in total agreement with the solid-state projection as four for the tungsten bound carbonyls and two for the diphos subunit (**3**) are expected. Nonetheless, the noticeable broadening of the detected peaks eludes that multiple bands have overlapping intensity. It is of interest to note that in the

positive ion EI-MS (CH_2Cl_2) spectrum, **10** is not detected. A sizable depletion of carbonyls ($[Cp_2Mo_2(CO)_{0-9}P_2W]^+$) with tungsten still bound continues on until even after the final W–P is severed. From this point stability is retained by binding to THF ($[Cp_2Mo_2(CO)_{3-4}P_2(THF)]^+$) after the loss of two more carbonyls. Following the loss of THF, several species of unbound $[Cp_2Mo_2(CO)_{0-4}P_2]^+$ are formed. The loss of carbonyl groups are rebound to molybdenum and tungsten in the form of $M(CO)_XTHF_X$.

Switching solvents (CH_2Cl_2/CH_3CN) for the positive ESI-MS affords larger species ($[Cp_{2-3}Mo_{2-4}(CO)_{4-12}P_{2-4}W_{1-2}]^+$), including the original complex **10**. The negative ion ESI-MS also shows steady patterns of larger complexes, $[Cp_4Mo_4P_4W(CO)_X]^-$ (X = 11, 9, 8) and $[Cp_2Mo_2P_4W(CO)_X]^-$ (X = 8, 9), retaining a P_4 subunit while exhibiting one rogue occasion of $[Cp_2Mo_2P_2W(CO)_{13}]^-$. The rest of the species present are simple tungsten and molybdenum carbonyls.

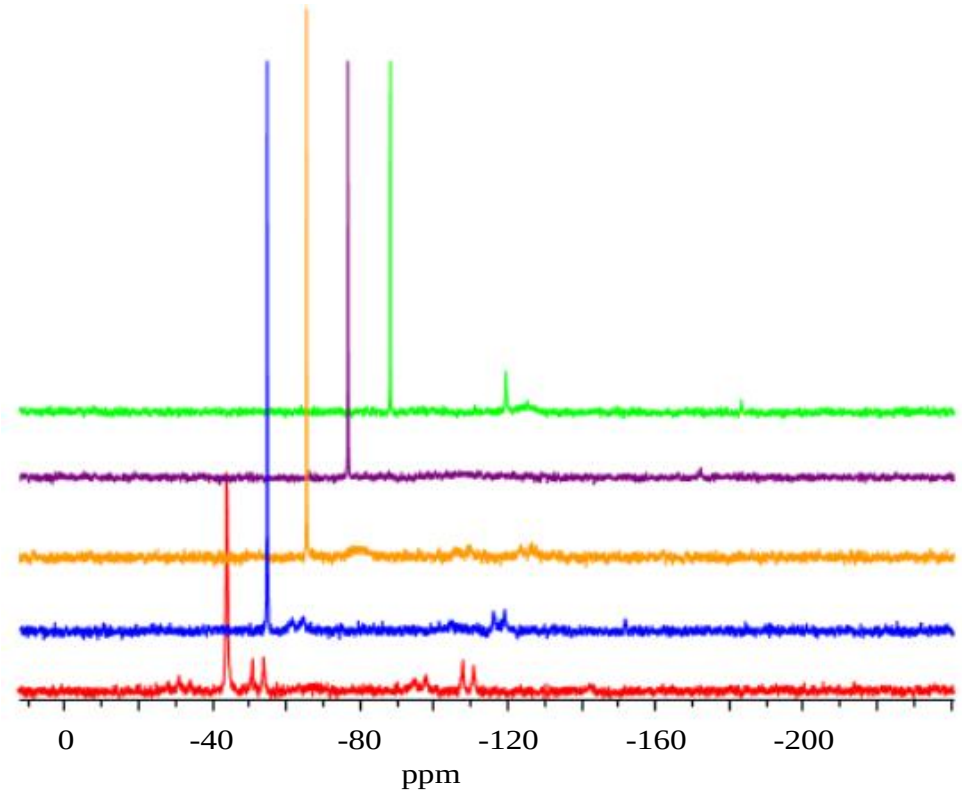

Figure 20. Variable temperature $^{31}P\{^1H\}$ NMR spectra of **10** in CD_2Cl_2/THF (3:1); From top to bottom: **27**, **0**, **–40**, **–80**, **–110** °C.

The dynamic behavior of **10** in a CD_2Cl_2/THF solution is detected from the variable temperature $^{31}P\{^1H\}$ NMR (Figure 20). When the temperature approaches –80 °C and continues to –110 °C two distinct doublets are produced representing the apparent binding of THF and subsequent separation of tungsten from the two phosphorus atoms (Scheme 4). The asymmetric environment is manifested by the two chemically inequivalent phosphorus atoms (–52.7 (d, P', $J_{P',P''}$ = 477.1 Hz), –109.5 (d, P'', $J_{P'',P'}$ = 477.1 Hz) @ –110 °C) and is in coexistence with the originally bound species.

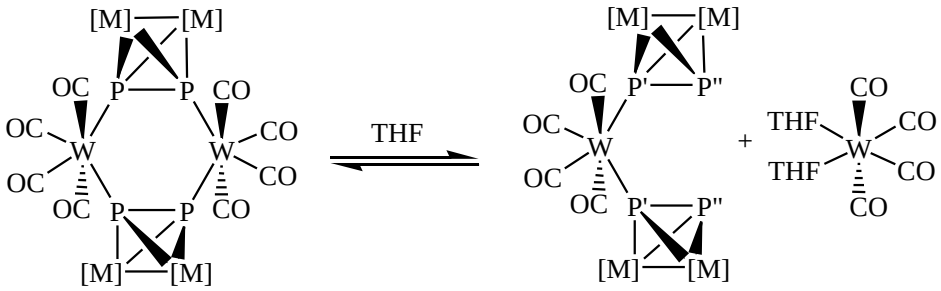

Scheme 4. Proposed equilibrium of **10** and **12** in a CD_2Cl_2/THF solution. [M] = $MoCp(CO)_2$ for **10** and $WCp(CO)_2$ for **12**.

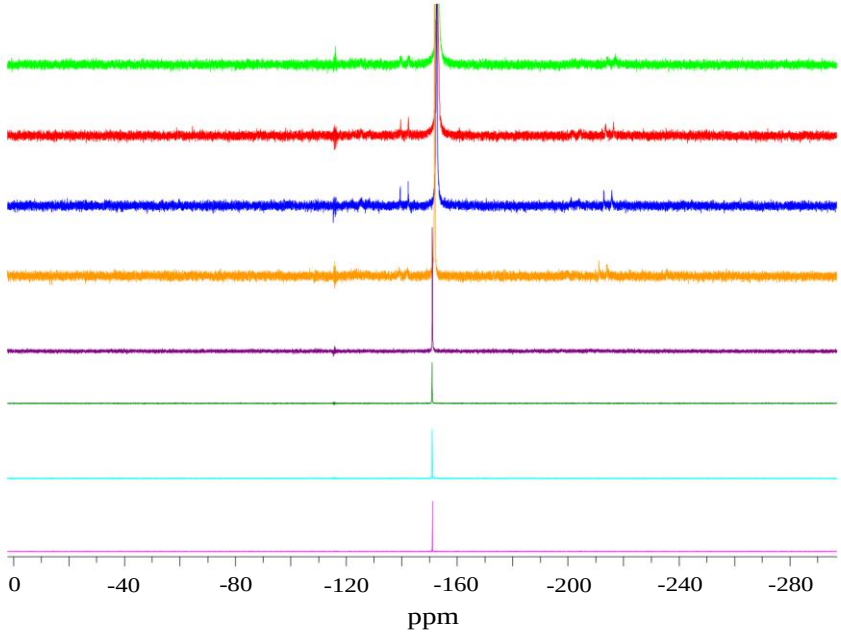

Figure 21. Variable temperature $^{31}P\{^1H\}$ NMR spectra of **12** in CD_2Cl_2/THF (3:1); From top to bottom: **–120**, **–110**, **–100**, **–80**, **–40**, **–20**, **0**, **27** °C.

The same is true of the dynamic behavior **12** in a CD_2Cl_2/THF solution. When the temperature approaches –80 °C and continues to –120 the variable temperature $^{31}P\{^1H\}$ NMR (Figure 21) displays two distinct doublets (–141.32 (d, P'', $J_{P'',P'}$ = 479.12 Hz), –153.11 (s), –215.62 (d, P', $J_{P',P''}$ = 479.12 Hz) @ –120 °C) representing the evident binding of THF and successive separation of tungsten from the two phosphorus atoms (Scheme 4). Complex **12** is synthesized by layering an **11**/THF with a solution of **9**/THF via cannula. Single maroon-brown crystals are obtained after the homogeneous solution is concentrated giving a product yield of 77.2%. The six membered ring complex of **12** is given regardless of the stoichiometric ratio of the starting materials.

The first noticeable similarity between the two analogs is the completely flat hexagonal (angle summation 720°) W,P,P,W,P,P structural pattern. In comparison with the first, which contains a bent chair-like configuration, **12** has similar W–P (2.508(3) and 2.529(4) Å) and shorter P–P (2.130(5) Å) bond lengths.[217] It should also be noted that the tungsten carbonyl configurations on either end are arranged in an octahedral structure. The orientation of the cyclopentadienyl groups are oriented in the exact same manner as those in

10, and the carbonyls located opposite and on the tungsten carbonyl subunits together emit two broad peaks in the IR spectrum. In the absence of the $WCp(CO)_2$ substituents the center of the molecule has an approximate D_{2h} symmetry. It is important to realize that even though all these similarities exist, the ^{31}P NMR detects severe differences in electron density around the phosphorus atoms of the two analogs regardless of temperature. In spite of the subtle differences in electronegativity between the tetrahedrally positioned tungsten and molybdenum, the phosphorus atoms in the tungsten analog (**12**) are significantly more shielded than the molybdenum complex (**10**). The same is true for the palladium (**2**) and platinum (**3**) complexes as the heavier platinum analog even though the electronegativity is practically equivalent and the metals are located in planar positions.

The positive ESI-MS for **12** contains many species of considerable molecular weight, none of which contains the original complex. Every group including W, P, Cp, and CO are subject to change in population in which the highest equivalence of phosphorus present is one equivalent. Variations of the starting material (**11**) with additions of carbonyl, tungsten, and phosphorus atoms are detected in the negative ESI-MS. No small fragments are identified, and THF or any other petty solvents are not used in the stabilization of any of the species.

Another plausible formation for complexes **1**, **2**, **10**, and **12** is thought to exist in the trans configuration forming either a monomer, dimer, or polymer (Figure 22). Inspection of the M–P bond reveals that it is may not be long enough to accommodate the steric bulk of the $MoCp(CO)_2$ configuration. Complexes **1** and **2** are bound in a square planar fashion and it is reasonable to believe that if they were bound in a trans configuration the preferred geometry around the metal center would also be square planar. While this argument could be biased for **10** and **12,** a previously reported structure involving datively bound phosphorus atoms to a $W(CO)_4$ subunit also confers that a six membered ring is more stable.[217] Yet, other somewhat analogous efforts in the literature show only a monosubstituted species.[218, 219]

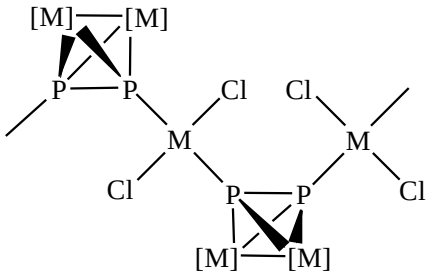

Figure 22. Explored trans possibility for **1**, **2**, **10**, and **12**. M = Pt, Pd, and W. X = Cl for **1** and **2**; and $(CO)_4$ for **10** and **12**. [M] = $MoCp(CO)_2$ for **1**, **2**, and **10**; and $WCp(CO)_2$ for **12**.

X-ray Data Collection for **1**. A light brown, thin plate having approximate dimensions of 0.109 x 0.043 x 0.013 mm, was mounted on an Oxford Diffraction Gemini Ultra diffractometer. All intensity measurements were performed using the omega scan method (λ = 1.5418 Å) with a graphite crystal incident beam monochrometer. Cell constants were obtained from a Full-matrix least-squares on F^2.

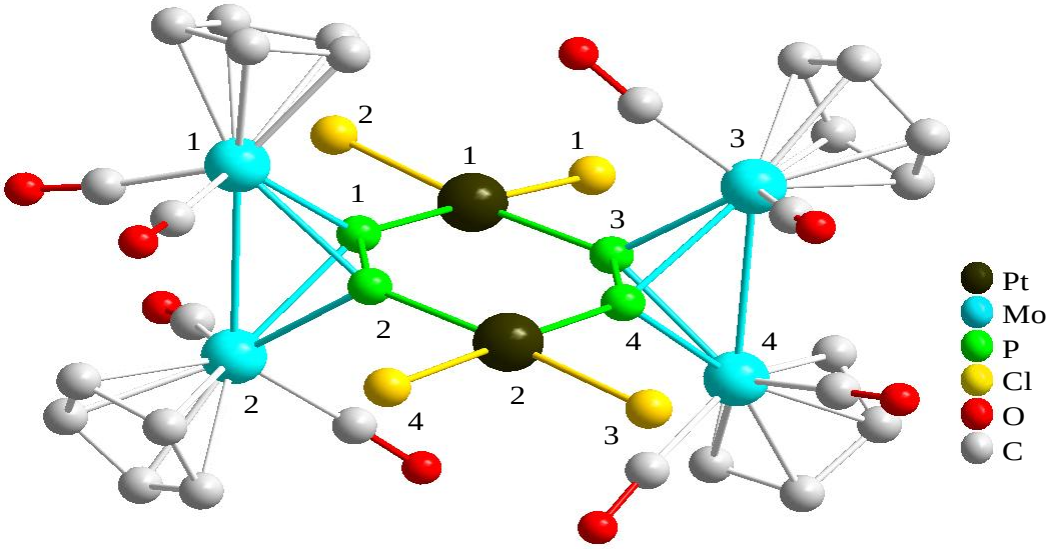

Figure 23. Solid-state projection of $C_{28}H_{20}Cl_4Mo_4O_8P_4Pt_2$ (**1**). Hydrogen atoms and CH_2Cl_2 are removed for clarity.

Table 3. Selected Bond Lengths (Å) and Angles (°) (**1**).

Pt(1)–Cl(1)	2.3471(18)	Pt(1)–Cl(2)	2.344(2)
Pt(1)–P(1)	2.2189(19)	Pt(1)–P(3)	2.2387(19)
Pt(2)–Cl(3)	2.352(2)	Pt(2)–Cl(4)	2.3457(18)
Pt(2)–P(2)	2.2406(19)	Pt(2)–P(4)	2.2241(18)
Mo(1)–P(1)	2.454(2)	Mo(1)–P(2)	2.502(2)
Mo(2)–P(1)	2.479(2)	Mo(2)–P(2)	2.474(2)
Mo(3)–P(3)	2.4703(19)	Mo(3)–P(4)	2.4808(19)
Mo(4)–P(3)	2.459(2)	Mo(4)–P(4)	2.488(2)
P(1)–P(2)	2.078(3)	P(3)–P(4)	2.074(2)

Cl(1)–Pt(1)–Cl(2)	91.40(7)	Cl(1)–Pt(1)–P(1)	177.47(8)
Cl(1)–Pt(1)–P(3)	86.55(6)	Cl(2)–Pt(1)–P(1)	88.97(7)
Cl(2)–Pt(1)–P(3)	174.92(7)	P(1)–Pt(1)–P(3)	93.28(7)
Cl(3)–Pt(2)–Cl(4)	90.86(7)	Cl(3)–Pt(2)–P(2)	176.66(7)
Cl(3)–Pt(2)–P(4)	88.81(7)	Cl(4)–Pt(2)–P(2)	87.45(7)
Cl(4)–Pt(2)–P(4)	178.63(8)	P(2)–Pt(2)–P(4)	92.81(7)
P(1)–Mo(1)–P(2)	49.57(6)	P(1)–Mo(2)–P(2)	49.60(6)
P(3)–Mo(3)–P(4)	49.54(6)	P(3)–Mo(4)–P(4)	49.58(6)
Pt(1)–P(1)–Mo(1)	142.28(9)	Pt(1)–P(1)–Mo(2)	135.59(9)
Pt(1)–P(1)–P(2)	135.41(10)	Mo(1)–P(1)–Mo(2)	78.22(6)
Mo(1)–P(1)–P(2)	66.40(8)	Mo(2)–P(1)–P(2)	65.07(7)
Pt(2)–P(2)–Mo(1)	149.07(9)	Pt(2)–P(2)–Mo(2)	131.93(9)
Pt(2)–P(2)–P(1)	131.23(10)	Mo(1)–P(2)–Mo(2)	77.43(6)
Mo(1)–P(2)–P(1)	64.03(8)	Mo(2)–P(2)–P(1)	65.33(7)
Pt(1)–P(3)–Mo(3)	134.18(9)	Pt(1)–P(3)–Mo(4)	145.63(9)
Pt(1)–P(3)–P(4)	130.92(10)	Mo(3)–P(3)–Mo(4)	78.38(6)
Mo(3)–P(3)–P(4)	65.50(7)	Mo(4)–P(3)–P(4)	65.94(8)

Pt(2)–P(4)–Mo(3)	142.40(9)	Pt(2)–P(4)–Mo(4)	136.73(9)
Pt(2)–P(4)–P(3)	135.44(10)	Mo(3)–P(4)–Mo(4)	77.64(6)
Mo(3)–P(4)–P(3)	64.97(7)	Mo(4)–P(4)–P(3)	64.48(8)

X-ray Data Collection for **2**. A light brown, thin plate having approximate dimensions of 0.130 x 0.030 x 0.010 mm, was mounted on an Oxford Diffraction Gemini Ultra diffractometer. All intensity measurements were performed using the omega scan method (λ = 0.71069 Å) with a graphite crystal incident beam monochrometer. Cell constants were obtained from a Full-matrix least-squares on F^2

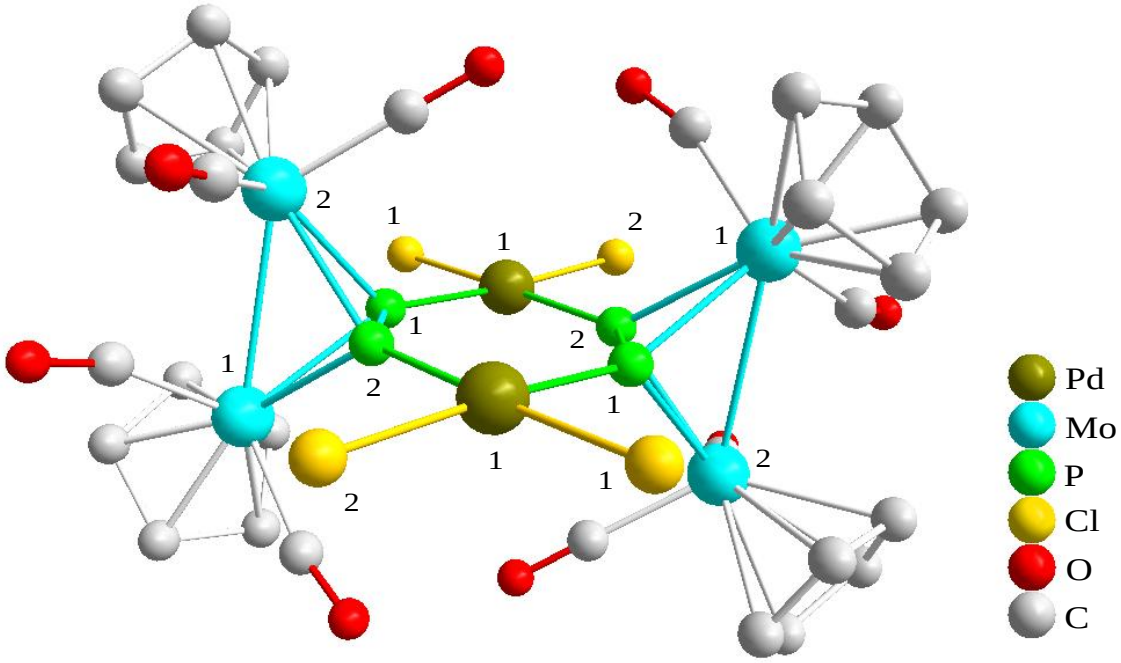

Figure 24. Solid-state projection of $C_{28}H_{20}Cl_4Mo_4O_8P_4Pd_2$ (**2**). Hydrogen atoms are removed for clarity.

Table 4. Selected Bond Lengths (Å) and Angles (°) (**2**).

Pd(1)–Cl(1)	2.3435(31)	Pd(1)–Cl(2)	2.3419(39)
Pd(1)–P(1)	2.2377(38)	Pd(1)–P(2)	2.2506(31)
Mo(1)–P(1)	2.4642(35)	Mo(1)–P(2)	2.4653(39)
Mo(2)–P(1)	2.4684(41)	Mo(2)–P(2)	2.4759(31)
P(1)–P(2)	2.0758(48)		

Cl(1)–Pd(1)–Cl(2)	93.647(135)	Cl(1)–Pd(1)–P(1)	87.935(126)
Cl(1)–Pd(1)–P(2)	175.919(131)	Cl(2)–Pd(1)–P(1)	178.273(131)
Cl(2)–Pd(1)–P(2)	86.236(186)	P(1)–Pd(1)–P(2)	92.236(130)
P(1)–Mo(1)–P(2)	49.808(121)	Pd(1)–P(1)–Mo(1)	138.934(163)
Pd(1)–P(1)–Mo(2)	132.027(160)	Pd(1)–P(1)–P(2)	136.031(201)
Mo(1)–P(1)–Mo(2)	78.313(104)	Mo(1)–P(1)–P(2)	65.126(142)

Mo(2)–P(1)–P(2)	65.362(133)	Mo(1)–P(2)–Mo(2)	78.150(105)
Mo(1)–P(2)–P(1)	65.066(146)	Pd(1)–P(2)–Mo(1)	132.036(168)
Mo(2)–P(2)–P(1)	64.989(131)	Pd(1)–P(2)–Mo(2)	148.126(160)
Pd(1)–P(2)–P(1)	131.213(199)		

X-ray Data Collection for **10**. A brown-black, prism having approximate dimensions of 0.120 x 0.120 x 0.110 mm, was mounted on an Oxford Diffraction Gemini Ultra diffractometer. All intensity measurements were performed using the omega scan method (λ = 1.5418 Å) with a graphite crystal incident beam monochrometer. Cell constants were obtained from a Full-matrix least-squares on F^2.

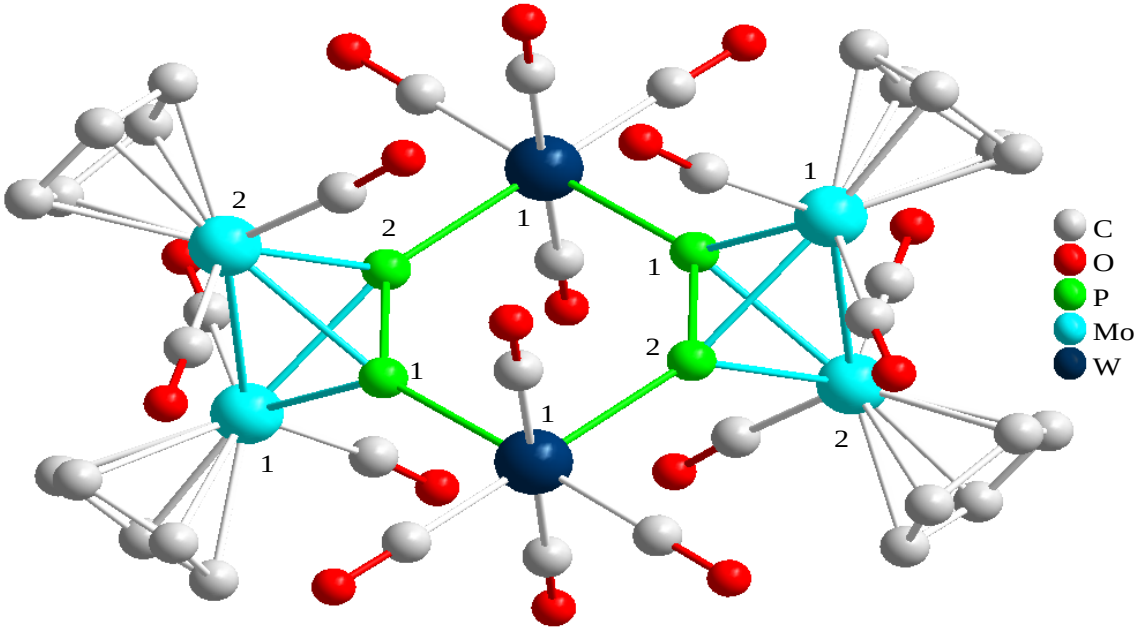

Figure 25. Solid-state projection of $C_{36}H_{20}Mo_4O_{16}P_4W_2(C_4H_8O)_2$ (**10**). Hydrogen atoms and C_4H_8O are removed for clarity.

Table 5. Selected Bond Lengths (Å) and Angles (°) (**10**).

W(1)–P(1)	2.5053(13)	W(1)–P(2)	2.5112(13)
Mo(1)–P(1)	2.4405(13)	Mo(1)–P(2)	2.5462(13)
Mo(2)–P(1)	2.5472(13)	Mo(2)–P(2)	2.4455(12)
P(1)–P(2)	2.0776(18)		

P(1)–W(1)–P(2)	89.30(4)	P(1)–Mo(1)–P(2)	49.19(4)
P(1)–Mo(2)–P(2)	49.13(4)	W(1)–P(1)–Mo(1)	140.18(5)
W(1)–P(1)–Mo(2)	140.84(5)	W(1)–P(1)–P(2)	135.70(7)
Mo(1)–P(1)–Mo(2)	74.39(4)	Mo(1)–P(1)–P(2)	68.06(5)
Mo(2)–P(1)–P(2)	62.88(5)	W(1)–P(2)–Mo(1)	143.68(5)
W(1)–P(2)–Mo(2)	137.99(5)	W(1)–P(2)–P(1)	135.00(7)
Mo(1)–P(2)–Mo(2)	74.33(4)	Mo(1)–P(2)–P(1)	62.76(5)

Mo(2)–P(2)–P(1)	67.99(5)

X-ray Data Collection for **12**. A red, prism having approximate dimensions of 0.062 x 0.056 x 0.054 mm, was mounted on an Oxford Diffraction Gemini Ultra diffractometer. All intensity measurements were performed using the omega scan method (λ = 0.71073 Å) with a graphite crystal incident beam monochrometer. Cell constants were obtained from a Full-matrix least-squares on F^2.

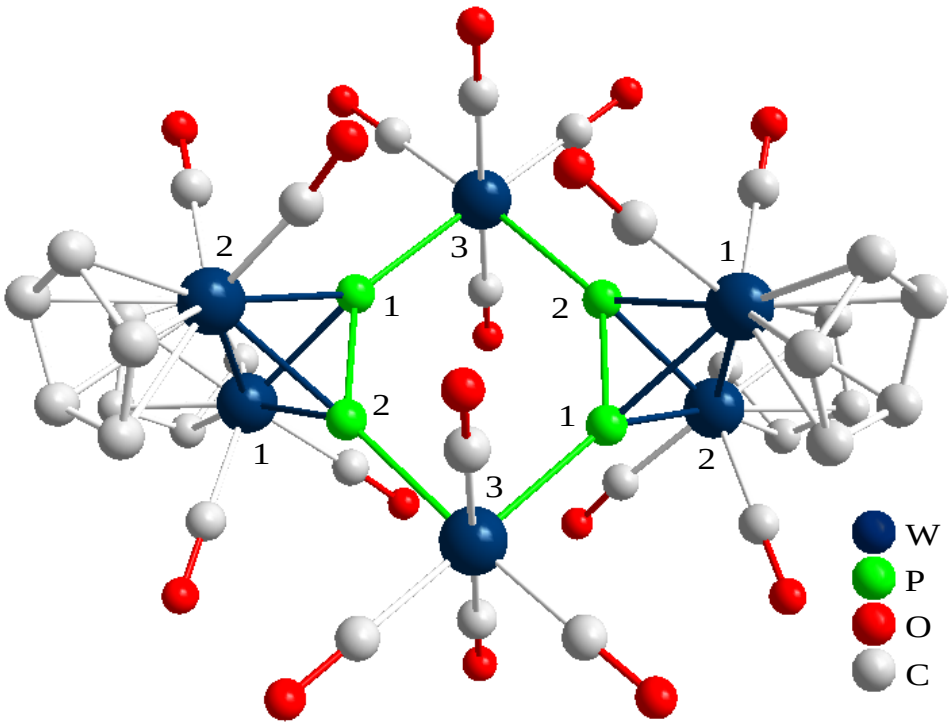

Figure 26. Solid-state projection of $C_{36}H_{20}O_{16}P_4W_6$ (**12**). Hydrogen atoms and C_4H_8O are removed for clarity.

Table 6. Selected Bond Lengths (Å) and Angles (°) (**12**).

W(3)–P(2)	2.5110(8)	W(3)–P(1)	2.5151(8)
W(2)–P(2)	2.4437(9)	W(2)–P(1)	2.5523(9)
W(1)–P(2)	2.5516(8)	W(1)–P(1)	2.4504(9)
P(1)–P(2)	2.0945(11)		

P(2)–W(3)–P(1)	89.76(3)	P(2)–W(2)–P(1)	49.51(3)
P(2)–W(1)–P(1)	49.46(2)	W(3)–P(2)–W(2)	140.32(3)
W(3)–P(2)–W(1)	141.15(3)	W(3)–P(2)–P(1)	135.41(5)
W(2)–P(2)–W(1)	74.19(2)	W(2)–P(2)–P(1)	67.94(3)
W(1)–P(2)–P(1)	62.75(3)	W(3)–P(1)–W(2)	144.05(4)
W(3)–P(1)–W(1)	138.09(3)	W(3)–P(1)–P(2)	134.82(5)
W(2)–P(1)–W(1)	74.06(2)	W(2)–P(1)–P(2)	62.55(3)
W(1)–P(1)–P(2)	67.79(3)		

2.3. Reactions with Group 11 Salts

Inorganic polymers have always been a fascinating field. Recently, multidimensional polymers and fullerene-type structures, derived from delocalized electron-rich phosphorus-bound metal substrates have attracted much attention.[181, 220-227] Still, there is no denying that this field is in its infancy. Although examples in the literature show it is possible for bidentate phosphorus ligands to simultaneously bind to the copper atom of a Cu_2X_2 (X = Cl[228-236], Br[231, 235-238], I[168, 231, 235, 237, 239-243]) square motif, none of these include any triphosphorus species. It is thus, in the author's interest to pursue exploration into these complexes. Previously performed research has shown that reactions with similar electron rich motifs have the potential of forming polymeric species.[172] If the initial binding of the two species is trans, the possibility of forming a polymer could be realized by extending the array of repeating units. These complexes, along with the featured species, can only realistically be characterized if a solid-state projection is obtained from single crystal X-ray diffraction.

2.3.1. Dimers Synthesized From a Triphosphanotungsten and CuX (X = Cl, Br, I)

The syntheses of complexes **14**–**16** (Scheme 5) are performed by carefully layering a solution of CuX/CH_3CN (X = Cl, Br, I) over a solution of **13**/CH_2Cl_2 with a cannula in a 2:1 ratio and placing the solution in a dark environment for two days at room temperature. The contents are then filtered with a fritted filter, layered with pentane, and cooled to 5 °C to give yellow crystals. The yield of **14** is somewhat lower due to the formation of a dark brown byproduct (**21**) that contains no traces of phosphorus. The product is separated by fractional crystallization. Likewise, the syntheses of the analogous molybdenum containing complexes **18**–**20** are similar in almost every aspect other than crystallization and, of course, a **17**/CH_2Cl_2 solution is used as the reactant.[180] All crystals of complexes **18**–**20** are obtained by slow depolarization of the solution by gentle layering with ether while only **18** and **20** are crystallized at a lower temperature (–28 °C). Complexes **18**–**20** are only slightly soluable in CH_3CN, CH_2Cl_2, and THF, but they are insoluble in hexanes and pentane.

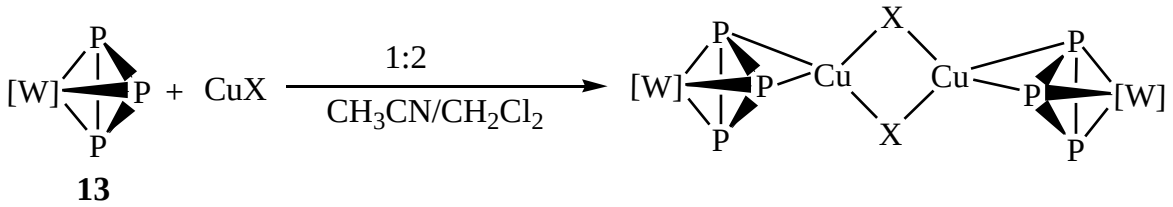

13

Scheme 5. Synthesis of **14**–**16**. X = Cl, Br, I. [W] = $W(CO)_2Cp^*$. Analogous reactions are also performed **18**–**20**. X = Cl, Br, I. [Mo] = $Mo(CO)_2Cp^*$. The complexes are isostructural with the exception of **20**; **20** is a polymer.

Complex **13** is synthesized by a known reaction,[244] however, it is not previously characterized by single crystal solid-state diffraction. The solid-state projection (Figure 27) shows tungsten bound by two carbonyl groups, pentamethylcyclopentadienyl, and the electron rich cyclotriphosphorus.

X-ray Data Collection for **13**. A yellow, thin plate having approximate dimensions of 0.060 x 0.060 x 0.030 mm, was mounted on an Oxford Diffraction Gemini Ultra diffractometer. All intensity measurements were performed using the omega scan method (λ = 1.54184 Å) with a graphite crystal incident beam monochrometer. Cell constants were obtained from a Full-matrix least-squares on F^2.

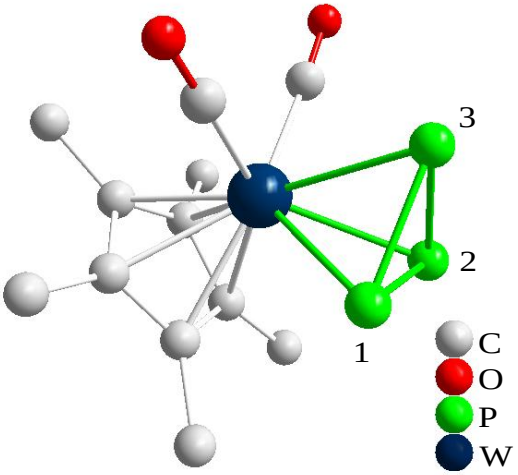

Figure 27. Solid-state projection of $C_{12}H_{15}O_2P_3W$ (**13**). Hydrogen atoms are removed for clarity. Selected bond lengths (Å): P1–P2 2.1558(1), P1–P3 2.1378(1), P2–P3 2.1831(0)

Complexes **14**–**16** possess carbonyl and pentamethylcyclopentadienyl substituents oriented in opposite directions just as in the original starting material. Each have approximately C_{2h} symmetry and contain a perfectly planar Cu_2X_2 rhombus (X = Cl, Br, I) configuration (angle summation of 360°). In comparison to the starting material (**13**, 2.183(9) Å), the P1–P2 bond lengths of the CuCl (**14**, 2.283(3) Å), CuBr (**15**, 2.2785(15) Å), and the CuI (**16**, 2.2717(16) Å) containing complexes are significantly longer (~0.1 Å) due to the slight weakening of the bond caused by the Cu^+ ion. The elongation (~0.1 Å) is also present in complexes **18** (CuCl analog, 2.2908(9) Å) and **19** (CuBr analog, 2.2785(9) Å) relative to their starting material (2.1703(8) Å). This elongation consequently causes a P1–P3–P2 bond angle increase (~3°) while the other phosphorus-phosphorus (P1–P3 and P2–P3) bond lengths remain consistent. The tungsten-carbonyl and molybdenum-carbonyl angles are also increased (~3–4° for **14**–**16** and ~2–4° for **18**–**20**) in comparison to the starting material, but the tungsten-carbon and molybdenum-carbon bond lengths associated with the pentamethylcyclopentadienyl group (C3–C7) remain constant. Each of the Cu_2X_2 rings contain an average CuX bond length that is elongated as the halide increases in atomic number (**14**, Cl = 2.305(2); **15**, Br = 2.431(1); **16,** I = 2.585(1); **18**, Cl = 2.328(1); **19**, Br = 2.436(1); **20**, I = 2.620(3) Å). The elongations for **14**–**16** (Cl to Br = 5.5%, Br to I = 6.4%) are more proportional to the increase in van der Waals radii (Cl to Br = 5.7%, Br to I = 7.0%) than the elongations for **18**–**20** (Cl to Br = 4.6%, Br to I = 7.5%). As one would expect, the distance between the copper atoms actually decreases when one compares the chloride containing analogs with the bromine containing species (**14** and **15**, –0.044 Å; **18** and **19**, –0.404 Å). The same pattern also exists for the bromine to iodine containing species (**15** and **16**, –0.026; **19** and **20**, –0.211 Å).

Previously synthesized molybdenum-arsenic complexes are the most similarly known analogs other than the ones presented in this thesis. Molybdenum-arsenic analogs for each of the three copper halide species (Cl, Br, and I) also show instances of elongation by the complimentary As1–As2 bonds.[245] Yet, these complexes demonstrate an intermolecular Cu···As binding mode which is not present in complexes **14**–**16**. It should be emphasized that even thou similarities exist, none of the analogous reactants presented and cited react analogously; proving this is extremely difficult without a solid-state projection.

X-ray Data Collection for **14**. A light yellow, flat prism having approximate dimensions of 0.17 x 0.09 x 0.03 mm, was mounted on an Oxford Diffraction Gemini Ultra diffractometer. All intensity measurements were performed using the omega scan method (λ = 1.54184 Å) with a graphite crystal incident beam monochrometer. Cell constants were obtained from a Full-matrix least-squares on F^2.

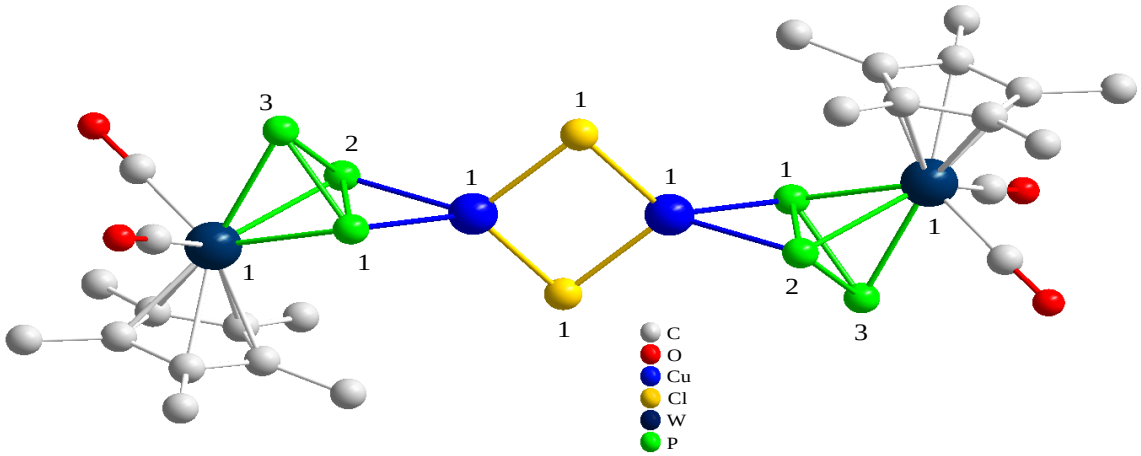

Figure 28. Solid-state projection of $C_{24}H_{30}Cl_2Cu_2O_4P_6W_2$ (**14**). Hydrogen atoms are removed for clarity.

X-ray Data Collection for **15**. A yellow, plate having approximate dimensions of 0.160 x 0.150 x 0.060 mm, was mounted on an Oxford Diffraction Gemini Ultra diffractometer. All intensity measurements were performed using the omega scan method (λ = 1.54184 Å) with a graphite crystal incident beam monochrometer. Cell constants were obtained from a Full-matrix least-squares on F^2.

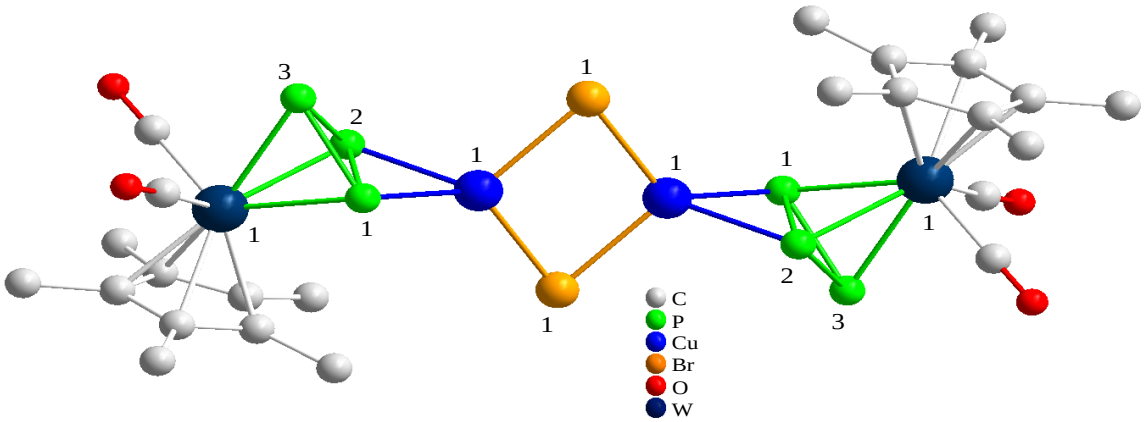

Figure 29. Solid-state projection of $C_{24}H_{30}Br_2Cu_2O_4P_6W_2$ (**15**). Hydrogen atoms are removed for clarity.

X-ray Data Collection for **16**. A yellow, flat prism having approximate dimensions of 0.160 x 0.150 x 0.080 mm, was mounted on an Oxford Diffraction Gemini Ultra diffractometer. All intensity measurements were performed using the omega scan method (λ = 0.71073 Å) with a graphite crystal incident beam monochrometer. Cell constants were obtained from a Full-matrix least-squares on F^2.

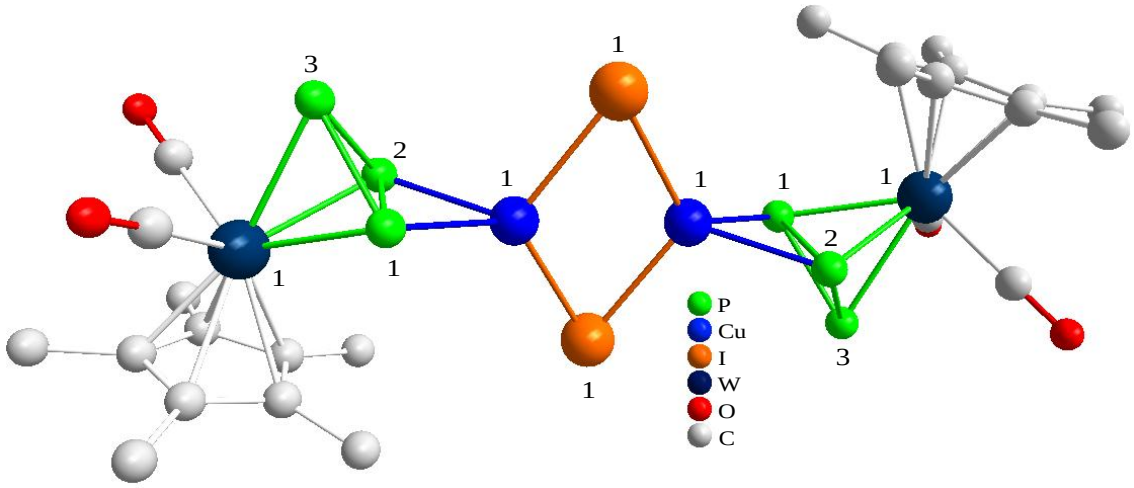

Figure 30. Solid-state projection of $C_{24}H_{30}Cu_2I_2O_4P_6W_2$ (**16**). Hydrogen atoms are removed for clarity.

Table 7. Selected bond lengths (Å) and angles (°) of compounds **13**–**16**.

	13	**14**	**15**	**16**
Cu(1)–X(1)		2.267(2)	2.3989(8)	2.5547(6)
Cu(1)–P(1)		2.312(2)	2.2998(13)	2.3522(12)
Cu(1)–P(2)		2.280(2)	2.3178(12)	2.3531(12)
Cu(1)–X(1)'		2.343(2)	2.4631(8)	2.6157(6)
P(1)–P(2)	2.183(9)	2.283(3)	2.2785(15)	2.2717(16)
P(1)–P(3)	2.137(10)	2.154(3)	2.1454(16)	2.1554(17)
P(2)–P(3)	2.156(10)	2.145(3)	2.1551(15)	2.1487(15)
X(1)–Cu(1)–P(1)		131.91(8)	125.21(4)	124.90(4)
X(1)–Cu(1)–P(2)		127.59(9)	131.07(4)	126.51(3)
X(1)–Cu(1)–X(1)'		97.14(7)	103.62(3)	114.28(2)
P(1)–Cu(1)–P(2)		59.61(7)	59.13(4)	57.74(4)
X(1)'–Cu(1)–P(1)		117.80(8)	120.64(4)	112.95(3)
X(1)'–Cu(1)–P(2)		122.67(8)	113.07(4)	108.62(3)
Cu(1)–X(1)–Cu(1)'		82.86(7)	76.38(3)	65.72(2)
Cu(1)–P(2)–P(1)		60.90(7)	60.04(4)	61.11(4)
Cu(1)–P(2)–P(3)		104.49(10)	104.06(5)	104.14(5)
P(2)–P(1)–P(3)	59.9(3)	57.73(9)	58.21(5)	58.00(5)
P(1)–P(2)–P(3)	59.0(3)	58.13(8)	57.80(5)	58.29(5)
P(1)–P(3)–P(2)	61.1(3)	64.14(9)	63.99(5)	63.71(5)

The formation of the polymer (**20**) is indeed fascinating! Considering the two analogous systems, evidence suggesting that the electronegativity difference of molybdenum (Pauling = 2.16) and tungsten (Pauling = 2.36) affect the configuration. The greater amount of electron density around the phosphorus atoms of the molybdenum analog allows this species to host two singlely bound copper atoms instead of one copper atom bound to two different phosphorus atoms on the same cyclotriphosphorus subunit. This added electron density, thus, increases the average length of the Cu–X bonds found in the molybdenum containing analogs (**14** and **18** = 0.024 Å, **15** and **19** = 0.005 Å, **16** and **20** = 0.0343 Å), which is advantageous in accommodating the steric bulk of the Cp* substituents. More importantly, this occurs with the least electronegative halide (iodine), which greatly reduces copper's relative electron deficient behavior.

The solid-state projections of complexes **14**–**16** are not in total agreement with the NMR spectra. A single peak is present in the ^{31}P NMR spectrum at room temperature, which means that the electron density of the phosphorus atoms is delocalized and resonates at a faster rate than the radio frequency pulse of the spectrometer. At lower temperatures this resonance slows. It is detectable and attributable to a change in the dative bond configuration between the copper and the phosphorus atoms. One bonded or two simultaneously bonded phosphorus atoms would create two separate peaks in the ^{31}P NMR spectrum.

The ^{31}P MAS-NMRs for **14**–**16** (Figure 34) are in agreement with the low temperature ^{31}P NMR in the case that two peaks are shown representing the bound and unbound phosphorus atoms. In contrast, the phosphorus atom peaks demonstrate a gradual deshielding as the halide is increased in atomic number. This is caused from the increased phosphorus-halide distance (as the atomic number of the halide increases) from which proximal electron

density from the lone pairs originates. Even though shouldered peaks are noticed for **15** and **16**, the integration of the two major peaks is 2:1 for the bound and unbound phosphorus atoms, respectively, just as in the spectrum for **14**. One source of subtle differences in chemical environments is the distance between the phosphorus atoms and the carbonyl groups. The two affected complexes (**15** and **16)** both have significant differences in their average P–O (0.0874 Å) and P–C (0.0623 Å) bond lengths that are surprisingly the same for both complexes. These averages (P–O, 0.05185 Å and P–C, 0.04275 Å) are not so different for **14** so any shouldering is not detected and the peak is only slightly broadened. The bound P1 and P2 phosphorus atoms are significantly more shielded than the unbound P3 (~107 ppm) for complexes **14**–**16**. This shows that even though the bond length is increased (~0.1 Å) it is not an electronegative effect induced by the copper. The P1 and P2 phosphorus atoms have, in fact, more electron density and the bond is elongated because of the strain of the copper bonding orbitals.

Very small instances of shouldering are noticed in the ^{65}Cu MAS-NMR for **14**–**16** (Figure 35) from minute occurrences of chemical inequality, however, given the symmetry of the X-ray projection the only source could be the arrangement of atoms given in the crystal packing of neighboring unit cells. While complexes **14** and **16** are consistent with each other a large upfield shift (~50 ppm) is noticed for **15**.

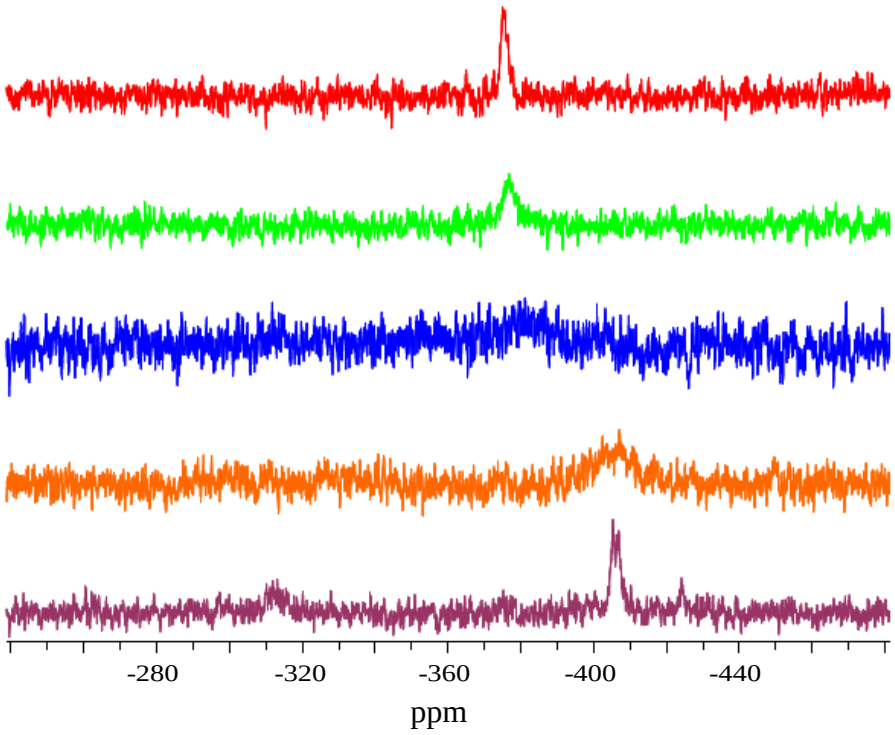

Figure 31. Variable temperature $^{31}P\{^{1}H\}$ NMR spectra of **14** in THF-d_8/CH_2Cl_2 (2:1); From top to bottom: **27**, **0**, **–40**, **–80**, **–120** °C. **–120** °C, δ = –313.2 (b), –407.0 (b).

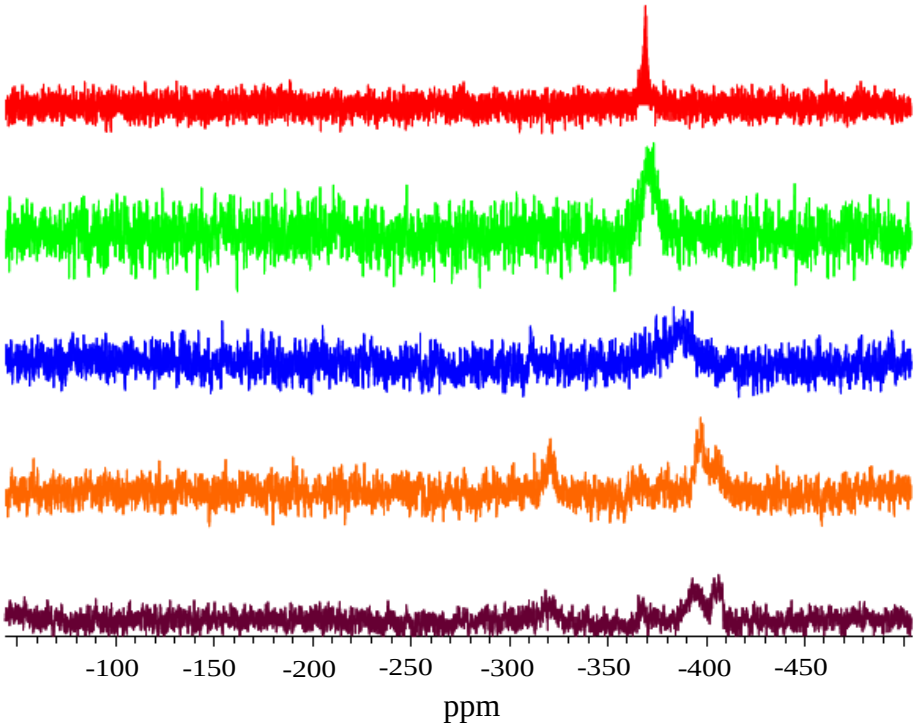

Figure 32. Variable temperature $^{31}P\{^{1}H\}$ NMR spectra of **15** in THF-d_8/CH_2Cl_2 (2:1); From top to bottom: **27**, **0**, **–40**, **–80**, **–120** °C. **–120** °C, δ = –318.4 (b), –393.2 (b), –406.3 (b).

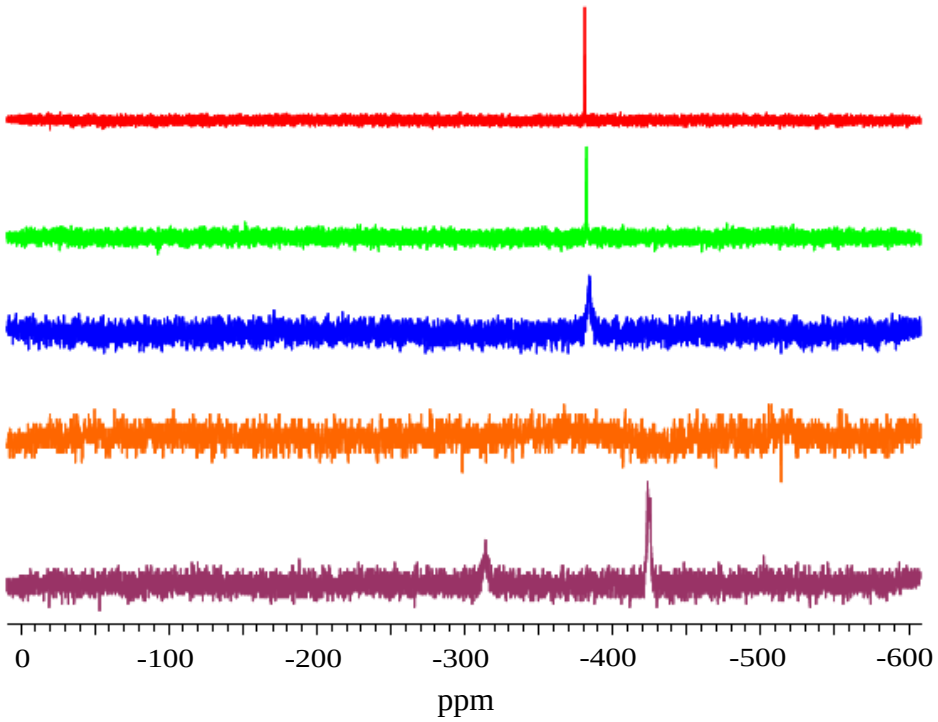

Figure 33. Variable temperature $^{31}P\{^{1}H\}$ NMR spectra of **16** in THF-d_8/CH_2Cl_2 (2:1); From top to bottom: **27**, **0**, **–40**, **–80**, **–120** °C. **–120** °C, δ = –314.1 (b), –423.7 (b).

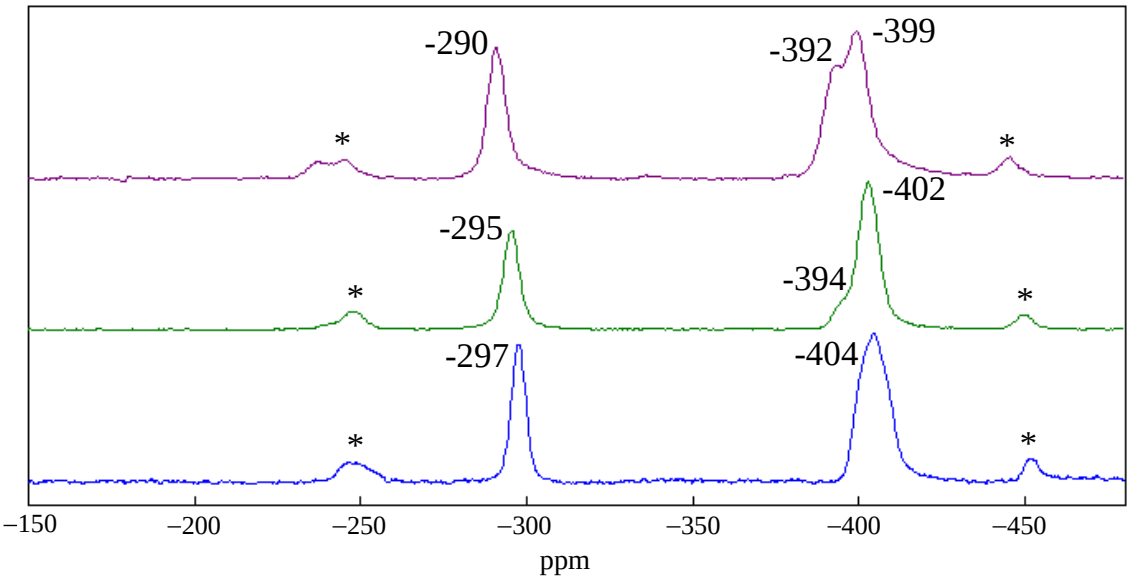

Figure 34. ^{31}P MAS-NMR spectra for **14**–**16** (202.405 MHz, spinning frequency 25 kHz, RT): **16** (violet), **15** (green), and **14** (blue). The asterisks mark the sidebands.

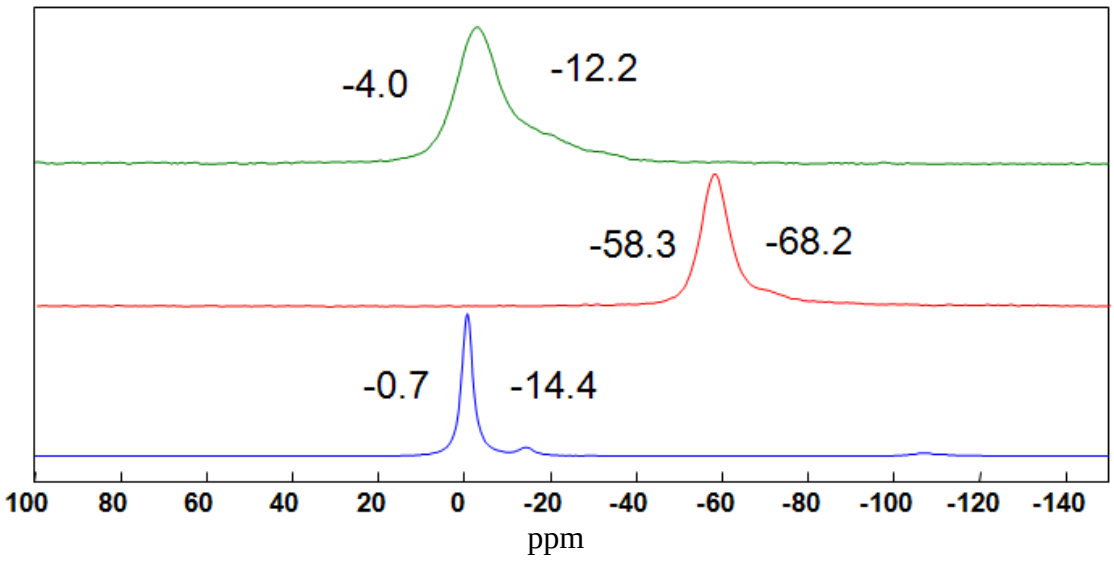

Figure 35. ^{65}Cu MAS-NMR spectra for **14**–**16** (142.105 MHz, spinning frequency 25 kHz, RT): **16** (green), **15** (red), and **14** (blue).

The positive ion electrospray mass spectrum (ESI-MS) for **14** reveals many species of **13** bound to a multiple array of copper chloride, acetonitrile, and ammonium species. Deviations of this pattern include the most abundant species of $[Cu_{X+1}Cl_X(CH_3CN)_2]^+$ (X = 1,2) and one instance of CuCl bound to **13** with a loss of one CO group to form $[CuClCp^*W(CO)P_3]^+$. Furthermore, the negative ESI-MS shows the presence of only copper halides in the form $[Cu_XCl_{X+1}]^-$ (X = 1–7).

The positive ESI-MS for the bromide analog (**15**) also shows instances where **13** is bound to a variety of ammonium, copperbromide, ethylhydroxyl, and acetonitrile species. Other species involving **13** without the cyclotriphosphorus group are bound to all the

previously mentioned species with the exception of the ethylhydroxyl group. The most significant observation is that the intact **15** is detected and bound to Cu^{+} in one case and $[Cu(CuCH_3CO)_2]^{+}$ in the other. Every signal, except for one (exception, $CuBr_2^{-}$), in the negative ESI-MS contains complex **13** in combination with ammonium, copperbromide, and ethylhydroxyl groups.

Of the tungsten containing complexes **14**–**16**, **16** is the most susceptible to dissociation when passed through a high potential electrical field. The positive and negative ESI-MS show no detection of **16** or **13**. The largest fragment seen is **13** without the cyclotriphosphorus substituent. All other species are miscellaneous combinations of ammonium, copperiodide, ethylhydroxyl, and acetonitrile.

While a steady increase in thermal decomposition temperature is noticed from the melting points of complexes **14**–**16** (**14** = 95–97, **15** = 96–100, **16** = 153), complexes **18**–**20** (**18** = 167, **19** = 153, **20** = 180–187) show a slight deviation for the bromine analog. Nevertheless, in accordance with their solid-state structures, two carbonyl signals are recorded in the IR spectra for all the species.

2.3.2. Phosphorus Free Negatively Charged Polymer

Never before has this means of synthesis produced a polymer absent of phosphorus, let alone a negatively charged one. What is really remarkable is that the featured polymer is the first and only example to the contrary. In sharp contrast to the vast number positive and neutral polymers, most negatively charged species reported in the literature are externally charged inorganic compounds composed of metal oxides in which the material is, many times, layered and excited by an external source.[246-251] The unexpectedly synthesized inorganic polymer (**21**) hosts a plethora of novel characteristics, as it is unprecedented in both charge, structure, as well as the tungsten-copper-carbon cage subunit. Never before in the literature has a crystal substructure, containing a pattern of a WCu_3 bound backbone integrated by carbon atoms, ever been reported, yet many other examples include sulfur, selenium, nitrogen, halides (Cl, Br), and phosphorus.[‡]

The reaction sequence for the featured product involves an unexpected rearrangement in which phosphorus is totally eliminated (Scheme 6). Tungsten is formally reduced from 0 to –1 while retaining an 18 electron count and, thus, contains the negative charge for each polymer unit while each of the copper atoms formally posses 16 electrons. When syntheses using copper bromide and iodide salts are attempted, the analogues of the polymer are not obtained.

Polymer **21** is the byproduct of **14** obtained by layering a $CuCl/CH_3CN$ solution over a solution of **13**/CH_2Cl_2 at room temperature. The substance is placed in a dark environment for 2 days. After the mixture is filtered, layered with pentane, and cooled, (5 °C) the dark brown crystals are separated and collected. The crystals are readily soluble in CH_3CN, slightly in $CHCl_3$, even less in CH_2Cl_2, and not appreciably in pentane.

[‡] Cambridge Crystal Database.

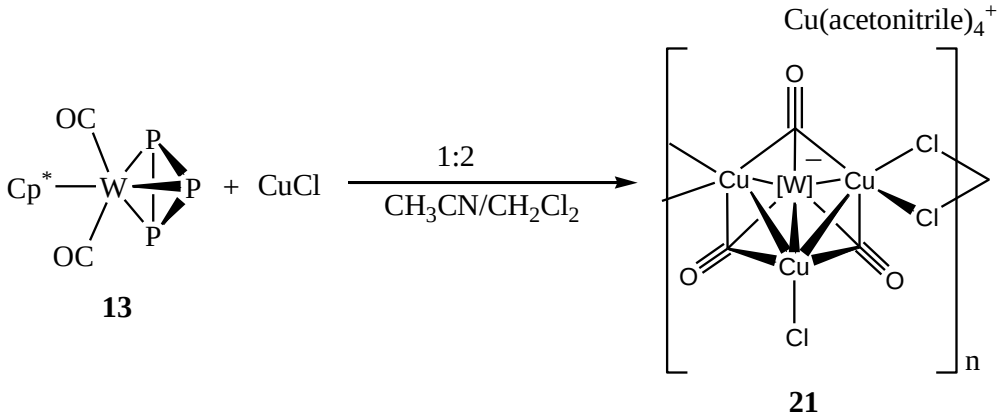

Scheme 6. Synthesis of polymer **21**. [W] = WCp*.

The solid-state structure of **21** (Figure 36) shows the *Cv* symmetric copper-carbon-bound tungstenate clusters bridged by chloride atoms. Moreover, the syndiotactic nature of this polymer is typified by the oppositely oriented clusters (in comparison with its neighbors), which are similarly oriented with every second subunit. Although each of the tungsten–C (carbonyl) bond lengths (1.991(3), 1.997(3), and 2.001(2) Å) remain unchanged from the starting material (1.995(19) and 2.009(17) Å)[244], a copper–C (carbonyl) bond is not present in the starting material. Yet, even though it may appear to be longer than many of the bonds listed in the literature (1.650–1.868 Å),[252-264] some bonds have similar lengths,[265, 266] however, it is not the longest example present in the literature.[267, 268] The lengthening can be accounted for in terms of the electronic effects provided by the surrounding inorganic substituents. It is thought that the tungsten atom and the geometry of the substructure influences the elongation of the Cu–C (carbonyl) and not the chlorides.[265, 269] The W–Cu (2.6074(2)–2.6761(5) Å) and Cu–Cu (2.7547–2.7589(6) Å) bond lengths are also in agreement with the W–Cu (2.602–3.134, mean 2.729 Å) and Cu–Cu (2.295–3.575, mean 2.747 Å) values registered in the Cambridge Crystal Database.

Two types of Cu–Cl bonds are present; there is the apical Cu(3)–Cl(3) (2.1505(9) Å) located on the WCu_3 unit and the analogous bridging Cu(1)–Cl(1) (2.2671(9) Å) and Cu(2)–Cl(2) (2.2435(9) Å) units. The extra electronic density of the WCu_3 unit and the steric hindrance supported by the bridging unit account for the difference in the Cu–Cl bond's length (0.1 Å). The angle summation of the Cu_2Cl_2 bridging units (360°) demonstrates that the motif is perfectly planar.

X-ray Data Collection for **21**. A dark brown, flat prism having approximate dimensions of 0.28 x 0.22 x 0.13 mm, was mounted on an Oxford Diffraction Gemini Ultra diffractometer. All intensity measurements were performed using the omega scan method (λ = 0.71073 Å) with a graphite crystal incident beam monochrometer. Cell constants were obtained from a Full-matrix least-squares on F^2.

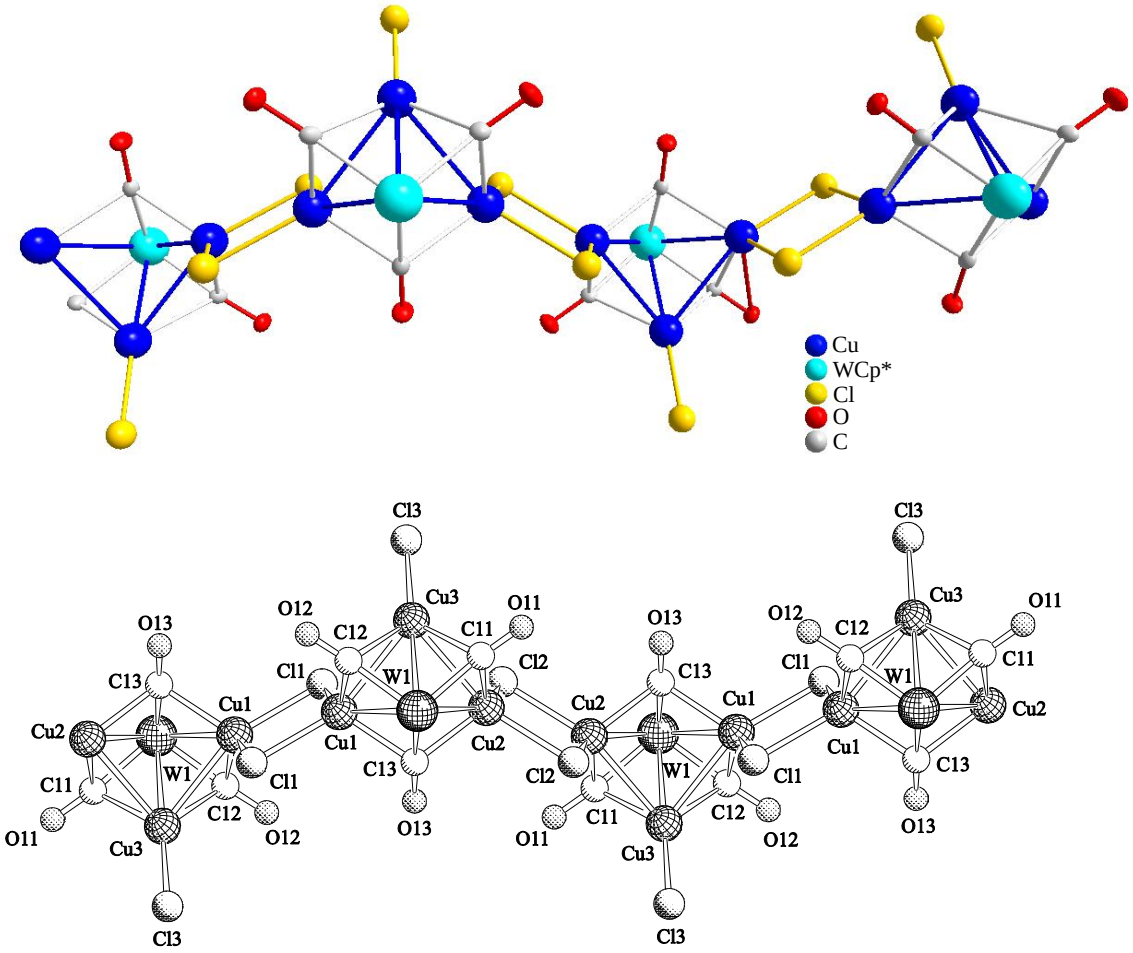

Figure 36. Solid-state projection of $C_{13}H_{15}Cl_3Cu_3O_3W$ (**21**). Cp* units connected to tungsten; $Cu^+(acetonitrile)_4$ units; and hydrogen atoms omitted for clarity. Selected bond lengths [Å] and angles [°]: W(1)–Cu(1) 2.6761(5), W(1)–Cu(2) 2.6638(4), W(1)–Cu(3) 2.6074(4), W(1)–C(11) 1.991(3), W(1)–C(12) 1.997(3), W(1)–C(13) 2.001(2), Cu(1)–Cl(1) 2.3843(10), Cu(1)–C(12) 2.182(2), Cu(1)–C(13) 2.150(3), Cu(1)–Cl(1) 2.2671(9), Cu(2)–Cl(2) 2.4151(11), Cu(2)–C(11) 2.182(2), Cu(2)–C(13) 2.162(3), Cu(2)–Cl(2) 2.2435(9), Cu(3)–Cl(3) 2.1505(9), Cu(3)–C(11) 2.193(3), Cu(3)–C(12) 2.231(3), O(11)–C(11) 1.172(4), O(12)–C(12) 1.171(4), O(13)–C(13) 1.176(3), Cu(1)–Cu(3) 2.7589(6), Cu(2)–Cu(3) 2.7545(7), Cl(1)–Cu(1)–Cl(1) 95.06(3), Cu(1)–Cl(1)–Cu(1) 84.94(3), Cl(2)–Cu(2)–Cl(2) 93.77(4), Cu(2)–Cl(2)–Cu(2) 86.23(4).

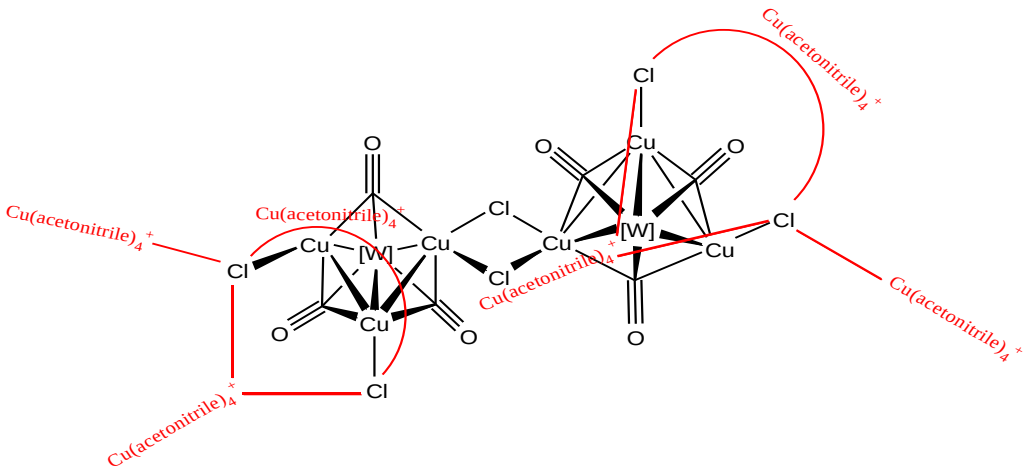

Figure 37. Proximal sites for Cu^{+}(acetonitrile)$_4$ on **21**. [W] = WCp*. Each shape represents a different configuration: Y = the same methyl group is in close proximity to two chloride atoms; I = one methyl group is in close proximity to one chloride; C = 2 different methyl groups tetrahedrally positioned.

The counter cation also plays a role in the crystal structure by being present in close proximity (1.65–1.87 Å) to a number of different chloride atoms in a specific pattern (Figure 37). For clarity, these are displayed with lines representing each of the CH_3 groups on the terminal ends of the copper^{+}(acetonitrile) molecules. The counter cations are in close proximity to the chlorides on every other Cl_2Cu_2 ring and every non-ring bound chloride (noted as Cl3 in Figure 36) and are, in addition, simultaneously bound to other polymer units in the same fashion.

Also in agreement with the solid-state projection, three different peaks representing the copper^{+}(acetonitrile) counter cation are detected in the ^{1}H NMR as being unbound, and two other peaks that are proximal. The second sets of shifted acetonitrile signals in the ^{1}H and ^{13}C NMR (2.37 ppm, 2H and 2.20 ppm, 1H; 109.18 ppm, CN and 1.88 ppm, Me in the ^{13}C) agree with the solid-state projection and shows that this configuration also remains in solution. Two carbonyl peaks detected in the ^{13}C NMR, one bonded to both CuCl bridges (C13–O13, 235.79 ppm) and other two bound to one CuCl bridge (C11–O11 and C12–O12, 220.46 ppm), are also in agreement with the solid-state projection. No other species associated with byproduct or transient stages are detected. More detailed studies show that the infrared radiation measurement detected three different carbonyl peaks (1997, 1894, and 1802), as one would expect from the solid-state projection. In spite of the high degree of crystallinity shown from the solid-state projection the polymer is cracked at relatively low temperatures (melting point, 112 °C). It seems clear from the largest cations detected in the positive ion electrospray ionization (510.1 (76) $Cp^*_2W(CO)_2^{+}$, 849.1 (76) $CuCl[Cp^*W(CO)_2]_2^{+}$) that the CuCl bond is the weakest bond in the polymer and is the main source of decomposition under heat.

2.3.3. Polymers Synthesized From a Tungsten(I))diphosphorus and CuX (X = Cl, Br, I)

The isotactic dicarbonylcyclopentadienyltungsten(I)diphosphorus (**11**) containing polymers presented are only the third examples of their kind and are only comparable to their chromium and molybdenum analogs.[166, 168, 172] The syntheses of polymers **22**–**24** are performed by slowly layering a cold (0 °C) CuX/CH_3CN (X = Cl, Br, I) solution on a cold (0

°C) solution of **11**/CH_2Cl_2 in a 2:1 ratio. After the solution is kept at 0 °C for a period of 7 days, red crystals are formed (Scheme 7). Each of the copper halide containing species are isostructural to each other forming an extended array of repeating units bound in a trans configuration affording the formation of three polymers. A further investigation on the reactivity of these polymers is futile mainly because of the lack of solubility in aprotic solvents including hexane, pentane, CH_2Cl_2, THF, chloroform, and DMSO.

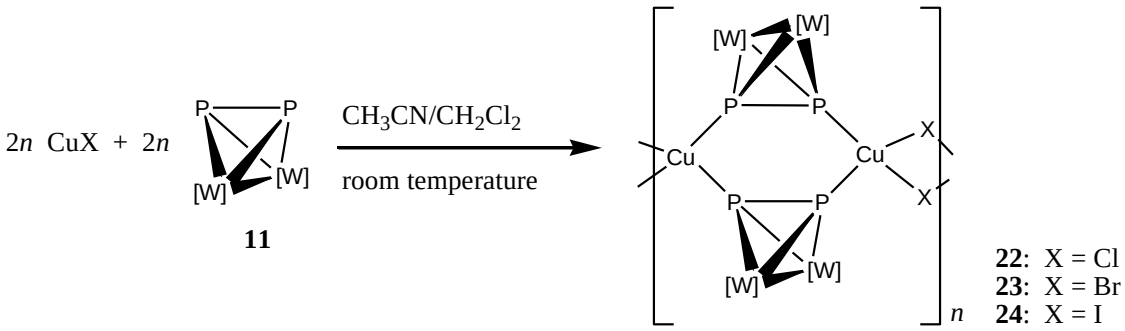

Scheme 7. Synthesis of **22**, **23**, and **24**. [W] = $WCp(CO)_2$.

The basal unit (**11**) has been previously synthesized,[154] but the solid-state crystal structure is not reported. The structure (Figure 38) forms a tetrahedral W_2P_2 framework in which cyclopentadienyl and carbonyl substituents are attached to the tungsten. The electron-rich phosphorus atoms provide lone pairs of electrons in which electrophillic metals can attach.

X-ray Data Collection for **11**. A red, prism having approximate dimensions of 0.062 x 0.056 x 0.054 mm, was mounted on an Oxford Diffraction Gemini Ultra diffractometer. All intensity measurements were performed using the omega scan method (λ = 0.71073 Å) with a graphite crystal incident beam monochrometer. Cell constants were obtained from a Full-matrix least-squares on F^2.

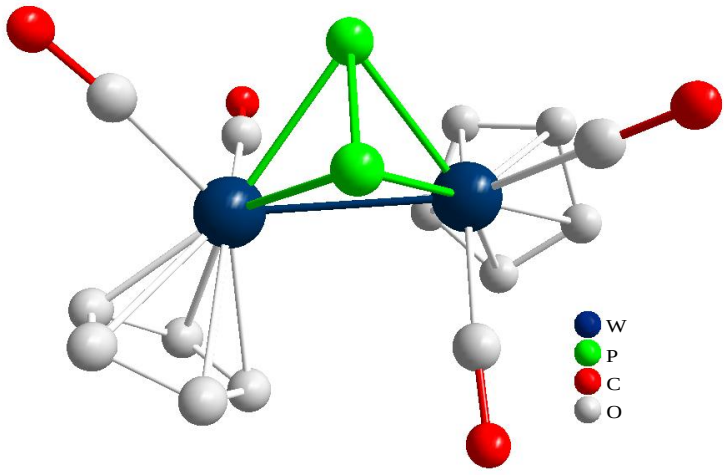

Figure 38. Solid-state projection of $C_{14}H_{10}O_4P_2W_2$ (**11**). Hydrogen atoms and C_4H_8O are removed for clarity. P–P bond length: 2.0951(18) Å.

The cyclopentadienyl and carbonyl groups for complexes **22**–**24** are located in opposite directions just as in the original starting material (**11**) and each of the Cu_2X_2 rhombi (X = Cl, Br, I) configurations have an angle summation of 360°. In contrast, inspection of the angle summations of the Cu_2P_4 rings reveals that they are not perfectly flat. Slight differences from of the ideal 720° are seen in each of the Cl (719.0°), Br (719.4°), and I (719.6°) analogs. Even though all three polymers are, for practical purposes, eclipsable in their conformations, only **22** belongs to a point group other than its identity (C_2). The cyclopentadienyl and carbonyl substituents of polymers **23** and **24** are not superimposable under any other symmetry operations. Although, the P–P bond length of the basal unit (**11**) is virtually unaffected when it is bound to the Cu^+ ion, the bond length is slightly elongated as the halide substitution is heavier. The inductive affect of the halide dictates the electron affinity of the Cu^+ ion and is demonstrated by the increase in the Cu–P bond length of approximately 0.02 Å from the Cl, Br, and I containing polymers. The Cu_2X_2 rings contain an average Cu–X bond length that is elongated as the halide increases in atomic number (**22**, Cl = 2.344(1) Å; **23**, Br = 2.471(1) Å; **24**, I = 2.640(1) Å), which is similar to the increase in van der Waals radii (Cl to Br = 5.5%, Br to I = 6.4%), however, no pattern is noticed in distance between the copper atoms (**22** = 4.930(2), **23** = 4.941(2), **24** = 4.858 (2) Å). Incidentally, the pattern of the Cu···Cu···Cu linearity is increasingly interrupted as the atomic number of the halide is increased (**22** = 180.00(0)°, **23** = 176.61(4)°, **24** = 168.49(3)°). The P–P bond lengths slightly increase (~0.01 Å) as the metal of the basal unit changes from chromium, molybdenum, and the featured tungsten analogs.[168, 172] Other significant bond lengths (Cu–P, Cu–X) do not exhibit any pattern of change.

X-ray Data Collection for **22**. A red, rod having approximate dimensions of 0.150 x 0.050 x 0.020 mm, was mounted on an Oxford Diffraction Gemini Ultra diffractometer. All intensity measurements were performed using the omega scan method (λ = 1.54184 Å) with a graphite crystal incident beam monochrometer. Cell constants were obtained from a Full-matrix least-squares on F^2.

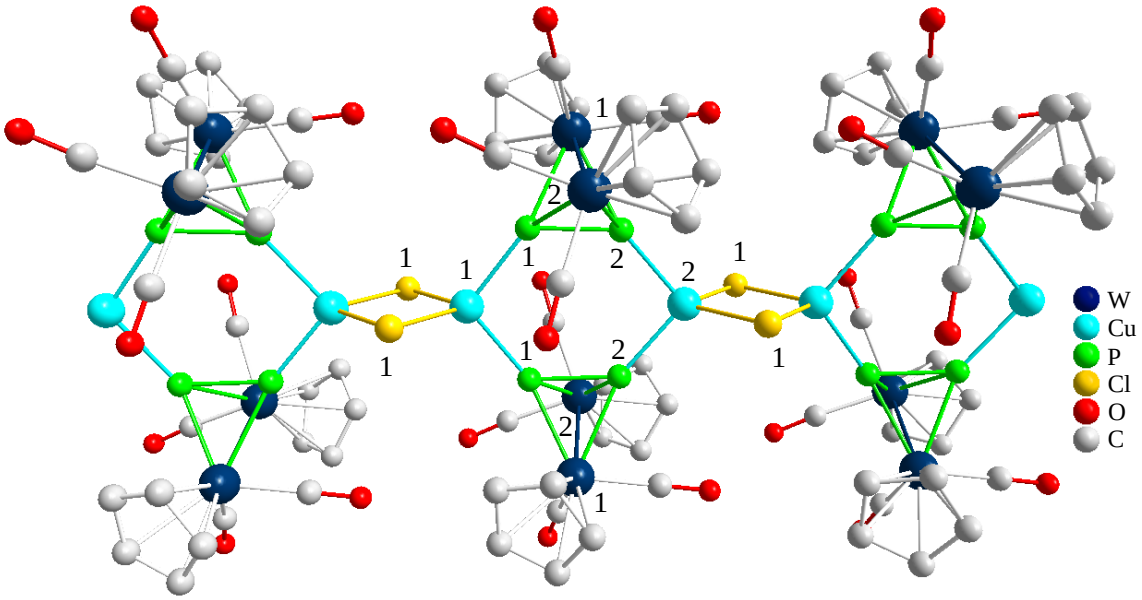

Figure 39. Solid-state projection of $C_{14}H_{10}ClCuO_4P_2W_2$ (**22**). Hydrogen atoms are removed for clarity.

X-ray Data Collection for **23**. A red-orange, rod having approximate dimensions of 0.190 x 0.030 x 0.010 mm, was mounted on an Oxford Diffraction Gemini Ultra diffractometer. All intensity measurements were performed using the omega scan method (λ = 1.54184 Å) with a graphite crystal incident beam monochrometer. Cell constants were obtained from a Full-matrix least-squares on F^2.

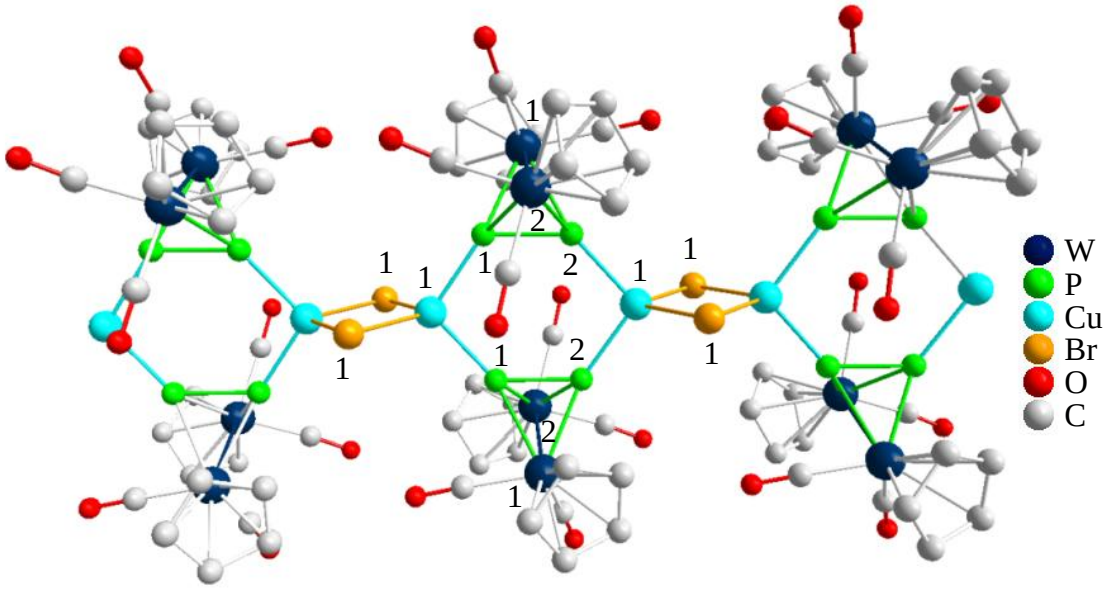

Figure 40. Solid-state projection of $C_{14}H_{10}BrCuO_4P_2W_2$ (**23**). Hydrogen atoms are removed for clarity.

X-ray Data Collection for **24**. A red-orange, rod having approximate dimensions of 0.16 x 0.03 x 0.03 mm, was mounted on an Oxford Diffraction Gemini Ultra diffractometer. All intensity measurements were performed using the omega scan method (λ = 1.54184 Å) with a graphite crystal incident beam monochrometer. Cell constants were obtained from a Full-matrix least-squares on F^2.

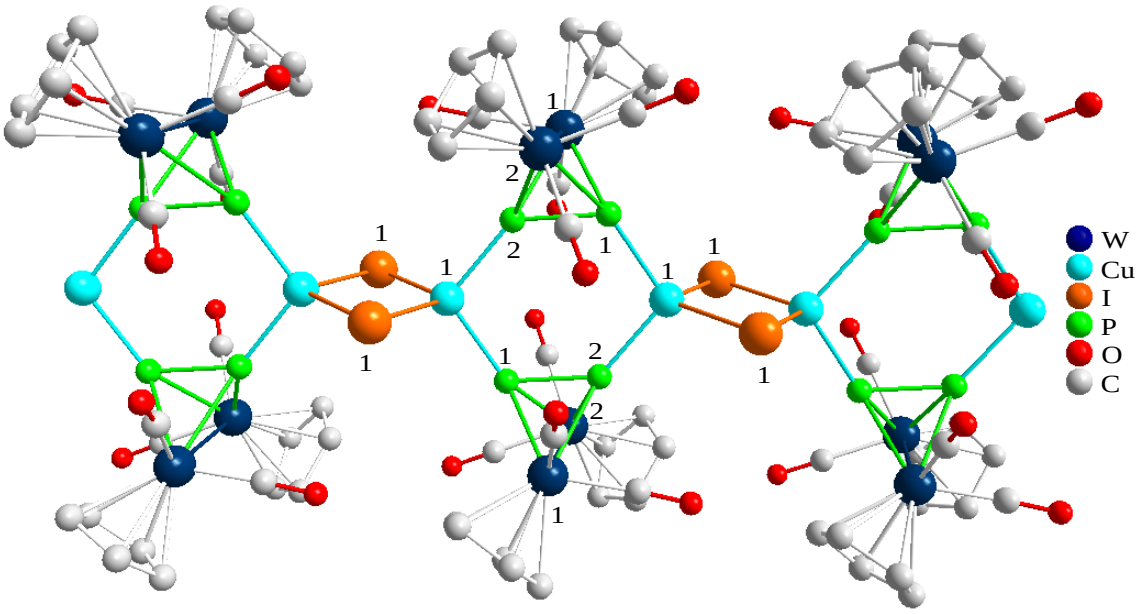

Figure 41. Solid-state projection of $C_{14}H_{10}ICuO_4P_2W_2$ (**24**). Hydrogen atoms and C_2H_3N are removed for clarity.

Table 8. Comparison of selected bond lengths (Å) and angles (°) in compounds **22**–**24**.

	22 (X = Cl)	**23** (X = Br)	**24** (X = I)
P–P	2.087(2)	2.093(2)	2.100(2)
Cu–P	2.2669(15)	2.2861(19)	2.3069(17)
	2.2920(15)	2.2923(19)	2.3070(17)
Cu–X	2.3417(14)	2.4669(11)	2.6089(9)
	2.3460(14)	2.4755(11)	2.6708(9)
P–Cu–P	99.59(7)	102.85(7)	107.18(5)
	105.55(7)	102.85(7)	107.70(5)
P1–Cu–X	109.30(4)	112.20(5)	107.18(5)
	116.81(4)	112.31(6)	111.88(5)
P2–Cu–X	113.83(4)	112.86(6)	107.70(5)
	115.61(4)	113.62(5)	117.79(5)
X–Cu–X	99.27(6)	103.33(4)	105.57(3)
	99.52(6)	103.33(4)	105.57(3)
Cu–X–Cu	80.61(5)	76.67(4)	74.43(3)
Cu···Cu···Cu	180.00(0)	176.61(4)	168.49(3)

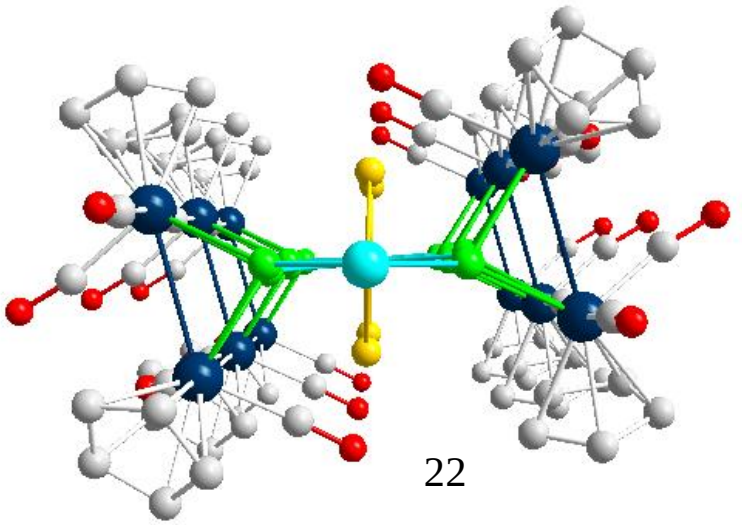

22

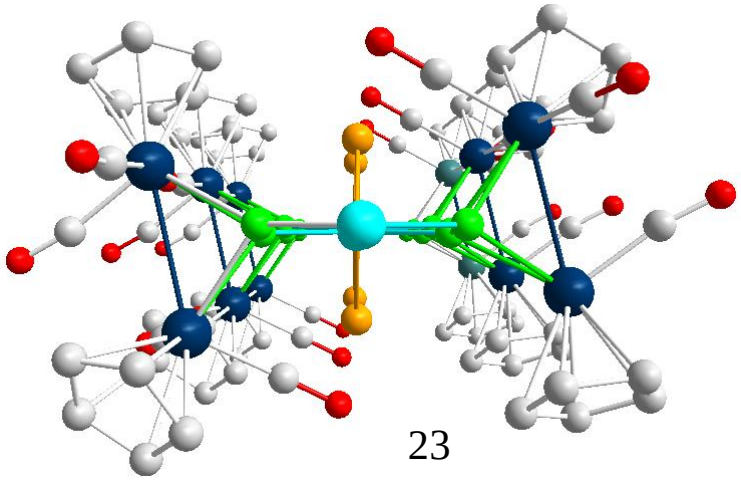

23

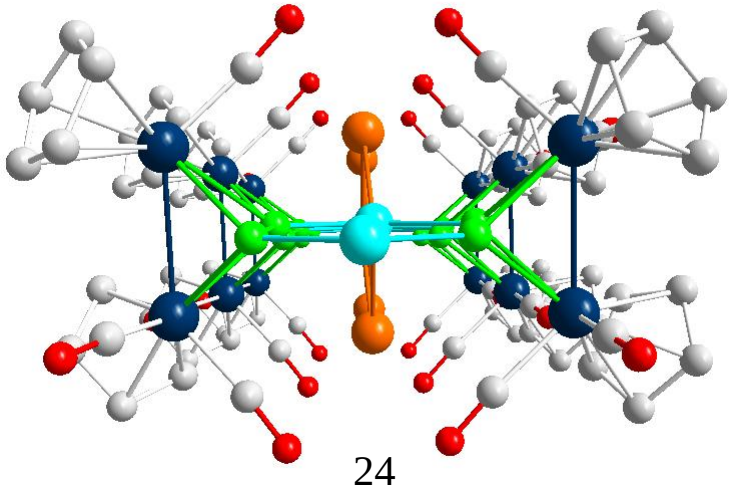

24

Figure 42. View down the crystallographic y-axis of complexes **22**, **23**, and **24**.

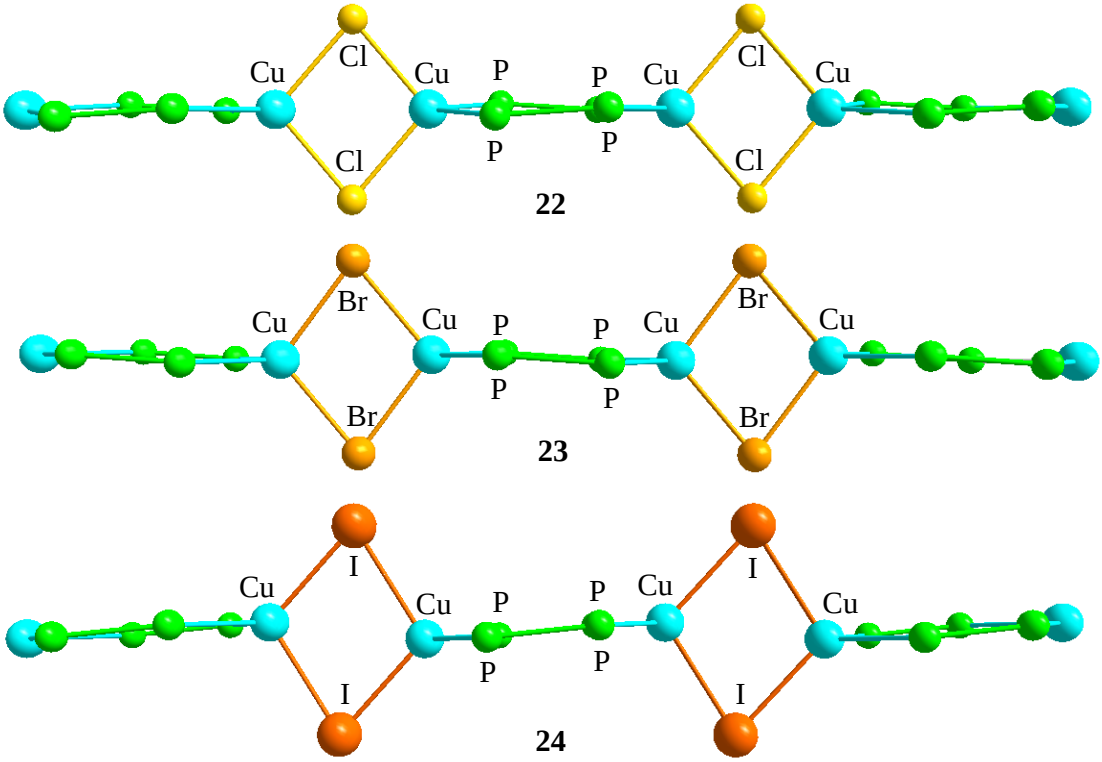

Figure 43. View of the structures of **22**–**24** perpendicular to the faces of the Cu_2X_2 rings. Tungsten atoms and their ancillary ligands are omitted for clarity.

The fine differences in complexes **22**–**24** are not only obvious in the side view and the view down the y-axis, but they also have an effect on the ^{31}P MAS-NMR spectrum. Differences in signals are noticed between the P1 and P2 atoms as a result from their interstitial differences between other atoms, but theses differences are not so pronounced for **24**. The most obvious and arguably the most influential atom is copper. The divergences in the bonded and nonbonded copper distances for **22** (0.0251 and 0.1109 Å) and **23** (0.0062 and 0.1424 Å) are significant, but the difference in **24** is virtually unchanged for the bonded copper and can be considered chemically equivalent, however, the nonbonding distance is considerably different (0.2416 Å). The second most influential atom in the polymers is tungsten and even though the average W–P1 and W–P2 distance deviations are small in **22** (0.003 Å), the differences in **23** (0.0151 Å) and **24** (0.0144 Å) are significant. Other sources of divergence include the average carbon (**22**, 0.0535; **23**, 0.0386; **24**, 0.0270 Å) and oxygen (**22**, 0.1739; **23**, 0.1775; **24**, 0.0236 Å) distances.

From this data it would seem that the strongest influence on the difference of chemical shift between the P1 and P2 atoms is caused from the most abundant carbon and oxygen atoms. The greatest difference in distance, however, comes from the oxygen. This is noticed from the comparison of the ^{31}P MAS-NMR spectra of **22**–**24** (Figures 44–46) as **22** and **23** have two sets of markedly different peaks and that of **24** is distorted to the point where it seems as if a single multiplet is created. The simulated spectrum below shows that the peak is truly made up of two closely positioned quartets although the simulation does not show the $^1J_{PP}$ coupling.

The greatest influence on the chemical shift of the phosphorus atoms comes from the positioning of the oxygen atom located on the carbonyl groups. Both of the phosphorus atoms in the iodide analog (**24**) are shifted upfield relative to **22** and **23** and they have the lowest average distance from the oxygen atoms (**22**, P1 = 4.1550, P2 = 4.3289 Å; **23**, P1 =

4.3272, P2 = 4.1497 Å; **24**, P1 = 4.0434, P2 = 4.0670 Å). This means that the closer the oxygen atom is to the phosphorus the more shielded it is and, thus, the more upfield the signal is shifted.

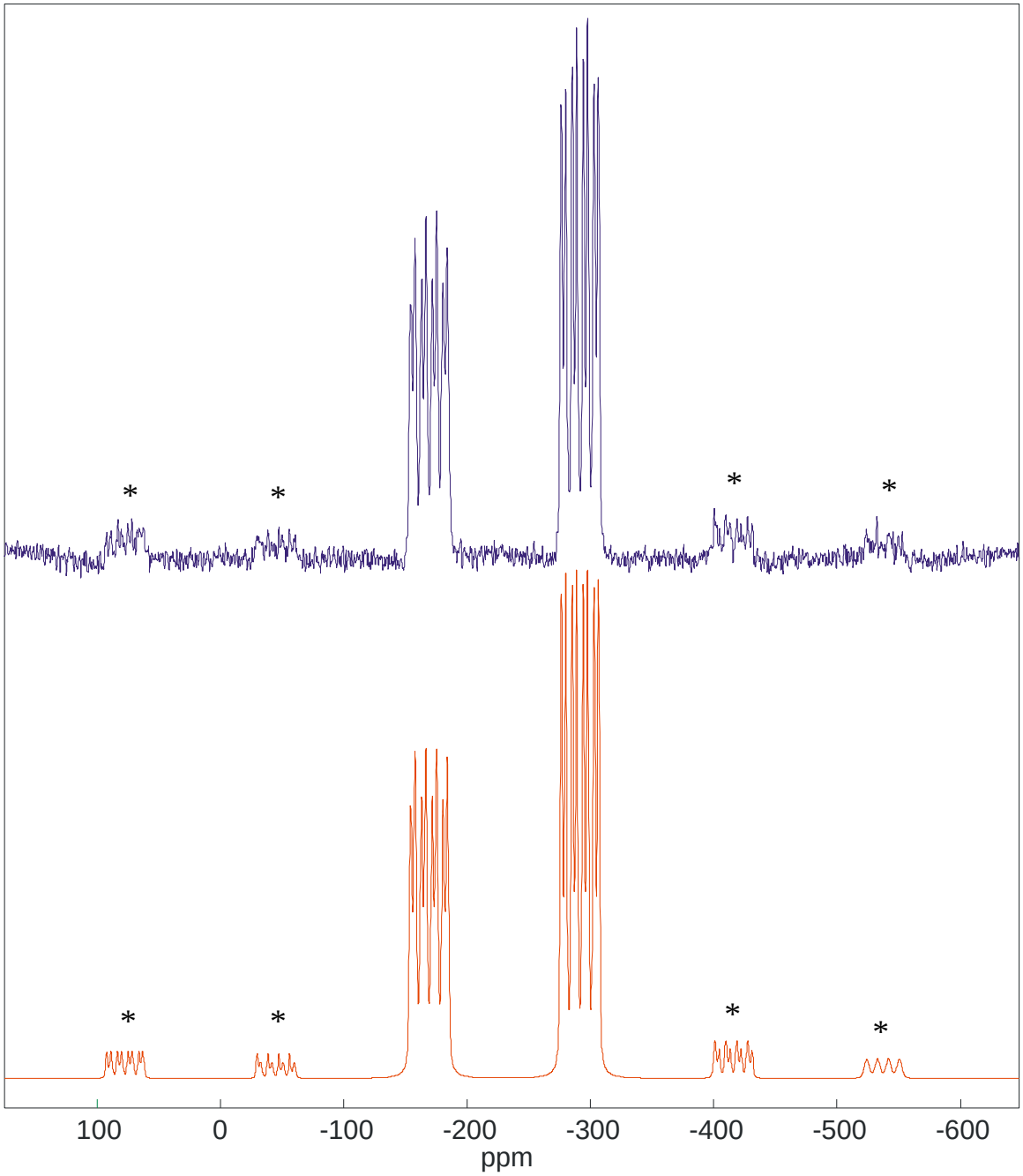

Figure 44. ^{31}P MAS-NMR spectra for **22**. Top spectrum (blue), experimental; bottom spectrum (red), simulated. **^{31}P MAS-NMR** (121.49 MHz, spinning frequency 30 kHz, RT) δ = –169.03 ($^{1}J_{PP}$ = 411.99 Hz; $^{1}J_{CuP}$ = 1057.94, 1057.95 Hz; P1), –291.31 ($^{1}J_{PP}$ = 427.18 Hz; $^{1}J_{CuP}$ = 1070.15, 1078.29 Hz; P2). **^{31}P MAS-NMR (simulated)** δ = –169.08 ($^{1}J_{PP}$ = 432.53 Hz; $^{1}J_{CuP}$ = 1060.12, 1060.09 Hz; P1), –291.48 ($^{1}J_{PP}$ = 428.28 Hz; $^{1}J_{CuP}$ = 1075.52, 1075.71 Hz; P2). Spinning side bands = *.

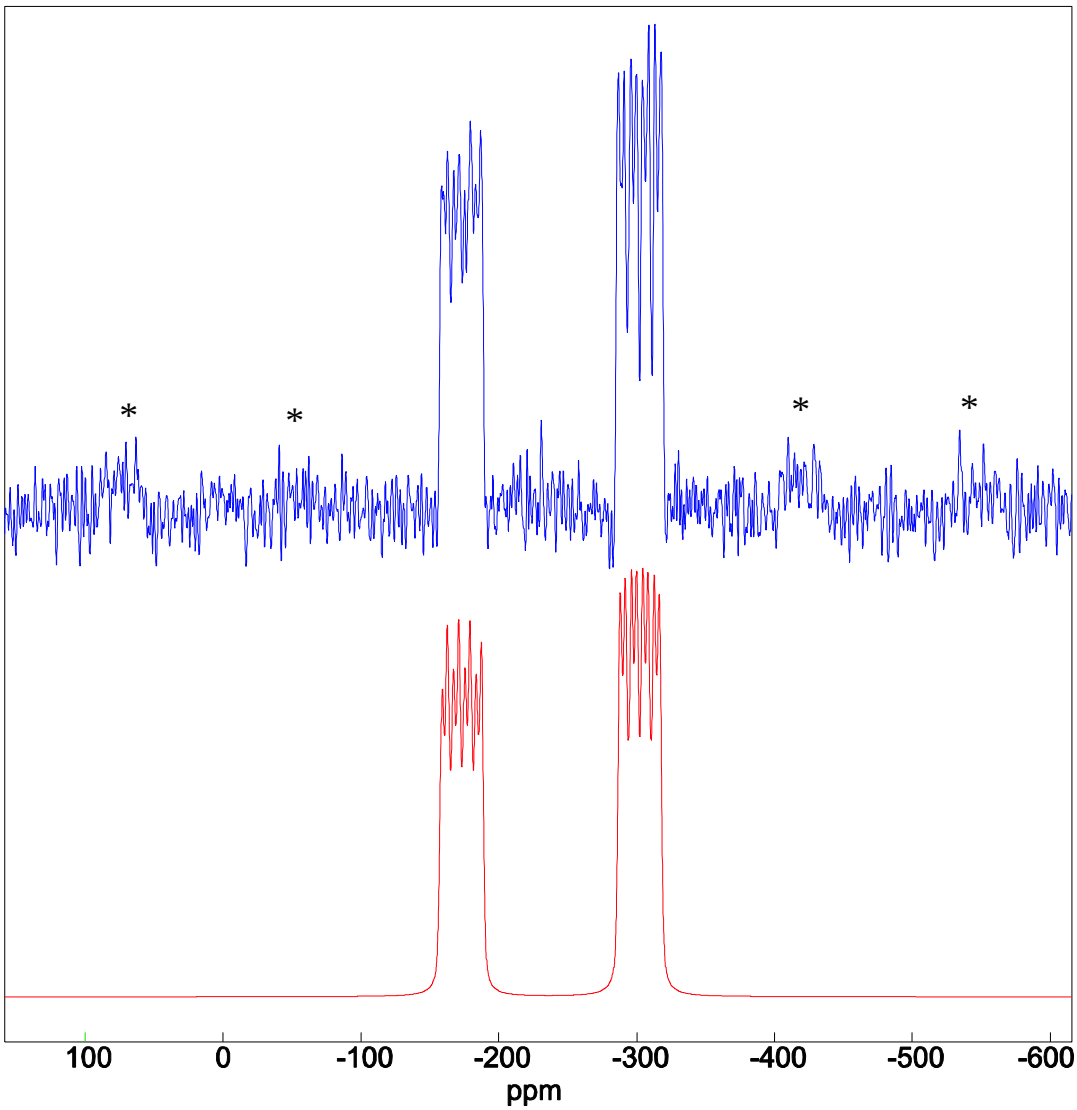

Figure 45. ^{31}P MAS-NMR spectra for **23**. Top spectrum (blue), experimental; bottom spectrum (red), simulated. **^{31}P MAS-NMR** (121.49 MHz, spinning frequency 30 kHz, RT) δ = –172.63 ($^{1}J_{PP}$ = 474.55 Hz; $^{1}J_{CuP}$ = 962.32, 974.52 Hz; P2), –302.24 ($^{1}J_{PP}$ = 515.75 Hz; $^{1}J_{CuP}$ = 1066.08, 1082.36 Hz; P1). **^{31}P MAS-NMR (simulated)** δ = –173.18 ($^{1}J_{PP}$ = 470.16 Hz; $^{1}J_{CuP}$ = 1000.00, 1000.00 Hz; P2), –302.21 ($^{1}J_{PP}$ = 458.25 Hz; $^{1}J_{CuP}$ = 1000.00, 1000.00 Hz; P1). Spinning side bands = *.

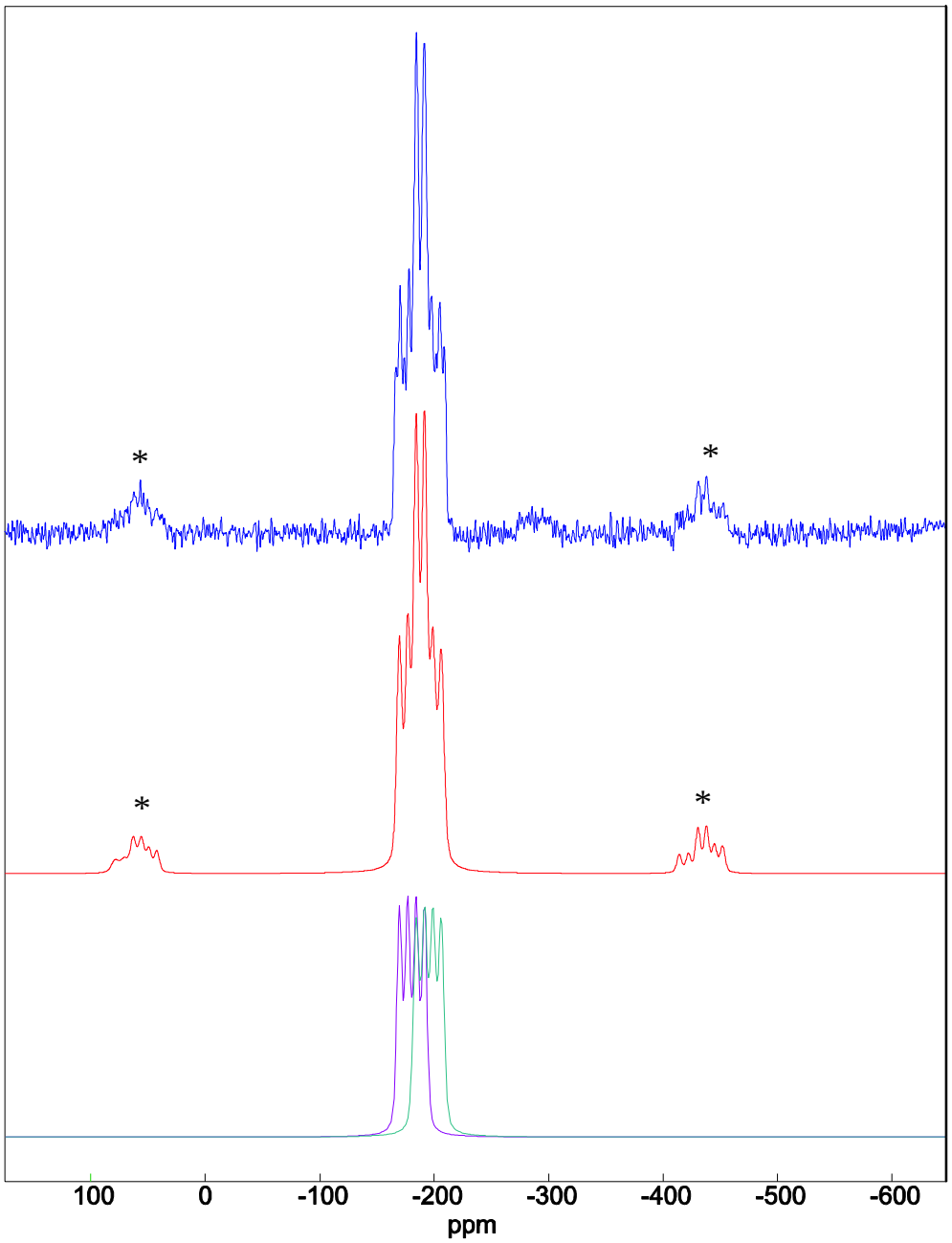

Figure 46. ^{31}P MAS-NMR spectra for **24**. Top spectrum (blue), experimental; middle spectrum (red), simulated; bottom spectrum (purple and aqua), separated contributions of the simulated peak. **^{31}P MAS-NMR** (121.46 MHz, spinning frequency 30 kHz, RT) δ = –187.75 ($^{1}J_{PP}$ = 472.91 Hz; $^{1}J_{CuP}$ = 890.90, 903.10 Hz; P1 and P2). **^{31}P MAS-NMR (simulated)** δ = –169.92 ($^{1}J_{CuP}$ = 891.77, 887.63 Hz; P1 and P2). **Separated peaks of ^{31}P MAS-NMR (simulated)** Purple = P1, Aqua = P2. Spinning side bands = *.

The most noteworthy peaks in the positive ion electrospray for **22** possess the intact basal unit (**11**) or some variation of it. The $[Cu\{Cp_2W_2(CO)_xP_2\}]^+$ (X = 3 and 4) accommodates only one loss of CO while other species like $[CuCl\{Cp_2W_2(CO)_2P_2\}]^+$ and $[Cu_2Cl_2\{Cp_4W_4(CO)_3P_2\}]^+$ vary the number chloride, tungsten, CO, and Cp groups in relation to each other and the basal unit. The loss of carbonyl by the basal unit is present in the other miscellaneous cations and anions detected.

The ESI-MS for the bromide analog (**23**) also shows the basal unit in multiple combinations with NH_4 and CH_3CN while experiencing variations in the number of CO groups (1, 2, 3, 4, 5, 6, and 7). This variation is continued when examples of CuBr are attached in the mono and disubstituted $[CuBr\{Cp_2W_2(CO)P_2\}]^+$ and $[Cu_2Br_2\{Cp_4W_4(CO)_5P_4\}]^+$ are present. Finally, the faint presence of the intact product is identified in accompaniment with $(NH_4)(CH_3CO)$.

The ESI-MS for the iodide analog (**24**) also shows the basal unit in multiple combinations with NH_4 and CH_3CN while experiencing variations in the number of CO groups. The $[(NH_4)_2I(CH_3CN)_2\{Cp_2W_2(CO)_4P_2\}]^+$ species replaces Cu with NH_4 followed by the transition to $Cu_{n+1}Cl_n$ (n = 1,2) containing species. The carbonyl count is unaltered in the monosubstituted species and is consistently reduced to one in the disubstituted species. Only one instance of NH_4 alternate for Cu is present in the disubstituted species.

The IR spectra for **22**–**24** show 5 bands with the exception of **24** having one of the bands overlapping with another. One would expect a multiple of 2n bands in the IR for the asymmetric and symmetric stretches of the two carbonyl groups attached to each tungsten, but with an infinite polymer one or more of these bands could be overlapping each other in the spectrum. Simpler molecules such as the dimers normally do not have such overlaps.

2.3.3.1. A Tungsten(I))diphosphorus, ^{t}Bu Analog and CuBr

Different varieties in the unbound unit, while seemingly trivial to the novice chemist, create variation in crystal formation. While the ^{t}Bu substituted unbound and bound unit are analogous to formations of the unsubstituted species, only the isotactic, bromine containing polymer is successful in crystallization whereas the chlorine, bromine, and iodine polymers are obtained for the unsubstituted species. This phenomenon demonstrates the trend of increasing difficulty in crystallization as heavier substituted subunits are reacted.

The subunit is synthesized in a two-part, modified procedure. First, tungsten hexacarbonyl is treated with ^{t}Bu-cyclopentadiene while refluxing for 18 h in decalin forming $[Mo(^tBu\text{-}C_5H_4)(CO)_3]_2$.[179] Then, the mixture is charged with white phosphorus and refluxed for another 16 h. After the mixture is cooled and the solvent is evaporated the contents are purified on a column of SiO_2.[270] The polymer is formed by gently layering a cold (0 °C) **25**/CH_2Cl_2 solution with a CuBr/CH_3CN solution. The complex is crystallized by concentration, layering with pentane, and cooling (4 °C) in darkness for 7 days (Scheme 8). Attempts to synthesize the CuCl and CuI analogs using the same procedure proved to be inconclusive due to lack of single crystals produced. All substance produced was amorphous and immesurable by X-ray diffraction.

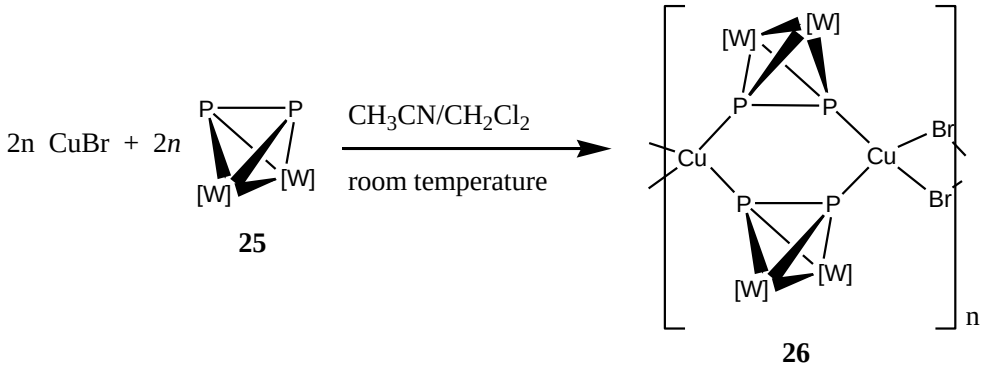

25 **26**

Scheme 8. Syntheses of **26** [W] = $W(Cp\text{-}^tBu)(CO)_2$.

The synthesis or characterization of complex **25**, the basal subunit, has never before been reported. The solid-state projection (Figure 47) shows tungsten bound by two carbonyl groups, *tert*-butylcyclopentadienyl, and the electron rich diphosphorus in a tetrahedral W_2P_2 framework. The lone pair on the phosphorus atoms provides attachment sites for metals.

X-ray Data Collection for **25**. A yellow, rod having approximate dimensions of 0.090 x 0.040 x 0.010 mm, was mounted on an Oxford Diffraction Goniometer Xcalibur diffractometer. All intensity measurements were performed using the omega scans method (λ = 0.71073 Å) with a graphite crystal incident beam monochrometer. Cell constants were obtained from a Full-matrix least-squares on F^2.

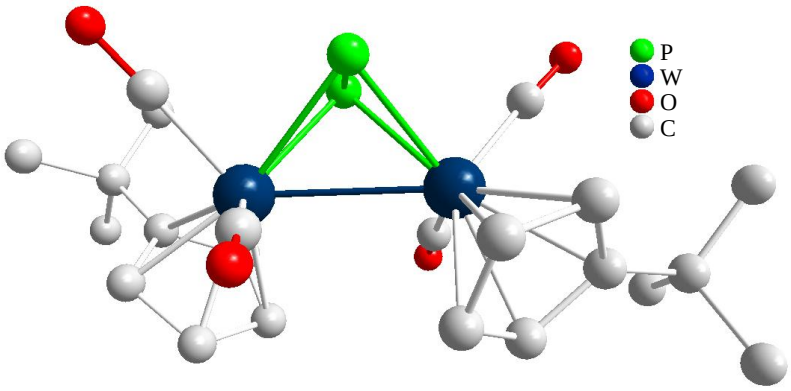

Figure 49. Solid-state projection of $C_{22}H_{26}O_4P_2W_2$ (**25**). Hydrogen atoms are removed for clarity. Selected bond lengths (Å): P–P 2.0983(24), W–W 3.0171(6).

The cyclopentadienyl and carbonyl groups for the unbound and bound unit are consistently located in opposite directions. Each of the Cu_2X_2 rhombi for the polymer (**26**) are perfectly flat as shown from their angle summations (360°). On the other hand the Cu_2P_4 rings deviate (angular summation, 717.7°) from the ideal 720°. This deviation is more noticeable in Figure 50 which depicts the perpendicular faces of the Cu_2X_2 rings. This is further proven by the lack of linearity (164.5°) of the Cu···Cu···Cu component; the breach is most severe when one compares it to the other unsubstituted polymers. If these slight deviations are ignored, the polymer exhibits C_2 symmetry. The P–P bond length is virtually unchanged when the unbound unit is compared to the polymer. The Cu–Br–Cu angle of the ^{t}Bu substituted polymer (**26**) is greatly reduced (25°) in comparison to the nonsubstituted analog (**23**) from the added steric bulk while the Cu–Br bond length remains constant.

X-ray Data Collection for **26**. A red to orange, flat rod having approximate dimensions of 0.2869 x 0.0303 x 0.0120 mm, was mounted on an Oxford Diffraction Goniometer Xcalibur diffractometer. All intensity measurements were performed using the omega scans method (λ = 1.54184 Å) with a graphite crystal incident beam monochrometer. Cell constants were obtained from a Full-matrix least-squares on F^2.

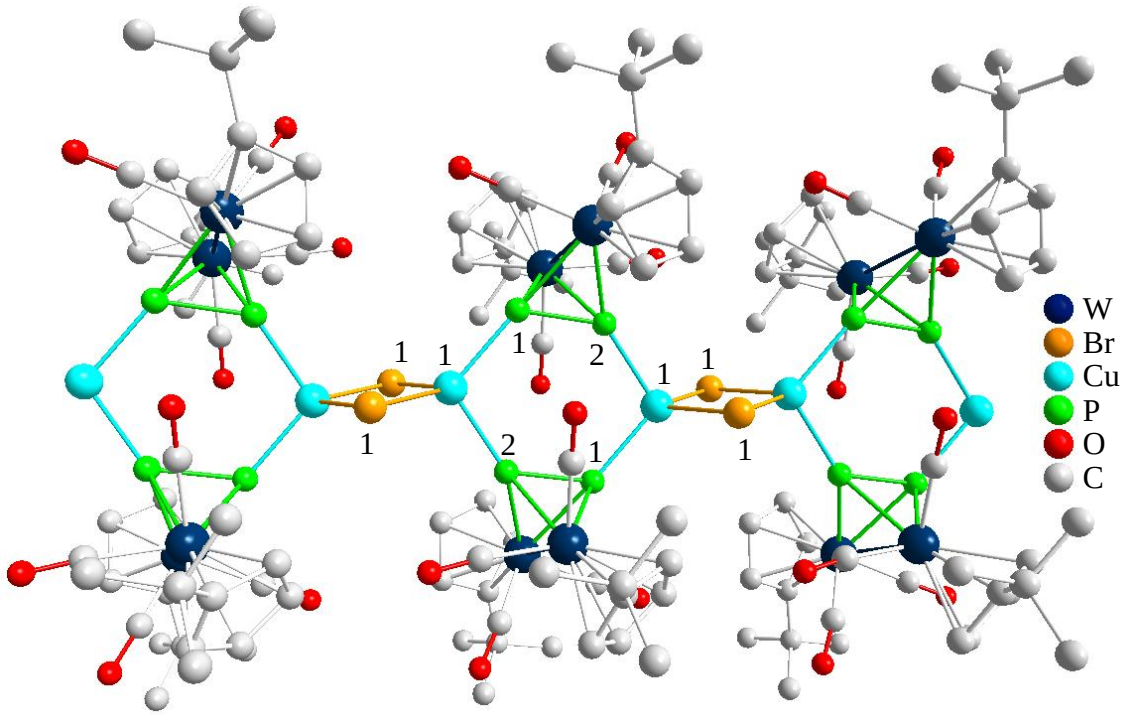

Figure 48. Solid-state projection of $C_{22}H_{26}BrCuO_4P_2W_2$ (**26**). Hydrogen atoms are removed for clarity. Selected bond lengths (Å) and angles (°): P-P 2.0973(20), Cu–P2 2.2938(18), Cu–P1 2.3113(17), Cu–Br 2.4964(9), Cu–Br' 2.4560(9), P1–Cu–P2 105.98(6), P1–Cu–Br 111.24(5), P1–Cu–Br' 122.81(5), P2–Cu–Br 106.84(5), Cu–Br' 2.4560(9), P2–Cu–Br' 106.99(5), Br–Cu–Br' 102.05(3), Cu–Br–Cu 77.96(3), Cu···Cu···Cu 164.50(3).

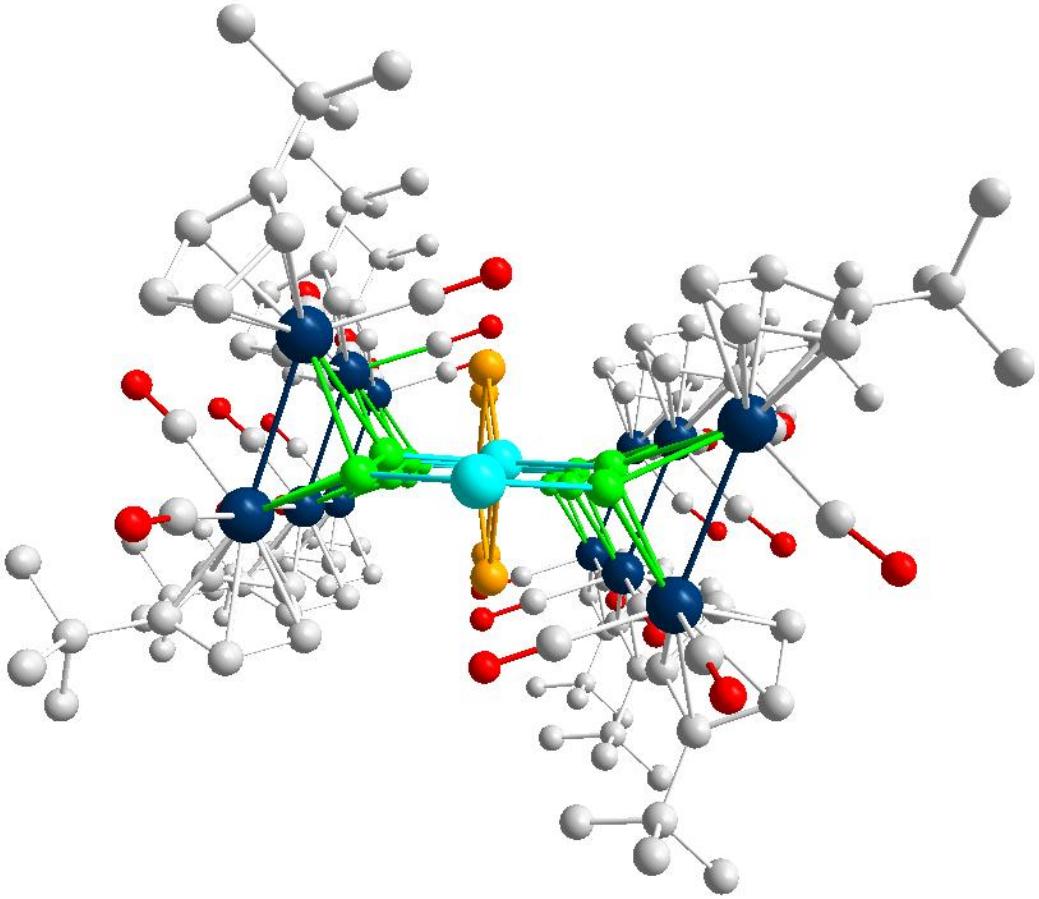

Figure 49. View down the crystallographic y-axis of complex **26**.

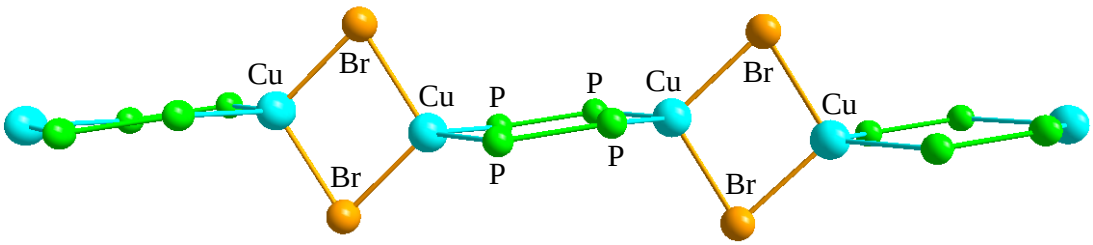

Figure 50. Structure of **26** perpendicular to the faces of the Cu_2Br_2 rings. Tungsten atoms and their ancillary ligands are omitted for clarity.

One fortunate and expected corollary from the presence of the ^{t}Bu group is increased solubility in common solvents such as THF, CH_2Cl_2, and CH_3CN while remaining insoluble in unsubstituted hydrocarbons like hexane or pentane. The greater differences and increased solubility allow NMR studies at both low temperature and room temperature. When temperatures are lowered to –80 °C, the resonance in solution is slower than the radio frequency pulse and four specific peaks are formed that represent the four chemically inequivalent phosphorus atoms. Even at room temperature variances between the unbound unit and the polymer are noticed in the ^{1}H NMR; the signals for the cyclopentadienyl ring and the ^{t}Bu groups are split from the polymer's lack of symmetry in comparison to the unbound

unit. One instance of splitting is also noted for the ^{t}Bu group in the $^{13}C\{^{1}H\}$ NMR of the polymer in comparison to the unbound unit.

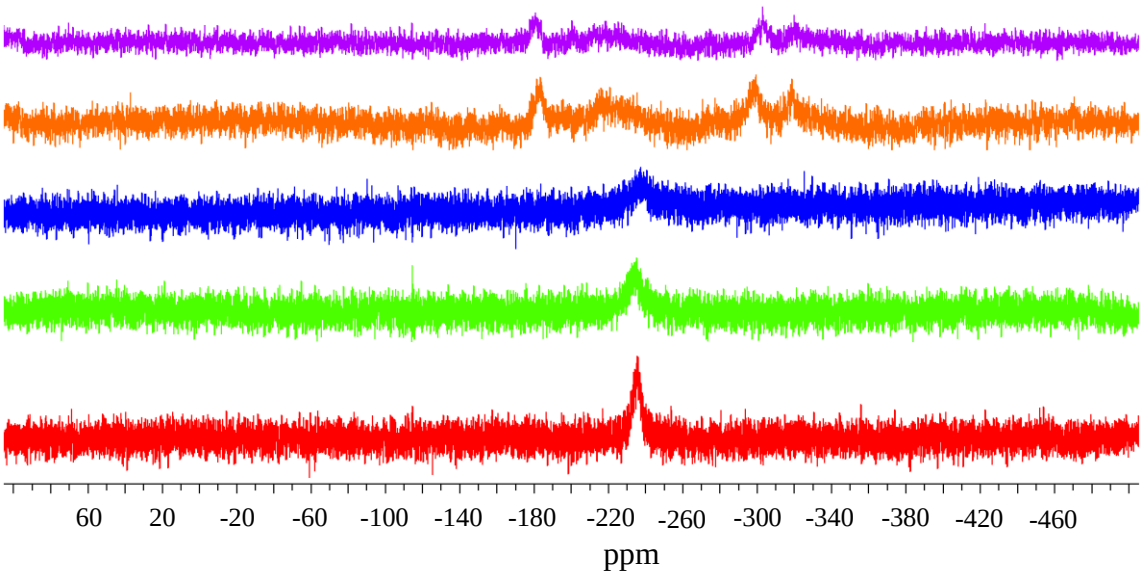

Figure 51. Variable temperature $^{31}P\{^{1}H\}$ NMR spectrum of **26** in THF-d_8/CH_2Cl_2 (3:1); From bottom to top: **27**, **0**, **–20**, **–80**, **–110** °C. **–110** °C, δ = –180.95 (s), –218.14 (s), –303.00 (s), –319.90 (s).

The ^{t}Bu group substitution adds enormous stability in comparison to the unsubstituted cyclopentadienyl analogs. The positive ESI-MS shows no instance of the $\{(^{t}BuCp)_2W_2(CO)_4P_2\}$ basal unit being damaged under measurement, every peak reported is attributed to the formula $Cu_NBr_{N-1}\{(^{t}BuCp)_2W_2(CO)_4P_2\}_X$. This increased stability is also manifested by a higher melting point (220–222 °C) when compared to the unsubstituted bromine analog (120–122 °C). Meanwhile, the negative ESI-MS shows species that contain CO groups, and if this assignment is correct, it is not certain what the source is as the basal units are the only species that contain CO groups. The other major species are the expected $Cu_{N-1}Br_N$ units.

The IR spectra for the unbound species shows only three peaks attributed to the CO groups. The polymer shows 5 and even though these peaks are shouldered, they are consistent with the unsubstituted chlorine and bromine analogs; the shouldering is even more intense for the iodine species causing the masking of one peak for a total count of 4. Ultimately, this phenomenon is the result of disrupted symmetry experienced by all of these similar species.

2.3.4. Polymers and Dimer Synthesized from reactions of Tungsten(I))diphosphorus and Triphosphanometal (metal = W and Mo) with AgX (X = PF_6^-, $CF_3SO_4^-$)

The formation of inorganic polymers using silver salts in combination of tri- and diphosphorus species is barely reported[160, 166, 180] even though attempts have already been made.[271-273] Besides the aforementioned reference,[180] no crystal structures are present in the literature containing a single silver atom hexa- or pentabound to phosphorus atoms. In this double boon of discoveries, polymers **29** and **32** are virtually unprecedented. Complexes **29**

and **30** are obtained by slowly layering a solution of CH_2Cl_2 and **27** or **11**, respectively, with a solution of $Ag^+(CF_3SO_3)^-$ in CH_3CN. Similarly, **31** and **32** are obtained by layering a cold solution (0 °C) of CH_2Cl_2 and **11** or **28**, respectively, with a solution of $Ag^+(PF_6)^-$ (in the case of **31**, 0 °C). Crystallization is obtained for **29** and **30** by slow evaporation of the solvent under reduced pressure and **30** is additionally cooled to 0 °C in a dark environment whereas **31** and **32** are crystallized by cooling (0 °C) in a dark environment without concentration.

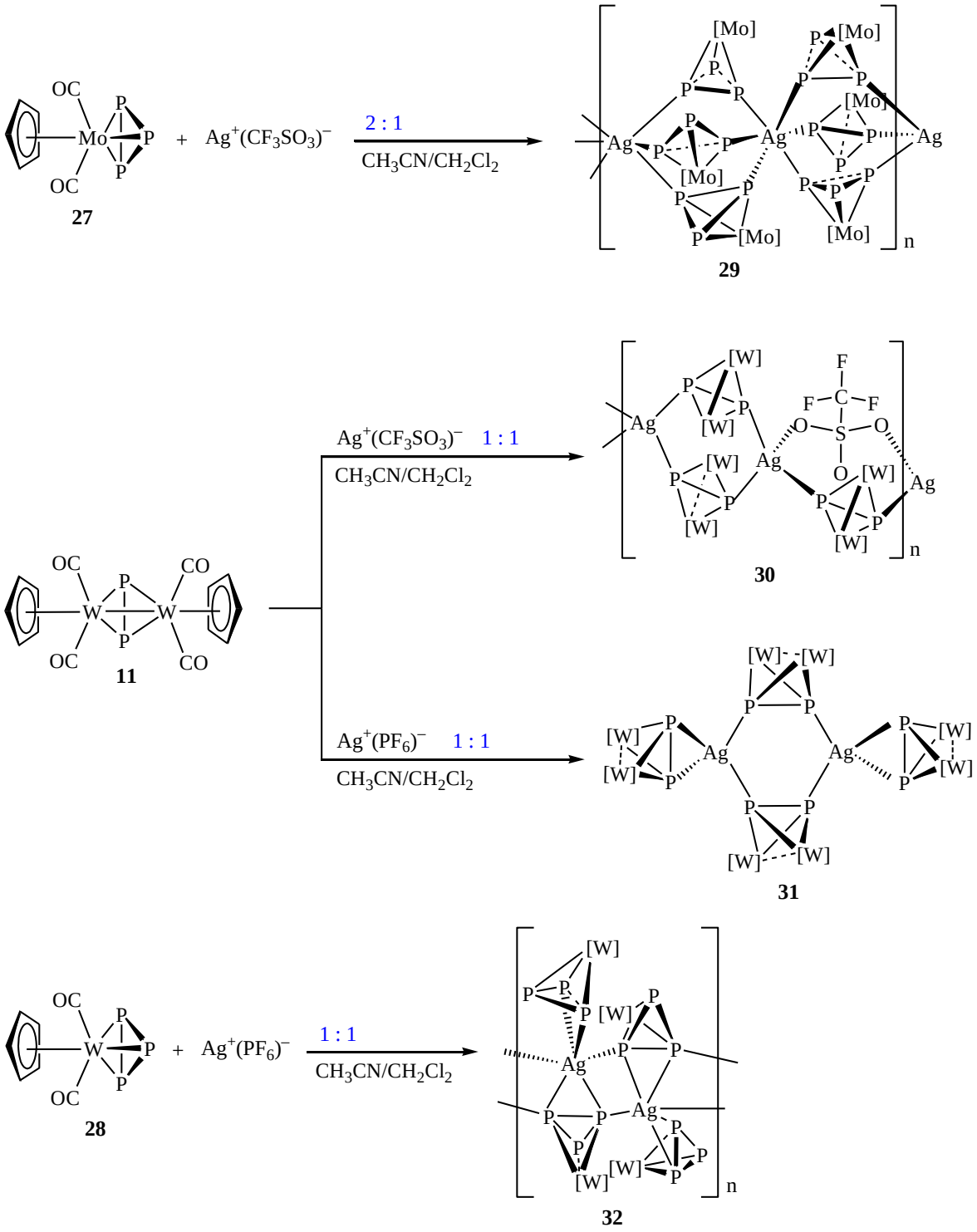

Scheme 9. Syntheses of **29**, **30**, **31**, and **32**.

Complex **27** is synthesized by a known reaction,[154] however, it is not previously characterized by single crystal X-ray diffraction. The solid-state projection (Figure 52) shows tungsten bound to two carbonyl groups, cyclopentadienyl, and the electron-rich cyclotriphosphorus. It is readily soluable in CH_2Cl_2 but moderately soluable in toluene and pentane.

X-ray Data Collection for **27**. A yellow, plate having approximate dimensions of 0.240 x 0.120 x 0.030 mm, was mounted on a Goniometer Xcalibur diffractometer. All intensity measurements were performed using the omega scans method (λ = 1.54184 Å) with a graphite crystal incident beam monochrometer. Cell constants were obtained from a Full-matrix least-squares on F^2.

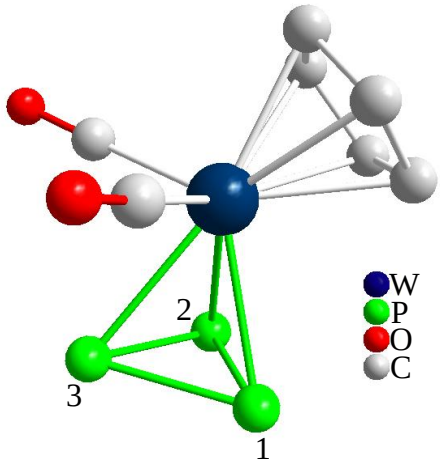

Figure 52. Solid-state projection of $C_7H_5O_2P_3W$ (**27**). Hydrogen atoms are removed for clarity. Selected bond lengths (Å) and angles (°): P1–P2 2.1578(18), P2–P3 2.1480(23), P1–P3 2.1522(21), P1–P2–P3 59.978(71), P1–P3–P2 60.238(73), P2–P1–P3 59.784(72).

Complexes **29**–**32** possess carbonyl and cyclopentadienyl substituents oriented in opposite directions just as in the original starting materials. Polymer **29** is eclipsed perfectly along the z-axis and exhibits a C_3 rotation. If one were to ignore the orientations of the carbonyl and cyclopentadienyl groups, a higher order, S_6 symmetry would be assigned, however, the orientation of these groups is different from every second silver atom. The center AgP_6 configurations of each unit are pseudooctahedral from the angular distortion (up to 10°) caused by the steric effects of the MoP_3 subunits. There are also two sets of facially oriented Ag–P bonds that are noteworthy because of their differences in length (2.6574(16) and 2.7945(12) Å). The longer bond is on the same side as the Cp ring in all cases and is, therefore, a result of increased steric influence. On the other hand the P–P bond distances and P–P–P angles (60 ± 1°) are identical to all the other subunits, and the average P–P bond length is only slightly elongated (0.01 Å) in comparison to the unbound subunit[138] as a result of electron donation to silver. The Ag1–P1 bond length (2.7945(15) Å) is longer than any of the tetrahedral structures reported[166, 271-280] and is, in fact, legit because the polymer chain would not exist without it.

The second polymer, **32**, composed of analogous WP_3 subunits and silver salts, ($Ag^+PF_6^-$) is a true testament to the unpredictable behavior and structure produced. This structure has no higher symmetry other than its identity. Even though each silver atom is

consistently bound to one phosphorus atom on two subunits and two atoms on two subunits, the subunits themselves disrupt the consistent pattern of the polymer. The subunits are inconsistently bound to 1, 2, or 3 silver atoms, but the pattern for each numerical instance is fixed. For example, a subunit bound to one silver has two phosphorus atoms creating two different Ag–P bonds; a subunit bound to two silver atoms bind two phosphorus atoms to one silver atom and one to the other silver atom; and finally a subunit bound to three silver atoms has two bonds to one silver involving two phosphorus atoms and the same two phosphorus atoms have one bond each to two other silver atoms while the third phosphorus of the subunit remains unbound. The subunits 1–3 possess 2 short (2.145–2.161 Å), which are similar in length to the unbound unit, and 1 long (2.220–2.238 Å) P–P bond lengths and the fourth possesses 2 long and 1 short bond lengths whereas the previously mentioned complex **29** has only shorter (2.126–2.155 Å) P–P bond lengths. The complementary silver-phosphorus bond lengths are also exact for each identical subunit. Several Ag–P bond lengths (Ag1–P2, Ag1–P5, Ag1–P10, Ag2–P7) are longer (≥2.79 Å) than the range previously reported by tetrahedral structures[166, 271-280] and complexes **30** and **31** all contain Ag–P bond lengths which are well within this preestablished range (2.34–2.77 Å). These extraordinary bond lengths are a result of poor metal orbital overlap caused by the constrained P–Ag–P bond angles with the exception of Ag1–P10 which is a result of steric hindrance.

Polymer **30** has an array of syndiotactically arranged triflate groups imbedded in the backbone of the structure tethering two silver atoms together by means of two oxygen atoms. Each of these Ag–O bonds differ in length (2.3870(136) Å and 2.4851(205) Å) and reflect the difference in the two distinct sets of Ag_2P_4 rings. The O–S–O bond angle is affected by this as each of the angles are different from each other and the largest of these angles is the O21CS–O22 (132 °). The backbone of this polymer shows that every other Ag_2P_4 ring is consistently pointing down and the other is pointed up and is accompanied by a difference in P–P (2.100(4) and 2.084(6) Å) and Ag–P (Ag1–P1 2.477(3), Ag1–P2 2.437(3) Ag2–P5 2.497(4), Ag2–P6 2.459(4) Å) bond lengths whereas the triflate containing rings have the same P–P and Ag–P bond lengths throughout the entire structure. The three sets of P–P (2.092(5) Å) lengths have an average bond length that is practically identical to the P–P (2.095(2) Å) bond length of the unbound unit. Each of the seven-atom, triflate-containing rings are indeed not flat, however, both of the chemically different six-atom Ag_2P_4 rings are as observed from their angle summations (720°). The pseudotetrahedrally bound silver atoms orient each adjacent ring perpendicular to the latter in the chain, and amid all of these patterns this structure has no higher symmetry other than its identity.

Complex **31** is a single molecule with a nearly flat Ag_2P_4 core (angle summation 718°). The core has a mirror plane perpendicular to the ring bisecting the two silver atoms and the side units have a C_2 rotation, but the entire molecule itself has no symmetry other than its identity. The P–P bond lengths around the ring (2.1063(21) Å) are similar to those in the rings of polymer **30** as well as the unbound unit, and they are shorter (0.05 Å) than the units outside the ring. The inner silver-phosphorus bonds (Ag1–P3 2.4714(17) Å and Ag1–P4 2.4819(13) Å) are shorter than those of the external ones (Ag1–P1 2.6874(13) Å and Ag1–P2 2.6085(16) Å). This evidence suggests that the relatively elongated Ag–P bonds are a result of steric strain on the metal bonding orbitals as the P–P bond constrains the P–Ag–P angle. With an electronic effect, withdrawn electron density would be expected to contribute, strengthen, and ultimately shorten the Ag–P bonds. This pattern is also noted for the molybdenum analog.[166] The pseudotetrahedral structure of the silver atoms places the P–P bond of the side unit not in a right angle, but closer to 45° instead.

X-ray Data Collection for **29**. A yellow, hexagonal column having approximate dimensions of 0.238 x 0.048 x 0.032 mm, was mounted on an Oxford Diffraction Gemini Ultra diffractometer. All intensity measurements were performed using the omega scan method (λ = 1.5418 Å) with a graphite crystal incident beam monochrometer. Cell constants were obtained from a Full-matrix least-squares on F^2.

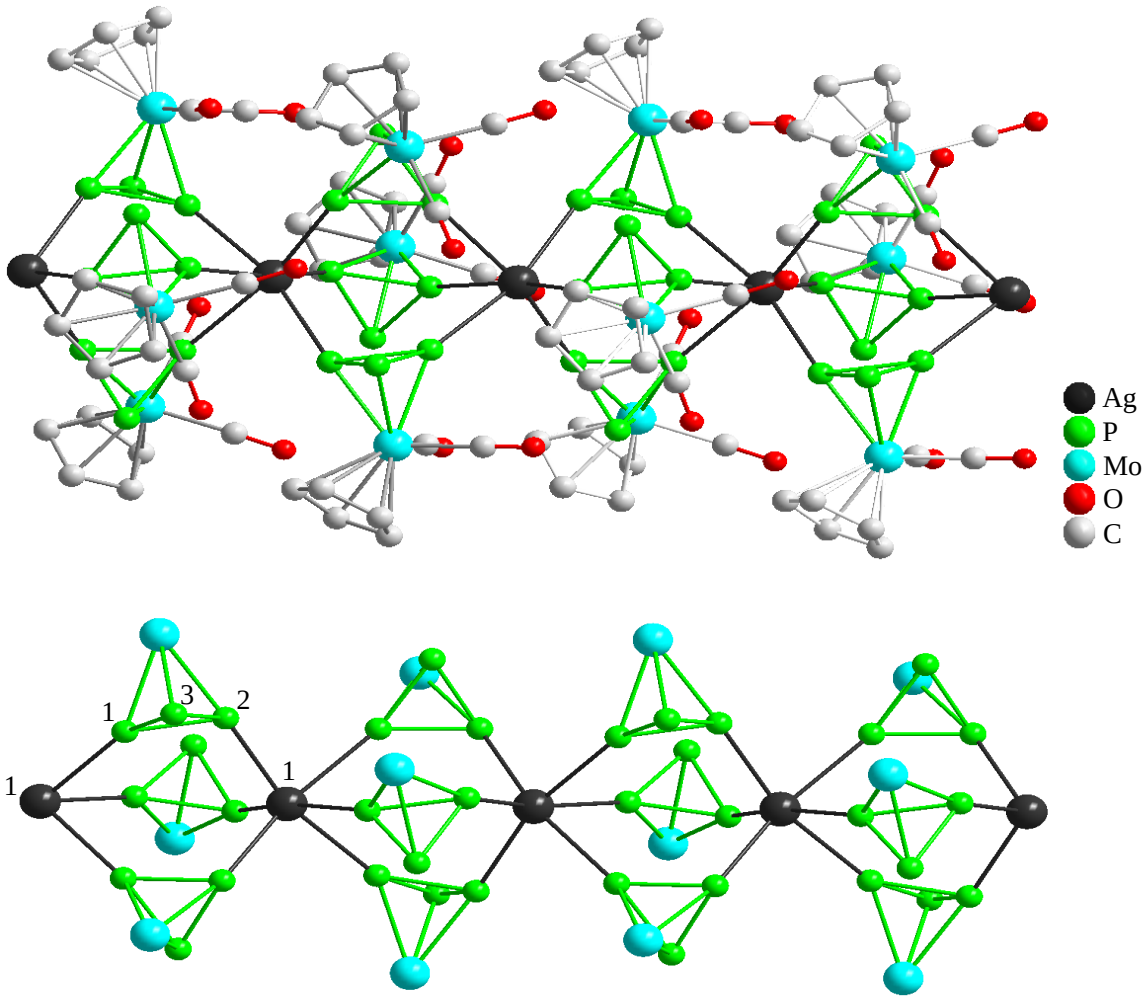

Figure 53. Top: Solid-state projection of $C_{21}H_{15}AgMo_3O_6P_9$ (**29**). Bottom: Backbone of the solid-state projection of $C_{21}H_{15}AgMo_3O_6P_9$ with the exclusion of Cp and CO groups. Triflate counterions and hydrogen atoms are removed for clarity. Selected bond lengths (Å) and angles (°): P1–P2 2.1263(15), P2–P3 2.1553(21), P1–P3 2.1409(19), Ag1–P1 2.7945(15), Ag1–P2 2.6574(11), P1–P2–P3 59.997(56), P2–P1–P3 60.675(57), P1–P3–P2 59.328(64).

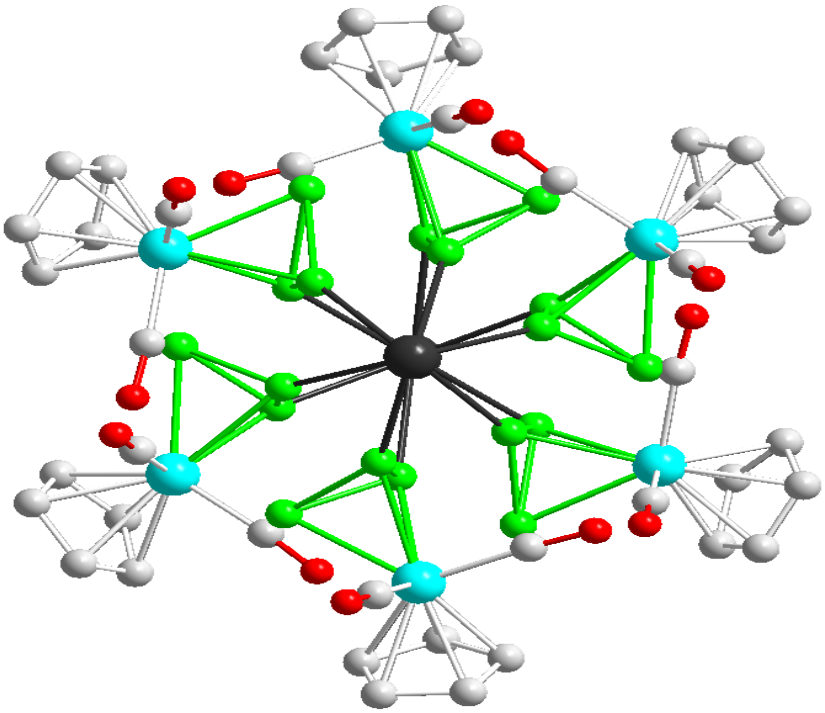

Figure 54. Side view down the crystallographic y-axis of **29**.

X-ray Data Collection for **30**. A red, parallelepiped having approximate dimensions of 0.130 x 0.080 x 0.050 mm, was mounted on an Oxford Diffraction Gemini Ultra diffractometer. All intensity measurements were performed using the omega scan method (λ = 1.5418 Å) with a graphite crystal incident beam monochrometer. Cell constants were obtained from a Full-matrix least-squares on F^2.

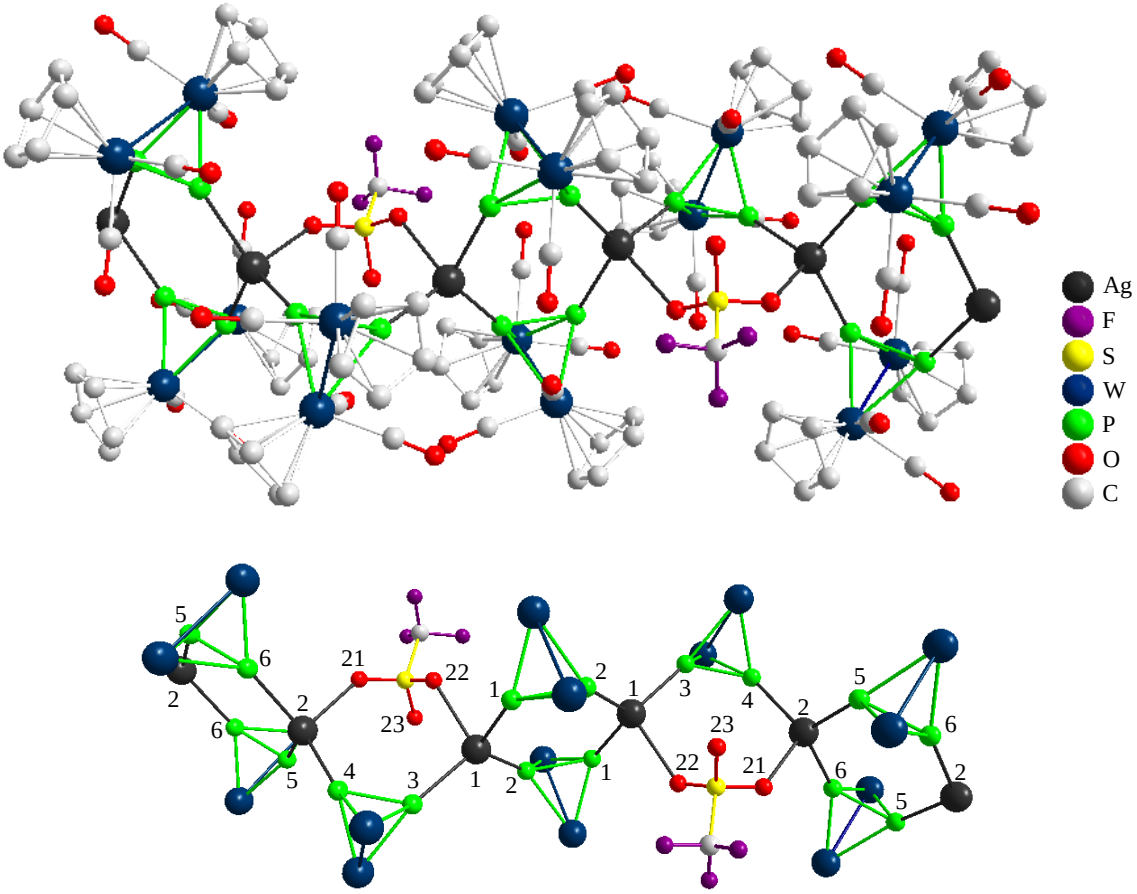

Figure 55. Top: Solid-state projection of $C_{42}H_{30}Ag_2O_{12}P_6W_6$ (**30**). Bottom: Backbone of the solid-state projection of $C_{42}H_{30}Ag_2O_{12}P_6W_6$ with the exclusion of Cp and CO groups. Triflate counterions, acetonitrile units, and hydrogen atoms are removed for clarity. Selected bond lengths (Å) and angles (°): P1–P2 2.1002(44), P3–P4 2.0912(45), P5–P6 2.0837(50), Ag1–P1 2.4766(33), Ag1–P2 2.4365(33), Ag1–P3 2.4549(32), Ag2–P4 2.4424(32), Ag2–P5 2.4965(40), Ag2–P6 2.4591(36), Ag1–O22 2.4851(205), Ag2–O21 2.3870(136), S1–O21 1.3776(140), S1–O22 1.2910(221), S1–O23 1.5388(150), P1–Ag1–P2 116.596(112), P3–Ag1–O22 102.878(382), P4–Ag2–O21 111.690(338), P5–Ag2–P6 119.357(129), O21–S1–O23 100.205(865), O22–S1–O23 110.743(1016), O21–S1–O22 131.734(1062).

X-ray Data Collection for **31**. A red, prism having approximate dimensions of 0.433 x 0.286 x 0.181 mm, was mounted on an Oxford Diffraction Gemini Ultra diffractometer. All intensity measurements were performed using the omega scan method (λ = 0.71073 Å) with a graphite crystal incident beam monochrometer. Cell constants were obtained from a Full-matrix least-squares on F^2.

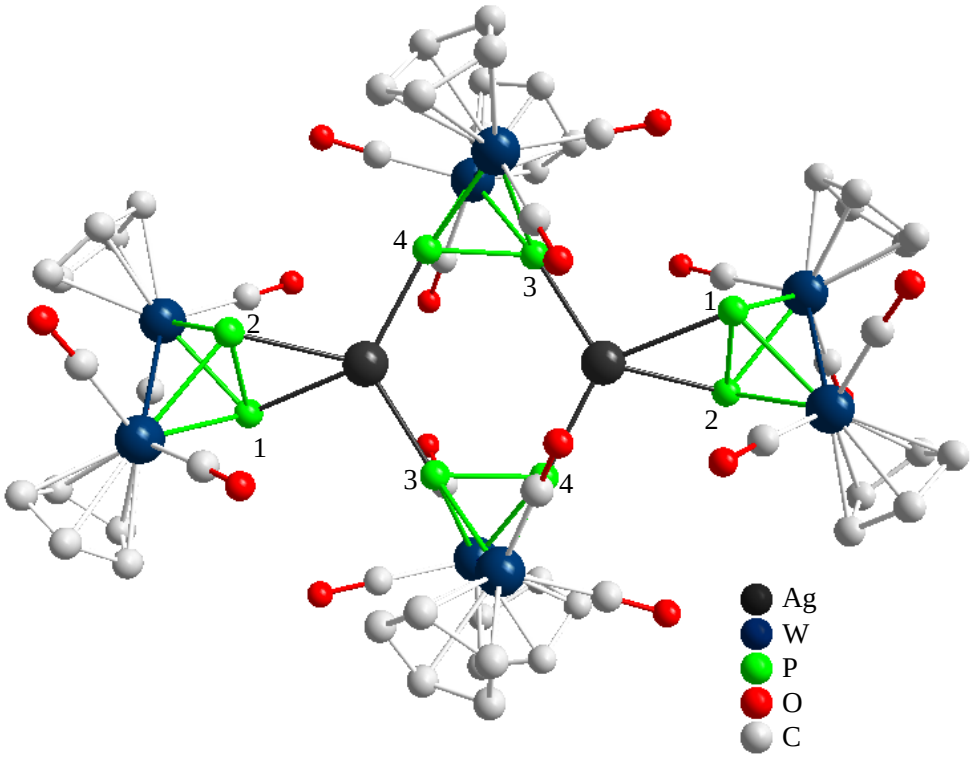

Figure 56. Solid-state projection of $C_{56}H_{40}Ag_2O_{16}P_8W_8$ (**31**). PF_6^- counterions, acetonitrile, dichloromethane, and hydrogen atoms are removed for clarity. Selected bond lengths (Å) and angles (°): P1–P2 2.1611(18), P3–P4 2.1063(21), Ag1–P1 2.6874(13), Ag1–P2 2.6085(16), Ag1–P3 2.4714(17), Ag1–P4 2.4819(13), P1–Ag1–P2 48.139(47), P3–Ag1–P4 120.214(47).

X-ray Data Collection for **32**. A yellow, plate having approximate dimensions of 0.244 x 0.081 x 0.017 mm, was mounted on an Oxford Diffraction Gemini Ultra diffractometer. All intensity measurements were performed using the omega scan method (λ = 1.5418 Å) with a graphite crystal incident beam monochrometer. Cell constants were obtained from a Full-matrix least-squares on F^2.

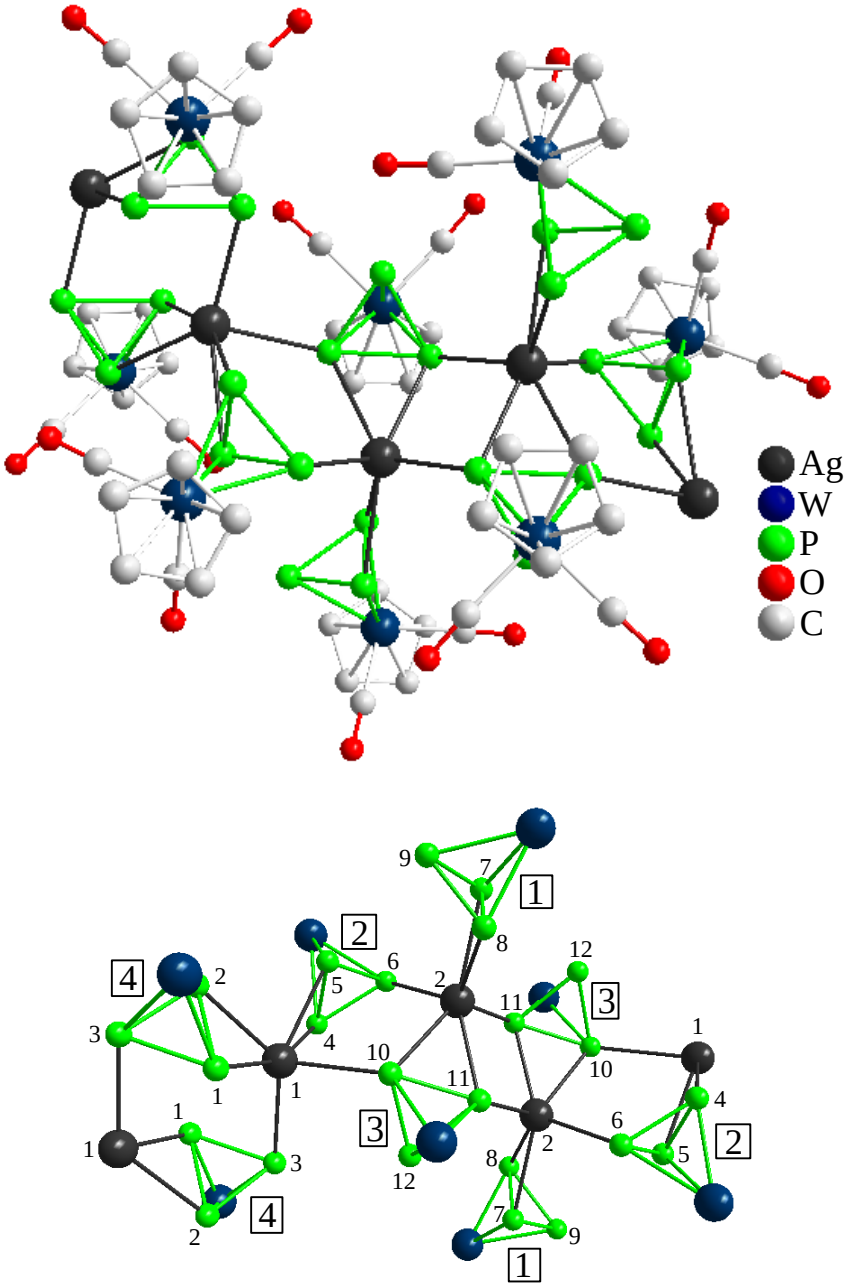

Figure 57. Top: Solid-state projection of $C_{28}H_{20}Ag_2O_8P_{12}W_4$ (**32**). Bottom: Backbone of the solid-state projection of $C_{28}H_{20}Ag_2O_8P_{12}W_4$ with the exclusion of Cp and CO groups, the large numbers in boxes show identical subunits. PF_6^- counterions and hydrogen atoms are removed for clarity. Selected bond lengths (Å) and angles (°): P1–P2 2.2217(21), P2–P3 2.1399(33), P1–P3 2.2166(24), P4–P5 2.2384(24), P5–P6 2.1606(28), P4–P6 2.1503(33), P7–P8 2.2196(26), P8–P9 2.1531(24), P7–P9 2.1521(30), P10–P11 2.2322(25), P11–P12 2.1541(34), P10–P12 2.1445(26), Ag1–P1 2.6554(19), Ag1–P2 2.7963(17), Ag1–P3 2.6401(22), Ag1–P4 2.6243(18), Ag1–P5 2.7946(22), Ag1–P10 2.8417(18), Ag2–P6 2.6535(16), Ag2–P7 2.7892(23), Ag2–P8 2.6033(22), Ag2–P10 2.7662(23), Ag2–P11 2.6826(20), P1–P2–P3 61.057(86), P1–P3–P2 61.294(83), P2–P1–P3 57.65(8), P4–P5–P6 58.494(79), P4–P6–P5 62.562(84), P5–P4–P6 58.944(82), P7–P8–P9 58.941(93), P7–P9–P8 62.070(95), P8–P7–P9 58.989(91), P10–P11–P12 58.505(85), P10–P12–P11 62.569(93), P11–P10–P12 58.926(84), P1–Ag1–P2 48.013(48), P4–Ag1–P5 48.671(55), P7–Ag2–P8 48.460(65), P10–Ag2–P11 48.510(63).

Other phenomena are detected in solution-state, low-temperature ^{31}P NMR of complexes **29** and **32.** Complex **30** is not soluble enough to conduct low temperature ^{31}P NMR in CD_2Cl_2 or CD_2Cl_2/THF, and complex **31** is not soluble enough in CD_2Cl_2, THF, DMSO, or CD_3Cl to perform any solution-state NMR at room temperature or low temperature. One peak is detected at room temperature for **29** in the solution and solid-state ^{31}P NMR**,** and at low temperature solution-state (–120 °C) there are two signals that integrate two to one. At this temperature the electronic resonance about the silver-phosphorus bonds is slower than the radio frequency pulse of the ^{31}P NMR and the two chemically inequivalent phosphorus atoms are discernable. The two bound to silver are represented by the larger of the two peaks (–386.0 ppm) and the unbound is represented by the smaller (–301.3 ppm). A single peak representing the resonance is also detected at room temperature for **32** and then disappears at temperatures –40 to –80 °C; it reappears again at –100 °C 32 ppm upfield from the other measurements while other peaks become more visible at lower temperatures. Three other prominent peaks include a doublet, a triplet, and a septet. The resonance of the phosphorus atoms on subunits 2, 3, and 4 is uninterrupted as the temperature is lowered. The doublet represents the two unbound phosphorus atoms on subunit 1 resulting from silver being bound to only one phosphorus atom, and the unbound phosphorus on subunit 3 is detected by the triplet. The severed bond is most likely the Ag2–P7 since it is the weaker of the two (2.7892(23) Å). This effect is apparent at 0 °C and is the most distinct at –20 °C. The PF_6^- counter anion is not detected in the ^{19}F NMR, but it is detected in the ^{31}P NMR as a septet, and the triflate anion for **29** and **30** is also detectable.

Diagnostic ^{31}P NMR studies conducted at room temperature show little differences in comparison to the unbound units. Complexes **29** and **32** show very little differences in their chemical shifts and the peaks are still singlets; complex **30** also shows a singlet, but it is relatively shielded (about 31 ppm) perhaps by the differences in dielectric constants of the solvent. The IR is also consistent for all the silver complexes with their corresponding unbound units showing two peaks in the carbonyl region.

The ^{31}P MAS-NMR spectrum for **30** (Figure 60) is reported in spite of the insufficient solubility for low temperature solution-state ^{31}P NMR experiments. A few assumptions must be made on the account that only two peaks are detected. It is understood that the polymer dilutes the difference in sensitivity of the different phosphorus atoms as noted by the 1:1 integration of the two peaks and, of course, the lack of others. The phosphorus atoms P1, P2, P5, and P6 are represented at –268 ppm because their positions in identical subunits and because of the relatively greater shielding caused from the smaller P···π electron distance of the oxygen atoms. The remaining P3 and P4 are less proximal and, thus, downfield (–201 ppm).

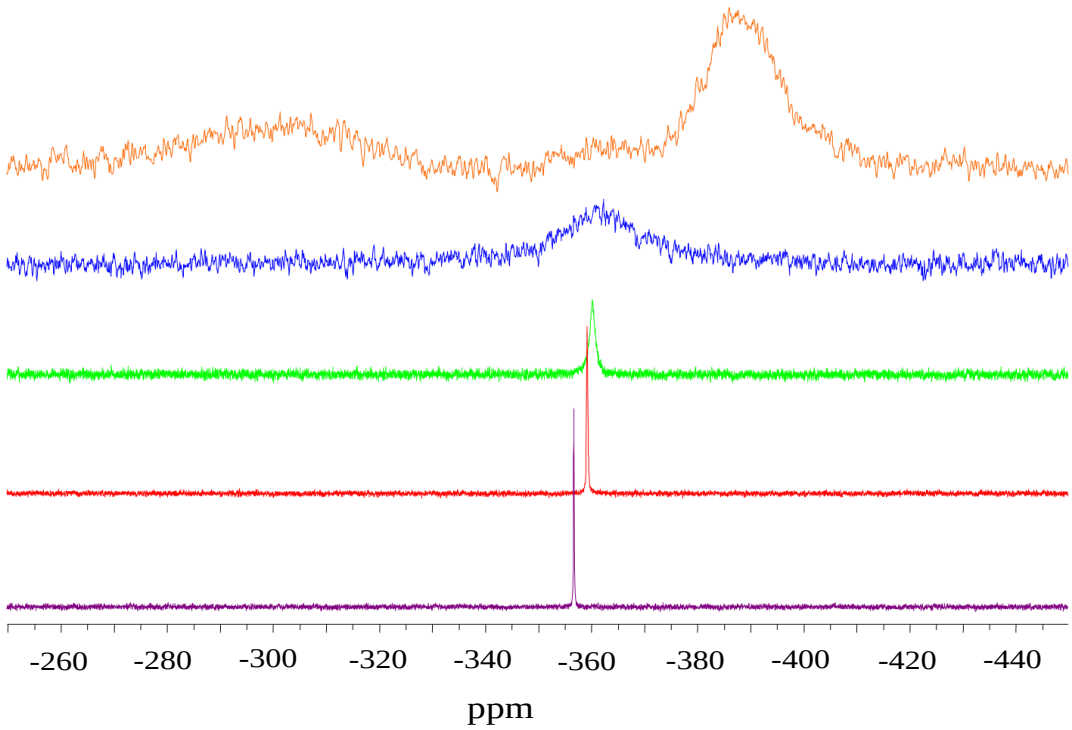

Figure 58. Variable temperature $^{31}P\{^{1}H\}$ NMR spectra of **29** in THF-d_8/CH_2Cl_2 (3:1); From bottom to top: **27**, **0**, **–40**, **–80**, **–120** °C.

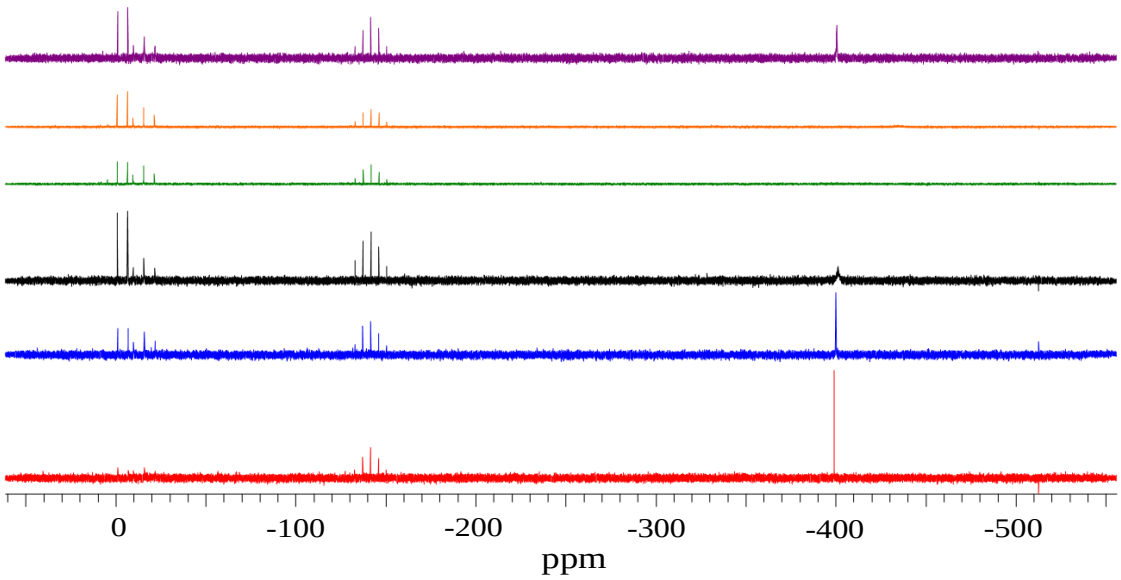

Figure 59. Variable temperature $^{31}P\{^{1}H\}$ NMR spectra of **32** in THF-d_8/CH_2Cl_2 (3:1); From bottom to top: **27**, **0**, **–20**, **–40**, **–80**, **–100** °C.

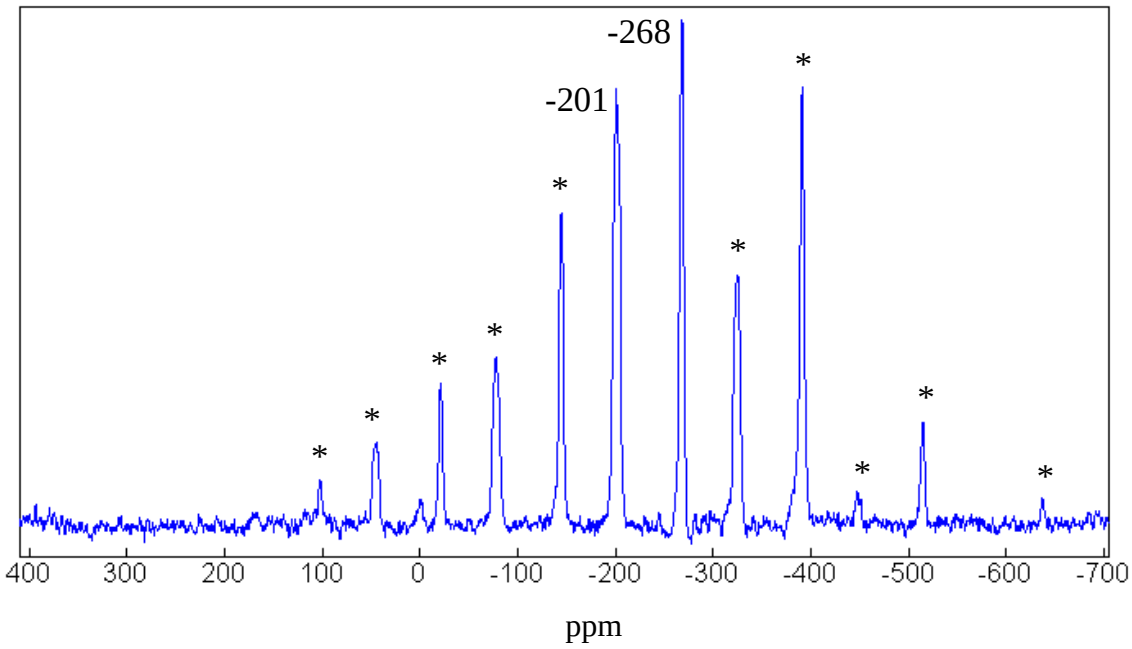

Figure 60. ^{31}P MAS-NMR spectrum for **30** (161.9 MHz, spinning frequency 23 kHz, RT). The asterisks mark the sidebands.

Astonishingly, the MoP_3 subunit remains in one piece throughout the analysis of the positive ESI-MS for complex **29** in CH_3CN and CH_2Cl_2/CH_3CN solutions, and every species has at least on silver atom bound to it. The triflate anion is the only species detected in the negative ion ESI-MS. The positive ion ESI-MS for **30** is not as populated, but every species in the CH_3CN and CH_2Cl_2/CH_3CN solutions also contains the unscathed starting material, W_2P_2, bound to at least one equivalent of silver. Triflate is detected in the negative ion ESI-MS with the one example of the intact W_2P_2 subunit bond to triflate in the CH_3CN solution.

Analogous complexes with the $Ag^+PF_6^-$ salt are not as robust; not all cases have a silver bound to the complex and the subunits are vulnerable to deterioration. Complex **31** does contain deteriorated isolated and silver bound species, but also shows the tendency to lose CO (most commonly 2) and also to breakdown to the more stable tungstenhexacarbonyl. The counterion (PF_6^-) also shows a great binding affinity for CH_3CN as depicted in the negative ESI-MS and in one instance is bound to silver and the deteriorated subunit. Complex **32** is markedly more robust under positive ESI-MS showing only two instances of carbonyl loss and every species except for one is accompanied by silver. Only the counterion (PF_6^-) is detected in the negative ESI-MS.

2.4. Phosphorus Free Monomers

Research related to structures containing a WCl_5 unit is largely motivated by the development of tungsten-nitrogen bonds for the characterization of catalytic intermediates.[54, 230, 281-295] Incidentally, this pursuit also includes tungsten bound to thio,[296] oxo,[297-303] and alkyne[54, 304-307] groups, however, no instance of a tungsten-cyclopentadienyl connection is proven by X-ray crystallography. $WCp^*Cl_5(SbCl_3)_3$ (**33**) is synthesized by layering a cold (0 °C) tungstencyclotriphosphorus (**28**)/CH_2Cl_2 solution with an antimonypentachloride (**11**)/CH_2Cl_2 solution. Two chlorides from each equivalent of **11** are ionically exchanged to tungsten reducing antimony +5 to its more stable +3 formal charge (Scheme 9). The destination of phosphorus is unknown, but it was not included in the product, therefore, the

side-product is not of interest for full characterization. Since the exchange of chloride is so rampant and the yield is not ideal (~35.7%, relative to $SbCl_5$) it is possible that PCl_X is created.

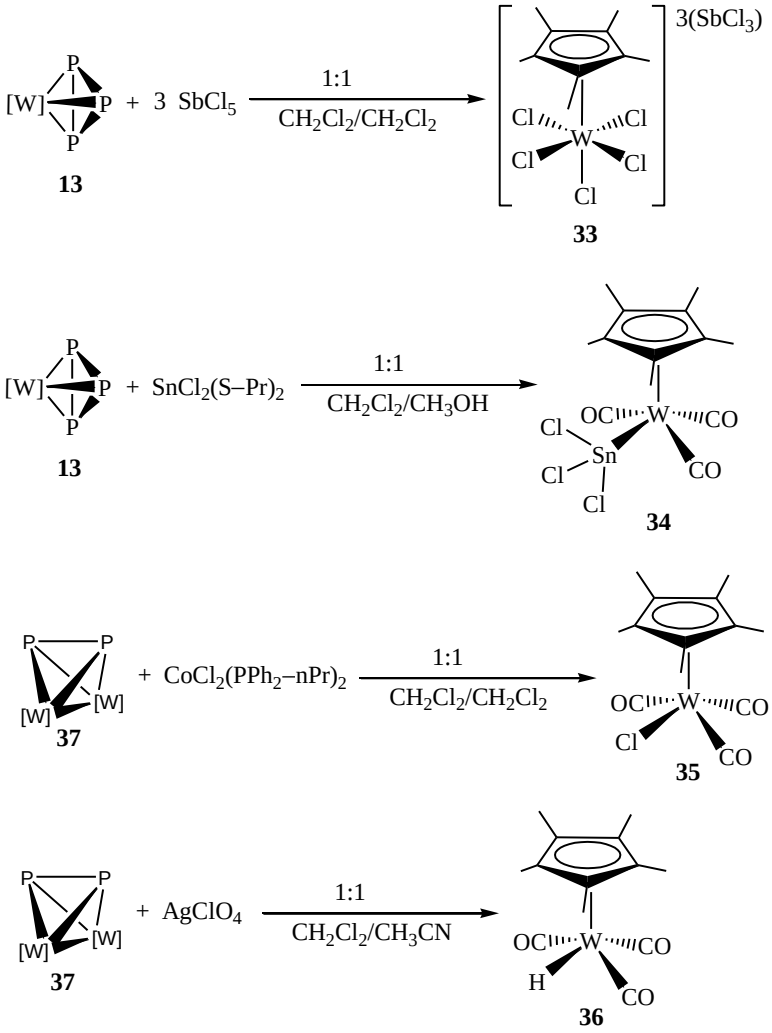

Scheme 9. Synthesis of **33**, **34**, **35**, **36**. [W] = $W(CO)_2Cp^*$.

X-ray Data Collection for **33**. A red-brown, prism having approximate dimensions of 0.220 x 0.170 x 0.100 mm, was mounted on an Oxford Diffraction Gemini Ultra diffractometer. All intensity measurements were performed using the omega scan method (λ = 0.71073 Å) with a graphite crystal incident beam monochrometer. Cell constants were obtained from a Full-matrix least-squares on F^2.

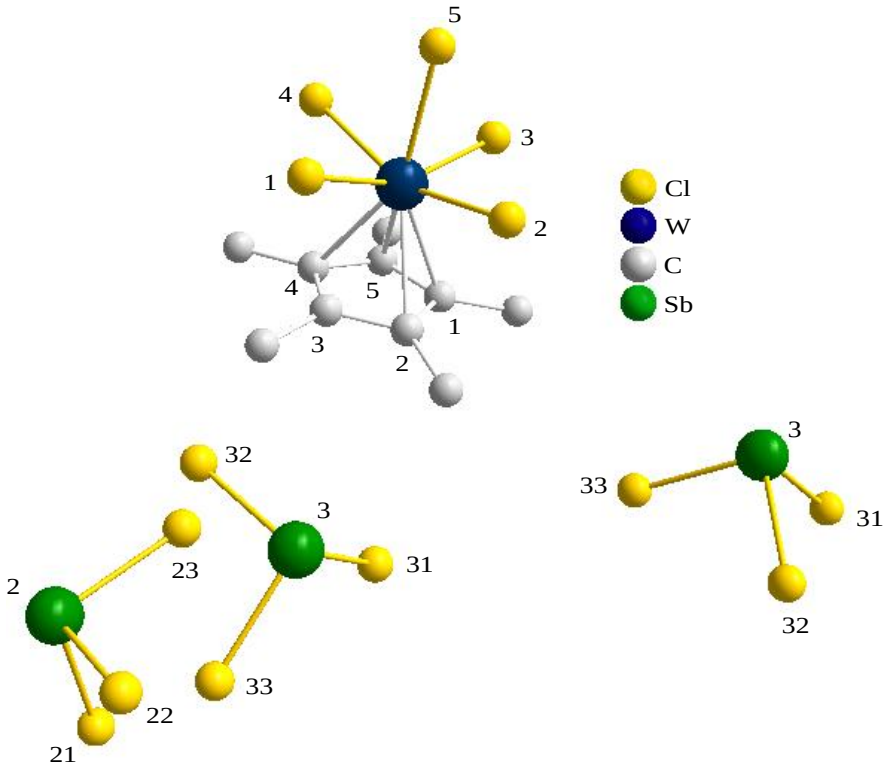

Figure 61. Solid-state projection of $C_{10}H_{15}Cl_5W(Cl_3Sb)_3$ (**33**). Hydrogen atoms are removed for clarity. Selected bond lengths (Å) and angles (°): W–Cl1 2.3644(6), W–Cl2 2.3310(7), W–Cl3 2.3426(7), W–Cl4 2.3751(7), W–Cl5 2.4826(7), W–C1 2.4057(29), W–C2 2.4663(30), W–C3 2.4929(31), W–C4 2.4624(32), W–C5 2.4158(30), Sb3–Cl31 2.3849(8), Sb3–Cl32 2.3700(8), Sb3–Cl33 2.3479(9), Sb2–Cl21 2.3896(8), Sb2–Cl22 2.3757 (8), Sb2–Cl23 2.3457(9). Cl5–W–Cl1 78.560(24), Cl5–W–Cl2 78.035(25), Cl5–W–Cl3 77.363(23), Cl5–W–Cl4 77.907(24).

There are many striking structural deviations in **33** shown by the X-ray projection. Perhaps the most obvious is the angle constriction (11.4–12.6°) of the equatorial chloride ligands from the ideal 90° caused by the steric hindrance from the Cp*. Second, the W–C bonds distances of the Cp* ligand vary (2.4057(29)–2.4929(31) Å). This is a direct result of the proximal alignment of the equatorial chloride ligands as the carbons closer to these chloride ligands are elongated greater. The electron density of the lone pair stored in the P_Z orbital of the chloride obviously donates to an antibonding orbital of the W–C bond (t_{1u} (σ*)), and, accordingly, weakens the W–C bond. If this were purely only an electronegative effect, the inner ring C–C bonds would also be significantly distorted, which is not true in this case. This donation does not vary the related equatorial W–Cl bond lengths in the same way, however, the axial W–Cl is drastically elongated (0.108–0.152 Å) in comparison and is caused from Jahn-Teller distortion (Figure 62). To avoid unequal occupation of the e_g (σ*) and the t_{2g} binding orbitals, the structure of **33** distorts separating the x^2-y^2 (b_{1g}) and z^2 (a_{1g}) binding orbitals (formerly e_g) as well as the *xz* (e_g) and *yz* (e_g) orbitals from the *xy* (b_{2g}) orbital (formerly t_{2g}). With the loss of degeneracy, the newly formed e_g binding orbital is, thus, completely and equally occupied.

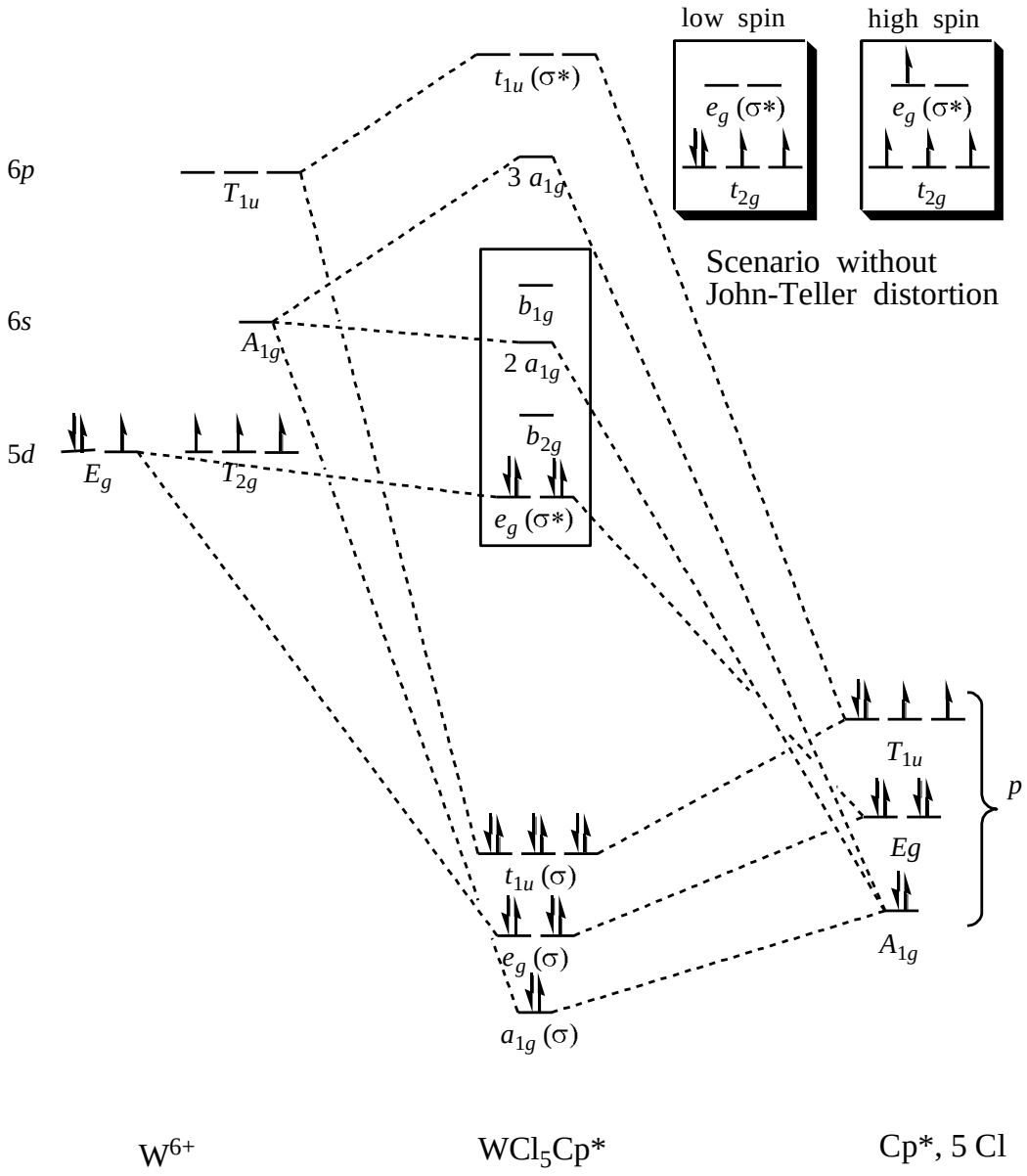

Figure 62. Molecular orbitals (σ) for **33** under the influence of Jahn-Teller distortion. Symmetry labels of the atomic orbitals are capitalized and the labels of the molecular orbitals are in lower case. π orbitals are omitted for clarity. Adapted from Messler and Tarr's "Inorganic Chemistry 2nd Ed.".[216]

Complexes proven by single crystal X-ray diffraction containing a W–Sn–Cl motif are common in the literature and some examples are very similar in comparison (Table 9).[308-312] In comparison to the known complexes in the literature, **34** has the shortest W–Sn bond length which is directly dictated by the π donor or acceptor ability of the substituent connected to Sn. Throughout all of the examples tungsten is consistently bound to 3 highly π accepting carbonyls and tin is bound to one slightly π donating Cl^-. The first three examples are the shortest because of the highest population of the π donating Cl^- groups for R'', and R' serves as a control by possessing organic substituents, yet, it is interesting to note that the Cp substituent is relatively more π accepting than the Cp*. The next two examples have a longer W–Sn bond length as the chloride substituent count is reduced to two and R' remains constant and, as a result, the *t*-Bu and $Os_3(CO)_{12}Cl$ substituents have little difference in π acceptor

abilities. Nevertheless, the last entry also has the same R' value, but the W–Sn bond is the longest since the $PhCN(Me)_2$ group is a stronger π acceptor than the Cl^- is a π donor, thus the net effect is a π acceptor ligand. The second and third to the last examples also embody the greater π accepting abilities of the Cp ligand in comparison to the Cp* ligand.

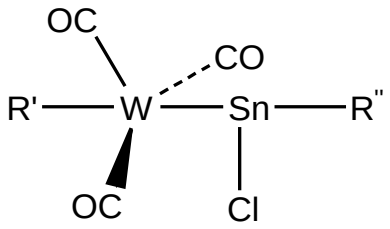

R'	R''	W–Sn bond length (Å)
Cp*	Cl, Cl	2.7034(5)
$((Me)CNN(CO)_2PhCp$	Cl, Cl	2.7138(9)
Cp	Cl, Cl	2.7244(3)
Cp	Cl, *t*-Bu	2.7518(6)
Cp	Cl, $Os_3(CO)_{12}Cl$	2.7557(68)
Cp*	Me, Me	2.7865(3)
Cp	Bu, Bu	2.7960(5)
Cp	Cl, $PhCN(Me)_2$	2.8204(3)

Table 9. Closely related complexes and their substituents' effect on the W–Sn bond lengh.[308-312]

Complexes **34**, **35**, and **36** show the same differences of W–C bond lengths associated with the Cp* ligand because of electron donation of different carbonyls, and electron withdrawing effects of $SnCl_3$, chloride, and hydrogen ligands. As previously mentioned, the carbonyl group has an effect, but it is smaller than the heteroligands which effect the W–C elongation in the following order H>Cl>$SnCl_3$. The $SnCl_3$ ligand has the largest inductive force of electron withdrawal as the threefold presence of chloride accentuates the electronegativity. The tungsten then becomes more positive and withdraws more electron density from the Cp* group causing the W–C bond to possess greater electron density. Another consideration is the steric hindrance of the ligand (cone angle = 118°) could also cause the W–C bond to lengthen. Elimination of tin to a pure chloride ligand contains no cone angle and a lesser electron withdrawal effect. Consequently, this creates a longer W–C bond. The final and most effective ligand is the hydride, which is too small and near to tungsten to be formally detected by X-ray diffraction, however, the similarity of the OC–W–CO angles with the other complexes certainly confirms its presence. It has no electron withdrawing capacity and, thus, the largest W–C bond is present. The movement of electron density away from the W–C bond causes an increase of electron density in the Cp* ring and the C–C bonds of the rings are shortened as the W–C bonds are lengthened.

X-ray Data Collection for **34**. A clear crystal having approximate dimensions of 0.125 x 0.105 x 0.026 mm, was mounted on an Oxford Diffraction Gemini Ultra diffractometer. All intensity measurements were performed using the omega scan method (λ = 1.54178 Å) with a graphite crystal incident beam monochrometer. Cell constants were obtained from a Full-matrix least-squares on F^2.

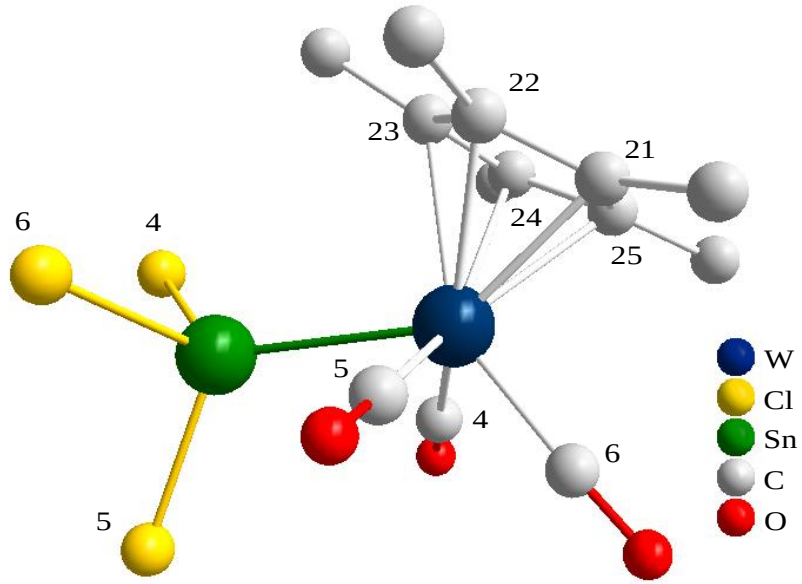

Figure 63. Solid-state projection of $C_{13}H_{15}Cl_3O_3SnW$ (**34**). Hydrogen atoms are removed for clarity. Selected bond lengths (Å) and angles (°): Sn–Cl4 2.3543(16), Sn–Cl5 2.3532(17), Sn–Cl6 2.3532(18), Sn–W 2.7034(5), W–C21 2.2813(67), W–C22 2.3305(56), W–C23 2.3630(61), W–C24 2.3517(64), W–C25 2.2944(68). Sn–W–C5 75.404(195), Sn–W–C4 73.910(193), C5–W–C6 77.467(268), C6–W–C4 79.327(265). $SnCl_3$ cone angle = 118°.

X-ray Data Collection for **35**. A clear crystal was mounted on an Oxford Diffraction Gemini Ultra diffractometer. All intensity measurements were performed using the omega scan method (λ = 1.54178 Å) with a graphite crystal incident beam monochrometer. Cell constants were obtained from a Full-matrix least-squares on F^2.

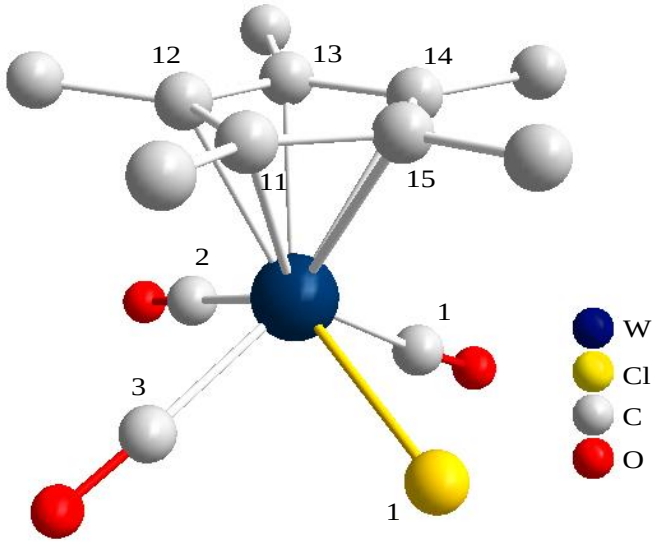

Figure 64. Solid-state projection of $C_{13}H_{15}ClO_3W$ (**35**). Hydrogen atoms are removed for clarity. Selected bond lengths (Å) and angles (°): W–Cl1 2.4995(8), W–C11 2.3294(11), W–C12 2.2950(9), W–C13 2.3021(7), W–C14 2.3671(7), W–C15 2.4079(10). Cl1–W–C1 79.001(13), C1–W–C2 79.222(12), C2–W–C3 77.737(13), C3–W–C1 78.178(11).

X-ray Data Collection for **36**. A clear crystal was mounted on an Oxford Diffraction Gemini Ultra diffractometer. All intensity measurements were performed using the omega scan method (λ = 1.54184 Å) with a graphite crystal incident beam monochrometer. Cell constants were obtained from a Full-matrix least-squares on F^2.

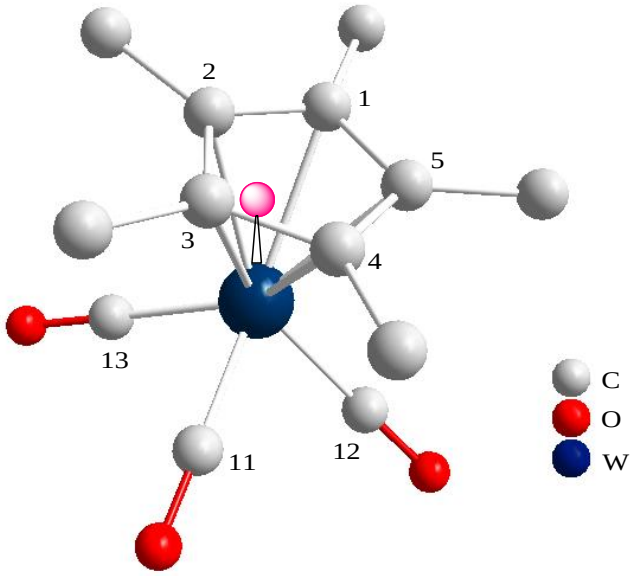

Figure 65. Solid-state projection of $C_{13}H_{15}O_3W$ (**36**). The pink atom marks the position of the undetected hydrogen atom. Hydrogen atoms are removed for clarity. Selected bond lengths (Å) and angles (°): W–C1 2.4108(0), W–C2 2.3704(0), W–C3 2.3097(0), W–C4 2.3090(0), W–C5 2.3783(0). C13–W–C11 77.808(0), C11–W–C12 77.591(0).

III. Experimental

3.1. General Remarks

3.1.1. Atmosphere and Solvents

All manipulations are performed using standard Schlenk and dry-box techniques under an atmosphere of nitrogen or argon. All solvents are degassed and distilled from appropriate drying agents under an atmosphere of dry, oxygen-free nitrogen prior to use. CH_2Cl_2 and CH_3CN is distilled from CaH_2. Pentane, hexane, toluene, xylene, and THF is distilled from K/benzophenone. All deuterated solvents are degassed and stored over molecular sieves, which had previously been dried for several hours under high vacuum at 200 °C.

3.1.2. Starting Materials

The following reactants are acquired commercially (company) and stored under an inert atmosphere as received: Cp (Aldrich), $AgSO_3CF_3$ (Fluka), $AgPF_6$ (Aldrich), CuCl (Strem), CuBr (Strem), and CuI (Aldrich). The complexes **3**, **27**,[177, 270] **4**,[313] **5**, **7**,[314, 315] **6**, **8**,[314, 315] **9**,[316] and **11**[219] as well as compounds Cp*,[317, 318] NaCp,[177] and ^{t}BuCp[319] are synthesized from known methods.

3.1.3. Characterization Methods

The melting points are measured with mercury and recorded on a Büchi, SMP-20 and are uncorrected. The infrared spectroscopy is recorded on a Varian, Scimitar FTS 800. These instruments are provided by the work group of professor doctor Manfred Scheer.

Elemental analyses are performed on an Elementar, Vario EL III and the electrospray ionization is performed with a Thermo Quest Finnigan TSQ 7000. All nuclear magnetic resonance spectra are recorded on a Bruker AVANCE-400 NMR spectrometer. Samples are referenced against TMS (^{1}H, ^{13}C), $CFCl_3$ (^{19}F), and 85% H_3PO_4 (^{31}P) as external standards. Chemical shifts are reported in ppm, according to the δ-scale, and the coupling constants J in Hz. The NMR spectra are processed using the 1D-WINNMR program. All X-ray crystallographic analyses are performed by the X-ray crystallography department of the University of Regensburg. The data were collected on an Oxford Diffraction Gemini Ultra or Goniometer Xcalibur CCD diffractometer. The structures are solved using either SIR-97[320]or SHELXS-97[321] and refined using SHELXL-97[321] with anisotropic displacements for non-hydrogen atoms. Hydrogen atoms are located in idealized positions and refined isotropically according to the riding model. Pictorial representations of the structures are generated using the Diamond program.[322] These instruments and services are provided by the University of Regensburg Central Analytic Department.

The solid-state ^{31}P MAS-NMR spectra of compounds **22**–**24** and **29** were recorded by Dr. Christian Gröger (research group of Prof. Dr. Dr. Kalbitzer, University of Regensburg) on a Bruker AVANCE300 solid-state spectrometer in 2.5 mm probes. All spectra are acquired at 121.50 MHz at spinning rates of 30 kHz, and samples are referenced against NaH_2PO_4 as an external standard. All ^{31}P MAS-NMR simulations were performed on a 2008 version of DMfit.[323]

The solid-state ^{31}P MAS-NMR and ^{65}Cu MAS-NMR spectra of **14**–**16** and **30** were recorded by Dr. Jinjun Ren (research group of Prof. Hellmut Eckert, University of Münster). The solid-state ^{31}P MAS-NMR spectrum of **14**–**16** were recorded on a Bruker DSX500 solid-state spectrometer in 2.5 mm probes. The spectra were acquired at 202.41 MHz using single-pulse acquisition spinning rates of 25 and 30 kHz. A rotor synchronised Hahn spin-echo sequence, generated with 90° pulse lengths of 1.8 μs and relaxation delays of 2 minutes (256 scans), was used to record the spectra. The solid-state ^{31}P MAS-NMR spectrum of **30** was recorded on a Bruker DSX400 solid-state spectrometer in 2.5 mm probes. The spectrum was acquired at 161.90 MHz using single-pulse acquisition spinning rates of 25 and 30 kHz. A rotor synchronised Hahn spin-echo sequence, generated with 90° pulse lengths of 4.4 μs and relaxation delays of 10 minutes (264 scans), was used to record the spectrum. The samples were referenced against 1M H_3PO_4 as an external standard. The ^{65}Cu MAS-NMR spectra of **14**–**16** were recorded on a Bruker DSX500 solid-state spectrometer in 2.5 mm probes. The spectrum was acquired at 142.11 MHz using a single-pulse acquisition spinning rate of 25 kHz. A rotor synchronised Hahn spin-echo sequence, generated with 30° pulse lengths of 1 μs and relaxation delays of 2 seconds (1024 scans), was used to record the spectra. The samples were referenced against CuI as an external standard.

3.2. Protocol

Bis(1*P*,2*P*-bis(dicarbonylcyclopentadienylmolybdenum(I))diphosphorus-κ^2*P*,*P*)bis(dichloroplatinum(II)) (1). A solution of **3** (100 mg, 0.202 mmol) in CH_2Cl_2 (10 mL) is added at room temperature to a solution of **4**, **5**, or **6** (0.202 mmol) in CH_2Cl_2 (10 mL), and the color of the mixture changes from orange into brown instantly. Further stirring for 2 days at 25 °C leads to the formation of the product, which is collected via filtration, washed with CH_2Cl_2 (3 × 5 mL), and dried under vacuum. Single brown X-ray quality crystals are obtained by layering the Mo_2P_2/CH_2Cl_2 solution over a cold (0 °C) **4**, **5**, or **6**/CH_2Cl_2 solution.

Product yield (relative to **3** using **5):** 0.076 g, 49.9%.

M.P.: 147 °C (decomposition).

^{1}H NMR (400.13 MHz, DMSO-d_6, 27 °C): δ = 5.91 (s, 20 H, Cp).

^{13}C{^{1}H} NMR (100.63 MHz, DMSO-d_6, 27 ºC): δ = 218.518 (s, CO), 89.12 (s, Cp).

^{31}P{^{1}H} NMR (161.94 MHz, DMSO-d_6, 27 °C): δ = –123.82 (non, $^1J_{P',P''}$ = 253.2 Hz and $^1J_{P',Pt}$ = 2051.1 Hz; $^1J_{P'',P'}$ = 157.8 Hz and $^2J_{P'',Pt}$ = 1629.3 Hz).

IR (KBr): ν = 3093 (w), 2014 (vs; CO), 1977 (vs; CO), 1632 (w), 1419 (w), 1260 (w), 1071 (w), 1022 (w), 834 (m), 548 (w), 487 (m), 432 (m).

Positive ion EI-MS (CH_3OH, RT): *m/z* (%) = 496.058 (9) $[Cp_2Mo_2(CO)_4P_2]^+$, 439.9 (12) $[Cp_2Mo_2(CO)_2P_2]^+$, 384.0 (41) $[Cp_2Mo_2P_2]^+$, 322.01 (14) $[Pt(CO)_2Cl_2]^+$, 267.1 (3) $[PtCl_2]^+$, 124.1 (100) $[Mo(CO)]^+$.

Elemental analysis: Calculated (%) for $C_{28}H_{20}Mo_4O_8P_4Pt_2Cl_4$ (1693.89): C 21.25, H 1.42; found: C 21.93, H 1.48.

$[Mo_2P_2Cp^*PtCl_2]_2$.

Positive ion ESI-MS (CH_3CN/CH_2Cl_2, + 10 mmol/L $NH_4^+CH_3CO^-$, RT): *m/z* (%) = 653.0 (100) $[Cp^*_2Mo_2(CO)_4P_2NH_4]^+$, 625.1 (75) $[Cp^*_2Mo_2(CO)_3P_2NH_4]^+$, 597.1 (16) $[Cp^*_2Mo_2(CO)_2P_2NH_4]^+$, 569.1 (45) $[Cp^*_2Mo_2(CO)P_2NH_4]^+$.

Negative ion ESI-MS (CH_3CN/CH_2Cl_2, + 10 mmol/L $NH_4^+CH_3CO^-$, RT): *m/z* (%) = 597.9 (34) $[(NH_4)_{10}(CH_3CO)_4Cl_7]^-$, 179.0 (64) $[NH_4Cl(CH_3CO)(CH_3CN)_2]^-$, 133.1 (16) $[NH_4(CH_3CO)_2CO]^-$.

Positive ion EI-MS (CH_3OH, RT): *m/z* (%) = 578.2 (6) $[Cp^*_2Mo_2(CO)_2P_2]^+$, 526.2 (38) $[Cp^*_2Mo_2P_2]^+$, 496.3 (100) $[Cp^*_2Mo_2P]^+$, 458.3 (73) $[Pt_2Cl_2]^+$, 265.2 (37) $[PtCl_2]^+$.

Bis(1*P*,2*P*-bis(dicarbonylcyclopentadienylmolybdenum(I))diphosphorus-κ^2*P*,*P*)bis(dichloropaladium(II)) (2). A cold (0 °C) solution of **7** (61 mg, 0.202 mmol) in CH_2Cl_2 (10 mL) is layered with a solution of **3** (100 mg, 0.202 mmol) in CH_2Cl_2 (10 mL), and the color of the solution turns dark instantly. After about one week small brown X-ray quality crystals are formed. Substitution of **7** with **8** yields the same structure.

Product yield (relative to 3): 0.057 g, 42.3%.

M.P.: 151 °C (decomposition).

^{1}H NMR (400.13 MHz, DMSO-d_6, 27 °C): δ = 5.98 (s, 20 H, Cp).

^{13}C{^{1}H} NMR (100.63 MHz, DMSO-d_6, 27 ºC): δ = 225.93 (s, CO), 86.47 (s, Cp).

^{31}P{^{1}H} NMR (161.98 MHz, DMSO-d_6, 27 °C): δ = 0.086 (s), –43.09 (s), –84.26 (s).

IR (KBr): ν = 2963 (w), 1950 (s, CO), 1908 (s, CO), 1417 (w), 1261 (s), 1095 (s), 1020 (s), 910 (w), 863 (w), 799 (s), 741 (w), 690 (w), 568 (m), 531 (m), 498 (m), 463 (m), 449 (m).

Positive ion EI-MS (CH_3OH, RT): *m/z* (%) = 496.1 (10) $[Cp_2Mo_2(CO)_4P_2]^+$, 440.1 (21) $[Cp_2Mo_2(CO)_2P_2]^+$, 412.1 (6) $[Cp_2Mo_2(CO)P_2]^+$, 384.2 (72) $[Cp_2Mo_2P_2]^+$, 355.1 (14) $[Pd_2Cl_4]^+$, 330.1 (12) $[MoPd(CO)_2Cl_2]^+$, 319.3 (10) $[Pd_2Cl_3]^+$, 205.3 (38) $[Pd(CO)Cl_2]^+$, 124.2 (100) $[Mo(CO)]^+$.

Positive ion ESI-MS (CH_3CN/CH_2Cl_2, RT): *m/z* (%) = 1184.7 (22) $[Cp_2Mo_2(CO)_2P_2Pd_3(CH_3CN)_9]^+$, 1151.6 (13) $[Cp_2Mo_2(CO)_2P_2Pd_5(CH_3CN)_3]^+$, 1053.6 (17) $[Cp_2Mo_2(CO)_2P_2Pd(CH_3CN)_{11}]^+$, 807.3 (13) $[Cp_2Mo_2(CO)_2P_2Pd(CH_3CN)_5]^+$, 583.2 (72) $[Pd_2(CH_3CN)_9]^+$, 542.2 (100) $[Pd_2(CH_3CN)_8]^+$, 501.1 (79) $[Pd_2(CH_3CN)_7]^+$, 454.3 (36) $[Pd_4(CH_3CN)]^+$.

Negative ion ESI-MS (CH_3CN/CH_2Cl_2, RT): *m/z* (%) = 531.0 (72) $[(PdCl_2)_3]^-$, 513.0 (86) $[MoCl_6(CH_3CN)_5]^-$, 459.0 (35) $[PdCl_3(CH_3CN)_6]^-$, 421.3 (39) $[Mo_2Cl_3(CH_3CN)_3]^-$, 391.0 (26) $[MoCl_6(CH_3CN)_2]^-$, 372.3 (100) $[PdCl_4(CH_3CN)_3]^-$, 294.1 (54) $[PdCl_3(CH_3CN)_2]^-$.

Elemental analysis: Calculated (%) for $C_{28}H_{20}Mo_4O_8P_4Pd_2Cl_4$: C 24.97, H 1.50; found: C 24.98, H 1.52.

$[Mo_2P_2Cp^*PdCl_2]_2$.

Positive ion ESI-MS (CH_3CN/CH_2Cl_2, + 10 mmol/L $NH_4^+CH_3CO^-$, RT): *m/z* (%) = 1338.8 (3) $[\{Cp^*_2Mo_2(CO)_2P_2\}_2PdCl_2]^+$, 676.0 (25) $[Cp^*_2Mo_2(CO)_4P_2CH_3CN]^+$, 631.9 (51) $[Cp^*_2Mo_2(CO)_5P]^+$, 603.9 (100) $[Cp^*_2Mo_2(CO)_4P]^+$, 569.0 (62) $[Cp^*_2Mo_2(CO)P_2+NH_4]^+$.

Negative ion ESI-MS (CH_3CN/CH_2Cl_2, + 10 mmol/L $NH_4^+CH_3CO^-$, RT): *m/z* (%) = 599.9 (16) $[(NH_4)_{10}(CH_3CO)_4Cl_7]^-$, 454.9 (100) $[Pd_2Cl_6CO]^-$, 222.9 (54) $[NH_4Cl(CH_3CO)(CH_3CN)_3]^-$, 179.0 (85) $[NH_4Cl(CH_3CO)(CH_3CN)_2]^-$, 133.1 (19) $[NH_4(CH_3CO)_2CO]^-$.

Bis(1*P*,2*P*-bis(dicarbonylcyclopentadienylmolybdenum(I))diphosphorus-κ^2*P,P*)bis(tetracarbonyltungsten(0)) (10). A solution of **3** (100 mg, 0.202 mmol) in THF (5 mL) is layered with a solution of $W(CO)_5$THF (**9**) in THF (0.028 M, 7.2 mL). The solution is concentrated and cooled to 5 °C giving maroon-brown X-ray quality crystals.

Product yield (relative to 3): 0.133 g, 76.2%

M.P.: 145–148 °C (decomposition).

^{1}H NMR (400.13 MHz, CD_2Cl_2, 27 °C): δ = 5.32 (s, 20 H, Cp), 3.68 (m, THF), 1.82 (m, THF).

^{13}C{^{1}H} NMR (100.63 MHz, CD_2Cl_2, 27 ºC): δ = 191.43 (s, CO), 87.25 (s, Cp), 68.15 (s, THF), 25.98 (s, THF).

^{31}P{^{1}H} NMR (161.95 MHz, CD_2Cl_2, 27 °C): δ = –43.12.

^{31}P{^{1}H} NMR (CD_2Cl_2/THF (3:1), 161.98 MHz, 27 °C): δ = –41.63 (s).

^{31}P{^{1}H} NMR (CD_2Cl_2/THF (3:1), 161.98 MHz, 0 °C): δ = –41.79 (s).

^{31}P{^{1}H} NMR (CD_2Cl_2/THF (3:1), 161.98 MHz, –40 °C): δ = –41.63 (s).

^{31}P{^{1}H} NMR (CD_2Cl_2/THF (3:1), 161.98 MHz, –80 °C): δ = –43.11 (s), –51.42 (d, P', $J_{P',P''}$ = 503.99 Hz), –106.01 (d, P'', $J_{P'',P'}$ = 503.99 Hz).

^{31}P{^{1}H} NMR (CD_2Cl_2/THF (3:1), 161.98 MHz, –110 °C): δ = –44.20 (s), –52.66 (d, P', $J_{P',P''}$ = 477.11 Hz), –109.53 (d, P'', $J_{P'',P'}$ = 477.11 Hz).

IR (KBr): ν = 3447 (br), 2964 (s), 1983 (s, CO), 1944 (s, CO), 1417 (w), 1262 (s), 1097 (s), 1022 (s), 866 (w), 801 (s), 703 (w), 575 (m), 459 (w) cm^{-1}.

Positive ion EI-MS (CH_2Cl_2, RT): *m/z* (%) = 819.6 (6) $[Cp_2Mo_2(CO)_9P_2W]^+$, 789.5 (2) $[Cp_2Mo_2(CO)_8P_2W]^+$, 763.6 (4) $[Cp_2Mo_2(CO)_7P_2W]^+$, 734.6 (3) $[Cp_2Mo_2(CO)_6P_2W]^+$, 679.6 (7) $[Cp_2Mo_2(CO)_4P_2W]^+$, 651.6 (26) $[Cp_2Mo_2(CO)_3P_2W]^+$, 623.9 (9) $[Cp_2Mo_2(CO)_2P_2W]^+$, 595.8 (9) $[Cp_2Mo_2(CO)P_2W]^+$, 567.7 (52) $[Cp_2Mo_2(CO)_4P_2(THF)]^+$ or $[Cp_2Mo_2P_2W]^+$, 537.8 (16) $[Cp_2Mo_2(CO)_3P_2(THF)]^+$, 495.8 (13) $[Cp_2Mo_2(CO)_4P_2]^+$, 439.8 (23) $[Cp_2Mo_2(CO)_2P_2]^+$,

412.9 (3) $[Cp_2Mo_2(CO)P_2]^+$, 381.9 (72) $[Cp_2Mo_2P_2]^+$, 353.8 (17) $[Mo(CO)_4(THF)_2]^+$, 351.9 (51) $[W(CO)_6]^+$, 268.0 (100) $[W(CO)]^+$, 240.0 (33) $[W(CO)_2]^+$, 212.0 (32) $[W(CO)]^+$, 207.1 (41) $[Mo(CO)_4]^+$, 151.1 (15) $[Mo(CO)_2]^+$.

Positive ion ESI-MS (CH_2Cl_2/CH_3CN, RT): *m/z* (%) = 1584.9 (8) $[Cp_4Mo_4(CO)_{16}P_4W_2]^+$, 1405.8 (16) $[Cp_3Mo_4(CO)_{12}P_4W_2]^+$, 820.0 (31.3) $[Cp_2Mo_2(CO)_9P_2W]^+$, 680.6 (100) $[Cp_2Mo_2(CO)_4P_2W]^+$.

Elemental analysis: Calculated (%) for $C_{36}H_{20}Mo_4O_{16}P_4W_2(C_4H_8O)_2$: C 30.58, H 2.10; found: C 29.90, H 2.24.

Bis(1*P*,2*P*-bis(dicarbonylcyclopentadienyldiphosphorustungsten(I))-κ^2*P*,*P'*)bis(tetracarbonyltungsten(0)) (12). A solution of **11** (0.050 g, 0.074 mmol) in THF (5 mL) is layered with a solution of $W(CO)_5THF$ in THF (0.028 M, 2.7 mL). The solution is concentrated and cooled to 5 °C for 7 days giving X-ray quality maroon-brown crystals.

Product yield (relative to 11): 0.059 g, 77.2%

M.P.: 155–160 °C (decomposition).

^{1}H NMR (400.13 MHz, CD_2Cl_2, 27 °C): δ = 5.32 (s, 20 H, Cp), 3.68 (m, THF), 1.84 (m, THF).

^{13}C{^{1}H} NMR (100.63 MHz, CD_2Cl_2, 27 ºC): δ = 191.78 (s, CO), 84.25 (s, Cp), 68.28 (s, THF), 25.98 (s, THF).

^{31}P{^{1}H} NMR (161.98 MHz, CD_2Cl_2, 27 °C): δ = –152.45.

^{31}P{^{1}H} NMR (CD_2Cl_2/THF (3:1), 161.98 MHz, 27 °C): δ = –151.21 (s).

^{31}P{^{1}H} NMR (CD_2Cl_2/THF (3:1), 161.98 MHz, 0 °C): δ = –151.04 (s).

^{31}P{^{1}H} NMR (CD_2Cl_2/THF (3:1), 161.98 MHz, –20 °C): δ = –115.89 (s), –151.01 (s).

^{31}P{^{1}H} NMR (CD_2Cl_2/THF (3:1), 161.98 MHz, –40 °C): δ = –115.86 (s), –151.21 (s).

^{31}P{^{1}H} NMR (CD_2Cl_2/THF (3:1), 161.98 MHz, –80 °C): δ = –115.86 (s), –151.21 (s), –212.77 (d, P', $J_{P',P''}$ = 454.82 Hz).

^{31}P{^{1}H} NMR (CD_2Cl_2/THF (3:1), 161.98 MHz, –100 °C): δ = –141.00 (d, P'', $J_{P'',P'}$ = 456.69 Hz), –152.69 (s), –214.41 (d, P', $J_{P',P''}$ = 456.69 Hz).

^{31}P{^{1}H} NMR (CD_2Cl_2/THF (3:1), 161.98 MHz, –110 °C): δ = –141.15 (d, P'', $J_{P'',P'}$ = 454.56 Hz), –152.98 (s), –215.04 (d, P', $J_{P',P''}$ = 454.56 Hz).

^{31}P{^{1}H} NMR (CD_2Cl_2/THF (3:1), 161.98 MHz, –120 °C): δ = –141.32 (d, P'', $J_{P'',P'}$ = 479.12 Hz), –153.11 (s), –215.62 (d, P', $J_{P',P''}$ = 479.12 Hz).

IR (KBr): ν = 3115 (w), 2963 (m), 2359 (w), 1999 (s), 1916 (s), 1417 (w), 1261 (s), 1095 (s), 1020 (s), 799 (s), 703 (w), 593 (w), 566 (m), 523 (m), 451 (m) cm^{-1}.

Positive ion ESI-MS (CH_3CN, RT): *m/z* (%) = 1406.2 (100) $[Cp_4W_5(CO)_7P]^+$.

Negative ion ESI-MS (CH_3CN, RT): *m/z* (%) = no peak.

Positive ion ESI-MS (CH_2Cl_2/CH_3CN, RT): *m/z* (%) = 1746.2 (13) $[Cp_3W_6(CO)_{16}]^+$, 1703.0 (8) $[Cp_4W_6(CO)_{11}P]^+$, 1451.0 (45) $[Cp_4W_4(CO)_{13}P]^+$, 1406.2 (100) $[Cp_4W_5(CO)_7P]^+$.

Negative ion ESI-MS (CH_2Cl_2/CH_3CN, RT): *m/z* (%) = 1057.7 (63) $[Cp_2W_3(CO)_9P_4]^-$, 703.0 (100) $[Cp_2W_2(CO)_5P_2]^-$,

Elemental analysis: Calculated (%) for $C_{36}H_{20}Mo_4O_{16}P_4W_2(C_4H_8O)$: C 23.93, H 1.41; found: C 24.36, H 1.49.

1*Cl*,2*Cl*-bis(dicarbonyl(pentamethylcyclopentadienyl)cyclotriphosphanotungsten(0)-κ^2*P*,*P'*copper(I))-μ-dichloride (14). A solution of **13** (0.050 g, 0.161 mmol) in CH_2Cl_2 (10 mL) is layered with a solution of CuCl (0.032 g, 0.322 mmol) in CH_3CN (10 mL) and placed in a dark environment for 2 days at 22 °C. The contents are filtered with a fritted filter, concentrated, layered with pentane (2 mL), and cooled to 5 °C giving yellow plate-like X-ray quality crystals.

Product yield (relative to 13): 0.035 g, 38.3%.

M.P.: 95–97 °C (decomposition).

^{1}H NMR (400.13 MHz, $CDCl_3$, 27 °C): δ = 2.20 (s, 20 H, Cp*), 2.00 (s, 10 H, Cp*).

^{13}C{^{1}H} NMR (100.63 MHz, $CDCl_3$, 27 ºC): δ = 220.46 (s, CO), 106.54 (s, Cp* (C)), 11.54 (s, Cp* (CH_3)).

^{31}P{^{1}H} NMR (161.95 MHz, CD_2Cl_2, 27 °C): δ = –374.91 (s, P_3).

^{31}P{^{1}H} NMR (THF-d_8/CH_2Cl_2 (2:1), 161.98 MHz, 27 °C): δ = –375.08 (s).

^{31}P{^{1}H} NMR (THF-d_8/CH_2Cl_2 (2:1), 161.98 MHz, 0 °C): δ = –376.80 (s).

^{31}P{^{1}H} NMR (THF-d_8/CH_2Cl_2 (2:1), 161.98 MHz, –40 °C): δ = no signal.

^{31}P{^{1}H} NMR (THF-d_8/CH_2Cl_2 (2:1), 161.98 MHz, –80 °C): δ = –407.25 (s).

^{31}P{^{1}H} NMR (THF-d_8/CH_2Cl_2 (2:1), 161.98 MHz, –120 °C): δ = –313.16 (b), –406.97 (b).

Solid-state ^{31}P MAS-NMR (202.41 MHz, 27 °C): δ = –290 (s, 1 P), –392 and –399 (s, 2 P).

Solid-state ^{65}Cu MAS-NMR (142.11 MHz, 27 °C): δ = –4.0 and –12.2 (s).

IR (KBr): ν = 2963 (w), 1996 (s, CO), 1923 (s, CO), 1477 (m), 1451 (m), 1381 (m), 1261 (s), 1096 (s), 1028 (s), 867 (w), 800 (s), 704 (s), 558 (w), 574 (m), 506 (m), 449 (s), 451 (m), 418 (m) cm^{-1}.

Positive ion ESI–MS (CH_3CN, RT): *m/z* (%) = 1046.7 (9) $[Cu_5Cl_5\{Cp^*W(CO)_2P_3\}(CH_3CN)_2]^+$, 978.9 (10) $[Cu_5Cl_5\{Cp^*W(CO)_2P_3\}CH_3CNNH_4]^+$, 947.2 (20) $[Cu_4Cl_4\{Cp^*W(CO)_2P_3\}(CH_3CN)_2]^+$, 879.2 (15) $[Cu_4Cl_4\{Cp^*W(CO)_2P_3\}NH_4]^+$, 824.2 (70) $[Cu_3Cl_3\{Cp^*W(CO)_2P_3\}CH_3CNNH_4]^+$, 781.1 (12) $[Cu_3Cl_3\{Cp^*W(CO)_2P_3\}NH_4]^+$, 624.1 (21) $[CuCl\{Cp^*W(CO)_2P_3\}CH_3CNNH_4]^+$, 608.2 (48) $[CuCl\{Cp^*W(CO)_2P_3\}CH_3CN]^+$, 585.9 (31) $[CuCl\{Cp^*W(CO)_2P_3\}NH_4]^+$, 567.1 (21) $[CuCl\{Cp^*W(CO)_2P_3\}]^+$, 537.1 (58) $[CuCl\{Cp^*W(CO)P_3\}]^+$, 486.1 (99) $[\{Cp^*W(CO)_2P_3\}NH_4]^+$, 342.7 (98) $[Cu_3Cl_2(CH_3CN)_2]^+$, 244.8 (100) $[Cu_2Cl(CH_3CN)_2]^+$.

Negative ion ESI–MS (CH_3CN, RT): *m/z* (%) = 726.4 (2) $[Cu_7Cl_8]^-$, 628.5 (6) $[Cu_6Cl_7]^-$, 530.6 (47) $[Cu_5Cl_6]^-$, 430.6 (5) $[Cu_4Cl_5]^-$, 332.6 (3) $[Cu_3Cl_4]^-$, 232.7 (6) $[Cu_2Cl_3]^-$, 134.9 (100) $[CuCl_2]^-$.

Elemental analysis: Calculated (%) for $C_{24}H_{30}Cl_2Cu_2O_4P_6W_2$: C 25.42, H 2.67; found: C 25.68, H 2.74.

1*Br*,2*Br*-bis(dicarbonyl(pentamethylcyclopentadienyl)cyclotriphosphanotungsten(0)-κ^2*P,P'*copper(I))-μ-dibromide (15). A solution of **13** (0.050 g, 0.161 mmol) in CH_2Cl_2 (10 mL) is layered with a solution of CuBr (0.046 g, 0.322 mmol) in CH_3CN (10 mL) and placed in a dark environment for 2 days at 22 °C. The contents are filtered with a fritted filter, concentrated, layered with pentane (2 mL), and cooled to 5 °C giving yellow plate-like X-ray quality crystals.

Product yield (relative to 13): 0.063 g, 63.9%

M.P.: 96–100 °C (decomposition).

^{1}H NMR (400.13 MHz, CD_2Cl_2, 27 °C): δ = 2.19 (s, 24 H, Cp*), 1.97 (s, 6 H, Cp*).

^{13}C{^{1}H} NMR (100.63 MHz, CD_2Cl_2, 27 °C): δ = 219.31 (s, CO), 103.91 (s, Cp* (C)), 11.63 (s, Cp* (CH_3)).

^{31}P{^{1}H} NMR (161.95 MHz, CD_2Cl_2, 27 °C): δ = –369.01 (s, P_3).

^{31}P{^{1}H} NMR (THF-d_8/CH_2Cl_2 (2:1), 161.94 MHz, 27 °C): δ = –369.22 (s).

^{31}P{^{1}H} NMR (THF-d_8/CH_2Cl_2 (2:1), 161.94 MHz, 0 °C): δ = –373.42 (s).

^{31}P{^{1}H} NMR (THF-d_8/CH_2Cl_2 (2:1), 161.94 MHz, –40 °C): δ = –383.60 (s).

^{31}P{^{1}H} NMR (THF-d_8/CH_2Cl_2 (2:1), 161.94 MHz, –80 °C): δ = –320.46 (b), –397.25 (b), 403.58 (b)

^{31}P{^{1}H} NMR (THF-d_8/CH_2Cl_2 (2:1), 161.94 MHz, –120 °C): δ = –318.44 (b), –393.15 (b), –406.29 (b).

Solid-state ^{31}P MAS-NMR (202.41 MHz, 27 °C): δ = –295 (s, 1 P), –394 and –402 (s, 2 P).

Solid-state ^{65}Cu MAS-NMR (142.11 MHz, 27 °C): δ = –58.3 and –68.2 (s).

IR (KBr): ν = 2963 (w), 1996 (s, CO), 1925 (s, CO), 1477 (w), 1381 (m), 1261 (s), 1096 (s), 1029 (s), 865 (w), 800 (s), 703 (w), 558 (w), 505 (m), 449 (w) cm^{-1}.

Positive ion ESI-MS ($CH_2Cl_2/CH_3CN/CH_3OH$ + 10 mmol/L $NH_4^+CH_3CO^-$, RT): *m/z* (%) = 1499.5 (8) $[CuBr\{Cp^*W(CO)_2P_3\}_2Cu(CuCH_3CO)_2]^+$, 1283.4 (13) $[CuBr\{Cp^*W(CO)_2P_3\}_2Cu]^+$, 1249.4 (9) $[Cu_2Br\{Cp^*W(CO)_2P_3\}_2(CuCH_3CO)]^+$, 1185.4 (41) $[Cu_2Br\{Cp^*W(CO)_2P_3\}_2CH_3CN]^+$, 947.3 (20) $[\{Cp^*W(CO)_2\}_2(CH_3CN)_2(NH_4)_2Br]^+$, 849.1 (83) $[\{Cp^*W(CO)_2\}_2NH_4(CH_3CN)_2]^+$, 822.1 (40) $[Cu_3Br_3\{Cp^*W(CO)_2\}NH_4]^+$, 488.0 (100) $[\{Cp^*W(CO)_2P_3\}NH_4]^+$.

Negative ion ESI-MS ($CH_2Cl_2/CH_3CN/CH_3OH$ + 10 mmol/L $NH_4^+CH_3CO^-$, RT): *m/z* (%) = 1527.2 (9) $[\{Cp^*W(CO)_2P_3\}_2Cu_2Br_4]^-$, 703.0 (33) $[Br\{Cp^*W(CO)_2P_3\}NH_4(CH_3CO)_2]^-$, 631.1 (59) $[\{Cp^*W(CO)_2P_3\}Br]^-$, 222.7 (100) $[CuBr_2]^-$,

Elemental analysis: Calculated (%) for $C_{24}H_{30}Br_2Cu_2O_4P_6W_2$: C 23.57, H 2.47; found: C 23.40, H 2.49.

1*I*,2*I*-bis(dicarbonyl(pentamethylcyclopentadienyl)cyclotriphosphanotungsten(0)-κ^2*P*,*P*')copper(I))-μ-diiodide (16). A solution of **13** (0.050 g, 0.161 mmol) in CH_2Cl_2 (10 mL) is layered with a solution of CuI (0.062 g, 0.322 mmol) in CH_3CN (10 mL) and placed in a dark environment for 2 days at 22 °C. The contents are filtered with a fritted filter, concentrated, layered with pentane (3 mL), and cooled to 5 °C giving yellow plate-like X-ray quality crystals.

Product yield (relative to 13): 0.076 g, 71.7%

M.P.: 110 °C (decomposition).

^{1}H NMR (400.13 MHz, $CDCl_3$, 27 °C): δ = 2.20 (s, 20 H, Cp*), 2.00 (s, 10 H, Cp*).

^{13}C{^{1}H} NMR (100.63 MHz, $CDCl_3$, 27 ºC): δ = 214.22 (s, CO), 103.30 (s, Cp* (C)), 11.50 (s, Cp* (CH_3)).

^{31}P{^{1}H} NMR (161.94 MHz, $CDCl_3$, 27 °C): δ = –379.14 (s, P_3).

^{31}P{^{1}H} NMR (THF-d_8/CH_2Cl_2 (2:1), 161.98 MHz, 27 °C): δ = –381.17 (s).

^{31}P{^{1}H} NMR (THF-d_8/CH_2Cl_2 (2:1), 161.98 MHz, 0 °C): δ = –382.46 (s).

^{31}P{^{1}H} NMR (THF-d_8/CH_2Cl_2 (2:1), 161.98 MHz, –40 °C): δ = –384.35 (s).

^{31}P{^{1}H} NMR (THF-d_8/CH_2Cl_2 (2:1), 161.98 MHz, –80 °C): δ = no signal.

^{31}P{^{1}H} NMR (THF-d_8/CH_2Cl_2 (2:1), 161.98 MHz, –120 °C): δ = –314.09 (b), –423.68 (b).

Solid-state ^{31}P MAS-NMR (202.41 MHz, 27 °C): δ = –297 (s, 1 P), –404 (s, 2 P).

Solid-state ^{65}Cu MAS-NMR (142.11 MHz, 27 °C): δ = –0.7 and –14.4 (s).

IR (KBr): ν = 2963 (w), 2919 (w), 2361 (w), 1997 (s, CO), 1895 (s, CO), 1479 (w), 1384 (m), 1261 (m), 1095 (s), 1031 (s), 801 (s), 574 (m), 524 (w), 476 (w), 419 (w) cm^{-1}.

Positive ion ESI-MS ($CH_2Cl_2/CH_3CN/CH_3OH$ + 10 mmol/L $NH_4^+CH_3CO^-$, RT): *m/z* (%) = 1301.4 (0.6) $[\{W(CO)_2Cp^*\}_2(CuCH_3CO)_5NH_4]^+$, 1069.2 (1.9) $[\{W(CO)_2Cp^*\}_2(CuCH_3CO)_3]^+$, 907.1 (1.4) $[\{W(CO)_2Cp^*\}(CuCH_3CO)_5]^+$, 733.2 (82) $[\{W(CO)_2Cp^*\}Cu_2INH_4(CH_3CO)_2]^+$, 719 (16) $[\{W(CO)_2Cp^*\}(NH_4CH_3CO)_5CH_3CN]^+$, 531.0 (12) $[(CuCH_3CO)_5]^+$, 503.0 (6) $[(CuI)_2(NH_4CH_3CO)_2]^+$, 476.0 (12) $[(NH_4I)_3CH_3CN]^+$, 397.0 (16) $[(NH_4I)_2CuCH_3CO]^+$, 383.0 (100) $[Cu_4(CH_3CO)_3]^+$, 369.0 (61) $[(NH_4)_4I_2CH_3CO]^+$.

Negative ion ESI-MS ($CH_2Cl_2/CH_3CN/CH_3OH$ + 10 mmol/L $NH_4^+CH_3CO^-$, RT): *m/z* (%) = 407.7 (41) $[CuCH_3CONH_4I_2CO]^-$, 380.7 (15) $[CuCH_3CONH_4I_2]^-$, 316.7 (100) $[CuI_2]^-$, 127.0 (12) $[I]^-$.

Elemental analysis: Calculated (%) for $C_{24}H_{30}I_2Cu_2O_4P_6W_2$: C 21.89, H 2.30; found: C 21.64, H 2.40.

1*Cl*,2*Cl*-(tri-μ-carbonyl-dicopper-(chloro)copper(pentamethylcyclopentadienyl)tungstenate(1-)-κ^2*Cl*^{1},*Cl*^{2}-dichloride-tetraacetonitrilecopper(I) (21). [Identical procedure for **14**] A solution of **13** (0.050 g, 0.161 mmol) in CH_2Cl_2 (10 mL) is layered with a solution of CuCl (0.032 g, 0.322 mmol) in CH_3CN (10 mL) and placed in a dark environment for 2 days at 22 °C. The contents are filtered with a fritted filter, concentrated, layered with pentane (2 mL), and cooled to 5 °C giving dark brown X-ray quality crystals.

Product yield (relative to 13): 0.018 g, 12.0%

M.P.: = 112 °C (decomposition).

^{1}H NMR (400.13 MHz, $CDCl_3$, 27 °C): δ = 2.05 (s, 15 H, Cp*), 2.00 (s, 9 H, CH_3– unbound acetonitrile), 2.20 (s, 1 H, CH_3–Cl bound acetonitrile, unbound H), 2.37 (s, 2 H, CH_3–Cl bound acetonitrile, bound H).

^{13}C{^{1}H} NMR (100.63 MHz, $CDCl_3$, 27 ºC): δ = 235.79 (s, CO, acetonitrile side), 220.46 (s, CO, bound to CuCl bridge), 116.30 (s, CN, unbound acetonitrile), 109.18 (s, CN bound acetonitrile), 106.54 (s, Cp*, C), 12.09 (s, CH_3, bound acetonitrile), 11.54 (s, Cp*, CH_3), 1.880 (s, CH_3, unbound acetonitrile).

IR (KBr): ν = 2982 (w), 2964 (w), 2917 (w), 1997 (s; CO), 1894 (s; CO), 1802 (s; CO), 1478 (m), 1451 (m), 1427 (w), 1381 (m), 1261 (w), 1097 (w), 1071 (w), 1031 (m), 799 (m), 643 (w), 617 (w), 574 (m), 513 (w), 489 (m), 475 (m), 419 (m) cm^{-1}.

Positive ion ESI-MS (CH_3CN + 10 mmol/L $NH_4^+CH_3CO^-$, RT): *m/z* (%) = 849.1 (76) $[CuCl\{Cp^*W(CO)_2\}]_2^+$, 510.1 (76) $[Cp^*_2W(CO)_2]^+$, 459.2 (42) $[\{Cp^*W(CO)_2\}(CH_3CN)_2]^+$, 444.1 (100) $[Cu_4Cl_3(CH_3CN)_2]^+$, 416.1 (24) $[\{Cp^*W(CO)_2\}CH_3CN]^+$, 403.1 (44) $[Cu_3Cl_2(CH_2Cl_2)NH_4(CH_3CO)]^+$.

Negative ion ESI-MS (CH_3CN + 10 mmol/L $NH_4^+CH_3O^-$, RT): *m/z* (%) = 232.7 (68) $[Cu_2Cl_3]^-$, 134.9 (100) $[CuCl_2]^-$.

Elemental analysis: Calculated (%) for $C_{21}H_{27}Cl_3Cu_4N_4O_3W$: C 27.18, H 2.93; found: C 27.67, H 3.31.

Bis(1*P*,2*P*-bis(dicarbonylcyclopentadienyltungsten(I))diphosphorus-κ^2*P*,*P'*copper(I))-μ-dichloride (22). A solution of **11** (0.050 g, 0.0742 mmoles) in CH_2Cl_2 (10 mL, 0 °C) is slowly layered with a solution of CuCl (0.015 g, 0.148 mmoles) in CH_3CN (10 mL, 0 °C) producing only a slight reaction at the surface. The vessel is kept at 0 °C for a period of 7 days. Maroon X-ray quality crystals are collected.

Product yield (relative to 11): 0.075 g, 65.4%

M.P.: 108–110 °C (decomposition).

^{31}P MAS-NMR (121.49 MHz, spinning frequency 30 kHz, RT) δ = –169.03 ($^1J_{PP}$ = 411.99 Hz; $^1J_{CuP}$ = 1057.94, 1057.95 Hz; P1), –291.31 ($^1J_{PP}$ = 427.18 Hz; $^1J_{CuP}$ = 1070.15, 1078.29 Hz; P2).

^{31}P MAS-NMR (simulated) δ = –169.08 ($^1J_{PP}$ = 432.53 Hz; $^1J_{CuP}$ = 1060.12, 1060.09 Hz; P1), –291.48 ($^1J_{PP}$ = 428.28 Hz; $^1J_{CuP}$ = 1075.52, 1075.71 Hz; P2).

IR (KBr): *ν* = 3110 (w), 2963 (w), 2359 (w), 2340 (w), 2001 (s; CO), 1949 (s; CO), 1921 (s; CO), 1852 (s; CO), 1823 (s; CO), 1416 (m), 1355 (vw), 1261 (m), 1094 (s), 1020 (s), 937 (vw), 866 (w), 847 (m), 799 (s), 703 (w), 606 (w), 575 (w), 545 (w), 511 (m), 474 (s), 438 (m) cm^{-1}.

Positive ion ESI-MS (CH_3CN + 10 mmol/L $NH_4^+CH_3CO^-$, RT): *m/z* (%) = 1406.8 (7) $[Cu_2Cl_2\{Cp_4W_4(CO)_3P_2\}]^+$, 775.7 (18) $[CuCl\{Cp_2W_2(CO)_2P_2\}]^+$, 738.8 (23) $[Cu\{Cp_2W_2(CO)_4P_2\}]^+$, 711.8 (23) $[Cu\{Cp_2W_2(CO)_3P_2\}]^+$, 287.8 (29) $[(NH_4)_3(CH_3CO)_3CH_3CNCu]^+$, 285.8 (43) $[(NH_4)_4(CH_3CO)_4CH_3CN]^+$, 246.7 (16) $[(NH_4)_3(CH_3CO)_3Cu]^+$, 244.7 (22) $[(NH_4)_4(CH_3CO)_4]^+$, 198.8 (12) $[(NH_4)_2Cl(CH_3CO)CH_2Cl_2]^+$, 185.8 (13) $[(NH_4)_2(CH_3CO)_2Cu]^+$, 152 (100) $[CuNH_4Cl]^+$, 144.9 (39) $[Cu(CO)NH_4Cl]^+$, 117.0 (12) $[CuNH_4Cl]^+$.

Negative ion ESI-MS (CH_3CN + 10 mmol/L $NH_4^+CH_3CO^-$, RT): *m/z* (%) = 214.6 (23) $[(NH_4)_2(CH_3CO)_2Cl(CO)_2]^-$, 212.5 (14) $[Cu(NH_4)(CH_3CO)_2Cl]^-$, 162.6 (15) $[CuCl_2(CO)]^-$, 160.6 (17) $[NH_4(CH_3CO)_2(CO)_2]^-$, 136.8 (13) $[NH_4Cl(CH_3CO)CH_3CN]^-$, 134.7 (42) $[CuCl_2]^-$, 132.7 (34) $[NH_4(CH_3CO)_2CO]^-$, 125.7 (27) $[(CH_3CO)(CH_3CN)_2]^-$, 123.7 (32) $[NH_4(CH_3CO)Cl]^-$, 105.9 (21) $[NH_4(CH_3CO)_2]^-$.

Elemental analysis: Calculated (%) for $C_{28}H_{20}Cl_2Cu_2O_8P_4W_4$: C 21.81, H 1.31; found: C 22.05, H 1.52.

Bis(1*P*,2*P*-bis(dicarbonylcyclopentadienyltungsten(I))diphosphorus-κ^2*P*,*P'*copper(I))-μ-dibromide (23). A solution of **11** (0.050 g, 0.0742 mmoles) in CH_2Cl_2 (10 mL, 0 °C) is slowly layered with a solution of CuBr (0.021 g, 0.148 mmoles) in CH_3CN (10 mL, 0 °C) producing only a slight reaction at the surface. The vessel is kept at 0 °C for a period of 7 days. Red X-ray quality crystals are collected.

Product yield (relative to 11): 0.098 g, 81.3%

M.P.: 120–122 °C (decomposition).

^{31}P MAS-NMR (121.49 MHz, spinning frequency 30 kHz, RT) δ = –172.63 ($^{1}J_{PP}$ = 474.55 Hz; $^{1}J_{CuP}$ = 962.32, 974.52 Hz; P2), –302.24 ($^{1}J_{PP}$ = 515.75 Hz; $^{1}J_{CuP}$ = 1066.08, 1082.36 Hz; P1).

^{31}P MAS-NMR (simulated) δ = –173.18 ($^{1}J_{PP}$ = 470.16 Hz; $^{1}J_{CuP}$ = 1000.00, 1000.00 Hz; P2), –302.21 ($^{1}J_{PP}$ = 458.25 Hz; $^{1}J_{CuP}$ = 1000.00, 1000.00 Hz; P1).

IR (KBr): ν = 3118 (w), 2963 (w), 2002 (s; CO), 1952 (s; CO), 1923 (s; CO), 1850 (s; CO), 1821 (s; CO), 1415 (m), 1261 (s), 1096 (s), 1057 (s), 1022 (s), 845 (m), 802 (s), 707 (vw), 575 (w), 545 (w), 513 (m), 474 (w), 441 (m) cm^{-1}.

Positive ion ESI-MS (CH_3CN + 10 mmol/L $NH_4^+CH_3CO^-$, RT): *m/z* (%) = 1695.0 (1) $[(NH_4)(CH_3CO)Cu_2Br_2\{Cp_4W_4(CO)_8P_4\}]^+$, 1551.0 (6) $[Cu_2Br_2\{Cp_4W_4(CO)_5P_4\}]^+$, 1407.0 (14) $[CuBr\{Cp_2W_2(CO)P_2\}]^+$, 775.7 (100) $[(NH_4)\{Cp_2W_2(CO)_4P_2\}(CH_3CN)_2]^+$ or $[(NH_4)\{Cp_2W_2(CO)_7P_2\}]^+$, 747.8 (17) $[(NH_4)\{Cp_2W_2(CO)_3P_2\}(CH_3CN)_2]^+$ or $[(NH_4)\{Cp_2W_2(CO)_6P_2\}]^+$, 719.7 (13) $[(NH_4)\{Cp_2W_2(CO)_5P_2\}]^+$ or $[(NH_4)\{Cp_2W_2(CO)_2P_2\}(CH_3CN)_2]^+$, 375.6 (50) $[Cu_3(CH_3CO)_2(NH_4)Br]^+$, 334.6 (13) $[(NH_4)_5(CH_3CO)_5CO]^+$, 277.8 (27) $[Cu_3(CH_3CO)_2]^+$, 259.7 (22) $[Cu(NH_4)_2Br_2]^+$.

Negative ion ESI-MS (CH_3CN + 10 mmol/L $NH_4^+CH_3CO^-$, RT): *m/z* (%) = 410.5 (2) $[(NH_4)_3Cu(CH_3CO)_4Br(CH_3CN)]^-$, 366.5 (4) $[(NH_4)Cu(CH_3CO)Br_2(CH_3CN)_2]^-$, 313.5 (7) $[(NH_4)_2Cu(CH_3CO)_4Br(CH_3CN)]^-$, 268.5 (20) $[Cu(CH_3CO)Br(CH_3CN)_2]^-$, 222.6 (100) $[CuBr_2]^-$.

Elemental analysis: Calculated (%) for $C_{28}H_{20}Br_2Cu_2O_8P_4W_4$: C 20.62, H 1.24; found: C 22.65, H 1.61.

Bis(1*P*,2*P*-bis(dicarbonylcyclopentadienyltungsten(I))diphosphorus-κ^2*P*,*P'*copper(I))-μ-diiodide (24). A solution of **11** (0.050 g, 0.0742 mmoles) in CH_2Cl_2 (10 mL, 0 °C) is slowly layered with a solution of CuI (0.028 g, 0.148 mmoles) in CH_3CN (10 mL, 0 °C) producing only a slight reaction at the surface. The vessel is kept at 0 °C for a period of 7 days. Red X-ray quality crystals are collected.

Product yield (relative to 11): 0.104 g, 81.3%

M.P.: 107–109 °C (decomposition).

^{31}P MAS-NMR (121.46 MHz, spinning frequency 30 kHz, RT) δ = –187.75 ($^{1}J_{PP}$ = 472.91 Hz; $^{1}J_{CuP}$ = 890.90, 903.10 Hz; P1 and P2).

^{31}P MAS-NMR (simulated) δ = –169.92 ($^{1}J_{CuP}$ = 891.77, 887.63 Hz; P1 and P2).

IR (KBr): ν = 3118 (w), 2963 (w), 2361 (w), 2285 (w), 2251 (w), 1986 (s; CO), 1973 (s; CO), 1916 (s; CO), 1867 (s; CO), 1417 (m), 1261 (m), 1105 (m), 1060 (m), 1025 (w), 1012 (m), 916 (w), 863 (w), 850 (m), 829 (s), 804 (m), 560 (m), 526 (m), 496 (m), 471 (m), 454 (m) cm^{-1}.

Positive ion ESI-MS (CH_3CN + 10 mmol/L $NH_4^+CH_3CO^-$, RT): *m/z* (%) = 1596.8 (2) $[Cu_3I_2\{Cp_4W_4(CO)P_4\}]^+$, 1551.0 (1) $[(NH_4)Cu_2I_2\{Cp_4W_4(CO)P_4\}]^+$, 1406.9 (8) $[Cu_2I\{Cp_4W_4(CO)P_4\}]^+$, 967.7 (10) $[Cu_2I(CH_3CN)\{Cp_2W_2(CO)_4P_2\}]^+$, 919.7 (6) $[(NH_4)_2I(CH_3CN)_2\{Cp_2W_2(CO)_4P_2\}]^+$, 775.8 (100) $[NH_4(CH_3CN)_2\{Cp_2W_2(CO)_4P_2\}]^+$, 747.9 (7) $[NH_4(CH_3CN)_2\{Cp_2W_2(CO)_3P_2\}]^+$, 719.9 (6) $[NH_4(CH_3CN)_2\{Cp_2W_2(CO)_2P_2\}]^+$.

Negative ion ESI-MS (CH_3CN + 10 mmol/L $NH_4^+CH_3CO^-$, RT): *m/z* (%) = 698.4 (5) $[Cu_3I_4]^-$, 650.5 (7) $[(NH_4)Cu_2I_4]^-$, 604.4 (4) $[(NH_4)_2CuI_4]^-$, 506.5 (9) Cu_2I_3, 460.5 (11) $[CuI_3NH_4]^-$, 414.5 (5) $[CuI_2(CO)_2CH_3CN]^-$, 360.6 (9) $[(NH_4)_2(CH_3CO)_2I(CO)_4]^-$, 316.6 (100) $[CuI_2]^-$, 270.5 (100) $[NH_4I_2]^-$, 222.5 (42) $[I(CO)_2CH_3CN]^-$, 126.8 (27) $[I]^-$.

Elemental analysis: Calculated (%) for $C_{28}H_{20}I_2Cu_2O_8P_4W_4(CH_3CN)$: C 21.27, H 1.45, N 1.55; found: C 21.33, H 1.70, N 1.43.

Bis(dicarbonyl(*t*-butylcyclopentadienyl)tungsten(I))diphosphorus (25). In a 100-mL, two-necked, round-bottomed flask equipped with a magnetic stirring bar, argon inlet, and a reflux condenser connected to a mineral oil bubbler, $[W(^tBu\text{-}C_5H_4)(CO)_3]_2$ (1.6 g, 2.0 mmol) is dissolved in n-decalin (60 mL). White phosphorus (0.5 g, 4.0 mmol) is added at room temperature through the second neck of the flask. The mixture is stirred and heated to maintain a gentle reflux for 16 h. The mixture is then cooled to room temperature and concentrated under reduced pressure. CH_2Cl_2 and SiO_2 are added and stirred until the contents are removed from the glass and then concentrated under reduced pressure forming a black-brown powder. The powder is applied under argon to a column (25 x 2.0) cm, which is filled with SiO_2 and pentane. Elution with pentane-toluene (10:1) affords a faint yellow fraction, which after evaporation to dryness gives yellow crystals of $W(^tBu\text{-}C_5H_5)(CO)_2(\eta^3\text{-}P_3)$. Further elution with pure toluene afford a red fraction, which after evaporation to dryness gives X-ray quality red crystals of the featured complex, $W(^tBu\text{-}C_5H_5)(CO)_2(\mu\text{-}\eta^3\text{-}P_2)$.

Product yield relative to $[W(^tBu\text{-}C_5H_4)(CO)_3]_2$: 1.024 g, 65.3%

M.P.: = 162–166 °C.

^{1}H NMR (400.13 MHz, CD_2Cl_2, 27 °C): δ = 5.19 (q, J_{HH} = 1.78 Hz, 2 H, Cp), 1.28 (s, 10 H, ^{t}Bu).

^{13}C{^{1}H} NMR (100.63 MHz, CD_2Cl_2, 27 °C): δ = 212.53 (s, CO), 118.03 (s, Cp), 86.02 (s, Cp), 82.43 (s, ^{t}Bu), 32.23 (s, ^{t}Bu).

^{31}P{^{1}H} NMR (161.98 MHz, CD_2Cl_2, 27 °C): δ = –150.73 (s).

IR (KBr): ν = 3112 (w), 2960 (w), 2906 (w), 2873 (w), 2358 (w), 1945 (s; CO), 1901 (s; CO), 1881 (s; CO), 1481 (w), 1468 (w), 1404 (w), 1368 (w), 1262 (m), 1096 (m), 1021 (m), 926 (w), 907 (w), 873 (w), 849 (m), 825 (s), 800 (s), 703 (w), 676 (w), 570 (m), 551 (w), 530 (m), 503 (m), 481 (m), 466 (m), 447 (m), 402 (m) cm^{-1}.

Elemental analysis: Calculated (%) for $C_{22}H_{26}O_4P_2W_2$: C 33.70, H 3.34; found: C 33.49, H 3.73.

Bis(1*P*,2*P*-bis(dicarbonyl(*t*-butylcyclopentadienyl)tungsten(I)) diphosphorus-κ^2*P*,*P'*copper(I))-μ-dibromide (26). A cold (0 °C) solution of **25** (0.050 g, 0.0693 mmoles) in CH_2Cl_2 (10 mL) is slowly layered with a solution of CuBr (0.020 g, 0.0693 mmoles) in CH_3CN (10 mL). After 2 days of diffusion, the solution is concentrated, layered with pentane (appr. 4.5 mL), and placed in a cold (4 °C) environment for 7 days giving X-ray quality crystals.

Product yield (relative to 25): 0.055 g, 85.6%

M.P.: = 220–222 °C (decomposition).

^{1}H NMR (400.13 MHz, CD_2Cl_2, 27 °C): δ = 5.34 (t, J_{HH} = 2.06 Hz, 2 H, Cp), 5.32 (t, J_{HH} = 1.04 Hz, 2 H, Cp), 1.97 (s, 1 H, ^{t}Bu), 1.30 (s, 9 H, ^{t}Bu).

^{13}C{^{1}H} NMR (100.63 MHz, CD_2Cl_2, 27 ºC): δ = 220.98 (s, CO), 119.56 (s, Cp), 88.27 (s, Cp), 83.66 (s, Cp), 32.30 (s, ^{t}Bu), 32.22 (s, ^{t}Bu).

^{31}P{^{1}H} NMR (161.95 MHz, CD_2Cl_2, 27 °C): δ = –196.16 (s).

^{31}P{^{1}H} NMR (THF-d_8/CH_2Cl_2 (3:1), 161.94 MHz, 27 °C): δ = –235.54 (s).

^{31}P{^{1}H} NMR (THF-d_8/CH_2Cl_2 (3:1), 161.94 MHz, 0 °C): δ = –236.34 (s).

^{31}P{^{1}H} NMR (THF-d_8/CH_2Cl_2 (3:1), 161.94 MHz, –20 °C): δ = –237.39 (s).

^{31}P{^{1}H} NMR (THF-d_8/CH_2Cl_2 (3:1), 161.94 MHz, –80 °C): δ = –183.59 (s), –220.61 (s), –299.64 (s), –318.88 (s).

^{31}P{^{1}H} NMR (THF-d_8/CH_2Cl_2 (3:1), 161.94 MHz, –110 °C): δ = –180.95 (s), –218.14 (s), –303.00 (s), –319.90 (s).

Positive ion ESI-MS (CH_2Cl_2/CH_3CN, RT): *m/z* (%) = 2988.2 (1) $[Cu_5Br_4\{(^tBuCp)_2W_2(CO)_4P_2\}_3]^+$, 2844.4 (1) $[Cu_4Br_3\{(^tBuCp)_2W_2(CO)_4P_2\}_3]^+$, 2701.7 (1) $[Cu_3Br_2\{(^tBuCp)_2W_2(CO)_4P_2\}_3]^+$, 2558.6 (1) $[Cu_2Br\{(^tBuCp)_2W_2(CO)_4P_2\}_3]^+$, 2062.6 (2) $[Cu_4Br_3\{(^tBuCp)_2W_2(CO)_4P_2\}_2]^+$, 1918.8 (4) $[Cu_3Br_2\{(^tBuCp)_2W_2(CO)_4P_2\}_2]^+$, 1775.0 (16) $[Cu_2Br\{(^tBuCp)_2W_2(CO)_4P_2\}_2]^+$, 1631.3 (48) $[Cu\{(^tBuCp)_2W_2(CO)_4P_2\}_2]^+$, 887.8 (100) $[Cu\{(^tBuCp)_2W_2(CO)_4P_2\}CH_3CN]^+$.

Negative ion ESI-MS (CH_2Cl_2/CH_3CN, RT): *m/z* (%) = 510.5 (1) $[Cu_3Br_4]^-$, 366.5 (6) $[Cu_2Br_3]^-$, 266.6 (6) $[CuBr_2CH_3CN]^-$, 234.8 (60) $[(CO)(CH_3CN)_5]^-$, 222.7 (100) $[CuBr_2]^-$, 178.7 (9) $[(CO)_2(CH_3CN)_3]^-$.

IR (KBr): ν = 2962 (w), 2906 (w), 2364 (s), 2345 (w), 1999 (s; CO), 1943 (s; CO), 1919 (s; CO), 1859 (s; CO), 1839 (s; CO), 1479 (w), 1465 (w), 1448 (w), 1399 (w), 1364 (w), 1262 (m), 1148 (w), 1095 (m), 1022 (m), 898 (w), 844 (m), 801 (m), 735 (w), 702 (w), 569 (w), 538 (w), 516 (w), 478 (w), 442 (m) cm^{-1}.

Elemental analysis: Calculated (%) for $C_{22}H_{26}BrCuO_4P_2W_2$: C 28.49, H 2.83; found: C 28.09, H 2.73.

Tris(dicarbonylcyclopentadienylcyclotriphosphanomolybdenum(0)-κ^2*P,P*)silver(I)triflate (29). A solution of **27** (0.095 g, 0.306 mmoles) in CH_2Cl_2 (10 mL) is slowly layered with a solution of $Ag^+(CF_3SO_3)^-$ (0.040 g, 0.153 mmoles) in CH_3CN (10 mL). After a period of 7 days a yellow-orange solution is observed with precipitate. The precipitate is separated with a fritted filter and the supernatant is collected. This orange solution is evaporated slowly under reduced pressure as orange X-ray quality crystals form on the side of the flask.

Product yield (relative to 27): 0.097 g, 80.1%

M.P.: = 108–110 °C (decomposition).

^{1}H NMR (400.13 MHz, CD_2Cl_2, 27 °C): δ = 5.39 (s, 15 H, Cp).

^{13}C{^{1}H} NMR (100.63 MHz, CD_2Cl_2, 27 ºC): δ = 221.33 (s, CO), 86.98 (s, Cp).

^{31}P{^{1}H} NMR (161.95 MHz, CD_2Cl_2, 27 °C): δ = –355.33 (s).

^{31}P{^{1}H} NMR (THF-d_8/CH_2Cl_2 (3:1), 161.94 MHz, 27 °C): δ = –356.73 (s).

^{31}P{^{1}H} NMR (THF-d_8/CH_2Cl_2 (3:1), 161.94 MHz, 0 °C): δ = –359.23 (s).

^{31}P{^{1}H} NMR (THF-d_8/CH_2Cl_2 (3:1), 161.94 MHz, –40 °C): δ = –360.19 (s).

^{31}P{^{1}H} NMR (THF-d_8/CH_2Cl_2 (3:1), 161.94 MHz, –80 °C): δ = –362.33 (s).

^{31}P{^{1}H} NMR (THF-d_8/CH_2Cl_2 (3:1), 161.94 MHz, –120 °C): δ = –301.36 (s (br), 1 P, unbound), –386.02 (s (br), 2 P, silver bound).

^{19}F NMR (282.38 MHz, CD_2Cl_2, 27 °C): δ = –77.79 (s, CF_3, triflate).

^{1}H NMR (400.13 MHz, CD_3CN, 27 °C): δ = 5.42 (s, 15 H, Cp).

^{13}C{^{1}H} NMR (100.63 MHz, CD_3CN, 27 ºC): δ = 221.33 (d, 1.95 Hz, CO), 87.66 (s, Cp).

^{31}P{^{1}H} NMR (161.94 MHz, CD_3CN, 27 °C): δ = –357.42 (s).

^{19}F NMR (282.38 MHz, CD_3CN, 27 °C): δ = –78.06 (s, CF_3, triflate).

Solid-state ^{31}P MAS-NMR (121.45 MHz, 27 °C): δ = –346.545 (s).

IR (KBr): ν = 1987 (s; CO), 1926 (s; CO), 1417 (w), 1261 (m), 1176 (w), 1153 (w), 1031 (m), 840 (w), 821 (m), 637 (m), 550 (w), 517 (w), 501 (w), 755 (w), 446 (w) cm^{-1}.

Positive ion ESI-MS (CH_3CN, RT): *m/z* (%) = 1296.7 (1) $[Ag\{CpMo(CO)_2P_3\}_3AgCF_3SO_3]^+$, 1081.2 (2) $[Ag\{CpMo(CO)_2P_3\}_3CH_3CN]^+$, 1027.6 (4) $[Ag\{CpMo(CO)_2P_3\}_2AgCF_3SO_3CH_3CN]^+$, 986.6 (5) $[Ag\{CpMo(CO)_2P_3\}_2AgCF_3SO_3]^+$, 726.7 (26) $[Ag\{CpMo(CO)_2P_3\}_2]^+$, 459.9 (100) $[Ag\{CpMo(CO)_2P_3\}CH_3CN]^+$, 418.9 (12) $[Ag\{CpMo(CO)_2P_3\}]^+$.

Negative ion ESI-MS (CH_3CN, RT): *m/z* (%) = 149.1 (100) $CF_3SO_3^-$.

Positive ion ESI-MS (CH_2Cl_2/CH_3CN, RT): *m/z* (%) = 1081.4 (4) $[Ag\{CpMo(CO)_2P_3\}_3CH_3CN]^+$, 1027.6 (2) $[Ag\{CpMo(CO)_2P_3\}_2AgCF_3SO_3CH_3CN]^+$, 986.6 (3) $[Ag\{CpMo(CO)_2P_3\}_2AgCF_3SO_3]^+$, 726.6 (55) $[Ag\{CpMo(CO)_2P_3\}_2]^+$, 459.7 (100) $[Ag\{CpMo(CO)_2P_3\}CH_3CN]^+$, 418.7 (28) $[Ag\{CpMo(CO)_2P_3\}]^+$.

Negative ion ESI-MS (CH_2Cl_2, RT): *m/z* (%) = 148.9 (100) $[CF_3SO_3]^-$.

Elemental analysis: Calculated (%) for $C_{22}H_{15}AgF_3Mo_3O_9P_9S$: C 22.26, H 1.27, S 2.70; found: C 22.55, H 1.43, S 2.18.

Tris(1*P*,2*P*-bis(dicarbonylcyclopentadienyltungsten(I))diphosphorus-κ^3*P,P',P''*)bis(disilver(I)-κ^2*O,O'*-triflate)triflate (30). A solution of **11** (0.050 g, 0.074 mmoles) in CH_2Cl_2 (10 mL) is slowly layered with a solution of $Ag^+(CF_3SO_3)^-$ (0.019 g, 0.074 mmoles) in CH_3CN (10 mL). After a period of 7 days the contents are filtered by a fritted filter and the supernatant is collected. This orange solution is evaporated slowly under reduced pressure and cooled to 4 °C for a week producing reddish orange X-ray quality crystals.

Product yield (relative to 11): 0.059 g, 90.9%

M.P.: = 118–121 °C (decomposition).

^{1}H NMR (400.13 MHz, CD_3CN, 27 °C): δ = 5.42 (s, 15 H, Cp).

^{13}C{^{1}H} NMR (100.63 MHz, CD_3CN, 27 ºC): δ = 85.77 (s, Cp).

^{31}P{^{1}H} NMR (161.93 MHz, CD_3CN, 27 °C): δ = –183.74 (s).

^{31}F NMR (282.38 MHz, CD_3CN, 27 °C): δ = –78.08 (s, CF_3, triflate).

Solid-state ^{31}P MAS-NMR (161.90 MHz, 27 °C): δ = –201 (s, 1 P), –268 (s, 1 P).

IR (KBr): ν = 3114 (w), 1940 (s; CO), 1901 (s; CO), 1627 (m), 1418 (m), 1356 (w), 1254 (s), 1167 (m), 1106 (w), 1032 (s), 920 (w), 824 (m), 765 (w), 638 (m), 565 (m), 532, (m), 519 (m), 476 (m), 460 (m), 450 (m) cm^{-1}.

Positive ion ESI-MS (CH_3CN, RT): *m/z* (%) = 1451.1 (90) $[\{Cp_2W_2(CO)_4P_2\}_2Ag]^+$, 820.0 (100) $[Cp_2W_2(CO)_4P_2AgCH_3CN]^+$.

Negative ion ESI-MS (CH_3CN, RT): *m/z* (%) = 148.9 (100) $[CF_3SO_3]^-$, 821.0 (0.30) $[\{Cp_2W_2(CO)_4P_2\}CF_3SO_3]^-$.

Positive ion ESI-MS (CH_2Cl_2/CH_3CN, RT): *m/z* (%) = 819.9 (100) $[Cp_2W_2(CO)_4P_2AgCH_3CN]^+$, 1451.2 (57) $[\{Cp_2W_2(CO)_4P_2\}_2Ag]^+$.

Negative ion ESI-MS (CH_2Cl_2, RT): *m/z* (%) = 148.9 (100) $[CF_3SO_3]^-$.

Elemental analysis: Calculated (%) for $C_{88}H_{60}Ag_4F_{12}O_{36}P_{12}S_4W_{12}$: C 20.89, H 1.20, S 2.54; found: C 21.23, H 1.51, S 2.19.

Bis(1*P*,2*P*-bis(dicarbonylcyclopentadienyltungsten(I))diphosphorus-κ*P*-κ*P*,*P*'silver(I)hexafluorophosphate (31). A solution of **11** (0.050 g, 0.0742 mmoles) in CH_2Cl_2 (10 mL) is slowly layered with a solution of $Ag^+(PF_6)^-$ (0.019 g, 0.0742 mmoles) in CH_3CN (10 mL) at 0 °C. The contents are stored in a cold (4 °C), dark environment for a period of 2 weeks affording red, prismatic X-ray quality crystals.

Product yield (relative to 11): 0.105 g, 78.3%

M.P.: = 226–232 °C (decomposition).

IR (KBr): ν = 3451 (w), 3121 (w), 2963 (w), 2923 (w), 2853 (w), 2853 (w), 2361 (w), 2342 (w), 1963 (s; CO), 1929 (s; CO), 1420 (w), 1262 (w), 1105 (w), 1064 (w), 1013 (w), 845 (m), 830 (m), 558 (w), 522 (w), 468 (w), 441 (w) cm^{-1}.

Positive ion ESI-MS (CH_3CN, RT): *m/z* (%) = 1451.1 (100) $[Ag\{Cp_2W(CO)_2P_2\}_2]^+$, 819.7 (11) $[AgCH_3CN\{Cp_2W(CO)_2P_2\}]^+$, 702.9 (5) $[\{Cp_2W(CO)_3P_2\}]^+$, 671.8 (10) $[\{Cp_2W(CO)_2P_2\}]^+$, 349.1 (19) $[W(CO)_6]^+$.

Negative ion ESI-MS (CH_3CN, RT): *m/z* (%) = 966.9 (86) $[AgPF_6\{Cp_2W(CO)_2P_2\}CH_3CN]^-$, 392.0 (14) $[PF_6(CH_3CN)_6]^-$, 328.8 (100) $[PF_6(CO)_2CH_3CNCH_2Cl_2]^-$, 312.8 (38) $[PF_6CH_3CNCH_2Cl_2]^-$.

Elemental analysis: Calculated (%) for: C 21.06, H 1.27; found: C 21.07, H 1.40.

Bis(dicarbonylcyclopentadienylcyclotriphosphanotungsten(0)-κ^2*P*,*P*)silver(I)hexafluorophosphate (32). A solution of **28** (0.050 g, 0.128 mmoles) in CH_2Cl_2 (10 mL, 0 °C) is slowly layered with a solution of $Ag^+(PF_6)^-$ (0.032 g, 0.128 mmoles) in CH_3CN (10 mL) using a thin walled cannula and placed in a dark environment at room temperature (22 °C). After a period of seven days the contents are filtered and the solution is cooled (5 °C) in darkness by which yellow, plate-shaped X-ray quality crystals are formed.

Product yield (relative to 28): 0.042 g, 84.0%.

M.P.: = 82–84 °C (decomposition).

^{1}H NMR (400.13 MHz, CD_2Cl_2, 27 °C): δ = 5.35 (s, 20 H, Cp)

^{13}C{^{1}H} NMR (100.61 MHz, CD_2Cl_2, 27 ºC): δ = 84.109 (s, Cp).

^{31}P{^{1}H} NMR (161.98 MHz, CD_2Cl_2, 27 °C): δ = –402.07 (s, P_3).

^{19}F NMR (282.40 MHz, CD_2Cl_2, 27 °C): δ = no signal.

^{31}P{^{1}H} NMR (THF-d_8/CH_2Cl_2 (3:1), 161.98 MHz, 27 °C): δ = –1.23 (s), –15.97 (s), –141.56 (sep, 710 Hz), –399.18 (s),.

^{31}P{^{1}H} NMR (THF-d_8/CH_2Cl_2 (3:1), 161.98 MHz, 0 °C): δ = –3.99 (d, 930 Hz), –15.95 (t, 972 Hz), –141.68 (sep, 710 Hz), –400.06 (s).

$^{31}P\{^{1}H\}$ NMR (THF-d_8/CH_2Cl_2 (3:1), 161.98 MHz, –20 °C): δ = –3.92 (d, 930 Hz), –15.90 (t, 976 Hz), –141.75 (sep, 710 Hz), –400.68 (s).

$^{31}P\{^{1}H\}$ NMR (THF-d_8/CH_2Cl_2 (3:1), 161.98 MHz, –40 °C): δ = –3.83 (d, 929 Hz), –15.75 (t, 968 Hz), –141.82 (sep, 711 Hz), –401.38 (s).

$^{31}P\{^{1}H\}$ NMR (THF-d_8/CH_2Cl_2 (3:1), 161.98 MHz, –80 °C): δ = –3.71 (d, 928 Hz), –15.53 (t, 964 Hz), –141.91 (sep, 711 Hz).

$^{31}P\{^{1}H\}$ NMR (THF-d_8/CH_2Cl_2 (3:1), 161.98 MHz, –100 °C): δ = –3.64 (d, 928 Hz), –15.58 (t, 960 Hz), –141.93 (sep, 712 Hz), –432.54 (s).

IR (KBr): v = 2361 (w), 1980 (s; CO), 1932 (s; CO), 1654 (w), 1416 (m), 1306 (m), 1149 (m), 1062 (m), 1003 (m), 912 (s), 834 (s), 559 (s), 514 (m), 453 (m), 428 (w) cm^{-1}.

Positive ion ESI-MS (CH_3CN, RT): *m/z* (%) = 190.0 (100) $[Ag(CH_3CN)_2]^+$, 519.79 (16) $[Ag\{CpW(CO)P_3\}CH_3CN]^+$, 547.8 (32) $[Ag\{CpW(CO)_2P_3\}CH_3CN]^+$, 905.65 (9) $[Ag\{CpW(CO)_2P_3\}_2]^+$, 1092.4 (0.7) $[AgPF_6\{CpW(CO)_2P_3\}_2CH_3CN]^+$, 1168.3 (0.4) $[\{CpW(CO)P_3\}\{CpW(CO)_2P_3\}_2]^+$, 1557.0 (0.4) $[Ag_2PF_6\{CpW(CO)_2P_3\}_3]^+$.

Negative ion ESI-MS (CH_3CN, RT): *m/z* (%) = 145.1 (100) $[PF_6]^-$.

Elemental analysis: Calculated (%) for $C_{28}H_{20}Ag_2O_8P_{12}W_4(PF_6)_2$: C 16.04, H 0.96; found: C 15.73, H 1.01.

Pentachloro(pentamethylcyclopentadienyl)tungsten(VI)tris(trichloroantimony(III)) (33). A solution of **13** (0.050 g, 0.107 mmoles) in cold (0 °C) CH_2Cl_2 (10 mL) is slowly layered with a solution of $SbCl_5$ (0.014 mL, 0.107 mmoles) in CH_2Cl_2 (10 mL) which gives a red solution. The solution is concentrated and placed in a cold (4°C) dark environment for 7 days. Maroon X-ray quality crystals are produced.

Product yield (relative to 13): 0.015 g, 11.9%
Product yield (relative to $SbCl_5$): 0.015 g, 35.7%

Tricarbonyl(trichlorotin(IV))(pentamethylcyclopentadienyl)tungsten(II) (34). A solution of **13** (0.050 g, 0.107 mmoles) in cold (0 °C) CH_2Cl_2 (10 mL) is slowly layered with a solution of $SnCl_2(S–Pr)_2$ (0.036 g, 0.107 mmoles) in EtOH (10 mL). The solution is allowed to diffuse for at least two days at room temperature, concentrated, and placed in a cold (4°C) dark environment for 14 days producing clear, X-ray quality crystals.

Product yield (relative to 13): 0.017 g, 25.3%

Tricarbonylchloro(pentamethylcyclopentadienyl)tungsten(II) (35). A solution of **37** (0.050 g, 0.0615 mmoles) in cold (0 °C) CH_2Cl_2 (10 mL) is slowly layered with a solution of $CoCl_2(PPh_2nPr)_2$ (0.036 g, 0.0615 mmoles) in CH_2Cl_2 (10 mL). The solution is allowed to diffusion for a minimal of 2 days and then placed in a cold (0 °C) dark environment producing clear, X-ray quality crystals.

Product yield (relative to 37): 0.005 g, 18.5%

Tricarbonyl(pentamethylcyclopentadienyl)tunsten(I) (36). A solution of **37** (0.050 g, 0.0615 mmoles) in cold (0 °C) CH_2Cl_2 (10 mL) is slowly layered with a solution of $AgClO_4$ (0.012 g, 0.0615 mmoles) in CH_3CN (10 mL). The solution is allowed to diffuse for a minimal of 14 days in a dark environment producing clear, X-ray quality crystals. The same product results when $AgClO_4$ is substituted with $(CoClCp^*)_2$ or AgF.

Product yield (relative to 37): 0.009 g, 36.3%

IV. Summary

4.1. Conclusions

The first six member Pt,P,P,Pt,P,P and Pd,P,P,Pd,P,P six member rings are synthesized, characterized, and proven by solid-state diffraction as well as the first example of a planar W,P,P,W,P,P ring. These rings, thus, offer greater stability than the formation of monomeric or trans configurations. These complexes are afforded through the treatment of **3** with the appropriate ML_2Cl_2 complex (M = Pt, Pd) [1] or tungsten pentacarbonyl (**9**) with [2], [3]. The NMR analysis also shows that each species except for **1** exhibits dynamic behavior in solution.

An analogous set of CuX (X = Cl, Br, I) bridged molybdenum- and tungsten-cyclotriphosphorus complexes (**14**–**16**) is synthesized, characterized, and proven by solid-state diffraction. A copper halide/acetonitrile solution is layered on a solution of **13**/CH_2Cl_2 [7] of which the phosphophorus free byproduct (**21**) of the CuCl treatment exhibits extraordinary properties. The solution-state ^{31}P NMR analysis shows that each of the copperhalide bridged tungsten-cyclotriphosphorus species exhibits dynamic behavior in solution while the ^{31}P MAS-NMR clearly defines different chemical environments for each phosphorus atom. In addition, concrete evidence from the difference in electronegativity of molybdenum and tungsten is thought to be the reason for the formation of the molybdenum-CuI polymer (**20**) and, furthermore, why the same accomplishment for the tungsten analog is not obtained.

The first phosphorus free polymer (**21**) obtained from the treatment of a cyclotriphosphorus or even a diphosphorus metal complex with CuCl [8] is synthesized, characterized, and proven by solid-state X-ray diffraction. The reactivity of this type is solely reserved to the CuCl reactant as the other CuBr and CuI reactants fail to produce analogous byproducts. The unprecedented backbone, negative charge, and presence of counterion activity make this complex truly unique in this field of chemistry.

An analogous set of CuX (X = Cl, Br, I) linked, isotactic tungsten-diphos inorganic polymers (**22**–**24**) is synthesized, characterized, and proven by solid-state diffraction. This is made possible by layering a copper halide/acetonitrile solution on a **11**/CH_2Cl_2 solution [6]. The solid-state NMR proves that the asymmetry induced by the unordered Cp and CO groups place the phosphorus atoms in chemically inequivalent environments. Asymmetry is also present in the ^{t}Bu substituted bromine analog (**26**) [9]. The ^{t}Bu group provides greater solubility and allows the species to be studied in solution-state NMR at room and low temperature. The low temperature NMR and X-ray diffraction confirms the asymmetry as all the phosphorus atoms are shown to be in different environments.

The first two examples of a silver atom bound to 6 phosphorus atoms are presented; these are also the first cyclotriphosphorus containing silver polymers reported. Ironically, the subunits (MP_3, M = Mo, W) are analogous with the only difference being the metal and counterion of the silver salt reacted, yet the structures are entirely different in nature. The molybdenum containing cyclotriphosphorus complex (**27**) creates a relatively simpler homogeneous polymer (**29**) [11], whereas the polymer (**32**) involving the tungsten species (**28**) contains four chemically different subunits [10]. Using the W_2P_2 subunit (**11**), a unique, triflate-incorporated polymer (**30**) [4] and a flat Ag_2P_4 ring (**31**) [5] are formed using the same procedure and different reactants, silver triflate and hexafluorophosphate, respectively. All of these reactions are carried out by layering a silver salt/acetonitrile solution on a solution of subunit (starting material)/CH_2Cl_2.

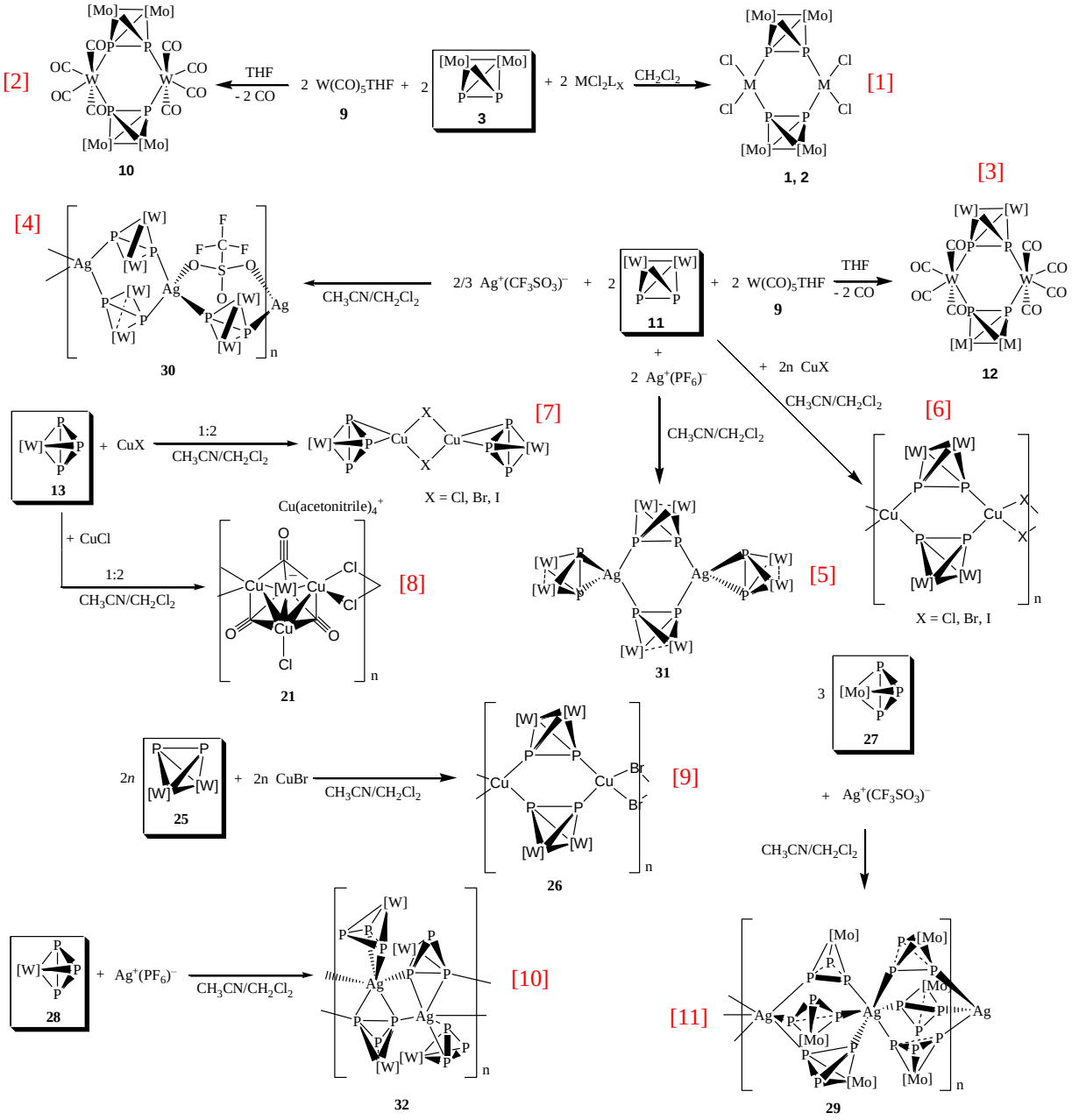

Scheme 10. Summary of all reactions involved in the synthesis of phosphorus containing products. [1] Synthesis of **1** (Pt) and **2** (Pd). MCl_2L_X = $(COD)PtCl_2$ (**4**, cis), $Pt(SMe_2)_2Cl_2$ (**5**, cis and trans mixture), $Pt(MeSPh)_2Cl_2$ (**6**, trans), $Pd(MeSPh)_2Cl_2$ (**7**, trans), and $Pd(SMe_2)_2Cl_2$ (**8**, cis and trans mixture). [Mo] = $MoCp(CO)_2$. [2] [Mo] = $MoCp(CO)_2$. [3] [W] = $WCp(CO)_2$. [4] [W] = $W(CO)_2Cp$. [5] [W] = $W(CO)_2Cp$. [6] [W] = $W(CO)_2Cp$. Syntheses of **22**–**24**. X = Cl (**22**), Br (**23**), I (**24**). [7] Syntheses of **14**–**16**. X = Cl (**14**), Br (**15**), I (**16**). [W] = $W(CO)_2Cp^*$. [8] A byproduct involved exclusively to the sythesis of **14**, [W] = WCp^*. [9] [W] = $W(Cp\text{-}^tBu)(CO)_2$. [10] $W(CO)_2Cp$. [11] [Mo] = $MoCp(CO)_2$.

Finally, an analogous set of phosphorus free complexes containing varieties of WCp^* is reported while in the pursuit of searching for new, compatible reactants. Unorthodox reactions with **37** and **13** produce text book examples of Jahn-Teller distortion and steric

effects associated with ligand substitution. This also reinforces the theory that basal units with larger substituents hinder the formation of phosphorus containing complexes.

4.2. Proposal

The success of this research has been limited to phosphorus rings with 6 or fewer phosphorus atoms per binding site, but the complexes involving more than 6 phosphorus atoms in the introduction have not been tested for reactivity. As the possibilities of phosphorus-rich structures wane, new subunits containing heterocycles involving mixed group 15 elements (except for N) demonstrate potential for forming new polymers.[174-176] In addition, new reactants must be explored just as the new platinum and palladium salts mentioned in this thesis.

More importantly is the lack of exploration of related antimony and bismuth subunits. For selection purposes, established subunits should be analogous or similar to the previously successful subunits. The complexes should contain a homogenous ring or if the ring is heterogeneous the varied atoms should be group 15 (except for N). The ring should be bound to a metal carbonyl and the molecule should contain no counterions (the reactants can contain counterions). The most successful ancillary ligand has been cyclopentadienyl or some variation, but heavier substituents on this ligand generally cause more difficulty in crystallization. Some appropriate examples of subunits containing antimony and bismuth[316-319] rings are already established, however, this area still remains relatively underdeveloped.

V. References

1. Zeise, W. C. *Ann. Phys. Chem.* **1831,** *21,* 497–541.
2. T. J. Kelly, P. L. P. *Nature*, **1951,** *168,* 1039.
3. Foust, A. S.; Foster, M. S.; Dahl, L. F. *J. Am. Chem. Soc.* **1969,** *91,* 5633–5.
4. Ginsberg, A. P.; Lindsell, W. E. *J. Am. Chem. Soc.* **1971,** *93,* 2082–4.
5. Vizi-Orosz, A.; Palyi, G.; Marko, L. *J. Organomet. Chem.* **1973,** *60,* C25–C26.
6. Schmettow, W.; Lipka, A.; Von Schnering, H. G. *Angew. Chem.* **1974,** *86,* 379–80.
7. Wichelhaus, W.; Von Schnering, H. G. *Naturwissenschaften* **1973,** *60,* 104.
8. Schmettow, W. Universität Münster, Münster, 1975.
9. Dahlmann, W.; Von Schnering, H. G. *Naturwissenschaften* **1972,** *59,* 420.
10. Konchenko, S. N.; Pushkarevsky, N. A.; Gamer, M. T.; Koeppe, R.; Schnoeckel, H.; Roesky, P. W. *J. Am. Chem. Soc.* **2009,** *131,* 5740–5741.
11. Dai, F.-R.; Xu, L. *Inorg. Chim. Acta* **2006,** *359,* 4265–4273.
12. Hanauer, T.; Aschenbrenner, J. C.; Korber, N. *Inorg. Chem.* **2006,** *45,* 6723–6727.
13. Kraus, F.; Korber, N. *Chem. Eur. J.* **2005,** *11,* 5945–5959.
14. Denk, M. K.; Hezarkhani, A. *Heteroat. Chem.* **2005,** *16,* 453–457.
15. Korber, N. *Phosphorus, Sulfur Silicon Relat. Elem.* **1997,** *124 & 125,* 339–346.
16. Korber, N.; Daniels, J.; von Schnering, H. G. *Angew. Chem. Int. Ed.* **1996,** *35,* 1107–1110.
17. Guerin, F.; Richeson, D. *Inorg. Chem.* **1995,** *34,* 2793–4.
18. Burkhardt, A.; Hoenle, W.; Wedig, U. *Angew. Chem.* **1991,** *103,* 850–2 (See also Angew Chem , Int Ed Engl , 1991, 30(7), 828–30).
19. Albright, T. A.; Yee, K. A.; Saillard, J. Y.; Kahlal, S.; Halet, J. F.; Leigh, J. S.; Whitmire, K. H. *Inorg. Chem.* **1991,** *30,* 1179–90.
20. Von Schnering, H. G.; Menge, G. *Z. Anorg. Allg. Chem.* **1981,** *481,* 33–40.
21. Burns, R. C.; Gillespie, R. J.; Barnes, J. A.; McGlinchey, M. J. *Inorg. Chem.* **1982,** *21,* 799–807.
22. Boehm, M. C.; Gleiter, R. *Z. Naturforsch., B: Chem. Sci.* **1981,** *36,* 498–500.
23. Bues, W.; Somer, M.; Brockner, W.; Gruenewald, D. *Naturwissenschaften* **1977,** *64,* 583–4.
24. Bianchini, C.; Di Vaira, M.; Meli, A.; Sacconi, L. *J. Am. Chem. Soc.* **1981,** *103,* 1448–52.
25. Di Vaira, M.; Midollini, S.; Sacconi, L. *J. Am. Chem. Soc.* **1979,** *101,* 1757–63.
26. Scherer, O. J.; Sitzmann, H.; Wolmershaeuser, G. *Angew. Chem.* **1984,** *96,* 979–80.
27. Scherer, O. J.; Schwalb, J.; Wolmershaeuser, G.; Kaim, W.; Gross, R. *Angew. Chem.* **1986,** *98,* 349–50.
28. Scherer, O. J.; Dave, T.; Braun, J.; Wolmershaeuser, G. *J. Organomet. Chem.* **1988,** *350,* C20–C24.
29. Di Vaira, M.; Stoppioni, P.; Peruzzini, M. *J. Chem. Soc., Dalton Trans.* **1990**, 109–13.
30. Goh, L. Y.; Wong, R. C. S.; Sinn, E. *J. Chem. Soc., Chem. Commun.* **1990**, 1484–5.
31. Scherer, O. J.; Hoebel, B.; Wolmershaeuser, G. *Angew. Chem.* **1992,** *104,* 1042–3 (See also Angew Chem , Int Ed Engl , 1992, 31(8), 1027–8).
32. Scherer, O. J.; Werner, B.; Heckmann, G.; Wolmershaeuser, G. *Angew. Chem.* **1991,** *103,* 562–3 (See also Angew Chem , Int Ed Engl , 1991, 30(5), 553–5).
33. Scherer, O. J.; Kemeny, G.; Wolmershaeuser, G. *Chem. Ber.* **1995,** *128,* 1145–8.
34. Scherer, O. J.; Berg, G.; Wolmershaeuser, G. *Chem. Ber.* **1996,** *129,* 53–8.
35. Peruzzini, M.; Marvelli, L.; Romerosa, A.; Rossi, R.; Vizza, F.; Zanobini, F. *Eur. J. Inorg. Chem.* **1999**, 931–933.
36. Bai, J.; Virovets, A. V.; Scheer, M. *Angew. Chem. Int. Ed.* **2002,** *41,* 1737–1740.

37. Bai, J.; Virovets, A. V.; Scheer, M. *Science* **2003,** *300*, 781–783.
38. Scheer, M.; Schindler, A.; Merkle, R.; Johnson, B. P.; Linseis, M.; Winter, R.; Anson, C. E.; Virovets, A. V. *J. Am. Chem. Soc.* **2007,** *129*, 13386–13387.
39. Pfitzner, A.; Braeu, M. F.; Zweck, J.; Brunklaus, G.; Eckert, H. *Angew. Chem. Int. Ed.* **2004,** *43*, 4228–4231.
40. Ruck, M.; Hoppe, D.; Wahl, B.; Simon, P.; Wang, Y.; Seifert, G. *Angew. Chem. Int. Ed.* **2005,** *44*, 7616–7619.
41. Haeser, M.; Schneider, U.; Ahlrichs, R. *J. Am. Chem. Soc.* **1992,** *114*, 9551–9.
42. Scherer, O. J.; Volmecke, T.; Wolmershauser, G. *Eur. J. Inorg. Chem.* **1999**, 945–949.
43. Goh, L. Y.; Wong, R. C. S.; Sinn, E. *Organometallics* **1993,** *12*, 888–94.
44. Von Schnering, H. G. *Angew. Chem.* **1981,** *93*, 44–63.
45. Rheingold, A. L., *Homoatomic Rings, Chains, and Macromolecules of Main-Group Elements*. 1977; 615 pp.
46. Wichelhaus, W.; Von Schnering, H. G. *Naturwissenschaften* **1975,** *62*, 180.
47. Ahlrichs, R.; Fenske, D.; Fromm, K.; Krautscheid, H.; Krautscheid, U.; Treutler, O. *Chem. Eur. J.* **1996,** *2*, 238–44.
48. Scherer, O. J.; Hilt, T.; Wolmershauser, G. *Angew. Chem. Int. Ed.* **2000,** *39*, 1426–1427.
49. Charles, S.; Eichhorn, B. W.; Rheingold, A. L.; Bott, S. G. *J. Am. Chem. Soc.* **1994,** *116*, 8077–86.
50. Charles, S.; Danis, J. A.; Fettinger, J. C.; Eichhorn, B. W. *Inorg. Chem.* **1997,** *36*, 3772–3778.
51. Charles, S.; Fettinger, J. C.; Eichhron, B. W. *J. Am. Chem. Soc.* **1995,** *117*, 5303–11.
52. Cossairt, B. M.; Cummins, C. C. *Angew. Chem. Int. Ed.* **2008,** *47*, 169–172.
53. Charles, S.; Fettinger, J. C.; Bott, S. G.; Eichhorn, B. W. *J. Am. Chem. Soc.* **1996,** *118*, 4713–14.
54. Barr, M. E.; Adams, B. R.; Weller, R. R.; Dahl, L. F. *J. Am. Chem. Soc.* **1991,** *113*, 3052–60.
55. Herberhold, M.; Frohmader, G.; Milius, W. *J. Organomet. Chem.* **1996,** *522*, 185–196.
56. Abicht, H. P.; Hoenle, W.; Von Schnering, H. G. *Z. Anorg. Allg. Chem.* **1984,** *519*, 7–23.
57. Chamizo, J. A.; Ruiz-Mazon, M.; Salcedo, R.; Toscano, R. A. *Inorg. Chem.* **1990,** *29*, 879–80.
58. Herberhold, M.; Frohmader, G.; Milius, W. *Phosphorus, Sulfur Silicon Relat. Elem.* **1994,** *93–94*, 205–8.
59. Kraus, F.; Hanauer, T.; Korber, N. *Angew. Chem. Int. Ed.* **2005,** *44*, 7200–7204.
60. Kraus, F.; Schmedt Auf der Gunne, J.; DiSalle Brian, F.; Korber, N. *Chem. Commun. (Camb)* **2006**, 218–9.
61. Scherer, O. J.; Sitzmann, H.; Wolmershaeuser, G. *Angew. Chem.* **1985,** *97*, 358–9.
62. Scherer, O. J.; Swarowsky, H.; Wolmershaeuser, G.; Kaim, W.; Kohlmann, S. *Angew. Chem.* **1987,** *99*, 1178–9.
63. Von Schnering, H. G.; Meyer, T.; Hoenle, W.; Schmettow, W.; Hinze, U.; Bauhofer, W.; Kliche, G. *Z. Anorg. Allg. Chem.* **1987,** *553*, 261–79.
64. Kerins, M. C.; Fitzpatrick, N. J.; Minh Tho, N. *Polyhedron* **1989,** *8*, 1135–8.
65. Hoffmann, R. *Prix Nobel* **1982**, 173–205.
66. Reddy, A. C.; Jemmis, E. D.; Scherer, O. J.; Winter, R.; Heckmann, G.; Wolmershaeuser, G. *Organometallics* **1992,** *11*, 3894–900.
67. Scherer, O. J.; Vondung, J.; Wolmershaeuser, G. *Angew. Chem.* **1989,** *101*, 1395–7.
68. Scherer, O. J.; Schwalb, J.; Swarowsky, H.; Wolmershaeuser, G.; Kaim, W.; Gross, R. *Chem. Ber.* **1988,** *121*, 443–9.

69. Hofmann, C.; Scherer, O. J.; Wolmershauser, G. *J. Organomet. Chem.* **1998,** *559*, 219–222.
70. Scherer, O. J.; Meiers, J.; Regitz, M.; Hofmann, M. A.; Karaghiosoff, K.; Wolmershauser, G. *Z. Anorg. Allg. Chem.* **2001,** *627*, 1532–1536.
71. Ginsberg, A. P.; Lindsell, W. E.; McCullough, K. J.; Sprinkle, C. R.; Welch, A. J. *J. Am. Chem. Soc.* **1986,** *108*, 403–16.
72. Friedrich, G.; Scherer, O. J.; Wolmershaeuser, G. *Z. Anorg. Allg. Chem.* **1996,** *622*, 1478–1486.
73. Koeppe, R.; Steiner, J.; Schnoeckel, H. *Z. Anorg. Allg. Chem.* **2003,** *629*, 2168–2172.
74. Rink, B.; Scherer, O. J.; Heckmann, G.; Wolmershaeuser, G. *Chem. Ber.* **1992,** *125*, 1011–16.
75. Scherer, O. J.; Brueck, T.; Wolmershaeuser, G. *Chem. Ber.* **1988,** *121*, 935–8.
76. Scherer, O. J.; Brueck, T.; Wolmershaeuser, G. *Chem. Ber.* **1989,** *122*, 2049–54.
77. Kudinov, A. R.; Loginov, D. A.; Starikova, Z. A.; Petrovskii, P. V.; Corsini, M.; Zanello, P. *Eur. J. Inorg. Chem.* **2002**, 3018–3027.
78. Baudler, M.; Etzbach, T. *Angew. Chem.* **1991,** *103*, 590–2 (See also Angew Chem , Int Ed Engl , 1991, 30(5), 580–2).
79. Scheer, M.; Deng, S.; Scherer, O. J.; Sierka, M. *Angew. Chem. Int. Ed.* **2005,** *44*, 3755–3758.
80. Scherer, O. J.; Hilt, T.; Wolmershaeuser, G. *Organometallics* **1998,** *17*, 4110–4112.
81. Scheer, M.; Gregoriades, L. J.; Virovets, A. V.; Kunz, W.; Neueder, R.; Krossing, I. *Angew. Chem. Int. Ed.* **2006,** *45*, 5689–5693.
82. Scherer, O. J.; Brueck, T. *Angew. Chem.* **1987,** *99*, 59.
83. Miluykov, V. A.; Sinyashin, O. G.; Scherer, O.; Hey-Hawkins, E. *Mendeleev Commun.* **2002**, 1–2.
84. Baudler, M.; Akpapoglou, S.; Ouzounis, D.; Wasgestian, F.; Meinigke, B.; Budzikiewicz, H.; Muenster, H. *Angew. Chem.* **1988,** *100*, 288–9.
85. Scheer, M.; Friedrich, G.; Schuster, K. *Angew. Chem.* **1993,** *105*, 641–3 (See also Angew Chem , Int Ed Engl , 1993, 32(4), 593–4).
86. Urnezius, E.; Brennessel, W. W.; Cramer, C. J.; Ellis, J. E.; Schleyer, P. v. R. *Science* **2002,** *295*, 832–834.
87. Baudler, M.; Etzbach, T. *Chem. Ber.* **1991,** *124*, 1159–60.
88. Lein, M.; Frunzke, J.; Frenking, G. *Inorg. Chem.* **2003,** *42*, 2504–2511.
89. Liu, Z.-Z.; Tian, W. Q.; Feng, J.-K.; Zhang, G.; Li, W.-Q.; Cui, Y.-H.; Sun, C.-C. *Eur. J. Inorg. Chem.* **2006**, 2808–2818.
90. Scherer, O. J.; Mohr, T.; Wolmershauser, G. *J. Organomet. Chem.* **1997,** *529*, 379–385.
91. Detzel, M.; Mohr, T.; Scherer, O. J.; Wolmershaeuser, G. *Angew. Chem.* **1994,** *106*, 1142–4 (See also Angew Chem , Int Ed Engl , 1994, 33(10), 1110–12).
92. Scherer, O. J.; Weigel, S.; Wolmershauser, G. *Chem. Eur. J.* **1998,** *4*, 1910–1916.
93. Koch, B.; Scherer, O. J.; Wolmershauser, G. *Z. Anorg. Allg. Chem.* **2000,** *626*, 1797–1802.
94. Scherer, O. J.; Braun, J.; Wolmershaeuser, G. *Chem. Ber.* **1990,** *123*, 471–5.
95. De los Rios, I.; Hamon, J.-R.; Hamon, P.; Lapinte, C.; Toupel, L.; Romerosa, A.; Peruzzini, M. *Angew. Chem. Int. Ed.* **2001,** *40*, 3910–3912.
96. Groeer, T.; Baum, G.; Scheer, M. *Organometallics* **1998,** *17*, 5916–5919.
97. Di Vaira, M.; Peruzzini, M.; Costantini, S. S.; Stoppioni, P. *J. Organomet. Chem.* **2006,** *691*, 3931–3937.
98. Di Vaira, M.; Frediani, P.; Costantini, S. S.; Peruzzini, M.; Stoppioni, P. *Dalton Trans.* **2005**, 2234–2236.

99. M.Di Vaira, M. P., S.S.Costantini, P.Stoppioni. *Private Communication*, **2006,** *Deposition: CCDC [606955]*,
100. Dapporto, P.; Midollini, S.; Sacconi, L. *Angew. Chem.* **1979,** *91*, 510.
101. Barbaro, P.; Di Vaira, M.; Peruzzini, M.; Costantini, S. S.; Stoppioni, P. *Chem. Eur. J.* **2007,** *13*, 6682–6690.
102. P.Barbaro, M. D. V., M.Peruzzini, S.Seniori Costantini, P.Stoppioni. *Private Communication*, **2006,** *CCDC [262403]*,
103. Akbayeva, D. N. *Russ. J. Coord. Chem.* **2007,** *33*, 661–668.
104. Akbayeva, D. N. *Russ. J. Coord. Chem.* **2006,** *32*, 329–334.
105. Di Vaira, M.; Ehses, M. P.; Peruzzini, M.; Stoppioni, P. *Eur. J. Inorg. Chem.* **2000**, 2193–2198.
106. Krossing, I.; Van Wullen, L. *Chem. Eur. J.* **2002,** *8*, 700–711.
107. Bihlmeier, A.; Gonsior, M.; Raabe, I.; Trapp, N.; Krossing, I. *Chem. Eur. J.* **2004,** *10*, 5041–5051.
108. Krossing, I. *J. Am. Chem. Soc.* **2001,** *123*, 4603–4604.
109. Santiso-Quinones, G.; Reisinger, A.; Slattery, J.; Krossing, I. *Chem. Commun.* **2007**, 5046–5048.
110. Peruzzini, M.; Gonsalvi, L.; Romerosa, A. *Chem. Soc. Rev.* **2005,** *34*, 1038–1047.
111. Tai, H.-C.; Krossing, I.; Seth, M.; Deubel, D. V. *Organometallics* **2004,** *23*, 2343–2349.
112. Scherer, O. J.; Swarowsky, M.; Wolmershaeuser, G. *Organometallics* **1989,** *8*, 841–2.
113. Yakhvarov, D.; Barbaro, P.; Gonsalvi, L.; Carpio, S. M.; Midollini, S.; Orlandini, A.; Peruzzini, M.; Sinyashin, O.; Zanobini, F. *Angew. Chem. Int. Ed.* **2006,** *45*, 4182–4185.
114. Power, M. B.; Barron, A. R. *Angew. Chem.* **1991,** *103*, 1403–4 (See also Angew Chem , Int Ed Engl , 1991, (30)10, 1353–4).
115. Krossing, I.; Raabe, I. *Angew. Chem. Int. Ed.* **2001,** *40*, 4406–4409.
116. Akbayeva, D. N.; Scherer, O. J. *Z. Anorg. Allg. Chem.* **2001,** *627*, 1429–1430.
117. Barr, M. E.; Dahl, L. F. *Organometallics* **1991,** *10*, 3991–6.
118. Scherer, O. J.; Berg, G.; Wolmershauser, G. *Chem. Ber.* **1995,** *128*, 635–9.
119. Scherer, O. J.; Schwarz, G.; Wolmershaeuser, G. *Z. Anorg. Allg. Chem.* **1996,** *622*, 951–957.
120. Smith, M. B.; March, J., *March's Advanced Organic Chemistry: Reactions, Mechanisms, and Structure, 5th Edition*. 2000; p 1824 pp.
121. Scherer, O. J.; Winter, R.; Wolmershaeuser, G. *Z. Anorg. Allg. Chem.* **1993,** *619*, 827–35.
122. Kraus, F.; Aschenbrenner, J. C.; Korber, N. *Angew. Chem. Int. Ed.* **2003,** *42*, 4030–4033.
123. Kraus, F.; Hanauer, T.; Korber, N. *Inorg. Chem.* **2006,** *45*, 1117–1123.
124. Scheer, M.; Becker, U.; Chisholm, M. H.; Huffman, J. C.; Lemoigno, F.; Eisenstein, O. *Inorg. Chem.* **1995,** *34*, 3117–19.
125. Uhl, W.; Benter, M. *Chem. Commun.* **1999**, 771–772.
126. Weber, D.; Mujica, C.; Von Schnering, H. G. *Angew. Chem.* **1982,** *94*, 869–70.
127. Fritz, G.; Hoppe, K. D.; Hoenle, W.; Weber, D.; Mujica, C.; Manriquez, V.; Von Schnering, H. G. *J. Organomet. Chem.* **1983,** *249*, 63–80.
128. Mujica, C.; Weber, D.; Von Schnering, H. G. *Z. Naturforsch., B: Chem. Sci.* **1986,** *41B*, 991–9.
129. Hoenle, W.; Von Schnering, H. G.; Fritz, G.; Schneider, H. W. *Z. Anorg. Allg. Chem.* **1990,** *584*, 51–70.
130. Dapporto, P.; Sacconi, L.; Stoppioni, P.; Zanobini, F. *Inorg. Chem.* **1981,** *20*, 3834–9.

131. Di Vaira, M.; Ehses, M. P.; Peruzzini, M.; Stoppioni, P. *Polyhedron* **1999,** *18,* 2331–2336.
132. Di Vaira, M.; Stoppioni, P. *Polyhedron* **1994,** *13,* 3045–51.
133. Bianchini, C.; Vaira, M. D.; Meli, A.; Sacconi, L. *Inorg. Chem.* **1981,** *20,* 1169–73.
134. Peruzzini, M.; Ramirez, J. A.; Vizza, F. *Angew. Chem. Int. Ed.* **1998,** *37,* 2255–2257.
135. Groer, T.; Scheer, M. *Z. Anorg. Allg. Chem.* **2000,** *626,* 1211–1216.
136. Brunner, H.; Klement, U.; Meier, W.; Wachter, J.; Serhadle, O.; Ziegler, M. L. *J. Organomet. Chem.* **1987,** *335,* 339–52.
137. Jutzi, P.; Kroos, R. *Chem. Ber.* **1988,** *121,* 1399–401.
138. Scherer, O. J.; Sitzmann, H.; Wolmershaeuser, G. *Acta Crystallogr., Sect. C: Cryst. Struct. Commun.* **1985,** *C41,* 1761–3.
139. Piro, N. A.; Cummins, C. C. *J. Am. Chem. Soc.* **2008,** *130,* 9524–9535.
140. Scherer, O. J.; Sitzmann, H.; Wolmershaeuser, G. *J. Organomet. Chem.* **1984,** *268,* C9–C12.
141. Umbarkar, S.; Sekar, P.; Scheer, M. *Dalton* **2000**, 1135–1137.
142. Goh, L. Y.; Chu, C. K.; Wong, R. C. S.; Hambley, T. W. *J. Chem. Soc., Dalton Trans.* **1989**, 1951–6.
143. Goh, L. Y.; Chen, W.; Wong, R. C. S. *Organometallics* **1999,** *18,* 306–314.
144. Di Vaira, M.; Peruzzini, M.; Stoppioni, P. *Acta Crystallogr., Sect. C: Cryst. Struct. Commun.* **1983,** *C39,* 1210–11.
145. Ghilardi, C. A.; Midollini, S.; Orlandini, A.; Sacconi, L. *Inorg. Chem.* **1980,** *19,* 301–6.
146. Bianchini, C.; Mealli, C.; Meli, A.; Sacconi, L. *Inorg. Chim. Acta* **1979,** *37,* L543–L544.
147. Vizi-Orosz, A. *J. Organomet. Chem.* **1976,** *111,* 61–4.
148. Chisholm, M. H.; Huffman, J. C.; Pasterczyk, J. W. *Inorg. Chim. Acta* **1987,** *133,* 17–18.
149. Stephens, F. H.; Johnson, M. J. A.; Cummins, C. C.; Kryatova, O. P.; Kryatov, S. V.; Rybak-Akimova, E. V.; McDonough, J. E.; Hoff, C. D. *J. Am. Chem. Soc.* **2005,** *127,* 15191–15200.
150. Vizi-Orosz, A.; Galamb, V.; Palyi, G.; Marko, L. *J. Organomet. Chem.* **1981,** *216,* 105–11.
151. Deng, S.; Schwarzmaier, C.; Eichhorn, C.; Scherer, O.; Wolmershaeuser, G.; Zabel, M.; Scheer, M. *Chem. Commun.* **2008**, 4064–4066.
152. Deng, S.; Schwarzmaier, C.; Zabel, M.; Nixon, J. F.; Timoshkin, A. Y.; Scheer, M. *Organometallics 28,* 1075–1081.
153. Herber, R. H.; Nowik, I.; Loginov, D. A.; Starikova, Z. A.; Kudinov, A. R. *Eur. J. Inorg. Chem.* **2004**, 3476–3483.
154. Schwalb, J. Chrom- und Wolframkomplexe mit Px-Liganden. University of Kaiserslautern, Kaiserslautern, 1988.
155. Eichhorn, C.; Scherer, O. J.; Sogding, T.; Wolmershauser, G. *Angew. Chem. Int. Ed.* **2001,** *40,* 2859–2861.
156. Scherer, O. J. *Acc. Chem. Res.* **1999,** *32,* 751–762.
157. Di Vaira, M.; Stoppioni, P. *Coord. Chem. Rev.* **1992,** *120,* 259–79.
158. Scherer, O. J. *Angew. Chem.* **1990,** *102,* 1137–55.
159. Peruzzini, M.; Abdreimova, R. R.; Budnikova, Y.; Romerosa, A.; Scherer, O. J.; Sitzmann, H. *J. Organomet. Chem.* **2004,** *689,* 4319–4331.
160. Gregoriades, L. J.; Wegley, B. K.; Sierka, M.; Brunner, E.; Groeger, C.; Peresypkina, E. V.; Virovets, A. V.; Zabel, M.; Scheer, M. *Chem. Asian J.* **2009,** *4,* 1578–1587.
161. Dielmann, F.; Merkle, R.; Heinl, S.; Scheer, M. *Z. Naturforsch., B: Chem. Sci.* **2009,** *64,* 3–10.

162. Dielmann, F.; Scheer, M. *Abstracts of Papers, 237th ACS National Meeting, Salt Lake City, UT, United States, March 22–26, 2009* **2009**, INOR–314.
163. Deng, S.; Schwarzmaier, C.; Vogel, U.; Zabel, M.; Nixon, J. F.; Scheer, M. *Eur. J. Inorg. Chem.* **2008**, 4870–4874.
164. Scheer, M. *Dalton Trans.* **2008**, 4372–4386.
165. Scheer, M.; Gregoriades, L. J.; Merkle, R.; Johnson, B. P.; Dielmann, F. *Phosphorus, Sulfur Silicon Relat. Elem.* **2008,** *183,* 504–508.
166. Scheer, M.; Gregoriades, L. J.; Zabel, M.; Bai, J.; Krossing, I.; Brunklaus, G.; Eckert, H. *Chem. Eur. J.* **2008,** *14,* 282–295.
167. Welsch, S.; Gregoriades, L. J.; Sierka, M.; Zabel, M.; Virovets, A. V.; Scheer, M. *Angew. Chem. Int. Ed.* **2007,** *46,* 9323–9326.
168. Scheer, M.; Gregoriades, L. J.; Zabel, M.; Sierka, M.; Zhang, L.; Eckert, H. *Eur. J. Inorg. Chem.* **2007**, 2775–2782.
169. Scheer, M.; Himmel, D.; Johnson, B. P.; Kuntz, C.; Schiffer, M. *Angew. Chem. Int. Ed.* **2007,** *46,* 3971–3975.
170. Johnson, B. P.; Dielmann, F.; Balazs, G.; Sierka, M.; Scheer, M. *Angew. Chem. Int. Ed.* **2006,** *45,* 2473–2475.
171. Scheer, M.; Bai, J.; Johnson, B. P.; Merkle, R.; Virovets, A. V.; Anson, C. E. *Eur. J. Inorg. Chem.* **2005**, 4023–4026.
172. Scheer, M.; Gregoriades, L.; Bai, J.; Sierka, M.; Brunklaus, G.; Eckert, H. *Chem. Eur. J.* **2005,** *11,* 2163–2169.
173. Bai, J.; Leiner, E.; Scheer, M. *Angew. Chem. Int. Ed.* **2002,** *41,* 783–786.
174. Gregoriades, L. J.; Balazs, G.; Brunner, E.; Groeger, C.; Wachter, J.; Zabel, M.; Scheer, M. *Angew. Chem. Int. Ed.* **2007,** *46,* 5966–5970.
175. Pronold, M.; Scheer, M.; Wachter, J.; Zabel, M. *Inorg. Chem.* **2007,** *46,* 1396–1400.
176. Gregoriades, L. J.; Krauss, H.; Wachter, J.; Virovets, A. V.; Sierka, M.; Scheer, M. *Angew. Chem. Int. Ed.* **2006,** *45,* 4189–4192.
177. Manning, A. R.; Hackett, P.; Birdwhistell, R.; Soye, P. *Inorg. Synth.* **1990,** *28,* 148–50.
178. Scherer, O. J.; Schwalb, J.; Sitzmann, H. *Inorg. Synth.* **1990,** *27,* 224–7.
179. Brunner, H.; Grassl, R.; Meier, W.; Wachter, J.; Nuber, B.; Ziegler, M. L. *J. Organomet. Chem.* **1992,** *434,* 63–78.
180. Gregoriades, L. J. Organometallic Pn-Ligand Complexes as Supramolecular Building Blocks. University of Regensburg, Regensburg, 2006.
181. Scheer, M.; Gregoriades, L.; Bai, J.; Sierka, M.; Brunklaus, G.; Eckert, H. *Chem. Eur. J.* **2005,** *11,* 2163–2169.
182. Bartsch, R.; Carmichael, D.; Hitchcock, P. B.; Meidine, M. F.; Nixon, J. F.; Sillett, G. J. D. *J. Chem. Soc., Chem. Commun.* **1988**, 1615–17.
183. Caliman, V.; Hitchcock, P. B.; Nixon, J. F. *Chem. Commun.* **1998**, 1537–1538.
184. Kesanli, B.; Charles, S.; Lam, Y.-F.; Bott, S. G.; Fettinger, J.; Eichhorn, B. *J. Am. Chem. Soc.* **2000,** *122,* 11101–11107.
185. Phillips, I. G.; Ball, R. G.; Cavell, R. G. *Inorg. Chem.* **1992,** *31,* 1633–41.
186. Shafaatian, B.; Akbari, A.; Nabavizadeh, S. M.; Heinemann, F. W.; Rashidi, M. *Dalton Trans.* **2007**, 4715–4725.
187. Keglevich, G.; Kerenyi, A.; Szelke, H.; Imre, T. *Transition Met. Chem.* **2006,** *31,* 306–309.
188. Catalano, V. J.; Malwitz, M. A.; Noll, B. C. *Inorg. Chem.* **2002,** *41,* 6553–6559.
189. Dey, S.; Jain, V. K.; Knoedler, A.; Kaim, W.; Zalis, S. *Eur. J. Inorg. Chem.* **2001**, 2965–2973.
190. Catalano, V. J.; Bennett, B. L.; Muratidis, S.; Noll, B. C. *J. Am. Chem. Soc.* **2001,** *123,* 173–174.

191. Deeming, A. J.; Cockerton, B. R.; Doherty, S. *Polyhedron*, **1997,** *16*, 1945–1956.
192. Kovacs, I.; Krautscheid, H.; Matern, E.; Fritz, G.; Pikies, J. *Z. Anorg. Allg. Chem.* **1997,** *623*, 1088–1092.
193. Krautscheid, H.; Matern, E.; Fritz, G.; Pikies, J. *Z. Anorg. Allg. Chem.* **1998,** *624*, 501–505.
194. Krautscheid, H.; Matern, E.; Fritz, G.; Pikies, J. *Z. Anorg. Allg. Chem.* **1998,** *624*, 1617–1621.
195. Krautscheid, H.; Matern, E.; Fritz, G.; Pikies, J. *Z. Anorg. Allg. Chem.* **2000,** *626*, 253–257.
196. Krautscheid, H.; Matern, E.; Pikies, J.; Fritz, G. *Z. Anorg. Allg. Chem.* **2000,** *626*, 2133–2135.
197. Slawin, A. M. Z.; Smith, M. B.; Woollins, J. D. *J. Chem. Soc., Dalton Trans.* **1997**, 3397–3401.
198. Caliman, V.; Hitchcock, P. B.; Nixon, J. F. *J. Chem. Soc., Chem. Commun.* **1995**, 1661–2.
199. Araujo, M. H.; Hitchcock, P. B.; Nixon, J. F.; Kuehner, U.; Stelzer, O. *Chem. Commun.* **2003**, 1092–1093.
200. Schmidpeter, A.; Steinmueller, F.; Sheldrick, W. S. *Z. Anorg. Allg. Chem.* **1989,** *579*, 158–72.
201. Leone, A.; Gischig, S.; Elsevier, C. J.; Consiglio, G. *J. Organomet. Chem.* **2007,** *692*, 2056–2063.
202. Gomez-Benitez, V.; Hernandez-Ortega, S.; Toscano, R. A.; Morales-Morales, D. *Inorg. Chim. Acta* **2007,** *360*, 2128–2138.
203. Steyl, G.; Kirsten, L.; Roodt, A. *Acta Crystallogr., Sect. E: Struct. Rep. Online* **2006,** *E62*, 1705–1707.
204. Meijboom, R.; Muller, A.; Roodt, A. *Acta Crystallogr., Sect. E: Struct. Rep. Online* **2006,** *E62*, 1603–1605.
205. Steyl, G. *Acta Crystallogr., Sect. E: Struct. Rep. Online* **2006,** *E62*, 1324–1325.
206. Kin-Chee, H.; McLaughlin, G. M.; McPartlin, M.; Robertson, G. B. *Acta Crystallogr., Sect. B: Struct. Sci* **1982,** *B38*, 421–5.
207. Johansson, M. H.; Otto, S. *Acta Crystallogr., Sect. C: Cryst. Struct. Commun.* **2000,** *C56*, 12–15.
208. Del Pra, A.; Zanotti, G. *Cryst. Struct. Commun.* **1979,** *8*, 737–42.
209. Del Pra, A.; Zanotti, G. *Inorg. Chim. Acta* **1980,** *39*, 137–41.
210. Otto, S.; Muller, A. J. *Acta Crystallogr., Sect. C: Cryst. Struct. Commun.* **2001,** *C57*, 1405–1407.
211. Grushin, V. V.; Bensimon, C.; Alper, H. *Inorg. Chem.* **1994,** *33*, 4804–6.
212. Schultz, G.; Subbotina, N. Y.; Jensen, C. M.; Golen, J. A.; Hargittai, I. *Inorg. Chim. Acta* **1992,** *191*, 85–90.
213. Alcock, N. W.; Nelson, J. H. *Acta Crystallogr., Sect. C: Cryst. Struct. Commun.* **1985,** *C41*, 1748–50.
214. Ferguson, G.; McCrindle, R.; McAlees, A. J.; Parvez, M. *Acta Crystallogr., Sect. B: Struct. Sci* **1982,** *B38*, 2679–81.
215. Woisetschlager, O. E.; Polborn, K.; Beck, W. *Department of Chemie Universität Munchen, Butenandtstr. 5–13 81377, Germany*, **2005**,
216. Miessler, G. L.; Tarr, D. A., *Inorg. Chem. Second Edition*. 1999; 640 pp.
217. Bourissou, D.; Canac, Y.; Gornitzka, H.; Marsden, C. J.; Baceiredo, A.; Bertrand, G. *Eur. J. Inorg. Chem.* **1999**, 1479–1488.
218. Davies, J. E.; Mays, M. J.; Raithby, P. R.; Shields, G. P.; Tompkin, P. K.; Woods, A. D. *Dalton* **2000**, 1925–1930.

219. Schwalb, J. Chrom- und Wolframkomplexe mit P_x-Liganden. Universität Kaiserslautern, Kaiserslautern, 1988.
220. Gregoriades, L. J.; Balazs, G.; Brunner, E.; Groeger, C.; Wachter, J.; Zabel, M.; Scheer, M. *Angew. Chem. Int. Ed.* **2007,** *46,* 5966–5970.
221. Scheer, M.; Schindler, A.; Merkle, R.; Johnson, B. P.; Linseis, M.; Winter, R.; Anson, C. E.; Virovets, A. V. *J. Am. Chem. Soc.* **2007,** *129,* 13386–13387.
222. Scheer, M.; Gregoriades, L. J.; Virovets, A. V.; Kunz, W.; Neueder, R.; Krossing, I. *Angew. Chem. Int. Ed.* **2006,** *45,* 5689–5693.
223. Johnson, B. P.; Dielmann, F.; Balazs, G.; Sierka, M.; Scheer, M. *Angew. Chem. Int. Ed.* **2006,** *45,* 2473–2475.
224. Scheer, M.; Bai, J.; Johnson, B. P.; Gregoriades, L.; Virovets, A. V. *Abstracts of Papers, 225th ACS National Meeting, New Orleans, LA, United States, March 23–27, 2003*, **2003**, INOR–091.
225. Bai, J.; Virovets, A. V.; Scheer, M. *Science* **2003,** *300,* 781–783.
226. Bai, J.; Leiner, E.; Scheer, M. *Angew. Chem. Int. Ed.* **2002,** *41,* 783–786.
227. Bai, J.; Virovets, A. V.; Scheer, M. *Angew. Chem. Int. Ed.* **2002,** *41,* 1737–1740.
228. Bayler, A.; Schier, A.; Schmidbaur, H. *Inorg. Chem.* **1998,** *37,* 4353–4359.
229. Diez, J.; Gamasa, M. P.; Gimeno, J.; Lanfranchi, M.; Tiripicchio, A. *J. Organomet. Chem.* **2001,** *637–639,* 677–682.
230. Doherty, S.; Robins, E. G.; Nieuwenhuyzen, M.; Knight, J. G.; Champkin, P. A.; Clegg, W. *Organometallics* **2002,** *21,* 1383–1399.
231. Effendy; Di Nicola, C.; Fianchini, M.; Pettinari, C.; Skelton, B. W.; Somers, N.; White, A. H. *Inorg. Chim. Acta* **2005,** *358,* 763–795.
232. Kuehl, O.; Blaurock, S.; Carls, T. *Inorg. Chem.* **2006,** *45,* 1723–1727.
233. Lipshutz, B. H.; Frieman, B.; Birkedal, H. *Org. Lett.* **2004,** *6,* 2305–2308.
234. Pinto, P.; Calhorda, M. J.; Felix, V.; Aviles, T.; Drew, M. G. B. *Monatshefte fuer Chemie,* **2000,** *131,* 1253–1265.
235. Tsuboyama, A.; Kuge, K.; Furugori, M.; Okada, S.; Hoshino, M.; Ueno, K. *Inorg. Chem.* **2007,** *46,* 1992–2001.
236. Zhang, D.; Dou, J.; Gong, S.; Li, D.; Wang, D. *Appl. Organomet. Chem.* **2006,** *20,* 632–637.
237. Ganesamoorthy, C.; Balakrishna, M. S.; George, P. P.; Mague, J. T. *Inorg. Chem.* **2007,** *46,* 848–858.
238. Aslanidis, P.; Cox, P. J.; Divanidis, S.; Tsipis, A. C. *Inorg. Chem.* **2002,** *41,* 6875–6886.
239. Deng, Y. H.; Yang, Y. L.; Yang, X. J. *Z. Kristallogr. - New Cryst. Struct.* **2006,** *221,* 316–318.
240. Wang, S.-Y.; Ji, S.-J.; Loh, T.-P. *J. Am. Chem. Soc.* **2007,** *129,* 276–277.
241. Lobana, T. S.; Sharma, R.; Sharma, R.; Mehra, S.; Castineiras, A.; Turner, P. *Inorg. Chem.* **2005,** *44,* 1914–1921.
242. Aslanidis, P.; Cox, P. J.; Divanidis, S.; Karagiannidis, P. *Inorg. Chim. Acta* **2004,** *357,* 1063–1076.
243. Zhang, D.; Dou, J.; Gong, S.; Li, D.; Wang, D. *Appl. Organomet. Chem.* **2006,** *20,* 632–637.
244. Scherer, O. J.; Schwalb, J.; Swarowsky, H.; Wolmershaeuser, G.; Kaim, W.; Gross, R. *Chem. Ber.* **1988,** *121,* 443–9.
245. Gregoriades, L. J.; Krauss, H.; Wachter, J.; Virovets, A. V.; Sierka, M.; Scheer, M. *Angew. Chem. Int. Ed.* **2006,** *45,* 4189–4192.
246. Adamczyk, L.; Kulesza, P. J.; Miecznikowski, K.; Palys, B.; Chojak, M.; Krawczyk, D. *J. Electrochem. Soc.* **2005,** *152,* 98–103.

247. Haque, S. A.; Koops, S.; Tokmoldin, N.; Durrant, J. R.; Huang, J.; Bradley, D. D. C.; Palomares, E. *Adv. Mater.* **2007,** *19*, 683–687.
248. Karnicka, K.; Chojak, M.; Miecznikowski, K.; Skunik, M.; Baranowska, B.; Kolary, A.; Piranska, A.; Palys, B.; Adamczyk, L.; Kulesza, P. J. *Bioelectrochem.* **2005,** *66*, 79–87.
249. Kulesza, P. J.; Karnicka, K.; Miecznikowski, K.; Chojak, M.; Kolary, A.; Barczuk, P. J.; Tsirlina, G.; Czerwinski, W. *Electrochim. Acta* **2005,** *50*, 5155–5162.
250. Seki, S.; Kobayashi, Y.; Miyashiro, H.; Usami, A.; Mita, Y.; Terada, N. *J. Electrochem. Soc.* **2006,** *153*, 1073–1076.
251. Wu, C.; Xu, T.; Gong, M.; Yang, W. *J. Membr. Sci.* **2005,** *247*, 111–118.
252. Carlton, L.; Lindsell, W. E.; McCullough, K. J.; Preston, P. N. *J. Chem. Soc., Chem. Commun.* **1983**, 216–18.
253. Costas, M.; Xifra, R.; Llobet, A.; Sola, M.; Robles, J.; Parella, T.; Stoeckli-Evans, H.; Neuburger, M. *Inorg. Chem.* **2003,** *42*, 4456–4468.
254. Doyle, G.; Eriksen, K. A.; Modrick, M.; Ansell, G. *Organometallics*, **1982,** *1*, 1613–18.
255. Floriani, C.; Chiesi-Villa, A.; Guastini, C.; Zanazzi, P. F. *J. Chem. Soc., Dalton Trans.* **1988**, 1607–15.
256. Gagne, R. R.; Kreh, R. P.; Dodge, J. A.; Marsh, R. E.; McCool, M. *Inorg. Chem.* **1982,** *21*, 254–61.
257. Geerts, R. L.; Huffman, J. C.; Folting, K.; Lemmen, T. H.; Caulton, K. G. *J. Am. Chem. Soc.* **1983,** *105*, 3503–6.
258. Pasquali, M.; Fiaschi, P.; Floriani, C.; Zanazzi, P. F. *J. Chem. Soc., Chem. Commun.* **1983**, 613–14.
259. Pasquali, M.; Floriani, C.; Gaetani-Manfredotti, A. *Inorg. Chem.* **1980,** *19*, 1191–7.
260. Pasquali, M.; Floriani, C.; Gaetani-Manfredotti, A. *Inorg. Chem.* **1981,** *20*, 3382–8.
261. Pasquali, M.; Floriani, C.; Venturi, G.; Gaetani-Manfredotti, A.; Chiesi-Villa, A. *J. Am. Chem. Soc.* **1982,** *104*, 4092–9.
262. Pasquali, M.; Marchetti, F.; Floriani, C. *Inorg. Chem.* **1978,** *17*, 1684–8.
263. Toth, A.; Floriani, C.; Pasquali, M.; Chiesi-Villa, A.; Gaetani-Manfredotti, A.; Guastini, C. *Inorg. Chem.* **1985,** *24*, 648–53.
264. Villacorta, G. M.; Lippard, S. J. *Inorg. Chem.* **1987,** *26*, 3672–6.
265. Blagg, A.; Shaw, B. L.; Thornton-Pett, M. *J. Chem. Soc., Dalton Trans.* **1987**, 769–75.
266. Doyle, G.; Eriksen, K. A.; Van Engen, D. *Inorg. Chem.* **1983,** *22*, 2892–5.
267. Doyle, G.; Eriksen, K. A.; Van Engen, D. *Organometallics*, **1985,** *4*, 2201–6.
268. Drake, S. R.; Johnson, B. F. G.; Lewis, J.; Nelson, W. W. J. H.; Vargas, M. D.; Adatia, T.; Braga, D.; Henrick, K.; McPartlin, M.; Sironi, A. *J. Chem. Soc., Dalton Trans.* **1989**, 1455–64.
269. Wiles, A. B.; Pike, R. D. *Organometallics*, **2006,** *25*, 3282–3285.
270. Scherer, O. J.; Schwalb, J.; Sitzmann, H. *Inorg. Synth.* **1990,** *27*, 224–7.
271. Airey, A. L.; Swiegers, G. F.; Willis, A. C.; Wild, S. B. *J. Chem. Soc., Chem. Commun.* **1995**, 695–6.
272. Airey, A. L.; Swiegers, G. F.; Willis, A. C.; Wild, S. B. *Inorg. Chem.* **1997,** *36*, 1588–1597.
273. Lu, X. L.; Leong, W. K.; Goh, L. Y.; Hor, A. T. S. *Eur. J. Inorg. Chem.* **2004**, 2504–2513.
274. Blake, C. J.; Cook, V. C.; Keniry, M. A.; Kitto, H. J.; Rae, A. D.; Swiegers, G. F.; Willis, A. C.; Zank, J.; Wild, S. B. *Inorg. Chem.* **2003,** *42*, 8709–8715.
275. Cotton, F. A.; Luck, R. L. *Acta Crystallogr., Sect. C: Cryst. Struct. Commun.* **1989,** *C45*, 1222–4.
276. Eisenmann, J.; Fenske, D.; Simon, F. *Z. Anorg. Allg. Chem.* **1995,** *621*, 1681–8.

277. Krishna, H.; Krishnamurthy, S. S.; Nethaji, M. *Polyhedron* **2006,** *25*, 3189–3200.
278. Schmitt, E. W.; Huffman, J. C.; Zaleski, J. M. *Chem. Commun.* **2001**, 167–168.
279. Uzelmeier, C. E.; Smucker, B. W.; Reinheimer, E. W.; Shatruk, M.; O'Neal, A. W.; Fourmigue, M.; Dunbar, K. R. *Dalton Trans.* **2006**, 5259–5268.
280. Venter, G. J. S.; Meijboom, R.; Roodt, A. *Acta Crystallogr., Sect. E: Struct. Rep. Online* **2006,** *E62*, 3453–3455.
281. Massa, W.; Kujanek, R.; Baum, G.; Dehnicke, K. *Angew. Chem.* **1984,** *96*, 149.
282. Homsy, N. K.; Roesky, H. W.; Noltemeyer, M.; Sheldrick, G. M. *J. Chem. Soc., Dalton Trans.* **1985**, 2205–7.
283. Godemeyer, T.; Dehnicke, K.; Fenske, D. *Z. Naturforsch., B: Chem. Sci.* **1985,** *40B*, 1005–9.
284. Godemeyer, T.; Berg, A.; Gross, H. D.; Mueller, U.; Dehnicke, K. *Z. Naturforsch., B: Chem. Sci.* **1985,** *40B*, 999–1004.
285. Kynast, U.; Willing, W.; Mueller, U.; Dehnicke, K. *Z. Anorg. Allg. Chem.* **1985,** *529*, 129–36.
286. Willing, W.; Hoesler, K.; Mueller, U.; Dehnicke, K. *Acta Crystallogr., Sect. C: Cryst. Struct. Commun.* **1987,** *C43*, 218–21.
287. Bradley, D. C.; Errington, R. J.; Hursthouse, M. B.; Short, R. L.; Aschroft, B. R.; Clark, G. R.; Nielson, A. J.; Rickard, C. E. F. *J. Chem. Soc., Dalton Trans.* **1987**, 2067–75.
288. Ashcroft, B. R.; Clark, G. R.; Nielson, A. J.; Rickard, C. E. F. *Polyhedron* **1986,** *5*, 2081–91.
289. Adel, J.; El Kholi, A.; Willing, W.; Mueller, U.; Dehnicke, K. *Chimia* **1988,** *42*, 70–1.
290. Vogler, S.; Massa, W.; Dehnicke, K. *Z. Naturforsch., B: Chem. Sci.* **1991,** *46*, 1625–8.
291. Vogler, S.; Dehnicke, K. *Z. Naturforsch., B: Chem. Sci.* **1992,** *47*, 301–4.
292. Weiher, U.; Dehnicke, K.; Fenske, D. *Z. Anorg. Allg. Chem.* **1979,** *457*, 105–14.
293. Chen, Q.; McClinton, D.; Zubieta, J. *Inorg. Chim. Acta* **1992,** *195*, 163–7.
294. Goerge, A.; Patt-Siebel, U.; Mueller, U.; Dehnicke, K. *Z. Naturforsch., B: Chem. Sci.* **1988,** *43*, 1633–8.
295. Lichtenhan, J. D.; Ziller, J. W.; Doherty, N. M. *Inorg. Chem.* **1992,** *31*, 2893–900.
296. Drew, M. G. B.; Fowles, G. W. A.; Page, E. M.; Rice, D. A. *J. Chem. Soc., Dalton Trans.* **1981**, 2409–13.
297. Fenske, D.; Stahl, K.; Hey, E.; Dehnicke, K. *Z. Naturforsch., B: Chem. Sci.*, **1984,** *39B*, 850–4.
298. Ovchinnikova, N. A.; Sinyakov, A. E.; Sergienko, V. S.; Aleksandrov, G. G. *Crystallogr. Rep.* **2003,** *48*, 602–605.
299. Lu, Y.-J.; Beer, R. H. *Polyhedron* **1996,** *15*, 1667–71.
300. Hofacker, P.; Werth, A.; Neuhaus, A.; Neumueller, B.; Weller, F.; Dehnicke, K.; Fenske, D. *Chem. Ztg* **1991,** *115*, 321–5.
301. Kanehisa, N.; Kai, Y.; Kasai, N.; Yasuda, H.; Nakayama, Y.; Nakamura, A. *Bull. Chem. Soc. Jpn.* **1992,** *65*, 1197–201.
302. Junk, P. C.; Atwood, J. L. *J. Chem. Soc., Chem. Commun.* **1995**, 1551–2.
303. Junk, P. C.; Atwood, J. L. *J. Chem. Soc., Dalton Trans.* **1997**, 4393–4400.
304. Stahl, K.; Weller, F.; Dehnicke, K. *Z. Anorg. Allg. Chem.* **1984,** *518*, 175–86.
305. Stahl, K.; Mueller, U.; Dehnicke, K. *Z. Anorg. Allg. Chem.* **1985,** *527*, 7–16.
306. Stahl, K.; Weller, F.; Dehnicke, K. *Z. Anorg. Allg. Chem.* **1986,** *533*, 73–82.
307. Kersting, M.; Dehnicke, K.; Fenske, D. *J. Organomet. Chem.* **1988,** *346*, 201–9.
308. Jurkschat, K.; Kaltenbrunner, U.; Schurmann, M. *Z. Kristallogr. - New Cryst. Struct.* **1999,** *214*, 473–474.
309. Padelkova, Z.; Cisarova, I.; Fejfarova, K.; Holubova, J.; Ruzicka, A.; Holecek, J. *Collect. Czech. Chem. Commun.* **2007,** *72*, 629–636.

310. Chen, S.-S.; Dou, Y.-Y.; Du, M.; Tang, L.-F. *J. Organomet. Chem.* **2006,** *691*, 3633–3639.
311. Braunschweig, H.; Bera, H.; Geibel, B.; Doerfler, R.; Goetz, D.; Seeler, F.; Kupfer, T.; Radacki, K. *Eur. J. Inorg. Chem.* **2007**, 3416–3424.
312. Firfiray, D. B.; Irving, A.; Moss, J. R. *J. Chem. Soc., Chem. Commun.* **1990**, 377–8.
313. Drew, D.; Doyle, J. R. *Inorg. Synth.* **1990,** *28*, 346–9.
314. Basato, M.; Cardinale, A.; Salvo, S.; Tubaro, C.; Benetollo, F. *Inorg. Chim. Acta* **2005,** *358*, 659–666.
315. Braunstein, P.; Bender, R.; Jud, J. *Inorg. Synth.* **1989,** *26*, 341–50.
316. Pronold, M. Darstellung supramolekularer Verbindungen aus $[(Cp^*Mo)_2E_2S_3]$ (E = P, As) und Kupfer(I)-Halogeniden. University of Regensburg, Regensburg, 2006.
317. Kohl, F. X.; Jutzi, P. *J. Organomet. Chem.* **1983,** *243*, 119–21.
318. Quindt, V.; Saurenz, D.; Schmitt, O.; Schar, M.; Dezember, T.; Wolmershauser, G.; Sitzmann, H. *J. Organomet. Chem.* **1999,** *579*, 376–384.
319. Riemschneider, R.; Reisch, A.; Horak, H. *Monatsh. Chem.* **1960,** *91*, 805–11.
320. Altomare, A.; Cascarano, G.; Giacovazzo, C.; Guagliardi, A. *J. Appl. Crystallogr.* **1993,** *26*, 343–50.
321. Sheldrick, G. M. *SHELXL–97*, University of Göttingen: 1997.
322. GbR, C. I. *Diamond Version 2.1e*, 2001.
323. Massiot, D.; Fayon, F.; Capron, M.; King, I.; Le Calve, S.; Alonso, B.; Durand, J.-O.; Bujoli, B.; Gan, Z.; Hoatson, G. *Magn. Reson. Chem.* **2002,** *40*, 70–76.

VI. Appendix

6.1. List of Abbreviations

°C = degrees centigrade, Celsius
Å = angstrom (1 x 10^{-10} m)
Ar = aryl
av. = average
Bu = butyl
Cy = cyclohexane
e^- = electron
EA = elemental analysis
EI-MS = electron impact mass spectrometry
ESI-MS = electrospray ionization mass spectrometry
Et = ethyl
h = hour
HOMO = highest occupied molecular orbital
IR = infrared
K = Kelvin
M = metal
M.P. = melting point
Me = methyl
MO = molecular orbital
nm = nanometers
NMR = nuclear magnetic resonance
non = nonet
Ph = phenyl
ppm = parts per million
R = organic substituent
RT = room temperature
^{t}Bu = *tert*-butyl
THF = tetrahydrofuran
UV, *uv* = ultraviolet
X = halogen

NMR
{^{1}H} = proton decoupled
at = apparent triplet
b = broad
d = doublet
dd = doublet of doublets
dt = doublet of triplets
Hz = hertz
I = nuclear-spin quantum number
J = coupling constant, Hz
m = multiplet
p = quintet
q = quartet
REDOR = Rotational Echo Double Resonance

REAPDOR = Rotational-Echo Adiabatic-Passage Double-Resonance
s = singlet
sep = septet
t = triplet
td = triplet of doublets
δ = chemical shift in ppm

X-ray
V = unit cell volume
Z = number of formula units in the unit cell
α = unit cell angle between b and c
β = unit cell angle between a and c
γ = unit cell angle between a and b
a = unit cell axis
b = unit cell axis
c = unit cell axis

IR
w = weak
m = medium
s = strong
v = very
b = broad

6.2. Index of Species

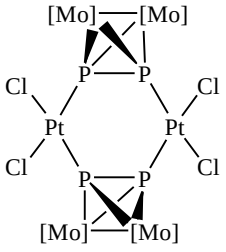

[Mo] = $MoCp(CO)_2$

IUPAC name: Bis(1*P*,2*P*-bis(dicarbonylcyclopentadienylmolybdenum(I))diphosphorus-$\kappa^2 P,P'$)bis(dichloroplatinum(II))
ID Number: 1

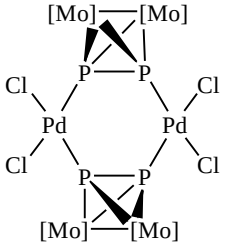

[Mo] = $MoCp(CO)_2$

IUPAC name: Bis(1*P*,2*P*-bis(dicarbonylcyclopentadienylmolybdenum(I))diphosphorus-$\kappa^2 P,P'$)bis(dichloropaladium(II))
ID Number: 2

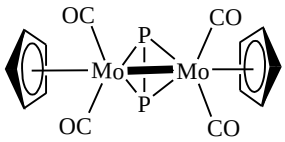

Unit short name: Mo_2P_2
IUPAC name: Bis(dicarbonylcyclopentadienylmolybdenum(I))diphosphorus
ID Number: 3

$(COD)PtCl_2$
IUPAC name: Cyclooctadienylplatinum(II) chloride
ID Number: 4

$Pt(SMe_2)_2Cl_2$
IUPAC name: Bis(dimethylsulfide)platinum(II) chloride
ID Number: 5

$Pt(MeSPh)_2Cl_2$
IUPAC name: Bis(methylphenylsulfide)platinum(II) chloride
ID Number: 6

$Pd(MeSPh)_2Cl_2$
IUPAC name: Bis(methylphenylsulfide)palladium(II) chloride
ID Number: 7

$Pd(SMe_2)_2Cl_2$
IUPAC name: Bis(dimethylsulfide)palladium(II) chloride
ID Number: 8

$W(CO)_5THF$
IUPAC name: Tungstenpentacarbonyltetrahydrofuran
ID Number: 9

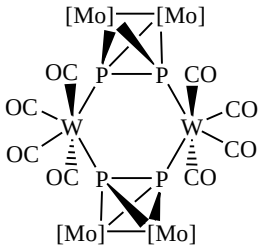

[Mo] = $MoCp(CO)_2$

IUPAC name: Bis(1*P*,2*P*-bis(dicarbonylcyclopentadienylmolybdenum(I))diphosphorus-κ^2P,P')bis(tetracarbonyltungsten(0))
ID Number: 10

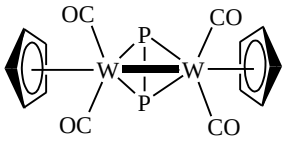

Unit short name: W_2P_2
IUPAC name: Bis(dicarbonylcyclopentadienyltungsten(I))diphosphorus
ID Number: 11

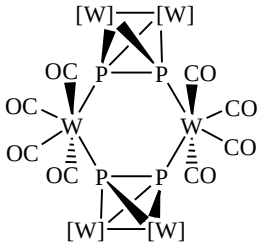

[W] = $WCp(CO)_2$

IUPAC name: Bis(1*P*,2*P*-bis(dicarbonylcyclopentadienyltungsten(I))diphosphorus-$\kappa^2 P,P'$)bis(tetracarbonyltungsten(0))
ID Number: 12

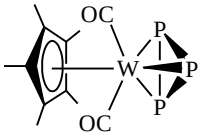

Unit short name: WP_3*
IUPAC name: dicarbonyl(pentamethylcyclopentadienyl)cyclotriphosphanotungsten(0)
ID Number: 13

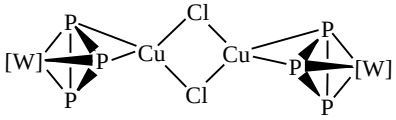

[W] = $W(CO)_2Cp^*$

IUPAC name: 1*Cl*,2*Cl*-bis(dicarbonyl(pentamethylcyclopentadienyl)cyclotriphosphanotungsten(0)- $\kappa^2 P,P'$copper(I))-μ-dichloride
ID Number: 14

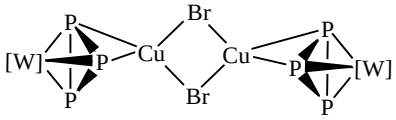

[W] = $W(CO)_2Cp^*$

IUPAC name: 1*Br*,2*Br*-bis(dicarbonyl(pentamethylcyclopentadienyl)cyclotriphosphanotungsten(0)- $\kappa^2 P,P'$copper(I))-μ-dibromide
ID Number: 15

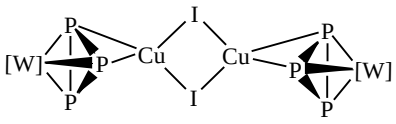

[W] = $W(CO)_2Cp^*$

IUPAC name: 1*I*,2*I*-bis(dicarbonyl(pentamethylcyclopentadienyl)cyclotriphosphanotungsten(0)- κ^2*P*,*P'*copper(I))-μ-diiodide
ID Number: 16

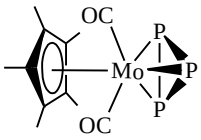

Unit short name: MoP_3^*
IUPAC name: dicarbonyl(pentamethylcyclopentadienyl)cyclotriphosphanomolybdenum(0)
ID Number: 17

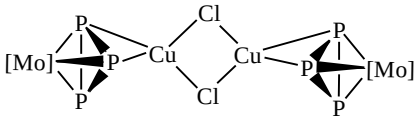

[Mo] = $Mo(CO)_2Cp^*$

IUPAC name: 1*Cl*,2*Cl*-bis(dicarbonyl(pentamethylcyclopentadienyl)cyclotriphosphanomolybdenum(0)-κ^2*P*,*P'*copper(I))-μ-dichloride
ID Number: 18

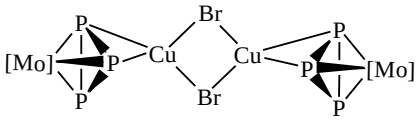

[Mo] = $Mo(CO)_2Cp^*$

IUPAC name: 1*Br*,2*Br*-bis(dicarbonyl(pentamethylcyclopentadienyl)cyclotriphosphanomolybdenum(0)-κ^2*P*,*P'*copper(I))-μ-dibromide
ID Number: 19

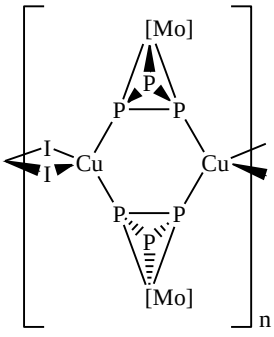

[Mo] = $Mo(CO)_2Cp^*$

IUPAC name: 1*I*,2*I*-bis(dicarbonyl(pentamethylcyclopentadienyl)cyclotriphosphanomolydenum(0)-κ^2*P*,*P'*copper(I))-μ-diiodide
ID Number: 20

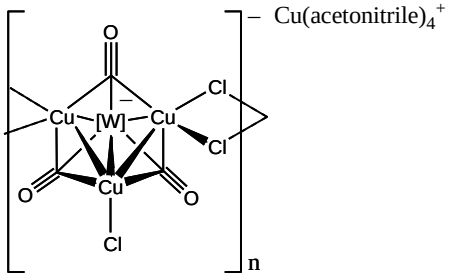

[W] = $W(CO)_2Cp^*$

IUPAC name: 1*Cl*,2*Cl*-(tri-μ-carbonyl-dicopper-(chloro)copper(pentamethylcyclopentadienyl)tungstenate(1-)-κ^2*Cl*^{1},*Cl*^{2}-dichloride-tetraacetonitrilecopper(I)
ID Number: 21

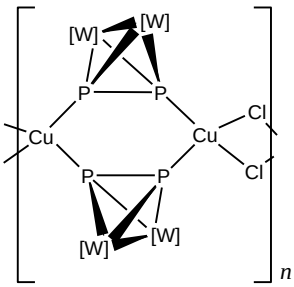

[W] = $WCp(CO)_2$

IUPAC name: Bis(1*P*,2*P*-bis(dicarbonylcyclopentadienyltungsten(I))diphosphorus-κ^2*P*,*P'*copper(I))-μ-dichloride
ID Number: 22

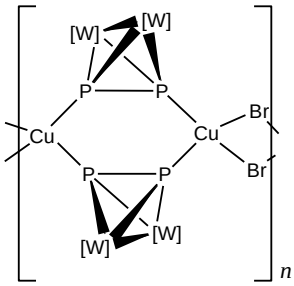

[W] = $WCp(CO)_2$

IUPAC name: Bis(1*P*,2*P*-bis(dicarbonylcyclopentadienyltungsten(I))diphosphorus-κ^2*P*,*P'*copper(I))-μ-dibromide
ID Number: 23

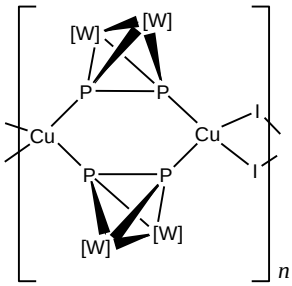

[W] = $WCp(CO)_2$

IUPAC name: Bis(1*P*,2*P*-bis(dicarbonylcyclopentadienyltungsten(I))diphosphorus-κ^2*P*,*P'*copper(I))-μ-diiodide
ID Number: 24

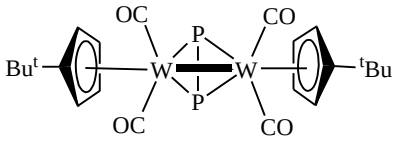

Unit short name: $W_2P_2(^tBu)$
IUPAC name: bis(dicarbonyl(*t*-butylcyclopentadienyl)tungsten(I))diphosphorus
ID Number: 25

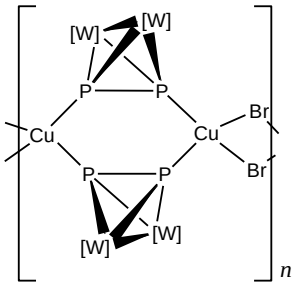

[W] = $W(Cp\text{-}^tBu)(CO)_2$

IUPAC name: Bis(1*P*,2*P*-bis(dicarbonyl(*t*-butylcyclopentadienyl)tungsten(I)) diphosphorus-κ^2*P*,*P'*copper(I))-μ-dibromide
ID Number: 26

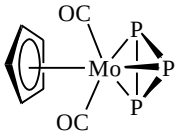

Unit short name: MoP_3
IUPAC name: dicarbonylcyclopentadienylcyclotriphosphanomolybdenum(0)
ID Number: 27

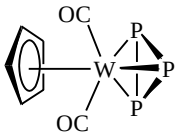

Unit short name: WP_3
IUPAC name: dicarbonylcyclopentadienylcyclotriphosphanotungsten(0)
ID Number: 28

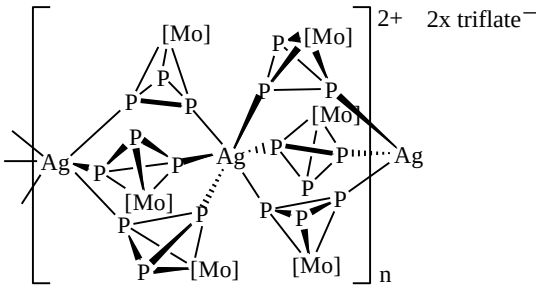

[Mo] = $Mo(CO)_2Cp$

IUPAC name: tris(dicarbonylcyclopentadienylcyclotriphosphanomolybdenum(0)-κ^2*P*,*P*)silver(I)triflate
ID Number: 29

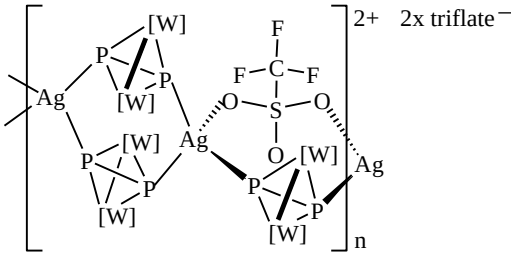

[W] = $WCp(CO)_2$

IUPAC name: Tris(1*P*,2*P*-bis(dicarbonylcyclopentadienyltungsten(I))diphosphorus-κ^3*P,P',P''*)bis(disilver(I)-κ^2*O,O'*-triflate)triflate
ID Number: 30

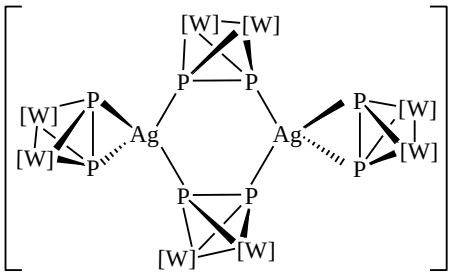

[W] = $WCp(CO)_2$

IUPAC name: Bis(1*P*,2*P*-bis(dicarbonylcyclopentadienyltungsten(I))diphosphorus- κ*P*-κ*P*,*P'*silver(I)hexafluorophosphate
ID Number: 31

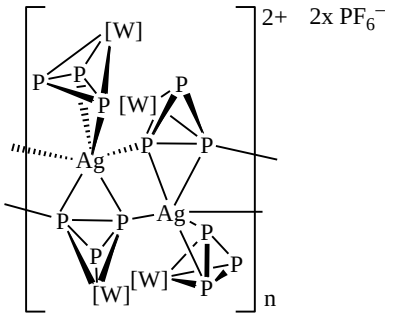

[W] = $WCp(CO)_2$

IUPAC name: Bis(dicarbonylcyclopentadienylcyclotriphosphanotungsten(0)-κ^2*P*,*P*)silver(I)hexafluorophosphate
ID Number: 32

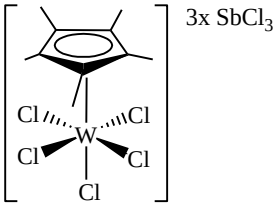

IUPAC name:
Pentachloro(pentamethylcyclopentadienyl)tungsten(VI)tris(trichloroantimony(III))
ID Number: 33

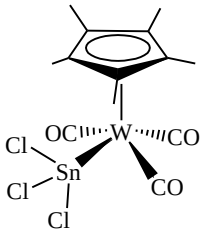

IUPAC name: tricarbonyl(trichlorotin(IV))(pentamethylcyclopentadienyl)tungsten(II)
ID Number: 34

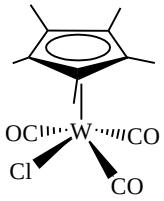

IUPAC name: tricarbonylchloro(pentamethylcyclopentadienyl)tungsten(II)
ID Number: 35

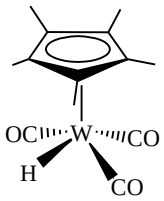

IUPAC name: tricarbonyl(pentamethylcyclopentadienyl)tungsten(I)
ID Number: 36

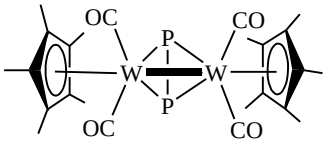

Unit short name: W_2P_2*
IUPAC name: bis(dicarbonyl(pentamethylcyclopentadienyl)tungsten(I))diphosphorus
ID Number: 37

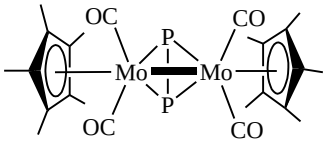

Unit short name: Mo_2P_2*
IUPAC name: bis(dicarbonyl(pentamethylcyclopentadienyl)molybdenum(I))diphosphorus
ID Number: 38

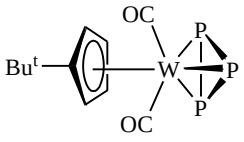

Unit short name: $WP_3(^tBu)$
IUPAC name: (dicarbonyl(*t*-butylcyclopentadienyl)cyclotriphosphanotungsten(0)
ID Number: 39

6.3 Crystallographic Data Tables

Table 6.3.1.	**1** ∗ 2(CH_2Cl_2)	
Empirical Formula	$C_{28}H_{20}Cl_4Mo_4O_8P_4Pt_2(CH_2Cl_2)_2$	
Formula weight	1693.89 g/mole	
Crystal size	0.109 x 0.043 x 0.013 mm	
Crystal description	thin plate	
Crystal color	brown	
Crystal system	triclinic	
Space group	$P\bar{1}$	
Unit cell dimensions	a = 10.9921(18) Å	α = 85.871(14)°
	b = 11.901(3) Å	β = 73.894(13)°
	c = 18.030(2) Å	γ = 77.701(16)°
Volume	2213.8(7) $Å^3$	
Z, Calculated density	2, 2.541 Mg/m^3	
Absorption coefficient	26.722 mm^{-1}	
F(000)	1576	
Measurement device type	Oxford Diffraction Gemini Ultra	
Measurement method	omega-scan	
Temperature	150(1) K	
Wavelength	1.5418 Å	
Monochromator	graphite	
θ range for data collection	2.55 to 62.77°	
Index ranges	$-12 \le h \le 12$, $-13 \le k \le 13$, $-20 \le l \le 20$	
Reflections collected / unique	18383 / 6978 [R(int) = 0.0323]	
Reflections greater I>2\s(I)	4838	
Absorption correction	semi-empirical from equivalents	
Max. and min. transmission	1.34719 and 0.45976	
Refinement method	Full-matrix least-squares on F^2	
Data / restraints / parameters	6978 / 0 / 505	
Goodness of fit on F^2	0.891	
Final R indices [I>2sigma(I)]	R1 = 0.0314, wR2 = 0.0759	
R indices (all data)	R1 = 0.0491, wR2 = 0.0799	
Largest diff. peak and hole	1.611 and -0.842 e.$Å^{-3}$	

Table 6.3.1-a. Atomic coordinates (x 10^4) and equivalent isotropic displacement parameters ($Å^2$ x 10^3) for **1**. U_{eq} is defined as one third of the trace of the orthogonalized U_{ij} tensor.

Atom	**x**	**y**	**z**	U_{eq}
Pt(1)	7439(1)	6497(1)	1487(1)	20(1)
Pt(2)	7577(1)	3351(1)	3586(1)	20(1)
Mo(1)	5746(1)	3415(1)	1592(1)	21(1)
Mo(2)	8753(1)	2811(1)	1132(1)	21(1)
Mo(3)	6264(1)	7128(1)	3949(1)	19(1)
Mo(4)	9267(1)	6407(1)	3434(1)	21(1)
Cl(1)	7718(2)	8409(1)	1385(1)	30(1)
Cl(2)	6987(2)	6632(2)	283(1)	34(1)
Cl(3)	8027(2)	3243(2)	4794(1)	30(1)
Cl(4)	7584(2)	1375(1)	3639(1)	32(1)

P(1)	7269(2)	4665(2)	1565(1)	21(1)
P(2)	7258(2)	3381(2)	2410(1)	20(1)
P(3)	7707(2)	6482(1)	2674(1)	20(1)
P(4)	7623(2)	5216(1)	3529(1)	20(1)
O(1)	5805(6)	848(5)	2168(4)	51(2)
O(2)	6677(6)	2685(5)	-139(3)	47(2)
O(3)	10686(6)	4020(5)	1622(3)	38(2)
O(4)	9191(6)	4207(5)	-433(3)	47(2)
O(5)	5688(6)	5674(5)	5492(3)	40(2)
O(6)	4162(6)	6314(5)	3389(3)	42(2)
O(7)	8642(6)	6084(6)	5246(3)	58(3)
O(8)	10818(6)	3873(5)	3252(3)	37(2)
C(1)	4123(8)	4675(8)	1208(5)	47(3)
C(2)	3712(9)	3612(8)	1427(5)	48(3)
C(3)	3605(8)	3434(8)	2225(5)	44(3)
C(4)	3922(8)	4376(7)	2501(5)	35(3)
C(5)	4269(8)	5144(7)	1877(5)	42(3)
C(6)	5853(8)	1751(7)	1943(5)	36(3)
C(7)	6425(8)	2936(7)	491(5)	33(3)
C(8)	9004(9)	892(6)	1557(5)	37(3)
C(9)	8618(8)	928(6)	863(4)	34(3)
C(10)	9583(9)	1313(6)	273(5)	37(3)
C(11)	10577(8)	1501(6)	579(4)	35(3)
C(12)	10203(8)	1228(7)	1379(5)	37(3)
C(13)	9972(8)	3612(7)	1438(4)	29(3)
C(14)	8988(8)	3761(6)	154(4)	30(3)
C(15)	5000(8)	8848(6)	3698(5)	33(3)
C(16)	4574(9)	8562(6)	4501(5)	39(3)
C(17)	5584(8)	8604(6)	4834(5)	33(3)
C(18)	6638(8)	8886(6)	4263(4)	33(3)
C(19)	6286(8)	9043(6)	3553(5)	32(3)
C(20)	5925(7)	6165(6)	4931(4)	27(3)
C(21)	4947(8)	6542(6)	3605(4)	26(3)
C(22)	10145(9)	7632(7)	2447(5)	43(3)
C(23)	11124(8)	6712(7)	2553(5)	38(3)
C(24)	11260(8)	6777(7)	3297(5)	37(3)
C(25)	10357(9)	7772(7)	3650(5)	42(3)
C(26)	9665(8)	8285(7)	3128(5)	39(3)
C(27)	8841(8)	6171(7)	4595(5)	36(3)
C(28)	10201(8)	4795(7)	3325(4)	33(3)
Cl(5)	6386(3)	1616(2)	8117(2)	78(1)
Cl(6)	6225(3)	-466(2)	9073(2)	82(1)
C(29)	5472(9)	949(7)	8918(5)	48(3)
Cl(7)	1867(4)	869(3)	2970(2)	91(2)
Cl(8)	1486(4)	310(3)	4590(2)	101(2)
C(30)	866(10)	1165(8)	3883(5)	57(4)

Table 6.3.1-b. Anisotropic displacement parameters ($Å^2$ x 10^3) for **1**. The anisotropic displacement factor exponent takes the form: $-2\pi^2 [h^2a^{*2}U_{11} + ... + 2hka^*b^*U_{12}]$.

Atom	U_{11}	U_{22}	U_{33}	U_{23}	U_{13}	U_{12}

Pt(1)	22(1)	18(1)	20(1)	1(1)	-5(1)	-4(1)
Pt(2)	21(1)	17(1)	20(1)	0(1)	-5(1)	-3(1)
Mo(1)	20(1)	22(1)	23(1)	-1(1)	-7(1)	-4(1)
Mo(2)	21(1)	18(1)	22(1)	-1(1)	-3(1)	-4(1)
Mo(3)	18(1)	17(1)	22(1)	-1(1)	-4(1)	-3(1)
Mo(4)	18(1)	22(1)	26(1)	-1(1)	-7(1)	-4(1)
Cl(1)	43(1)	19(1)	31(1)	3(1)	-11(1)	-11(1)
Cl(2)	49(1)	29(1)	28(1)	3(1)	-18(1)	-8(1)
Cl(3)	39(1)	28(1)	25(1)	2(1)	-13(1)	-5(1)
Cl(4)	52(1)	18(1)	29(1)	3(1)	-10(1)	-12(1)
P(1)	23(1)	17(1)	22(1)	-1(1)	-7(1)	-4(1)
P(2)	21(1)	18(1)	22(1)	1(1)	-6(1)	-5(1)
P(3)	20(1)	17(1)	22(1)	1(1)	-5(1)	-4(1)
P(4)	23(1)	17(1)	22(1)	1(1)	-8(1)	-4(1)
O(1)	49(4)	41(4)	61(4)	14(3)	-12(3)	-16(3)
O(2)	47(4)	68(4)	27(3)	-20(3)	-7(3)	-12(3)
O(3)	32(4)	52(4)	36(3)	1(3)	-15(3)	-15(3)
O(4)	58(5)	41(3)	30(3)	6(3)	0(3)	-4(3)
O(5)	45(4)	35(3)	31(3)	13(3)	-2(3)	-6(3)
O(6)	24(3)	57(4)	49(4)	-10(3)	-13(3)	-12(3)
O(7)	51(4)	93(5)	34(4)	2(3)	-19(3)	-17(4)
O(8)	38(4)	31(3)	42(3)	4(3)	-15(3)	-4(3)
C(1)	30(5)	65(6)	33(5)	6(4)	-11(4)	19(5)
C(2)	35(6)	58(6)	58(6)	-16(5)	-26(5)	-1(5)
C(3)	21(5)	42(5)	68(6)	-3(5)	-6(5)	-10(4)
C(4)	29(5)	35(5)	38(5)	-9(4)	-7(4)	0(4)
C(5)	27(5)	37(5)	53(6)	1(4)	-3(4)	-1(4)
C(6)	32(5)	30(5)	45(5)	8(4)	-10(4)	-8(4)
C(7)	29(5)	32(4)	39(5)	1(4)	-8(4)	-12(4)
C(8)	43(6)	19(4)	38(5)	11(4)	-2(4)	2(4)
C(9)	37(5)	16(4)	43(5)	-5(4)	3(4)	-9(4)
C(10)	44(6)	24(4)	37(5)	-6(4)	-5(4)	1(4)
C(11)	30(5)	29(4)	35(5)	-4(4)	1(4)	4(4)
C(12)	35(5)	32(4)	38(5)	-4(4)	-9(4)	8(4)
C(13)	26(5)	34(4)	22(4)	-2(3)	-2(4)	2(4)
C(14)	35(5)	23(4)	28(4)	0(4)	-2(4)	-6(4)
C(15)	33(5)	21(4)	44(5)	-3(4)	-21(4)	10(4)
C(16)	36(5)	22(4)	48(5)	-9(4)	7(4)	-2(4)
C(17)	38(5)	20(4)	35(4)	-13(3)	-2(4)	3(4)
C(18)	36(5)	16(4)	44(5)	-9(3)	-6(4)	-2(4)
C(19)	29(5)	12(4)	45(5)	-1(3)	1(4)	1(3)
C(20)	26(5)	20(4)	36(5)	-6(4)	-6(4)	-6(3)
C(21)	23(5)	28(4)	23(4)	-5(3)	1(4)	-2(4)
C(22)	46(6)	43(5)	52(6)	16(4)	-23(5)	-26(5)
C(23)	30(5)	37(5)	42(5)	1(4)	7(4)	-16(4)
C(24)	19(5)	40(5)	55(6)	-3(4)	-11(4)	-8(4)
C(25)	37(6)	47(5)	51(5)	0(4)	-12(5)	-25(5)
C(26)	22(5)	30(4)	61(6)	4(4)	-4(4)	-8(4)
C(27)	32(5)	47(5)	34(5)	1(4)	-12(4)	-13(4)
C(28)	27(5)	39(5)	31(4)	2(4)	-8(4)	-5(4)

Cl(5)	102(3)	56(2)	64(2)	3(1)	-1(2)	-22(2)
Cl(6)	69(2)	66(2)	85(2)	21(2)	-5(2)	16(2)
C(29)	43(6)	43(5)	58(6)	1(5)	-14(5)	-7(5)
Cl(7)	90(3)	105(3)	62(2)	-8(2)	-12(2)	6(2)
Cl(8)	107(3)	114(3)	80(2)	-11(2)	-56(2)	23(2)
C(30)	58(7)	35(5)	70(7)	-1(5)	-18(6)	8(5)

Table 6.3.2.	**2** $*$ $2(CH_2Cl_2)$
Empirical Formula	$C_{28}H_{20}Cl_4Mo_4O_8P_4Pd_2(CH_2Cl_2)_2$
Formula weight	1516.57
Crystal size	0.470 x 0.270 x 0.030 mm
Crystal description	plate
Crystal color	dark brown
Crystal system	triclinic
Space group	$P\bar{1}$
Unit cell dimensions	a = 9.0901(11) Å α = 78.016(10)°
	b = 10.9579(13) Å β = 86.775(10)°
	c = 11.8860(14) Å γ = 71.328(11)°
Volume	1097.1(2) $Å^3$
Z, Calculated density	1, 2.296 Mg/m^3
Absorption coefficient	21.820 mm^{-1}
F(000)	724
Measurement device type	Oxford Diffraction Gemini Ultra
Measurement method	omega-scan
Temperature	123 K
Wavelength	1.54184 Å
Monochromator	graphite
θ range for data collection	3.80 to 57.05°
Index ranges	$-9 \le h \le 9$, $-11 \le k \le 11$, $-12 \le l \le 12$
Reflections collected / unique	6571 / 2919 [R(int) = 0.0737]
Reflections greater I>2\s(I)	2186
Absorption correction	semi-empirical from equivalents
Max. and min. transmission	1.00000 and 0.14448
Refinement method	Full-matrix least-squares on F^2
Data / restraints / parameters	2919 / 0 / 300
Goodness of fit on F^2	0.990
Final R indices [I>2sigma(I)]	R1 = 0.0712, wR2 = 0.1740
R indices (all data)	R1 = 0.1098, wR2 = 0.1858
Largest diff. peak and hole	2.598 and -1.455 $e.A^{-3}$

Table 6.3.2-a. Atomic coordinates (x 10^4) and equivalent isotropic displacement parameters ($Å^2$ x 10^3) for **2**. U_{eq} is defined as one third of the trace of the orthogonalized U_{ij} tensor.

Atom	**x**	**y**	**z**	U_{eq}
Pd(1)	2873(1)	1126(1)	-1580(1)	33(1)
Mo(1)	2193(1)	137(1)	2156(1)	32(1)
Mo(2)	3157(1)	2677(1)	1512(1)	36(1)
Cl(1)	2755(4)	1039(4)	-3524(3)	56(1)
Cl(2)	480(4)	2794(3)	-1646(3)	43(1)

P(1)	3034(4)	1147(3)	287(3)	33(1)
P(2)	4749(4)	363(3)	1555(3)	34(1)
O(1)	3255(12)	-2407(10)	1103(10)	58(4)
O(2)	-975(12)	1167(10)	760(8)	51(3)
O(5)	-530(20)	3859(19)	1076(16)	52(7)
O(6)	4280(20)	2010(20)	4196(14)	55(7)
C(1)	2874(14)	-1459(14)	1466(11)	34(4)
C(2)	205(19)	810(14)	1254(13)	48(5)
C(3)	437(19)	210(17)	3651(10)	52(6)
C(4)	1119(16)	-1104(15)	3527(12)	46(5)
C(5)	2722(18)	-1443(19)	3783(12)	55(6)
C(6)	3030(18)	-370(17)	4047(12)	51(6)
C(7)	1660(20)	610(20)	3995(13)	66(7)
C(15)	2413(19)	4633(16)	403(15)	63(13)
C(16)	3730(20)	3861(17)	-45(14)	61(10)
C(17)	4949(17)	3594(15)	707(12)	42(9)
C(18)	4381(16)	4201(12)	1620(10)	41(10)
C(19)	2814(18)	4843(11)	1432(12)	52(10)
C(21)	760(30)	3460(30)	1190(30)	44(10)
C(22)	3930(40)	2250(40)	3300(30)	51(8)
C(11)	4933(15)	3737(15)	1752(10)	47(14)
C(12)	3388(18)	4606(11)	1794(11)	33(9)
C(13)	2610(20)	4020(16)	2723(12)	47(10)
C(14)	3680(20)	2789(19)	3256(13)	33(8)
O(4)	-320(20)	3450(20)	2350(20)	50(8)
C(8)	3360(30)	3580(30)	-220(20)	30(6)
C(9)	930(40)	3060(30)	2050(30)	31(10)
C(10)	5112(18)	2615(18)	2656(12)	38(7)
O(3)	3480(20)	4022(17)	-1123(15)	37(6)
Cl(5)	809(12)	-3902(10)	-4676(10)	95(4)
Cl(6)	4038(11)	-5151(10)	-4164(11)	83(4)
C(31)	2190(60)	-5320(50)	-3880(40)	72(16)
Cl(7)	3774(10)	-5620(11)	-3325(8)	64(3)
Cl(8)	1887(12)	-4754(11)	-5435(9)	79(4)
C(32)	2120(50)	-5640(50)	-4030(40)	52(12)

Table 6.3.2-b. Anisotropic displacement parameters ($Å^2$ x 10^3) for **2**. The anisotropic displacement factor exponent takes the form: $-2\pi^2[h^2a^{*2}U_{11} + ... + 2hka^*b^*U_{12}]$.

Atom	U_{11}	U_{22}	U_{33}	U_{23}	U_{13}	U_{12}
Pd(1)	34(1)	33(1)	39(1)	-12(1)	7(1)	-17(1)
Mo(1)	36(1)	36(1)	30(1)	-9(1)	4(1)	-19(1)
Mo(2)	33(1)	29(1)	49(1)	-11(1)	5(1)	-14(1)
Cl(1)	36(2)	90(3)	52(2)	-43(2)	-2(2)	-16(2)
Cl(2)	40(2)	42(2)	47(2)	-12(2)	7(1)	-11(2)
P(1)	39(2)	29(2)	34(2)	-11(1)	8(1)	-13(2)
P(2)	36(2)	31(2)	39(2)	-12(1)	6(1)	-16(2)
O(1)	48(6)	43(6)	89(8)	-25(6)	0(5)	-14(5)
O(2)	51(6)	54(6)	48(5)	-3(5)	-5(5)	-19(5)
O(5)	40(13)	44(11)	61(13)	-6(9)	1(9)	-1(10)
O(6)	79(14)	70(14)	30(10)	-9(9)	-14(9)	-41(12)

C(1)	24(7)	38(8)	44(7)	-7(6)	5(5)	-15(6)
C(2)	57(10)	49(9)	45(8)	-23(7)	5(7)	-19(8)
C(3)	61(10)	89(13)	18(6)	-16(7)	15(6)	-41(9)
C(4)	47(9)	53(9)	51(8)	-3(7)	11(7)	-41(8)
C(5)	46(9)	88(12)	40(8)	-13(8)	7(6)	-34(9)
C(6)	44(9)	92(12)	45(8)	-23(8)	8(7)	-54(10)
C(7)	68(12)	116(15)	52(9)	-59(10)	41(8)	-62(12)
C(15)	44(17)	37(16)	100(30)	16(17)	-10(16)	-18(14)
C(17)	38(14)	23(13)	62(18)	12(12)	1(13)	-20(12)
C(18)	60(20)	49(19)	29(14)	-5(12)	0(13)	-40(20)
C(19)	45(18)	26(14)	80(20)	-4(14)	9(18)	-11(14)
C(21)	36(18)	29(15)	50(20)	0(13)	10(13)	7(13)
C(11)	40(20)	50(20)	70(30)	-30(20)	6(17)	-30(20)
C(13)	41(17)	60(20)	40(16)	-36(15)	24(13)	-5(16)
O(4)	26(12)	52(13)	93(18)	-40(12)	11(11)	-26(10)
C(9)	50(20)	27(15)	21(16)	8(13)	-6(14)	-25(15)
O(3)	45(11)	32(10)	32(10)	-17(8)	11(8)	-5(9)
Cl(5)	83(7)	65(6)	110(8)	16(6)	7(6)	-10(5)
Cl(6)	68(6)	72(6)	107(9)	0(6)	9(5)	-31(5)
Cl(7)	55(5)	90(7)	54(6)	-11(5)	-5(4)	-32(5)
Cl(8)	70(7)	86(7)	80(6)	12(5)	-15(5)	-37(6)

Table 6.3.3.	**10** $*$ $2(C_4H_8O)$
Empirical Formula	$C_{36}H_{20}Mo_4O_{16}P_4W_2(C_4H_8O)_2$
Formula weight	1728.05
Crystal size	0.120 x 0.120 x 0.110 mm
Crystal description	prism
Crystal color	brown to black
Crystal system	monoclinic
Space group	$P2_1/n$
Unit cell dimensions	a = 10.22848(13) Å α = 90°
	b = 17.9710(2) Å β = 106.1811(15)°
	c = 14.5534(2) Å γ = 90°
Volume	2569.17(6) $Å^3$
Z, Calculated density	2, 2.234 Mg/m^3
Absorption coefficient	17.591 mm^{-1}
F(000)	1640
Measurement device type	Oxford Diffraction Gemini Ultra
Measurement method	omega-scan
Temperature	123 K
Wavelength	1.54184 Å
Monochromator	graphite
θ range for data collection	4.01 to 62.32°
Index ranges	$-11 \leq h \leq 11$, $-20 \leq k \leq 19$, $-16 \leq l \leq 12$
Reflections collected / unique	10251 / 3983 [R(int) = 0.0264]
Reflections greater I>2\s(I)	3478
Absorption correction	semi-empirical from equivalents
Max. and min. transmission	1.00000 and 0.23493
Refinement method	Full-matrix least-squares on F^2

Data / restraints / parameters	3983 / 0 / 325
Goodness of fit on F^2	0.979
Final R indices [I>2sigma(I)]	R1 = 0.0278, wR2 = 0.0660
R indices (all data)	R1 = 0.0322, wR2 = 0.0676
Largest diff. peak and hole	1.771 and -0.834 e.Å^{-3}

Table 6.3.3-a. Atomic coordinates (x 10^4) and equivalent isotropic displacement parameters (Å^2 x 10^3) for **10**. U_{eq} is defined as one third of the trace of the orthogonalized U_{ij} tensor.

Atom	**x**	**y**	**z**	U_{eq}
W(1)	7147(1)	-180(1)	4370(1)	13(1)
Mo(1)	9413(1)	2076(1)	5146(1)	13(1)
Mo(2)	9873(1)	1573(1)	3284(1)	14(1)
P(1)	8772(1)	867(1)	4391(1)	13(1)
P(2)	9129(1)	-1004(1)	5152(1)	13(1)
O(1)	10202(4)	1498(2)	7257(3)	37(1)
O(2)	12399(4)	2673(2)	5614(2)	27(1)
O(3)	6712(4)	1678(2)	2402(2)	30(1)
O(4)	9687(4)	3(2)	2337(3)	35(1)
O(5)	7253(4)	413(2)	6453(3)	30(1)
O(6)	4700(4)	867(2)	3394(2)	25(1)
O(7)	6929(4)	-761(2)	2272(2)	35(1)
O(8)	5166(4)	-1464(2)	4561(2)	25(1)
C(1)	9939(5)	1664(3)	6473(4)	24(2)
C(2)	11321(5)	2444(3)	5432(3)	17(2)
C(3)	7098(5)	2403(3)	4622(4)	23(2)
C(4)	7806(5)	2924(3)	4211(4)	24(2)
C(5)	8732(5)	3308(3)	4956(4)	22(2)
C(6)	8587(5)	3039(3)	5841(4)	23(2)
C(7)	7565(5)	2479(3)	5628(4)	21(2)
C(8)	7859(5)	1639(3)	2738(3)	20(2)
C(9)	9740(5)	562(3)	2712(3)	20(2)
C(10)	10047(5)	2616(3)	2392(3)	22(2)
C(11)	10444(5)	1975(3)	1961(3)	20(2)
C(12)	11643(5)	1691(3)	2603(3)	23(2)
C(13)	11988(5)	2145(3)	3413(3)	23(2)
C(14)	11014(6)	2722(3)	3290(3)	24(2)
C(15)	7197(5)	195(3)	5707(4)	19(2)
C(16)	5585(5)	489(3)	3759(3)	17(2)
C(17)	7053(5)	-545(3)	3035(3)	21(2)
C(18)	5891(5)	-995(3)	4490(3)	17(2)
O(20)	3918(4)	9330(2)	555(3)	37(1)
C(20)	2955(6)	9576(3)	-300(4)	34(2)
C(21)	3703(6)	9783(3)	1308(4)	35(2)
C(22)	2201(7)	9980(5)	1003(4)	48(2)
C(23)	1723(8)	9755(7)	-18(5)	89(4)

Table 6.3.3-b. Anisotropic displacement parameters (Å^2 x 10^3) for **10**. The anisotropic displacement factor exponent takes the form: $-2\pi^2[h^2a^{*2}U_{11} + ... + 2hka^*b^* U_{12}]$.

Atom	U_{11}	U_{22}	U_{33}	U_{23}	U_{13}	U_{12}
W(1)	13(1)	13(1)	12(1)	0(1)	3(1)	0(1)
Mo(1)	15(1)	11(1)	14(1)	-1(1)	4(1)	0(1)
Mo(2)	16(1)	13(1)	12(1)	2(1)	4(1)	0(1)
P(1)	15(1)	13(1)	12(1)	0(1)	3(1)	0(1)
P(2)	15(1)	11(1)	13(1)	1(1)	4(1)	0(1)
O(1)	56(3)	34(2)	19(2)	7(2)	6(2)	7(2)
O(2)	24(2)	30(2)	26(2)	-7(2)	4(2)	-3(2)
O(3)	24(2)	41(3)	22(2)	10(2)	2(2)	2(2)
O(4)	47(3)	26(2)	35(2)	-11(2)	14(2)	-4(2)
O(5)	33(2)	39(2)	20(2)	-6(2)	10(2)	-1(2)
O(6)	20(2)	23(2)	27(2)	3(2)	0(2)	6(2)
O(7)	36(2)	48(3)	20(2)	-10(2)	8(2)	-2(2)
O(8)	30(2)	17(2)	30(2)	-4(2)	12(2)	-13(2)
C(1)	24(3)	25(3)	24(3)	1(2)	8(2)	-1(2)
C(2)	17(3)	14(3)	19(2)	-3(2)	4(2)	1(2)
C(3)	22(3)	18(3)	29(3)	-2(2)	6(2)	2(2)
C(4)	26(3)	22(3)	23(3)	8(2)	5(2)	15(2)
C(5)	20(3)	9(3)	40(3)	0(2)	12(2)	1(2)
C(6)	24(3)	17(3)	25(3)	-9(2)	2(2)	9(2)
C(7)	23(3)	16(3)	27(3)	0(2)	13(2)	6(2)
C(8)	22(3)	21(3)	17(2)	1(2)	7(2)	-4(2)
C(9)	23(3)	21(3)	16(2)	4(2)	7(2)	1(2)
C(10)	25(3)	17(3)	25(3)	9(2)	11(2)	-2(2)
C(11)	23(3)	23(3)	15(2)	10(2)	8(2)	-2(2)
C(12)	26(3)	24(3)	26(3)	3(2)	19(2)	-4(2)
C(13)	20(3)	31(3)	19(2)	2(2)	5(2)	-7(2)
C(14)	36(3)	17(3)	21(2)	5(2)	13(2)	-6(2)
C(15)	18(3)	20(3)	20(3)	2(2)	7(2)	0(2)
C(16)	21(3)	18(3)	12(2)	-6(2)	6(2)	-1(2)
C(17)	23(3)	19(3)	20(3)	0(2)	7(2)	-1(2)
C(18)	21(3)	17(3)	14(2)	-3(2)	7(2)	5(2)
O(20)	42(2)	40(3)	29(2)	0(2)	9(2)	15(2)
C(20)	48(4)	28(3)	22(3)	-1(2)	5(3)	5(3)
C(21)	42(4)	33(4)	27(3)	-6(3)	6(3)	5(3)
C(22)	39(4)	75(5)	33(3)	-14(3)	13(3)	12(4)
C(23)	38(4)	178(11)	40(4)	-43(5)	-6(3)	35(5)

Table 6.3.4.	**11**	
Empirical Formula	$C_{14}H_{10}O_4P_2W_2$	
Formula weight	671.84	
Crystal size	0.128 x 0.092 x 0.066 mm	
Crystal description	parallelepiped	
Crystal color	orange	
Crystal system	monoclinic	
Space group	C2/c	
Unit cell dimensions	a = 13.4146(3) Å	α = 90°
	b = 7.2399(1) Å	β = 105.621(3)°
	c = 16.5646(5) Å	γ = 90°

Volume	1549.34(7) Å^3
Z, Calculated density	4, 2.880 Mg/m^3
Absorption coefficient	29.133 mm^{-1}
F(000)	1216
Measurement device type	Oxford Diffraction Gemini Ultra
Measurement method	omega-scan
Temperature	123 K
Wavelength	1.54184 Å
Monochromator	graphite
θ range for data collection	5.55 to 66.80°
Index ranges	$-15 \leq h \leq 15$, $-8 \leq k \leq 8$, $-15 \leq l \leq 19$
Reflections collected / unique	11262 / 1351 [R(int) = 0.0370]
Reflections greater I>2\s(I)	1318
Absorption correction	semi-empirical from equivalents
Max. and min. transmission	1.00000 and 0.25857
Refinement method	Full-matrix least-squares on F^2
Data / restraints / parameters	1351 / 0 / 100
Goodness of fit on F^2	1.118
Final R indices [I>2sigma(I)]	R1 = 0.0232, wR2 = 0.0612
R indices (all data)	R1 = 0.0238, wR2 = 0.0615
Largest diff. peak and hole	0.968 and -1.228 e.Å^{-3}

Table 6.3.4-a. Atomic coordinates (x 10^4) and equivalent isotropic displacement parameters (Å^2 x 10^3) for **11**. U_{eq} is defined as one third of the trace of the orthogonalized U_{ij} tensor.

Atom	**x**	**y**	**z**	U_{eq}
W(1)	4511(1)	227(1)	1573(1)	10(1)
P(1)	4242(1)	2606(2)	2560(1)	15(1)
O(1)	4494(3)	3300(5)	245(2)	25(1)
O(2)	6678(3)	-1012(6)	1400(3)	30(1)
C(1)	3540(4)	-2395(7)	1763(4)	23(2)
C(2)	2855(4)	-891(9)	1529(4)	27(2)
C(3)	2871(4)	-324(8)	713(4)	26(2)
C(4)	3587(4)	-1465(8)	451(4)	25(2)
C(5)	3999(4)	-2742(7)	1104(4)	23(2)
C(6)	4533(4)	2206(7)	748(3)	16(1)
C(7)	5905(4)	-512(7)	1491(3)	17(2)

Table 6.3.4-b. Anisotropic displacement parameters (Å^2 x 10^3) for **11**. The anisotropic displacement factor exponent takes the form: $-2\pi^2[h^2a^{*2}U_{11} + ... + 2hka^*b^*U_{12}]$.

Atom	U_{11}	U_{22}	U_{33}	U_{23}	U_{13}	U_{12}
W(1)	8(1)	8(1)	14(1)	0(1)	2(1)	-1(1)
P(1)	15(1)	12(1)	18(1)	-1(1)	3(1)	5(1)
O(1)	37(2)	16(2)	21(2)	7(2)	9(2)	2(2)
O(2)	19(2)	44(3)	28(2)	-1(2)	7(2)	11(2)
C(1)	29(3)	13(2)	24(3)	-3(2)	4(2)	-15(2)
C(2)	14(2)	31(3)	36(3)	-12(3)	9(2)	-14(2)
C(3)	15(3)	24(3)	33(4)	-1(2)	-2(3)	-7(2)
C(4)	23(3)	25(3)	23(3)	-7(2)	2(2)	-16(2)

C(5)	23(3)	13(2)	30(3)	-9(2)	4(2)	-11(2)
C(6)	18(2)	12(2)	17(2)	-5(2)	5(2)	1(2)
C(7)	19(3)	14(2)	18(3)	1(2)	5(2)	2(2)

Table 6.3.5.	**12** $*$ $2(C_4H_8O)$	
Empirical Formula	$C_{36}H_{20}O_{16}P_4W_6(C_4H_8O)_2$	
Formula weight	2079.65	
Crystal size	0.062 x 0.056 x 0.054 mm	
Crystal description	prism	
Crystal color	red	
Crystal system	monoclinic	
Space group	$P2_1/n$	
Unit cell dimensions	a = 10.2244(2) Å	α = 90°
	b = 17.9963(3) Å	β = 106.304(2)°
	c = 14.5618(2) Å	γ = 90°
Volume	2571.64(8) $Å^3$	
Z, Calculated density	2, 2.686 Mg/m^3	
Absorption coefficient	13.560 mm^{-1}	
F(000)	1896	
Measurement device type	Oxford Diffraction Gemini Ultra	
Measurement method	omega-scan	
Temperature	123 K	
Wavelength	0.71073 Å	
Monochromator	graphite	
θ range for data collection	2.91 to 30.75°	
Index ranges	$-14 \le h \le 14$, $-11 \le k \le 25$, $-15 \le l \le 20$	
Reflections collected / unique	17559 / 7969 [R(int) = 0.0281]	
Reflections greater I>2\s(I)	6312	
Absorption correction	semi-empirical from equivalents	
Max. and min. transmission	1.00000 and 0.82394	
Refinement method	Full-matrix least-squares on F^2	
Data / restraints / parameters	7969 / 0 / 325	
Goodness of fit on F^2	0.875	
Final R indices [I>2sigma(I)]	R1 = 0.0212, wR2 = 0.0303	
R indices (all data)	R1 = 0.0330, wR2 = 0.0313	
Largest diff. peak and hole	1.359 and -1.080 e.$Å^{-3}$	

Table 6.3.5-a. Atomic coordinates (x 10^4) and equivalent isotropic displacement parameters ($Å^2$ x 10^3) for **12**. U_{eq} is defined as one third of the trace of the orthogonalized U_{ij} tensor.

Atom	**x**	**y**	**z**	U_{eq}
W(1)	5130(1)	-1577(1)	6719(1)	10(1)
W(2)	5594(1)	-2079(1)	4861(1)	9(1)
W(3)	7861(1)	181(1)	5632(1)	9(1)
P(1)	4122(1)	-1008(1)	5151(1)	10(1)
P(2)	6240(1)	-870(1)	5616(1)	10(1)
O(6)	8302(2)	-1697(2)	7603(2)	24(1)
O(7)	5339(3)	-9(2)	7660(2)	27(1)
O(16)	2606(2)	-2690(1)	4402(2)	20(1)

O(17)	4784(3)	-1497(2)	2754(2)	29(1)
O(21)	10310(2)	-869(2)	6614(2)	23(1)
O(22)	7737(2)	-413(2)	3543(2)	26(1)
O(23)	9855(2)	1464(1)	5438(2)	21(1)
O(24)	8090(2)	765(2)	7726(2)	28(1)
C(1)	3011(3)	-2152(2)	6587(2)	19(1)
C(2)	3352(3)	-1689(2)	7402(2)	15(1)
C(3)	4565(3)	-1981(2)	8048(2)	16(1)
C(4)	4952(3)	-2618(2)	7619(2)	18(1)
C(5)	3986(3)	-2729(2)	6718(2)	17(1)
C(6)	7142(3)	-1655(2)	7264(2)	16(1)
C(7)	5272(3)	-571(2)	7281(2)	16(1)
C(11)	7213(3)	-2921(2)	5794(2)	16(1)
C(12)	7929(3)	-2407(2)	5382(2)	18(1)
C(13)	7443(3)	-2475(2)	4373(2)	17(1)
C(14)	6415(3)	-3042(2)	4163(2)	16(1)
C(15)	6274(3)	-3307(2)	5051(2)	16(1)
C(16)	3690(3)	-2460(2)	4574(2)	13(1)
C(17)	5055(3)	-1663(2)	3542(2)	17(1)
C(21)	9414(3)	-482(2)	6239(2)	13(1)
C(22)	7795(3)	-198(2)	4292(2)	14(1)
C(23)	9119(3)	987(2)	5520(2)	14(1)
C(24)	7952(3)	547(2)	6966(2)	13(1)
O(45)	3922(2)	5663(2)	5552(2)	31(1)
C(41)	3701(4)	5222(2)	6307(3)	27(1)
C(42)	2207(4)	5018(3)	6003(3)	40(1)
C(43)	1696(4)	5262(4)	4976(3)	71(2)
C(44)	2964(4)	5424(2)	4694(2)	26(1)

Table 6.3.5-b. Atomic coordinates (x 10^4) and equivalent isotropic displacement parameters ($Å^2$ x 10^3) for **12**. U_{eq} is defined as one third of the trace of the orthogonalized U_{ij} tensor.

Atom	U_{11}	U_{22}	U_{33}	U_{23}	U_{13}	U_{12}
W(1)	10(1)	10(1)	9(1)	2(1)	3(1)	0(1)
W(2)	10(1)	8(1)	11(1)	0(1)	3(1)	0(1)
W(3)	8(1)	9(1)	10(1)	0(1)	2(1)	0(1)
P(1)	9(1)	10(1)	10(1)	1(1)	2(1)	0(1)
P(2)	9(1)	10(1)	10(1)	1(1)	3(1)	-1(1)
O(6)	14(1)	38(2)	20(1)	8(1)	3(1)	2(1)
O(7)	40(2)	19(2)	24(1)	-5(1)	11(1)	-5(1)
O(16)	15(1)	23(2)	22(1)	-7(1)	6(1)	-5(1)
O(17)	43(2)	28(2)	14(1)	5(1)	4(1)	5(1)
O(21)	19(1)	23(2)	25(1)	3(1)	3(1)	6(1)
O(22)	25(1)	35(2)	17(1)	-5(1)	8(1)	-2(1)
O(23)	21(1)	18(2)	27(1)	-3(1)	12(1)	-8(1)
O(24)	27(1)	37(2)	19(1)	-9(1)	7(1)	-2(1)
C(1)	16(2)	23(2)	16(2)	5(2)	4(1)	-5(2)
C(2)	16(2)	16(2)	17(2)	4(1)	13(1)	0(1)
C(3)	19(2)	21(2)	11(2)	2(1)	8(1)	-2(2)
C(4)	22(2)	16(2)	18(2)	6(2)	8(1)	0(2)
C(5)	18(2)	14(2)	19(2)	1(2)	7(1)	-4(1)

C(6)	20(2)	18(2)	12(2)	4(1)	6(1)	-1(2)
C(7)	17(2)	20(2)	13(2)	3(2)	7(1)	0(2)
C(11)	16(2)	14(2)	20(2)	2(2)	6(1)	7(2)
C(12)	11(1)	16(2)	23(2)	-4(2)	1(1)	5(1)
C(13)	13(2)	17(2)	23(2)	-3(2)	11(1)	6(1)
C(14)	19(2)	10(2)	21(2)	-7(1)	7(1)	6(1)
C(15)	17(2)	5(2)	29(2)	1(2)	10(1)	2(1)
C(16)	16(2)	13(2)	9(2)	1(1)	3(1)	3(1)
C(17)	20(2)	12(2)	17(2)	0(2)	3(1)	3(2)
C(21)	15(2)	12(2)	13(2)	0(1)	5(1)	0(1)
C(22)	9(1)	16(2)	18(2)	-1(2)	4(1)	0(1)
C(23)	13(1)	18(2)	9(2)	-4(1)	1(1)	5(1)
C(24)	10(1)	14(2)	16(2)	-2(1)	3(1)	-2(1)
O(45)	34(1)	33(2)	24(1)	4(1)	8(1)	-15(1)
C(41)	32(2)	25(2)	22(2)	6(2)	3(2)	-7(2)
C(42)	36(2)	54(3)	29(2)	8(2)	9(2)	-20(2)
C(43)	31(2)	135(6)	39(3)	42(3)	-1(2)	-22(3)
C(44)	39(2)	20(2)	19(2)	2(2)	9(2)	-3(2)

Table 6.3.6.	**13**
Empirical Formula	$C_{12}H_{15}O_2P_3W$
Formula weight	467.99
Crystal size	0.060 x 0.060 x 0.030 mm
Crystal description	thin plate
Crystal color	yellow
Crystal system	monoclinic
Space group	$P2_1/n$
Unit cell dimensions	a = 11.9363(4) Å α = 90°
	b = 9.2134(2) Å β = 95.260(3)°
	c = 13.3688(3) Å γ = 90°
Volume	1464.03(7) $Å^3$
Z, Calculated density	4, 2.123 Mg/m^3
Absorption coefficient	17.660 mm^{-1}
F(000)	888
Measurement device type	Oxford Diffraction Gemini Ultra
Measurement method	omega-scan
Temperature	123 K
Wavelength	1.54184 Å
Monochromator	graphite
θ range for data collection	4.75 to 62.08°
Index ranges	$-13 \le h \le 9$, $-10 \le k \le 10$, $-15 \le l \le 15$
Reflections collected / unique	8193 / 2247 [R(int) = 0.0353]
Reflections greater I>2\s(I)	1799
Absorption correction	semi-empirical from equivalents
Max. and min. transmission	1.00000 and 0.60907
Refinement method	Full-matrix least-squares on F^2
Data / restraints / parameters	2247 / 0 / 168
Goodness of fit on F^2	1.110
Final R indices [I>2sigma(I)]	R1 = 0.0669, wR2 = 0.1857

R indices (all data)	R1 = 0.0776, wR2 = 0.1915
Largest diff. peak and hole	3.663 and -1.379 e.Å^{-3}

Table 6.3.6-a. Atomic coordinates (x 10^4) and equivalent isotropic displacement parameters (Å^2 x 10^3) for **13**. U_{eq} is defined as one third of the trace of the orthogonalized U_{ij} tensor.

Atom	**x**	**y**	**z**	U_{eq}
W(1)	9682(1)	844(1)	7623(1)	34(1)
P(1)	10318(6)	-1125(8)	8835(5)	78(2)
P(2)	8774(6)	-1628(7)	7936(6)	80(3)
P(3)	10319(5)	-1663(8)	7245(5)	75(3)
O(11)	7813(13)	1630(20)	9022(12)	83(7)
O(12)	7785(13)	612(17)	5851(12)	70(6)
C(1)	10058(15)	3221(16)	7160(15)	46(6)
C(2)	10474(14)	3026(19)	8154(13)	43(6)
C(3)	11384(13)	1977(19)	8239(15)	46(6)
C(4)	11473(14)	1522(19)	7195(13)	41(5)
C(5)	10666(17)	2280(20)	6566(14)	55(7)
C(6)	9210(20)	4330(20)	6760(20)	76(9)
C(7)	10180(20)	3970(20)	9065(18)	71(8)
C(8)	12150(19)	1580(30)	9085(17)	71(8)
C(9)	12395(17)	540(30)	6870(18)	65(8)
C(10)	10600(20)	2140(30)	5445(16)	75(9)
C(11)	8487(16)	1300(20)	8525(15)	52(6)
C(12)	8459(15)	686(18)	6491(12)	39(5)

Table 6.3.6-b. Anisotropic displacement parameters (Å^2 x 10^3) for **13**. The anisotropic displacement factor exponent takes the form: $-2\pi^2[h^2a^{*2}U_{11} + ... + 2hka^*b^*U_{12}]$.

Atom	U_{11}	U_{22}	U_{33}	U_{23}	U_{13}	U_{12}
W(1)	34(1)	28(1)	41(1)	-2(1)	6(1)	-3(1)
P(1)	85(4)	74(4)	73(4)	21(3)	0(3)	-4(3)
P(2)	88(5)	58(4)	95(5)	-2(3)	17(4)	-15(3)
P(3)	74(4)	79(5)	75(4)	-6(3)	17(3)	4(3)
O(11)	59(9)	123(15)	73(10)	-27(10)	33(8)	-10(10)
O(12)	58(9)	83(11)	65(9)	-21(8)	-17(8)	7(8)
C(1)	53(10)	8(7)	75(13)	13(8)	-4(9)	5(7)
C(2)	45(10)	38(9)	52(10)	-18(8)	34(8)	-11(8)
C(3)	20(8)	39(9)	74(12)	5(9)	-18(8)	-12(7)
C(4)	38(9)	33(9)	53(10)	-7(8)	10(8)	2(8)
C(5)	66(12)	47(11)	57(11)	-12(9)	36(10)	-33(10)
C(6)	69(15)	44(12)	110(20)	31(12)	-12(14)	4(11)
C(7)	75(15)	64(14)	74(14)	-46(12)	13(12)	-7(12)
C(8)	67(14)	72(15)	71(14)	7(12)	-9(11)	-20(12)
C(9)	44(11)	74(15)	78(14)	-16(12)	16(10)	6(10)
C(10)	93(17)	76(16)	56(12)	-22(11)	11(12)	25(13)
C(11)	49(11)	51(11)	56(11)	-25(9)	11(9)	-12(9)
C(12)	50(10)	35(9)	34(9)	1(7)	12(8)	5(8)

Table 6.3.7.	**14**
Empirical Formula	$C_{24}H_{30}Cl_2Cu_2O_4P_6W_2$
Formula weight	1133.98
Crystal size	0.17 x 0.09 x 0.03 mm
Crystal description	flat prism
Crystal color	light yellow
Crystal system	monoclinic
Space group	$P2_1/a$
Unit cell dimensions	a = 13.41920(10) Å α = 90°.
	b = 9.04130(10) Å β = 94.3130(10)°
	c = 13.76930(10) Å γ = 90°
Volume	1665.86(3) A^3
Z, Calculated density	2.261 Mg/m^3
Absorption coefficient	18.332 mm^{-1}
F(000)	1072
Measurement device type	Oxford Diffraction Gemini Ultra
Measurement method	omega-scan
Temperature	123 K
Wavelength	1.54184 Å
Monochromator	graphite
θ range for data collection	3.22 to 62.30°
Index ranges	$-15 \leq h \leq 15$, $-9 \leq k \leq 10$, $-15 \leq l \leq 15$
Reflections collected / unique	25110 / 2622 [R(int) = 0.0518]
Reflections greater I>2\s(I)	2160
Absorption correction	semi-empirical from equivalents
Max. and min. transmission	1.00000 and 0.12515
Refinement method	Full-matrix least-squares on F^2
Data / restraints / parameters	2622 / 0 / 186
Goodness of fit on F^2	1.038
Final R indices [I>2sigma(I)]	R1 = 0.0342, wR2 = 0.0855
R indices (all data)	R1 = 0.0423, wR2 = 0.0890
Largest diff. peak and hole	1.471 and -1.147 $e.A^{-3}$

Table 6.3.7-a. Atomic coordinates (x 10^4) and equivalent isotropic displacement parameters ($Å^2$ x 10^3) for **14**. U_{eq} is defined as one third of the trace of the orthogonalized U_{ij} tensor.

Atom	**x**	**y**	**z**	U_{eq}
W(1)	1917(1)	4610(1)	7056(1)	26(1)
Cu(1)	4234(1)	5014(1)	9124(1)	38(1)
Cl(1)	4282(1)	3667(2)	10515(1)	48(1)
P(1)	2940(1)	6211(2)	8241(1)	33(1)
P(2)	3728(1)	4253(2)	7586(1)	33(1)
P(3)	3434(1)	6263(3)	6789(1)	43(1)
O(11)	840(4)	7521(8)	6337(5)	59(2)
O(12)	2383(4)	3804(9)	4931(4)	65(2)
C(1)	1235(5)	3510(10)	8390(5)	41(3)
C(2)	458(5)	4245(8)	7829(5)	27(2)
C(3)	362(6)	3554(11)	6912(5)	46(3)
C(4)	1073(8)	2367(10)	6930(8)	62(4)
C(5)	1597(6)	2389(11)	7841(9)	66(4)

C(6)	1511(8)	3812(19)	9453(6)	125(7)
C(7)	-194(7)	5428(11)	8187(10)	85(5)
C(8)	-462(8)	3899(19)	6118(7)	126(7)
C(9)	1114(13)	1234(18)	6149(14)	199(10)
C(10)	2334(10)	1255(16)	8223(18)	199(11)
C(11)	1247(5)	6470(10)	6586(5)	38(3)
C(12)	2220(5)	4118(10)	5701(5)	39(3)

Table 6.3.7-b. Anisotropic displacement parameters ($Å^2$ x 10^3) for **14**. The anisotropic displacement factor exponent takes the form: $-2\pi^2[h^2a^{*2}U_{11} + ... + 2hka^*b^*U_{12}]$

Atom	U_{11}	U_{22}	U_{33}	U_{23}	U_{13}	U_{12}
W(1)	20(1)	36(1)	21(1)	0(1)	-2(1)	-5(1)
Cu(1)	29(1)	51(1)	33(1)	0(1)	-12(1)	5(1)
Cl(1)	41(1)	56(2)	44(1)	13(1)	-14(1)	-15(1)
P(1)	27(1)	36(1)	34(1)	-3(1)	-12(1)	2(1)
P(2)	22(1)	45(1)	32(1)	-6(1)	-4(1)	2(1)
P(3)	30(1)	58(2)	39(1)	11(1)	-7(1)	-16(1)
O(11)	35(3)	66(5)	73(4)	36(4)	-5(3)	-4(3)
O(12)	48(3)	113(6)	33(3)	-15(3)	4(3)	-25(4)
C(1)	16(4)	79(7)	27(4)	24(4)	-2(3)	-6(4)
C(2)	16(3)	29(4)	36(4)	1(3)	5(3)	-7(3)
C(3)	38(4)	75(7)	23(4)	8(4)	-3(3)	-36(5)
C(4)	61(6)	40(6)	91(7)	-26(5)	53(6)	-31(5)
C(5)	32(5)	47(6)	124(9)	33(6)	34(6)	7(4)
C(6)	68(7)	276(19)	27(5)	50(8)	-15(4)	-99(10)
C(7)	41(5)	46(7)	174(13)	-23(7)	57(7)	-16(5)
C(8)	71(7)	238(18)	60(6)	75(9)	-45(6)	-108(10)
C(9)	201(17)	143(14)	280(20)	-177(16)	207(18)	-140(14)
C(10)	67(8)	82(11)	460(30)	156(17)	103(14)	48(8)
C(11)	24(4)	47(6)	40(4)	18(4)	-10(3)	-10(4)
C(12)	26(4)	71(6)	21(4)	-2(4)	3(3)	-12(4)

Table 6.3.8.	**15**
Empirical Formula	$C_{24}H_{30}Br_2Cu_2O_4P_6W_2$
Formula weight	1222.88
Crystal size	0.160 x 0.150 x 0.060 mm
Crystal description	plate
Crystal color	yellow
Crystal system	monoclinic
Space group	$P2_1/a$
Unit cell dimensions	a = 13.29858(11) Å α = 90°
	b = 9.48002(8) Å β = 92.9243(7)°
	c = 13.53355(11) Å γ = 90°
Volume	1703.96(2) $Å^3$
Z, Calculated density	2, 2.384 Mg/m^3
Absorption coefficient	19.227 mm^{-1}
F(000)	1144
Measurement device type	Oxford Diffraction Gemini Ultra

Measurement method	omega-scan
Temperature	123 K
Wavelength	1.54184 Å
Monochromator	graphite
θ range for data collection	3.27 to 62.33°
Index ranges	$-15 \le h \le 15$, $-10 \le k \le 10$, $-15 \le l \le 15$
Reflections collected / unique	26445 / 2691 [R(int) = 0.0527]
Reflections greater I>2\s(I)	2595
Absorption correction	semi-empirical from equivalents
Max. and min. transmission	1.00000 and 0.05460
Refinement method	Full-matrix least-squares on F^2
Data / restraints / parameters	2691 / 0 / 186
Goodness of fit on F^2	1.100
Final R indices [I>2sigma(I)]	R1 = 0.0238, wR2 = 0.0631
R indices (all data)	R1 = 0.0247, wR2 = 0.0636
Largest diff. peak and hole	0.661 and -1.470 e.A^{-3}

Table 6.3.8-a. Atomic coordinates (x 10^4) and equivalent isotropic displacement parameters (Å^2 x 10^3) for **15**. U_{eq} is defined as one third of the trace of the orthogonalized U_{ij} tensor.

Atom	**x**	**y**	**z**	$\boldsymbol{U_{eq}}$
W(1)	1944(1)	332(1)	7047(1)	11(1)
Br(1)	4207(1)	1425(1)	10586(1)	26(1)
Cu(1)	4259(1)	3(1)	9123(1)	23(1)
P(1)	2994(1)	-1176(1)	8217(1)	17(1)
P(2)	3759(1)	726(1)	7552(1)	19(1)
P(3)	3501(1)	-1186(1)	6730(1)	23(1)
O(1)	926(2)	-2518(3)	6362(2)	27(1)
O(2)	2323(3)	1153(4)	4850(2)	31(1)
C(1)	1311(3)	-1484(4)	6591(3)	17(1)
C(2)	2214(3)	825(5)	5654(3)	21(1)
C(3)	1120(3)	1159(4)	8438(3)	15(1)
C(4)	398(3)	643(4)	7724(3)	14(1)
C(5)	440(3)	1495(4)	6855(3)	15(1)
C(6)	1201(3)	2543(4)	7034(3)	18(1)
C(7)	1622(3)	2332(4)	8019(3)	18(1)
C(8)	1257(3)	702(5)	9497(3)	22(1)
C(9)	-366(3)	-476(4)	7902(4)	22(1)
C(10)	-287(3)	1439(5)	5964(3)	24(1)
C(11)	1415(4)	3777(5)	6386(4)	29(2)
C(12)	2359(3)	3287(5)	8559(4)	29(1)

Table 6.3.8-b. Anisotropic displacement parameters (Å^2 x 10^3) for **15**. The anisotropic displacement factor exponent takes the form: $-2\pi^2[h^2a^{*2}U_{11} + ... + 2hka^*b^*U_{12}]$.

Atom	$\boldsymbol{U_{11}}$	$\boldsymbol{U_{22}}$	$\boldsymbol{U_{33}}$	$\boldsymbol{U_{23}}$	$\boldsymbol{U_{13}}$	$\boldsymbol{U_{12}}$
W(1)	13(1)	10(1)	10(1)	0(1)	0(1)	1(1)
Br(1)	25(1)	21(1)	30(1)	-6(1)	-10(1)	3(1)
Cu(1)	22(1)	24(1)	21(1)	0(1)	-7(1)	-3(1)
P(1)	18(1)	14(1)	17(1)	3(1)	-5(1)	0(1)

P(2)	16(1)	21(1)	21(1)	5(1)	-1(1)	-2(1)
P(3)	22(1)	28(1)	20(1)	-4(1)	-1(1)	11(1)
O(1)	30(2)	18(2)	33(2)	-8(1)	-6(1)	-2(1)
O(2)	43(2)	38(2)	13(2)	10(1)	8(1)	10(2)
C(1)	17(2)	22(2)	12(2)	1(2)	-2(2)	7(2)
C(2)	19(2)	19(2)	26(3)	-6(2)	1(2)	3(2)
C(3)	16(2)	17(2)	12(2)	-6(2)	3(2)	4(2)
C(4)	16(2)	14(2)	12(2)	-4(2)	0(2)	5(2)
C(5)	21(2)	12(2)	13(2)	-1(2)	0(2)	8(2)
C(6)	22(2)	12(2)	21(2)	-1(2)	7(2)	5(2)
C(7)	21(2)	15(2)	18(2)	-7(2)	3(2)	1(2)
C(8)	25(2)	28(2)	14(2)	-2(2)	0(2)	4(2)
C(9)	15(2)	20(2)	31(3)	2(2)	2(2)	0(2)
C(10)	30(2)	28(2)	14(2)	-5(2)	-5(2)	12(2)
C(11)	34(3)	16(2)	36(3)	9(2)	7(2)	5(2)
C(12)	25(2)	22(2)	39(3)	-10(2)	-5(2)	0(2)

Table 6.3.9.	**16**
Empirical Formula	$C_{24}H_{30}Cu_2I_2O_4P_6W_2$
Formula weight	1316.88
Crystal size	0.160 x 0.150 x 0.080 mm
Crystal description	flat prism
Crystal color	yellow
Crystal system	orthorhombic
Space group	*Pbca*
Unit cell dimensions	a = 10.0020(2) Å α = 90°
	b = 13.0351(3) Å β = 90°
	c = 26.8519(5) Å γ = 90°
Volume	3500.87(13) A^3
Z, Calculated density	4, 2.499 Mg/m^3
Absorption coefficient	9.815 mm^{-1}
F(000)	2432
Measurement device type	Oxford Diffraction Gemini Ultra
Measurement method	omega-scan
Temperature	123 K
Wavelength	0.71073 A
Monochromator	graphite
θ range for data collection	3.13 to 27.04°
Index ranges	$-12 \leq h \leq 12$, $-16 \leq k \leq 16$, $-33 \leq l \leq 31$
Reflections collected / unique	25690 / 3490 [R(int) = 0.0324]
Reflections greater I>2\s(I)	3005
Absorption correction	semi-empirical from equivalents
Max. and min. transmission	1.00000 and 0.63574
Refinement method	Full-matrix least-squares on F^2
Data / restraints / parameters	3490 / 0 / 186
Goodness of fit on F^2	1.087
Final R indices [I>2sigma(I)]	R1 = 0.0231, wR2 = 0.0481
R indices (all data)	R1 = 0.0309, wR2 = 0.0509
Largest diff. peak and hole	1.247 and -0.830 e.$Å^{-3}$

Table 6.3.9-a. Atomic coordinates (x 10^4) and equivalent isotropic displacement parameters (Å^2 x 10^3) for **16**. U_{eq} is defined as one third of the trace of the orthogonalized U_{ij} tensor.

Atom	**x**	**y**	**z**	U_{eq}
W(1)	10327(1)	2935(1)	6488(1)	16(1)
I(1)	11489(1)	942(1)	4630(1)	27(1)
Cu(1)	10053(1)	677(1)	5406(1)	26(1)
P(1)	8960(1)	1962(1)	5868(1)	20(1)
P(2)	10700(1)	1111(1)	6221(1)	23(1)
P(3)	8833(1)	1336(1)	6607(1)	26(1)
O(1)	7631(3)	3945(2)	6839(1)	34(1)
O(2)	11087(3)	2240(3)	7571(1)	34(1)
C(1)	8608(5)	3559(3)	6721(2)	22(1)
C(2)	10790(4)	2491(3)	7184(2)	21(1)
C(11)	12414(4)	3703(3)	6516(2)	21(1)
C(12)	12246(4)	3345(3)	6018(2)	20(1)
C(13)	11143(4)	3876(3)	5802(2)	19(1)
C(14)	10642(4)	4573(3)	6164(2)	18(1)
C(15)	11421(4)	4461(3)	6611(2)	20(1)
C(16)	13584(4)	3437(4)	6849(2)	30(2)
C(17)	13159(5)	2622(4)	5746(2)	29(1)
C(18)	10736(5)	3809(4)	5267(2)	25(1)
C(19)	9572(4)	5367(3)	6071(2)	23(1)
C(20)	11343(5)	5138(3)	7066(2)	28(1)

Table 6.3.9-b. Anisotropic displacement parameters (Å^2 x 10^3) for **16**. The anisotropic displacement factor exponent takes the form: $-2\pi^2[h^2a^{*2}U_{11} + ... + 2hka^*b^*U_{12}]$.

Atom	U_{11}	U_{22}	U_{33}	U_{23}	U_{13}	U_{12}
W(1)	18(1)	15(1)	15(1)	1(1)	0(1)	-1(1)
I(1)	23(1)	26(1)	31(1)	-8(1)	5(1)	-2(1)
Cu(1)	27(1)	24(1)	26(1)	-5(1)	1(1)	1(1)
P(1)	20(1)	20(1)	21(1)	-2(1)	-2(1)	1(1)
P(2)	26(1)	17(1)	25(1)	-1(1)	-3(1)	2(1)
P(3)	32(1)	22(1)	25(1)	1(1)	4(1)	-9(1)
O(1)	31(2)	34(2)	36(2)	3(2)	10(2)	12(2)
O(2)	39(2)	41(2)	21(2)	5(2)	-3(2)	0(2)
C(1)	31(3)	16(2)	19(2)	3(2)	1(2)	-4(2)
C(2)	21(2)	18(2)	25(2)	-3(2)	4(2)	0(2)
C(11)	17(2)	21(2)	24(2)	4(2)	-3(2)	-4(2)
C(12)	21(2)	16(2)	23(2)	6(2)	1(2)	-6(2)
C(13)	21(2)	18(2)	19(2)	6(2)	3(2)	-6(2)
C(14)	18(2)	11(2)	25(2)	5(2)	-2(2)	-4(2)
C(15)	19(2)	16(2)	25(2)	3(2)	-3(2)	-6(2)
C(16)	23(2)	28(3)	38(3)	3(2)	-11(2)	-4(2)
C(17)	27(2)	30(2)	31(3)	-1(2)	9(2)	0(2)
C(18)	28(2)	29(2)	19(2)	10(2)	4(2)	-3(2)
C(19)	26(2)	14(2)	28(2)	1(2)	-5(2)	1(2)
C(20)	35(3)	24(2)	24(2)	-2(2)	-6(2)	-3(2)

Table 6.3.10.	**21** ∗ ($C_8H_{12}CuN_4$)	
Empirical Formula	$C_{13}H_{15}Cl_3Cu_3OW(C_8H_{12}CuN_4)$	
Formula weight	927.86	
Crystal size	0.28 x 0.22 x 0.13 mm	
Crystal description	flat prism	
Crystal color	dark brown	
Crystal system	monoclinic	
Space group	$P2_1/c$	
Unit cell dimensions	a = 11.7685(3) Å	α = 90 deg.
	b = 20.8946(3) Å	β = 115.338(3) deg.
	c = 13.1979(3) Å	γ = 90 deg.
Volume	2933.13(13) $Å^3$	
Z, Calculated density	4, 2.101 Mg/m^3	
Absorption coefficient	7.063 mm^{-1}	
F(000)	1784	
Measurement device type	Oxford Diffraction Gemini Ultra	
Measurement method	omega-scan	
Temperature	123 K	
Wavelength	0.71073 Å	
Monochromator	graphite	
θ range for data collection	3.60 to 37.71°	
Index ranges	$-17 \leq h \leq 19$, $-34 \leq k \leq 35$, $-21 \leq l \leq 22$	
Reflections collected / unique	29767 / 14310 [R(int) = 0.0372]	
Reflections greater I>2\s(I)	9956	
Absorption correction	semi-empirical from equivalents	
Max. and min. transmission	1.00000 and 0.48831	
Refinement method	Full-matrix least-squares on F^2	
Data / restraints / parameters	14310 / 0 / 334	
Goodness of fit on F^2	1.009	
Final R indices [I>2sigma(I)]	R1 = 0.0357, wR2 = 0.0729	
R indices (all data)	R1 = 0.0647, wR2 = 0.0824	
Largest diff. peak and hole	2.015 and -1.441 e.$Å^{-3}$	

Table 6.3.10-a. Atomic coordinates (x 10^4) and equivalent isotropic displacement parameters ($Å^2$ x 10^3) for **21**. U_{eq} is defined as one third of the trace of the orthogonalized U_{ij} tensor.

Atom	**x**	**y**	**z**	$\boldsymbol{U_{eq}}$
W(1)	1392(1)	5615(1)	2716(1)	11(1)
Cu(1)	3589(1)	5131(1)	4177(1)	21(1)
Cu(2)	657(1)	5087(1)	4174(1)	19(1)
Cu(3)	1551(1)	4373(1)	2917(1)	19(1)
Cl(1)	5523(1)	5659(1)	4549(1)	25(1)
Cl(2)	-889(1)	5674(1)	4552(1)	22(1)
Cl(3)	1593(1)	3344(1)	2874(1)	26(1)
O(11)	-1058(2)	4787(1)	1961(2)	24(1)
O(12)	3217(2)	4863(1)	1964(2)	20(1)
O(13)	2632(2)	5916(1)	5305(2)	21(1)
C(1)	1434(3)	6276(1)	1300(3)	19(1)

C(2)	2017(3)	6609(1)	2343(2)	15(1)
C(3)	1075(3)	6719(1)	2750(2)	16(1)
C(4)	-70(3)	6440(1)	1968(2)	15(1)
C(5)	149(3)	6163(1)	1066(2)	17(1)
C(6)	2020(4)	6142(2)	516(3)	28(1)
C(7)	3348(3)	6850(2)	2853(3)	24(1)
C(8)	1195(3)	7104(2)	3748(3)	23(1)
C(9)	-1322(3)	6494(2)	2005(3)	24(1)
C(10)	-824(3)	5878(2)	19(3)	29(1)
C(11)	-61(3)	5026(1)	2355(2)	16(1)
C(12)	2578(3)	5082(1)	2354(2)	15(1)
C(13)	2201(3)	5716(1)	4384(2)	15(1)
Cu(4)	-5171(1)	6726(1)	39(1)	26(1)
N(21)	-4566(3)	5970(2)	1000(3)	32(1)
N(22)	-3939(3)	7131(2)	-454(3)	28(1)
N(23)	-5298(3)	7484(2)	941(3)	32(1)
N(24)	-6740(3)	6585(1)	-1346(3)	25(1)
C(21)	-4218(3)	5542(2)	1587(3)	25(1)
C(22)	-3780(4)	4983(2)	2289(4)	30(1)
C(23)	-3327(4)	7472(2)	-661(3)	32(1)
C(24)	-2570(5)	7918(3)	-952(5)	60(2)
C(25)	-5033(3)	7958(2)	1412(3)	24(1)
C(26)	-4690(3)	8563(2)	2005(3)	25(1)
C(27)	-7606(3)	6589(2)	-2164(3)	22(1)
C(28)	-8722(3)	6611(2)	-3229(3)	32(1)

Table 6.3.10-b. Anisotropic displacement parameters ($Å^2$ x 10^3) for **21**. The anisotropic displacement factor exponent takes the form: $-2\pi^2[h^2a^{*2}U_{11} + ... + 2hka^*b^*U_{12}]$.

Atom	U_{11}	U_{22}	U_{33}	U_{23}	U_{13}	U_{12}
W(1)	11(1)	11(1)	10(1)	0(1)	4(1)	0(1)
Cu(1)	15(1)	27(1)	16(1)	-1(1)	2(1)	7(1)
Cu(2)	22(1)	21(1)	16(1)	0(1)	11(1)	-4(1)
Cu(3)	23(1)	11(1)	26(1)	1(1)	13(1)	0(1)
Cl(1)	16(1)	28(1)	26(1)	9(1)	4(1)	1(1)
Cl(2)	28(1)	21(1)	24(1)	8(1)	17(1)	9(1)
Cl(3)	30(1)	15(1)	38(1)	2(1)	20(1)	1(1)
O(11)	18(1)	26(1)	24(1)	-1(1)	4(1)	-6(1)
O(12)	19(1)	22(1)	21(1)	-1(1)	10(1)	4(1)
O(13)	20(1)	26(1)	14(1)	-3(1)	6(1)	1(1)
C(1)	27(2)	17(1)	19(1)	7(1)	15(1)	3(1)
C(2)	17(1)	12(1)	17(1)	2(1)	7(1)	1(1)
C(3)	22(1)	13(1)	16(1)	0(1)	12(1)	2(1)
C(4)	14(1)	16(1)	15(1)	5(1)	6(1)	4(1)
C(5)	21(1)	15(1)	10(1)	3(1)	4(1)	3(1)
C(6)	43(2)	29(2)	26(2)	8(1)	27(2)	9(2)
C(7)	20(1)	18(1)	36(2)	-1(1)	12(1)	-3(1)
C(8)	34(2)	17(1)	20(1)	1(1)	15(1)	2(1)
C(9)	18(1)	23(2)	30(2)	10(1)	10(1)	6(1)
C(10)	31(2)	28(2)	18(1)	2(1)	0(1)	0(1)
C(11)	17(1)	18(1)	12(1)	-2(1)	5(1)	-1(1)

C(12)	16(1)	14(1)	13(1)	-1(1)	4(1)	1(1)
C(13)	15(1)	15(1)	16(1)	1(1)	8(1)	1(1)
Cu(4)	25(1)	22(1)	30(1)	5(1)	11(1)	-2(1)
N(21)	25(1)	32(2)	40(2)	8(1)	15(1)	-4(1)
N(22)	27(2)	30(2)	26(2)	0(1)	11(1)	-6(1)
N(23)	36(2)	32(2)	27(2)	3(1)	14(1)	-1(1)
N(24)	27(1)	21(1)	28(1)	-1(1)	13(1)	-1(1)
C(21)	15(1)	18(1)	43(2)	11(1)	14(1)	-1(1)
C(22)	31(2)	27(2)	38(2)	12(2)	19(2)	8(1)
C(23)	36(2)	36(2)	27(2)	-4(2)	17(2)	-13(2)
C(24)	73(4)	59(3)	65(4)	-14(3)	47(3)	-38(3)
C(25)	24(2)	28(2)	24(2)	5(1)	13(1)	0(1)
C(26)	23(2)	28(2)	25(2)	2(1)	10(1)	-1(1)
C(27)	19(1)	21(1)	30(2)	-4(1)	15(1)	-2(1)
C(28)	27(2)	39(2)	28(2)	-8(2)	9(2)	-5(2)

Table 6.3.11.	**22**
Empirical Formula	$C_{14}H_{10}ClCuO_4P_2W_2$
Formula weight	770.84
Crystal size	0.150 x 0.050 x 0.020 mm
Crystal description	rod
Crystal color	red
Crystal system	monoclinic
Space group	*C*2/*c*
Unit cell dimensions	*a* = 25.5190(3) Å α = 90°
	b = 7.9624(1) Å β = 93.0749(12)°
	c = 17.1325(2) Å γ = 90°
Volume	3476.18(7) $Å^3$
Z, Calculated density	8, 2.946 Mg/m^3
Absorption coefficient	28.664 mm^{-1}
F(000)	2800
Measurement device type	Oxford Diffraction Gemini Ultra
Measurement method	omega-scan
Temperature	123 K
Wavelength	1.54184 Å
Monochromator	graphite
θ range for data collection	3.47 to 66.77°
Index ranges	$-23 \le h \le 29$, $-9 \le k \le 9$, $-20 \le l \le 19$
Reflections collected / unique	7401 / 3018 [R(int) = 0.0306]
Reflections greater I>2\s(I)	2549
Absorption correction	semi-empirical from equivalents
Max. and min. transmission	1.00000 and 0.04892
Refinement method	Full-matrix least-squares on F^2
Data / restraints / parameters	3018 / 0 / 218
Goodness of fit on F^2	1.035
Final R indices [I>2sigma(I)]	R1 = 0.0278, wR2 = 0.0709
R indices (all data)	R1 = 0.0344, wR2 = 0.0743
Largest diff. peak and hole	0.958 and -1.867 $e.Å^{-3}$

Table 6.3.11-a. Atomic coordinates (x 10^4) and equivalent isotropic displacement parameters (Å^2 x 10^3) for **22**. U_{eq} is defined as one third of the trace of the orthogonalized U_{ij} tensor.

Atom	**x**	**y**	**z**	U_{eq}
W(1)	1530(1)	2634(1)	2389(1)	12(1)
W(2)	1035(1)	2337(1)	3980(1)	12(1)
Cu(1)	0	5650(1)	2500	14(1)
Cu(2)	0	-542(1)	2500	15(1)
Cl(1)	-85(1)	7550(2)	3529(1)	18(1)
P(1)	699(1)	3909(2)	2789(1)	13(1)
P(2)	672(1)	1296(2)	2701(1)	14(1)
O(6)	2382(2)	3392(6)	3710(2)	29(1)
O(7)	1691(2)	-1263(6)	2458(3)	31(2)
O(13)	1500(2)	5910(6)	4356(2)	32(2)
O(14)	-83(2)	3476(6)	4444(2)	30(1)
C(1)	1969(3)	4773(9)	1768(4)	33(2)
C(2)	2180(2)	3215(9)	1555(3)	26(2)
C(3)	1779(3)	2314(9)	1130(3)	27(2)
C(4)	1331(3)	3314(12)	1084(3)	42(3)
C(5)	1447(3)	4814(11)	1474(4)	45(3)
C(6)	2033(2)	3077(8)	3266(3)	20(2)
C(7)	1635(2)	185(8)	2463(3)	19(2)
C(8)	1660(2)	294(8)	4371(3)	26(2)
C(9)	1170(2)	-537(8)	4237(4)	26(2)
C(10)	831(2)	149(8)	4777(3)	24(2)
C(11)	1108(2)	1380(8)	5239(3)	24(2)
C(12)	1621(2)	1475(8)	4980(3)	23(2)
C(13)	1308(2)	4623(8)	4210(3)	18(2)
C(14)	323(2)	3107(8)	4257(3)	21(2)

Table 6.3.11-b. Anisotropic displacement parameters (Å^2 x 10^3) for **22**. The anisotropic displacement factor exponent takes the form: $-2\pi^2 [h^2a^{*2}U_{11} + ... + 2hka^*b^*U_{12}]$.

Atom	U_{11}	U_{22}	U_{33}	U_{23}	U_{13}	U_{12}
W(1)	9(1)	15(1)	11(1)	-1(1)	0(1)	-1(1)
W(2)	11(1)	14(1)	12(1)	1(1)	1(1)	2(1)
Cu(1)	15(1)	13(1)	15(1)	0	-2(1)	0
Cu(2)	14(1)	13(1)	18(1)	0	-1(1)	0
Cl(1)	26(1)	16(1)	12(1)	-1(1)	4(1)	-1(1)
P(1)	12(1)	14(1)	14(1)	2(1)	0(1)	2(1)
P(2)	11(1)	14(1)	17(1)	-2(1)	0(1)	-1(1)
O(6)	15(2)	50(3)	23(2)	-6(2)	-2(2)	-2(2)
O(7)	29(2)	23(3)	40(3)	-3(2)	6(2)	10(2)
O(13)	49(3)	20(3)	26(2)	-5(2)	-4(2)	-3(2)
O(14)	16(2)	48(3)	26(2)	2(2)	6(2)	14(2)
C(1)	46(4)	28(4)	27(3)	-2(3)	15(3)	-13(3)
C(2)	19(3)	39(4)	22(3)	3(3)	9(2)	-6(3)
C(3)	30(3)	41(4)	9(3)	-9(2)	7(2)	-12(3)
C(4)	27(3)	84(7)	14(3)	15(4)	-3(2)	-10(4)
C(5)	58(5)	49(5)	30(4)	29(4)	23(3)	26(4)
C(6)	15(3)	25(3)	20(3)	-6(2)	3(2)	-1(2)
C(7)	15(3)	21(4)	20(3)	-2(2)	4(2)	5(2)

C(8)	24(3)	33(4)	20(3)	7(3)	1(2)	14(3)
C(9)	35(3)	17(3)	24(3)	6(2)	-3(3)	9(3)
C(10)	25(3)	17(3)	28(3)	10(2)	-3(2)	-4(2)
C(11)	37(3)	22(3)	14(2)	7(2)	6(2)	11(3)
C(12)	19(3)	25(4)	23(3)	10(3)	-5(2)	3(2)
C(13)	25(3)	15(3)	14(2)	2(2)	-2(2)	5(2)
C(14)	21(3)	26(3)	15(2)	1(2)	-2(2)	-2(3)

Table 6.3.12.	**23**	
Empirical Formula	$C_{14}H_{10}BrCuO_4P_2W_2$	
Formula weight	815.29	
Crystal size	0.190 x 0.030 x 0.010 mm	
Crystal description	rod	
Crystal color	red to orange	
Crystal system	monoclinic	
Space group	$P2_1/n$	
Unit cell dimensions	a = 14.8287(2) Å	α = 90°
	b = 8.0031(1) Å	β = 111.303(2)°
	c = 16.2056(3) Å	γ = 90°
Volume	1791.80(5) $Å^3$	
Z, Calculated density	4, 3.022 Mg/m^3	
Absorption coefficient	29.046 mm^{-1}	
F(000)	1472	
Measurement device type	Oxford Diffraction Gemini Ultra	
Measurement method	omega-scan	
Temperature	123 K	
Wavelength	1.54184 Å	
Monochromator	graphite	
θ range for data collection	5.06 to 66.61°	
Index ranges	$-17 \leq h \leq 17$, $-9 \leq k \leq 9$, $-18 \leq l \leq 19$	
Reflections collected / unique	7496 / 3069 [R(int) = 0.0335]	
Reflections greater I>2\s(I)	2661	
Absorption correction	semi-empirical from equivalents	
Max. and min. transmission	1.00000 and 0.24599	
Refinement method	Full-matrix least-squares on F^2	
Data / restraints / parameters	3069 / 0 / 217	
Goodness of fit on F^2	1.015	
Final R indices [I>2sigma(I)]	R1 = 0.0346, wR2 = 0.0911	
R indices (all data)	R1 = 0.0406, wR2 = 0.0954	
Largest diff. peak and hole	1.702 and -1.972 $e.A^{-3}$	

Table 6.3.12-a.. Atomic coordinates (x 10^4) and equivalent isotropic displacement parameters ($Å^2$ x 10^3) for **23**. U_{eq} is defined as one third of the trace of the orthogonalized U_{ij} tensor.

Atom	**x**	**y**	**z**	U_{eq}
W(1)	8604(1)	5099(1)	1649(1)	16(1)
W(2)	7472(1)	4783(1)	-356(1)	16(1)
Br(1)	9021(1)	10072(1)	-1181(1)	21(1)

Cu(1)	9962(1)	8086(1)	-25(1)	19(1)
P(10)	9133(1)	3749(2)	490(1)	17(1)
P(12)	9006(1)	6355(2)	428(1)	17(1)
O(6)	6606(4)	8345(7)	-342(4)	41(2)
O(7)	8177(4)	5794(8)	-1894(3)	37(2)
O(16)	8330(4)	1235(7)	1751(3)	35(2)
O(17)	6429(3)	5892(8)	1242(3)	35(2)
C(1)	5885(4)	3973(9)	-720(4)	24(2)
C(2)	6119(5)	3846(10)	-1483(4)	28(2)
C(3)	6854(5)	2621(9)	-1320(5)	28(2)
C(4)	7055(5)	1945(9)	-466(5)	30(2)
C(5)	6449(5)	2763(10)	-104(4)	30(2)
C(6)	6976(5)	7070(10)	-348(5)	28(2)
C(7)	7919(5)	5458(10)	-1318(4)	25(2)
C(11)	8826(5)	5668(10)	3100(4)	25(2)
C(12)	8787(5)	7233(9)	2679(4)	29(2)
C(13)	9590(6)	7339(11)	2430(4)	37(2)
C(14)	10141(5)	5847(13)	2679(5)	38(3)
C(15)	9656(6)	4803(10)	3090(5)	31(3)
C(16)	8411(5)	2660(9)	1685(4)	23(2)
C(17)	7215(5)	5578(9)	1316(4)	23(2)

Table 6.3.12-b. Anisotropic displacement parameters ($Å^2$ x 10^3) for **23**. The anisotropic displacement factor exponent takes the form: $-2\pi^2[h^2a^{*2}U_{11} + ... + 2hka^*b^*U_{12}]$

Atom	U_{11}	U_{22}	U_{33}	U_{23}	U_{13}	U_{12}
W(1)	13(1)	21(1)	11(1)	0(1)	2(1)	1(1)
W(2)	13(1)	20(1)	11(1)	0(1)	1(1)	-2(1)
Br(1)	20(1)	22(1)	15(1)	-1(1)	-1(1)	0(1)
Cu(1)	16(1)	21(1)	19(1)	0(1)	4(1)	-1(1)
P(10)	15(1)	20(1)	15(1)	1(1)	5(1)	1(1)
P(12)	15(1)	19(1)	14(1)	-1(1)	3(1)	-3(1)
O(6)	38(3)	22(3)	48(3)	1(3)	-2(3)	4(2)
O(7)	36(3)	56(4)	18(2)	3(3)	9(2)	-14(3)
O(16)	42(3)	30(3)	36(3)	6(2)	17(2)	-5(2)
O(17)	23(3)	56(4)	25(3)	-1(3)	8(2)	5(3)
C(1)	14(3)	28(4)	23(3)	-10(3)	-2(3)	-13(3)
C(2)	21(3)	28(4)	22(3)	1(3)	-6(3)	-5(3)
C(3)	21(3)	32(4)	25(3)	-11(3)	3(3)	-10(3)
C(4)	22(3)	19(4)	37(4)	4(3)	-5(3)	-5(3)
C(5)	26(4)	41(5)	18(3)	3(3)	3(3)	-11(3)
C(6)	20(3)	30(4)	25(4)	12(3)	-4(3)	-3(3)
C(7)	16(3)	35(4)	15(3)	-3(3)	-5(3)	-6(3)
C(11)	20(3)	41(5)	15(3)	-9(3)	7(3)	2(3)
C(12)	34(4)	29(4)	21(3)	-6(3)	8(3)	5(3)
C(13)	45(4)	44(5)	13(3)	-11(3)	1(3)	-28(4)
C(14)	16(3)	75(7)	18(3)	-16(4)	-1(3)	-1(4)
C(15)	27(4)	40(5)	17(4)	-3(3)	-4(3)	13(3)
C(16)	23(3)	29(4)	16(3)	3(3)	5(3)	4(3)
C(17)	19(4)	32(4)	16(3)	0(3)	5(3)	5(3)

Table 6.3.13.	**24** ∗ (C_2H_3N)	
Empirical Formula	$C_{14}H_{10}CuIO_4P_2W_2(C_2H_3N)$	
Formula weight	903.34	
Crystal size	0.16 x 0.03 x 0.03 mm	
Crystal description	rod	
Crystal color	orangish red	
Crystal system	triclinic	
Space group	*P*-1	
Unit cell dimensions	*a* = 8.0130(2) Å	α = 83.920(3)°
	b = 11.4298(4) Å	β = 82.848(3)°
	c = 11.6073(4) Å	γ = 77.694(3)°
Volume	1027.11(6) A^3	
Z, Calculated density	2, 2.921 Mg/m^3	
Absorption coefficient	34.926 mm^{-1}	
F(000)	816	
Measurement device type	Oxford Diffraction Gemini Ultra	
Measurement method	omega-scan	
Temperature	123 K	
Wavelength	1.54184 Å	
Monochromator	graphite	
θ range for data collection	3.85 to 66.66°	
Index ranges	$-9 \leq h \leq 8$, $-13 \leq k \leq 13$, $-13 \leq l \leq 13$	
Reflections collected / unique	12960 / 3519 [R(int) = 0.0343]	
Reflections greater I>2\s(I)	3177	
Absorption correction	semi-empirical from equivalents	
Max. and min. transmission	1.00000 and 0.18509	
Refinement method	Full-matrix least-squares on F^2	
Data / restraints / parameters	3519 / 0 / 245	
Goodness of fit on F^2	1.073	
Final R indices [I>2sigma(I)]	R1 = 0.0269, wR2 = 0.0693	
R indices (all data)	R1 = 0.0313, wR2 = 0.0713	
Largest diff. peak and hole	1.347 and -1.400 $e.A^{-3}$	

Table 6.3.13-a. Atomic coordinates (x 10^4) and equivalent isotropic displacement parameters ($Å^2$ x 10^3) for **24**. U_{eq} is defined as one third of the trace of the orthogonalized U_{ij} tensor.

Atom	**x**	**y**	**z**	U_{eq}
W(1)	4174(1)	3227(1)	3515(1)	13(1)
W(2)	5740(1)	1333(1)	1854(1)	13(1)
I(1)	10420(1)	-1357(1)	3845(1)	21(1)
Cu(1)	7981(1)	38(1)	5161(1)	17(1)
P(1)	3558(2)	1197(1)	3650(1)	16(1)
P(2)	6103(2)	1183(1)	3930(1)	16(1)
O(1)	7862(6)	3735(4)	3515(4)	29(2)
O(2)	3777(8)	3178(5)	6229(4)	39(2)
O(8)	2238(6)	1886(4)	769(4)	25(1)
O(9)	5429(7)	-1363(4)	1927(4)	31(1)
C(1)	6515(8)	3510(5)	3522(5)	20(2)
C(2)	3967(9)	3138(6)	5249(5)	23(2)

C(3)	3615(9)	5170(5)	2594(6)	23(2)
C(4)	2644(8)	5181(5)	3695(6)	22(2)
C(5)	1449(8)	4407(6)	3713(6)	23(2)
C(6)	1664(9)	3948(6)	2612(6)	24(2)
C(7)	2989(8)	4415(6)	1916(5)	22(2)
C(8)	3495(8)	1701(5)	1203(5)	17(2)
C(9)	5533(8)	-385(6)	1953(5)	21(2)
C(10)	6791(8)	2256(6)	129(5)	23(2)
C(11)	7393(8)	996(6)	110(5)	21(2)
C(12)	8468(9)	625(7)	1020(6)	28(2)
C(13)	8547(8)	1656(7)	1575(6)	26(2)
C(14)	7521(8)	2667(6)	1012(5)	25(2)
N(1)	2814(10)	4338(6)	9038(5)	39(2)
C(15)	1863(10)	3839(6)	8765(5)	28(2)
C(16)	673(9)	3175(6)	8414(6)	32(2)

Table 6.3.13-b. Anisotropic displacement parameters ($Å^2$ x 10^3) for **24**. The anisotropic displacement factor exponent takes the form: $-2\pi^2[h^2a^{*2}U_{11} + ... + 2hka^*b^*U_{12}]$.

Atom	U_{11}	U_{22}	U_{33}	U_{23}	U_{13}	U_{12}
W(1)	16(1)	11(1)	12(1)	-1(1)	-1(1)	-2(1)
W(2)	15(1)	11(1)	12(1)	-2(1)	-1(1)	-1(1)
I(1)	21(1)	18(1)	24(1)	-10(1)	-5(1)	-1(1)
Cu(1)	19(1)	15(1)	17(1)	0(1)	-4(1)	-4(1)
P(1)	20(1)	14(1)	14(1)	-1(1)	0(1)	-4(1)
P(2)	19(1)	13(1)	15(1)	1(1)	-2(1)	-2(1)
O(1)	21(2)	36(3)	33(3)	-8(2)	-5(2)	-12(2)
O(2)	59(4)	39(3)	16(2)	-3(2)	-1(2)	-8(3)
O(8)	21(2)	26(2)	28(2)	1(2)	-5(2)	-5(2)
O(9)	51(3)	14(2)	29(2)	1(2)	-5(2)	-7(2)
C(1)	26(4)	20(3)	12(3)	-5(2)	0(2)	-2(3)
C(2)	28(3)	20(3)	18(3)	-1(2)	-1(3)	-2(3)
C(3)	29(4)	10(3)	29(3)	5(2)	-12(3)	1(3)
C(4)	25(3)	10(3)	29(3)	-6(2)	-8(3)	3(2)
C(5)	22(3)	21(3)	23(3)	-6(2)	-1(3)	6(3)
C(6)	24(3)	18(3)	30(3)	-9(3)	-14(3)	6(3)
C(7)	23(3)	20(3)	19(3)	1(2)	-6(3)	3(3)
C(8)	21(3)	12(3)	17(3)	-6(2)	1(3)	-4(2)
C(9)	26(3)	18(3)	18(3)	1(2)	-3(3)	-2(3)
C(10)	24(3)	29(3)	13(3)	5(2)	3(2)	-5(3)
C(11)	21(3)	26(3)	17(3)	-8(2)	4(3)	-5(3)
C(12)	24(3)	34(4)	21(3)	-8(3)	7(3)	1(3)
C(13)	12(3)	39(4)	25(3)	-9(3)	4(3)	-4(3)
C(14)	28(4)	25(3)	21(3)	-8(3)	12(3)	-10(3)
N(1)	66(5)	36(3)	23(3)	-1(3)	-8(3)	-27(3)
C(15)	51(5)	15(3)	17(3)	1(2)	-5(3)	-4(3)
C(16)	32(4)	28(4)	32(4)	-1(3)	-11(3)	3(3)

Table 6.3.14.	**25**	
Empirical Formula	$C_{22}H_{26}O_4P_2W_2$	
Formula weight	784.05 g/mole	
Crystal size	0.090 x 0.040 x 0.010 mm	
Crystal description	rod	
Crystal color	yellow	
Crystal system	monoclinic	
Space group	$C2_C$	
Unit cell dimensions	a = 30.630(5) Å	α = 90°
	b = 7.159(5) Å	β = 118.604(5)°
	c = 24.780(5) Å	γ = 90°
Volume	4771(4) $Å^3$	
Z, Calculated density	8, 2.183 Mg/m^3	
Absorption coefficient	9.796 mm^{-1}	
F(000)	2944	
Measurement device type	Goniometer Xcalibur	
Measurement method	omega scans	
Temperature	123 K	
Wavelength	0.71073 Å	
Monochromator	graphite	
θ range for data collection	1.51 to 25.00°	
Index ranges	$-26 \leq h \leq 36$, $-7 \leq k \leq 8$, $-29 \leq l \leq 25$	
Reflections collected / unique	7342 / 4088 [R(int) = 0.0259]	
Reflections greater I>2\s(I)	3533	
Absorption correction	semi-empirical from equivalent	
Max. and min. transmission	1.00000 and 0.31695	
Refinement method	Full-matrix least-squares on F^2	
Data / restraints / parameters	4088 / 0 / 271	
Goodness of fit on F^2	1.017	
Final R indices [I>2sigma(I)]	R1 = 0.0282, wR2 = 0.0785	
R indices (all data)	R1 = 0.0335, wR2 = 0.0810	
Largest diff. peak and hole	1.355 and -1.673 $e.Å^{-3}$	

Table 6.3.14-a. Atomic coordinates (x 10^4) and equivalent isotropic displacement parameters ($Å^2$ x 10^3) for **25**. U_{eq} is defined as one third of the trace of the orthogonalized U_{ij} tensor.

Atom	**x**	**y**	**z**	U_{eq}
W(1)	1283(1)	564(1)	5493(1)	18(1)
W(2)	2401(1)	707(1)	6238(1)	17(1)
P(1)	1822(1)	3023(2)	6286(1)	15(1)
P(2)	1819(1)	3049(2)	5437(1)	14(1)
O(1)	539(2)	3495(6)	5527(2)	35(1)
O(2)	1332(2)	-959(6)	6707(2)	23(1)
O(3)	3124(2)	3815(6)	6257(2)	26(1)
O(4)	2399(2)	-494(6)	5019(2)	23(1)
C(1)	724(2)	8(9)	4463(2)	18(2)
C(2)	615(2)	-1204(9)	4836(3)	21(2)
C(3)	1024(2)	-2451(8)	5149(3)	27(2)
C(4)	1386(2)	-2016(8)	4968(2)	19(2)
C(5)	1203(2)	-485(8)	4551(3)	19(2)

C(6)	357(2)	1301(9)	3947(3)	26(2)
C(7)	598(2)	3086(10)	3918(3)	41(2)
C(8)	198(4)	206(14)	3341(3)	63(3)
C(9)	-102(3)	1661(15)	4022(4)	58(3)
C(10)	814(2)	2447(8)	5511(3)	24(2)
C(11)	1325(2)	-338(8)	6272(2)	16(2)
C(12)	3119(2)	-909(7)	6926(2)	14(2)
C(13)	2946(2)	214(8)	7265(2)	14(1)
C(14)	2477(2)	-469(8)	7158(3)	17(2)
C(15)	2351(2)	-1993(7)	6746(2)	14(1)
C(16)	2735(2)	-2242(7)	6597(2)	17(2)
C(17)	3638(2)	-977(7)	7006(2)	16(2)
C(18)	3894(2)	-2689(9)	7420(3)	32(2)
C(19)	3942(2)	750(8)	7319(3)	26(2)
C(20)	3631(2)	-1275(9)	6388(3)	24(2)
C(21)	2846(2)	2711(7)	6246(2)	15(2)
C(22)	2385(2)	-42(8)	5456(2)	15(2)

Table 6.3.14-b. Anisotropic displacement parameters ($Å^2$ x 10^3) for **25**. The anisotropic displacement factor exponent takes the form: $-2\pi^2[h^2a^{*2}U_{11} + ... + 2hka^*b^*U_{12}]$.

Atom	U_{11}	U_{22}	U_{33}	U_{23}	U_{13}	U_{12}
W(1)	19(1)	19(1)	16(1)	1(1)	8(1)	-2(1)
W(2)	19(1)	15(1)	15(1)	0(1)	8(1)	-1(1)
P(1)	16(1)	11(1)	17(1)	-5(1)	6(1)	0(1)
P(2)	13(1)	10(1)	16(1)	4(1)	5(1)	-1(1)
O(1)	23(2)	24(2)	63(3)	1(2)	25(2)	4(2)
O(2)	21(2)	33(2)	17(2)	6(2)	11(2)	-1(2)
O(3)	21(2)	20(2)	33(2)	4(2)	11(2)	-5(2)
O(4)	29(2)	29(2)	15(2)	1(2)	15(2)	2(2)
C(1)	15(3)	29(3)	5(2)	-1(2)	1(2)	-10(2)
C(2)	17(3)	28(3)	17(3)	-1(2)	7(2)	-13(2)
C(3)	44(4)	16(3)	17(3)	-2(2)	11(3)	-8(3)
C(4)	23(3)	17(3)	10(3)	-8(2)	3(2)	-5(2)
C(5)	23(3)	20(3)	14(3)	-8(2)	8(3)	-10(2)
C(6)	16(3)	41(4)	21(3)	3(3)	8(2)	-5(3)
C(7)	27(3)	40(4)	40(4)	22(3)	4(3)	2(3)
C(8)	72(6)	71(6)	8(3)	1(4)	-12(4)	0(5)
C(9)	21(3)	108(8)	48(5)	39(5)	18(3)	17(4)
C(10)	22(3)	22(3)	27(3)	1(2)	11(3)	-6(3)
C(11)	14(3)	18(3)	14(3)	1(2)	5(2)	3(2)
C(12)	21(3)	13(3)	7(2)	7(2)	5(2)	6(2)
C(13)	17(3)	13(2)	8(2)	-3(2)	2(2)	-2(2)
C(14)	19(3)	21(3)	11(3)	8(2)	7(2)	5(2)
C(15)	15(2)	12(2)	14(3)	8(2)	6(2)	2(2)
C(16)	23(3)	9(2)	14(3)	1(2)	6(2)	-1(2)
C(17)	16(3)	16(3)	16(3)	-1(2)	9(2)	-1(2)
C(18)	21(3)	34(4)	39(4)	16(3)	12(3)	14(3)
C(19)	13(3)	32(4)	25(3)	-7(3)	3(3)	-4(2)
C(20)	21(3)	32(3)	27(3)	-8(3)	18(3)	-2(3)
C(21)	19(3)	10(3)	15(3)	1(2)	8(2)	3(2)

C(22)	15(3)	11(3)	11(3)	3(2)	1(2)	-2(2)

Table 6.3.15.	**26**	
Empirical Formula	$C_{22}H_{26}BrCuO_4P_2W_2$	
Formula weight	927.50 g/mole	
Crystal size	0.2869 x 0.0303 x 0.0120 mm	
Crystal description	flat rod	
Crystal color	redish orange	
Crystal system	monoclinic	
Space group	*C*2/*c*	
Unit cell dimensions	*a* = 27.4649(8) Å	α = 90°
	b = 7.8948(2) Å	β = 104.649(4)°
	c = 24.9063(9) Å	γ = 90°
Volume	5224.9(3) Å^3	
Z, Calculated density	8, 2.358 Mg/m^3	
Absorption coefficient	20.033 mm^{-1}	
F(000)	3456	
Measurement device type	Goniometer Xcalibur	
Measurement method	omega scans	
Temperature	123 K	
Wavelength	1.54184 Å	
Monochromator	graphite	
θ range for data collection	3.33 to 66.73°	
Index ranges	-21≤*h*≤32, -9≤*k*≤8, -29≤*l*≤28	
Reflections collected / unique	9051 / 4505 [R(int) = 0.0282]	
Reflections greater I>2\s(I)	3958	
Absorption correction	analytical	
Max. and min. transmission	0.800 and 0.162	
Refinement method	Full-matrix least-squares on F^2	
Data / restraints / parameters	4505 / 0 / 295	
Goodness of fit on F^2	1.049	
Final R indices [I>2sigma(I)]	R1 = 0.0301, wR2 = 0.0774	
R indices (all data)	R1 = 0.0347, wR2 = 0.0798	
Largest diff. peak and hole	2.134 and -0.886 e.Å^{-3}	

Table 6.3.15-a. Atomic coordinates (x 10^4) and equivalent isotropic displacement parameters (Å^2 x 10^3) for **26**. U_{eq} is defined as one third of the trace of the orthogonalized U_{ij} tensor.

Atom	**x**	**y**	**z**	$\boldsymbol{U_{eq}}$
W(1)	3317(1)	3259(1)	-1106(1)	20(1)
W(2)	3823(1)	2366(1)	110(1)	18(1)
Br(1)	1971(1)	-2721(1)	-671(1)	23(1)
Cu(1)	2504(1)	-554(1)	-101(1)	22(1)
P(1)	2994(1)	1307(2)	-455(1)	20(1)
P(2)	3012(1)	3905(2)	-276(1)	21(1)
O(1)	4421(2)	4613(6)	-786(2)	35(2)
O(2)	3590(2)	-443(5)	-1370(2)	34(1)
O(3)	4176(2)	6108(6)	384(2)	42(1)
O(4)	3315(2)	2476(6)	1102(2)	34(2)

C(1)	4020(2)	4027(8)	-859(2)	25(2)
C(2)	3507(2)	924(8)	-1253(3)	29(2)
C(3)	3225(2)	4107(8)	-2022(2)	24(2)
C(4)	2777(2)	3255(9)	-1982(2)	29(2)
C(5)	2548(2)	4249(11)	-1631(3)	44(2)
C(6)	2843(3)	5679(9)	-1468(3)	39(2)
C(7)	3263(2)	5616(7)	-1700(2)	27(2)
C(8)	3531(2)	3748(8)	-2437(3)	32(2)
C(9)	3507(3)	1868(10)	-2605(4)	51(3)
C(10)	4082(3)	4236(14)	-2218(4)	64(3)
C(11)	3291(4)	4784(11)	-2956(3)	57(3)
C(12)	4019(2)	4782(7)	272(3)	28(2)
C(13)	3495(2)	2452(7)	735(3)	26(2)
C(14)	4516(2)	1286(7)	760(2)	21(2)
C(15)	4689(2)	1936(8)	305(3)	24(2)
C(16)	4468(2)	967(7)	-175(3)	24(2)
C(17)	4154(2)	-280(7)	-38(2)	25(2)
C(18)	4181(2)	-92(7)	540(3)	24(2)
C(19)	4736(2)	1682(9)	1376(3)	31(2)
C(20)	4709(2)	3554(10)	1514(3)	39(2)
C(21)	4467(3)	634(10)	1736(3)	42(2)
C(22)	5291(2)	1117(10)	1505(3)	39(2)

Table 6.3.15-b. Anisotropic displacement parameters ($Å^2$ x 10^3) for **26**. The anisotropic displacement factor exponent takes the form: $-2\pi^2[h^2a^{*2}U_{11} + ... + 2hka^*b^*U_{12}]$.

Atom	U_{11}	U_{22}	U_{33}	U_{23}	U_{13}	U_{12}
W(1)	21(1)	16(1)	25(1)	2(1)	11(1)	2(1)
W(2)	19(1)	13(1)	25(1)	0(1)	9(1)	1(1)
Br(1)	23(1)	18(1)	28(1)	0(1)	6(1)	0(1)
Cu(1)	22(1)	15(1)	30(1)	0(1)	11(1)	1(1)
P(1)	22(1)	16(1)	27(1)	0(1)	11(1)	-1(1)
P(2)	21(1)	17(1)	28(1)	2(1)	12(1)	3(1)
O(1)	30(2)	38(3)	39(3)	4(2)	13(2)	-11(2)
O(2)	46(2)	22(2)	38(3)	-5(2)	17(2)	4(2)
O(3)	43(2)	15(2)	67(3)	-7(2)	14(2)	-6(2)
O(4)	31(2)	43(3)	34(3)	-4(2)	18(2)	-2(2)
C(1)	27(3)	23(3)	28(3)	4(2)	13(2)	1(2)
C(2)	32(3)	25(4)	31(3)	8(3)	12(2)	1(2)
C(3)	27(3)	23(3)	23(3)	3(2)	8(2)	-1(2)
C(4)	26(3)	39(4)	20(3)	12(3)	3(2)	-2(2)
C(5)	26(3)	63(5)	47(4)	24(4)	16(3)	16(3)
C(6)	50(4)	37(4)	33(4)	17(3)	19(3)	27(3)
C(7)	43(3)	18(3)	22(3)	9(2)	10(2)	4(3)
C(8)	37(3)	30(3)	33(3)	-6(3)	18(3)	-6(3)
C(9)	78(5)	35(4)	47(5)	-8(4)	30(4)	4(4)
C(10)	52(4)	99(8)	53(5)	-34(5)	33(4)	-33(5)
C(11)	106(7)	43(5)	32(4)	10(3)	35(4)	28(5)
C(12)	31(3)	17(3)	41(4)	8(3)	17(3)	6(2)
C(13)	26(3)	19(3)	37(4)	5(2)	13(3)	1(2)
C(14)	18(2)	15(3)	30(3)	2(2)	4(2)	7(2)

C(15)	19(2)	21(3)	35(3)	1(2)	11(2)	5(2)
C(16)	21(2)	23(3)	30(3)	-5(2)	8(2)	9(2)
C(17)	31(3)	14(3)	28(3)	-1(2)	5(2)	8(2)
C(18)	24(3)	13(3)	34(3)	5(2)	4(2)	5(2)
C(19)	23(3)	39(4)	33(3)	1(3)	12(2)	-1(2)
C(20)	29(3)	53(5)	34(4)	-12(3)	7(3)	-6(3)
C(21)	41(3)	54(5)	29(3)	3(3)	7(3)	-3(3)
C(22)	34(3)	55(5)	27(3)	-2(3)	6(3)	1(3)

Table 6.3.16.	**28**	
Empirical Formula	$C_7H_5O_2P_3W$	
Formula weight	397.86	
Crystal size	0.1130 x 0.0830 x 0.0389 mm	
Crystal description	parallelepiped	
Crystal color	pale yellow	
Crystal system	triclinic	
Space group	$P\bar{1}$	
Unit cell dimensions	a = 7.7617(12) Å	α = 92.327(9)°
	b = 8.2360(12) Å	β = 90.579(10)°
	c = 8.6287(8) Å	γ = 115.421(14)°
Volume	497.54(13) $Å^3$	
Z, Calculated density	2, 2.656 Mg/m^3	
Absorption coefficient	25.799 mm^{-1}	
F(000)	364	
Measurement device type	Goniometer Xcalibur	
Measurement method	omega scans	
Temperature	123 K	
Wavelength	1.54184 Å	
Monochromator	graphite	
θ range for data collection	5.13 to 66.26°	
Index ranges	$-9 \leq h \leq 9$, $-9 \leq k \leq 9$, $-7 \leq l \leq 9$	
Reflections collected / unique	2742 / 1661 [R(int) = 0.0217]	
Reflections greater I>2\s(I)	1589	
Absorption correction	Analytical	
Max. and min. transmission	0.460 and 0.191	
Refinement method	Full-matrix least-squares on F^2	
Data / restraints / parameters	1661 / 0 / 118	
Goodness of fit on F^2	1.061	
Final R indices [I>2sigma(I)]	R1 = 0.0237, wR2 = 0.0616	
R indices (all data)	R1 = 0.0250, wR2 = 0.0623	
Largest diff. peak and hole	0.889 and -1.090 e.$Å^{-3}$	

Table 6.3.16-a. Atomic coordinates (x 10^4) and equivalent isotropic displacement parameters (A^2 x 10^3) for **28**. U_{eq} is defined as one third of the trace of the orthogonalized U_{ij} tensor.

Atom	**x**	**y**	**z**	$\boldsymbol{U_{eq}}$
W(1)	2748(1)	2764(1)	2304(1)	15(1)
P(1)	1211(2)	-518(2)	2914(2)	25(1)
P(2)	3012(2)	1290(2)	4749(2)	26(1)

P(3)	4268(2)	590(2)	2777(2)	28(1)
O(1)	7166(5)	5224(5)	2558(5)	31(1)
O(2)	3313(6)	1562(6)	-1085(5)	33(1)
C(1)	5551(7)	4316(7)	2474(6)	19(2)
C(2)	3129(7)	1977(7)	154(6)	24(2)
C(3)	2343(8)	5279(7)	3086(7)	27(2)
C(4)	2075(8)	5029(7)	1446(7)	26(2)
C(5)	417(8)	3380(8)	1140(6)	26(2)
C(6)	-310(8)	2654(8)	2574(7)	28(2)
C(7)	880(8)	3826(8)	3765(6)	26(2)

Table 6.3.16-b. Anisotropic displacement parameters ($Å^2$ x 10^3) for **28**. The anisotropic displacement factor exponent takes the form: $-2\pi^2[h^2a^{*2}U_{11} + ... + 2hka^*b^*U_{12}]$.

Atom	U_{11}	U_{22}	U_{33}	U_{23}	U_{13}	U_{12}
W(1)	15(1)	16(1)	18(1)	4(1)	2(1)	8(1)
P(1)	22(1)	19(1)	33(1)	5(1)	2(1)	7(1)
P(2)	30(1)	29(1)	21(1)	8(1)	1(1)	15(1)
P(3)	25(1)	26(1)	41(1)	11(1)	8(1)	17(1)
O(1)	19(2)	29(2)	39(2)	2(2)	0(2)	6(2)
O(2)	42(2)	40(2)	22(2)	-3(2)	4(2)	22(2)
C(1)	18(3)	16(2)	20(3)	6(2)	1(2)	4(2)
C(2)	16(3)	26(3)	28(3)	2(2)	0(2)	8(2)
C(3)	26(3)	20(3)	40(3)	0(2)	-1(2)	14(2)
C(4)	32(3)	26(3)	32(3)	11(2)	6(2)	22(3)
C(5)	31(3)	36(3)	23(3)	4(2)	1(2)	25(3)
C(6)	18(3)	27(3)	43(3)	2(2)	2(2)	15(2)
C(7)	33(3)	32(3)	24(3)	-2(2)	2(2)	25(3)

Table 6.3.17.	**29** $*$ (CF_3O_3S)	
Empirical Formula	$C_{21}H_{15}AgMo_3O_6P_9(CF_3O_3S)$	
Formula weight	1186.83 g/mole	
Crystal size	0.238 x 0.048 x 0.032 mm	
Crystal description	hexagonal column	
Crystal color	yellow	
Crystal system	hexagonal	
Space group	$P6_3$	
Unit cell dimensions	a = 13.9763(5) Å	α = 90°
	b = 13.9763(5) Å	β = 90°
	c = 10.3040(4) Å	γ = 120°
Volume	1743.09(11) $Å^3$	
Z, Calculated density	2, 2.250 Mg/m^3	
Absorption coefficient	18.052 mm^{-1}	
F(000)	1140	
Measurement device type	Oxford Diffraction Gemini Ultra	
Measurement method	omega-scan	
Temperature	150(1) K	
Wavelength	1.5418 Å	
Monochromator	graphite	

θ range for data collection	3.65 to 63.09°
Index ranges	$-15 \leq h \leq 16$, $-16 \leq k \leq 16$, $-11 \leq l \leq 11$
Reflections collected / unique	32904 / 1877 [R(int) = 0.0451]
Reflections greater I>2\s(I)	1739
Absorption correction	semi-empirical from equivalents
Max. and min. transmission	1.35942 and 0.32986
Refinement method	Full-matrix least-squares on F^2
Data / restraints / parameters	1877 / 1 / 145
Goodness of fit on F^2	1.023
Final R indices [I>2sigma(I)]	R1 = 0.0196, wR2 = 0.0469
R indices (all data)	R1 = 0.0410, wR2 = 0.0803
Largest diff. peak and hole	0.991 and -0.314 e.Å^{-3}

Table 6.3.17-a. Atomic coordinates (x 10^4) and equivalent isotropic displacement parameters (Å^2 x 10^3) for **29**. U_{eq} is defined as one third of the trace of the orthogonalized U_{ij} tensor.

Atom	**x**	**y**	**z**	$\boldsymbol{U_{eq}}$
Ag(1)	0	0	7191(1)	35(1)
Mo(1)	3399(1)	554(1)	4733(1)	22(1)
P(1)	1405(1)	-200(1)	5421(1)	31(1)
P(2)	1713(1)	65(1)	3395(1)	34(1)
P(3)	1704(1)	-1323(1)	4319(1)	35(1)
O(1)	3337(3)	-318(3)	7570(3)	52(1)
O(2)	3508(3)	2718(2)	5772(3)	42(1)
C(1)	5283(3)	1419(3)	4711(6)	37(1)
C(2)	4960(3)	1829(3)	3640(5)	38(1)
C(3)	4361(3)	958(3)	2756(4)	33(1)
C(4)	4304(3)	-17(3)	3286(5)	35(1)
C(5)	4873(3)	280(3)	4494(4)	32(1)
C(6)	3366(3)	20(4)	6552(5)	36(2)
C(7)	3426(3)	1900(3)	5428(4)	31(1)
S(1)	3333	6667	2922(2)	39(1)
F(1)	2334(3)	6156(4)	5161(3)	95(2)
O(3)	2733(4)	5531(3)	2574(4)	79(2)
C(8)	3333	6667	4693(11)	46(2)

Table 6.3.17-b. Anisotropic displacement parameters (Å^2 x 10^3) for **29**. The anisotropic displacement factor exponent takes the form: $-2\pi^2[h^2a^{*2}U_{11} + ... + 2hka^*b^*U_{12}]$.

Atom	$\boldsymbol{U_{11}}$	$\boldsymbol{U_{22}}$	$\boldsymbol{U_{33}}$	$\boldsymbol{U_{23}}$	$\boldsymbol{U_{13}}$	$\boldsymbol{U_{12}}$
Ag(1)	33(1)	33(1)	37(1)	0	0	17(1)
Mo(1)	20(1)	24(1)	23(1)	-3(1)	0(1)	11(1)
P(1)	25(1)	39(1)	29(1)	0(1)	4(1)	18(1)
P(2)	27(1)	43(1)	28(1)	0(1)	-5(1)	16(1)
P(3)	27(1)	27(1)	47(1)	-4(1)	-1(1)	10(1)
O(1)	53(2)	75(3)	36(2)	14(2)	-2(2)	39(2)
O(2)	45(2)	31(2)	45(2)	-8(1)	5(2)	16(2)
C(1)	17(2)	44(2)	41(2)	-16(3)	1(2)	9(2)
C(2)	25(2)	32(2)	49(3)	-1(2)	13(2)	8(2)
C(3)	26(2)	38(2)	31(2)	-4(2)	8(2)	12(2)

C(4)	29(2)	35(2)	40(3)	-10(2)	8(2)	16(2)
C(5)	25(2)	43(2)	35(3)	-4(2)	-3(2)	22(2)
C(6)	29(2)	46(3)	37(3)	-2(2)	1(2)	22(2)
C(7)	26(2)	29(2)	35(2)	2(2)	1(2)	12(2)
S(1)	34(1)	34(1)	51(1)	0	0	17(1)
F(1)	55(2)	129(3)	64(3)	-30(2)	19(2)	19(2)
O(3)	112(3)	48(2)	62(3)	-2(2)	39(2)	29(2)
C(8)	41(2)	41(2)	55(5)	0	0	21(1)

Table 6.3.18.	**30** $*$ $5(C_2H_3N)$
Empirical Formula	$(C_{42}H_{30}Ag_2O_{12}P_6W_6)_2(CF_3O_3S)_4$, $5(C_2H_3N)$
Formula weight	5264.18
Crystal size	0.130 x 0.080 x 0.050 mm
Crystal description	parallelepiped
Crystal color	red
Crystal system	monoclinic
Space group	C2/c
Unit cell dimensions	a = 34.1794(8) Å α = 90°
	b = 15.4307(3) Å β = 97.745(2)°
	c = 27.0670(7) Å γ = 90°
Volume	14145.2(6) $Å^3$
Z, Calculated density	4, 2.433 Mg/m^3
Absorption coefficient	24.341 mm^{-1}
F(000)	9479
Measurement device type	Oxford Diffraction Gemini Ultra
Measurement method	omega-scan
Temperature	123 K
Wavelength	1.54184 Å
Monochromator	graphite
θ range for data collection	2.61 to 66.69°
Index ranges	$-40 \leq h \leq 40$, $-18 \leq k \leq 18$, $-31 \leq l \leq 29$
Reflections collected / unique	24599 / 11435 [R(int) = 0.0368]
Reflections greater I>2\s(I)	8441
Absorption correction	semi-empirical from equivalents
Max. and min. transmission	1.00000 and 0.58087
Refinement method	Full-matrix least-squares on F^2
Data / restraints / parameters	11435 / 5 / 792
Goodness of fit on F^2	1.057
Final R indices [I>2sigma(I)]	R1 = 0.0488, wR2 = 0.1174
R indices (all data)	R1 = 0.0685, wR2 = 0.1250
Largest diff. peak and hole	3.003 and -1.578 $e.Å^{-3}$

Table 6.3.18-a. Atomic coordinates (x 10^4) and equivalent isotropic displacement parameters ($Å^2$ x 10^3) for **30**. U_{eq} is defined as one third of the trace of the orthogonalized U_{ij} tensor.

Atom	**x**	**y**	**z**	U_{eq}
W(1)	-2636(1)	1755(1)	-1477(1)	47(1)
W(2)	-3165(1)	828(1)	-832(1)	48(1)

W(3)	-1640(1)	-1498(1)	458(1)	49(1)
W(4)	-1541(1)	-368(1)	1378(1)	40(1)
W(5)	-466(1)	-339(1)	-1411(1)	58(1)
W(6)	-310(1)	-2107(1)	-915(1)	70(1)
Ag(1)	-1992(1)	1483(1)	145(1)	46(1)
Ag(2)	-625(1)	152(1)	198(1)	49(1)
S(1)	-1146(1)	1874(3)	-357(2)	69(1)
P(1)	-2971(1)	2348(2)	-764(1)	48(1)
P(2)	-2494(1)	1495(2)	-585(1)	53(1)
P(3)	-1752(1)	102(2)	522(1)	54(1)
P(4)	-1167(1)	-331(2)	634(1)	44(1)
P(5)	-549(1)	-729(3)	-556(1)	58(1)
P(6)	34(1)	-757(3)	-700(1)	60(1)
F(1)	-841(6)	3383(9)	-477(5)	178(8)
F(2)	-911(5)	2589(9)	-1119(4)	148(7)
F(3)	-1377(5)	3177(11)	-933(7)	181(9)
O(1)	-2249(3)	3588(7)	-1273(5)	84(5)
O(2)	-3398(3)	2620(6)	-2053(3)	64(3)
O(3)	-2564(3)	-711(7)	-817(5)	88(5)
O(4)	-3056(4)	645(10)	325(5)	108(6)
O(5)	-1693(3)	-904(8)	-660(4)	85(5)
O(6)	-2551(4)	-1251(15)	392(6)	160(11)
O(7)	-757(3)	-1346(8)	1731(4)	83(4)
O(8)	-1089(3)	1382(6)	1519(4)	70(3)
O(9)	-108(5)	1447(9)	-1034(6)	121(7)
O(10)	305(4)	-592(15)	-1895(5)	149(8)
O(11)	-1227(3)	-2363(8)	-1047(5)	93(5)
O(21)	-790(4)	1446(9)	-267(5)	113(6)
O(22)	-1378(6)	2178(10)	-60(8)	180(10)
O(23)	-1372(5)	1263(10)	-745(5)	125(7)
O(46)	-290(5)	-2477(14)	277(6)	95(6)
C(1)	-2626(5)	1056(11)	-2218(5)	71(5)
C(2)	-2533(5)	451(11)	-1853(6)	71(6)
C(3)	-2174(4)	676(10)	-1568(6)	71(6)
C(4)	-2045(4)	1456(10)	-1768(6)	67(5)
C(5)	-2331(4)	1681(12)	-2184(6)	69(6)
C(6)	-2390(4)	2923(11)	-1350(5)	62(5)
C(7)	-3127(4)	2304(7)	-1838(4)	47(4)
C(8)	-3649(4)	751(8)	-1532(5)	56(4)
C(9)	-3614(5)	-80(9)	-1300(5)	66(5)
C(10)	-3720(5)	4(10)	-824(6)	69(5)
C(11)	-3820(4)	886(10)	-764(6)	66(5)
C(12)	-3780(4)	1342(9)	-1192(6)	62(5)
C(13)	-2776(4)	-131(8)	-828(6)	62(5)
C(14)	-3087(5)	723(11)	-90(7)	76(6)
C(15)	-1132(6)	-2472(8)	703(6)	78(6)
C(16)	-1275(6)	-2640(9)	204(6)	78(6)
C(17)	-1688(6)	-2896(10)	197(9)	104(8)
C(18)	-1781(9)	-2890(12)	679(12)	135(15)
C(19)	-1440(10)	-2630(10)	991(8)	118(11)
C(20)	-1684(4)	-1120(10)	-247(6)	63(5)

C(21)	-2227(5)	-1319(14)	414(7)	90(8)
C(22)	-1723(4)	-233(11)	2157(5)	67(5)
C(23)	-1997(3)	267(9)	1817(5)	55(4)
C(24)	-2206(4)	-313(11)	1496(6)	67(5)
C(25)	-2070(5)	-1140(11)	1618(6)	72(6)
C(26)	-1782(5)	-1096(11)	2012(6)	76(6)
C(27)	-1044(4)	-993(8)	1589(5)	51(4)
C(28)	-1251(4)	743(9)	1467(5)	55(5)
C(29)	-1153(4)	-327(13)	-1580(6)	74(6)
C(30)	-1027(5)	-957(13)	-1905(6)	82(6)
C(31)	-790(6)	-510(20)	-2211(6)	117(11)
C(32)	-777(7)	360(20)	-2093(8)	121(12)
C(33)	-1010(6)	474(16)	-1695(7)	101(9)
C(34)	-229(5)	790(13)	-1175(7)	80(6)
C(35)	24(5)	-521(16)	-1701(6)	101(8)
C(36)	-898(5)	-2254(11)	-998(7)	83(6)
C(37)	-1029(6)	2809(12)	-720(8)	87(7)
C(41)	-205(7)	-3538(17)	-952(9)	93(8)
C(42)	152(7)	-3147(16)	-803(8)	98(12)
C(43)	233(5)	-2604(14)	-1178(8)	88(6)
C(44)	-74(5)	-2660(13)	-1560(7)	88(6)
C(45)	-345(5)	-3237(14)	-1421(8)	88(6)
C(46)	-301(8)	-2320(20)	-134(9)	95(6)
C(47)	-170(14)	-3590(30)	-971(17)	93(8)
C(48)	181(15)	-3190(30)	-1054(16)	98(12)
C(49)	314(10)	-2680(20)	-638(13)	55(8)
C(50)	45(8)	-2771(19)	-297(12)	55(8)
C(51)	-254(9)	-3330(20)	-503(14)	55(8)
C(52)	-302(13)	-2080(30)	-1749(12)	63(8)
O(52)	-271(9)	-2137(19)	-2161(10)	63(8)
N(2)	-3942(7)	-533(17)	467(9)	99(8)
C(63)	-3420(7)	-307(17)	1301(8)	129(9)
C(64)	-3738(8)	-440(20)	836(10)	92(9)
N(3)	-3686(16)	-1360(40)	1991(19)	130(20)
C(65)	-3542(13)	-970(30)	1700(14)	72(12)
C(66)	-3420(7)	-307(17)	1301(8)	129(9)
S(2)	-1642(2)	3708(3)	-2533(2)	90(2)
F(4)	-1093(5)	2540(8)	-2332(5)	153(7)
F(5)	-940(5)	3589(13)	-2779(6)	164(9)
F(6)	-953(5)	3780(9)	-2002(5)	148(6)
O(24)	-1792(6)	3393(13)	-2106(6)	164(9)
O(25)	-1617(4)	4651(8)	-2567(5)	99(5)
O(26)	-1774(5)	3300(8)	-2998(5)	113(6)
C(38)	-1137(8)	3393(13)	-2432(7)	108(9)
N(1)	-2185(7)	-2592(15)	-1136(8)	61(6)
C(61)	-2086(8)	-1716(16)	-1886(9)	52(6)
C(62)	-2143(8)	-2192(17)	-1484(10)	61(7)

Table 6.3.18-b. Anisotropic displacement parameters (A^2 x 10^3) for **30**. The anisotropic displacement factor exponent takes the form: $-2\pi^2[h^2a^{*2}U_{11} + ... + 2hka^*b^*U_{12}]$

Atom	U_{11}	U_{22}	U_{33}	U_{23}	U_{13}	U_{12}
W(1)	38(1)	57(1)	48(1)	1(1)	13(1)	15(1)
W(2)	47(1)	44(1)	55(1)	-2(1)	18(1)	11(1)
W(3)	42(1)	47(1)	58(1)	-2(1)	4(1)	-7(1)
W(4)	33(1)	43(1)	45(1)	7(1)	11(1)	2(1)
W(5)	49(1)	83(1)	45(1)	0(1)	19(1)	12(1)
W(6)	36(1)	66(1)	104(1)	-3(1)	2(1)	9(1)
Ag(1)	46(1)	47(1)	45(1)	4(1)	12(1)	15(1)
Ag(2)	36(1)	55(1)	58(1)	6(1)	17(1)	6(1)
S(1)	44(2)	81(2)	84(3)	36(2)	21(2)	18(2)
P(1)	46(2)	51(2)	49(2)	-2(1)	15(1)	10(1)
P(2)	49(2)	57(2)	53(2)	8(2)	4(2)	15(2)
P(3)	57(2)	58(2)	51(2)	11(2)	15(2)	23(2)
P(4)	44(2)	40(1)	51(2)	-2(1)	17(1)	-3(1)
P(5)	44(2)	84(2)	48(2)	3(2)	13(2)	5(2)
P(6)	41(2)	76(2)	66(2)	-1(2)	13(2)	4(2)
F(1)	320(20)	117(10)	94(9)	13(7)	15(11)	-114(13)
F(2)	255(18)	124(10)	78(7)	35(7)	73(10)	23(11)
F(3)	169(14)	154(13)	213(17)	85(13)	4(12)	66(12)
O(1)	55(6)	69(7)	126(10)	9(6)	7(6)	-11(5)
O(2)	56(5)	68(6)	67(6)	4(5)	7(5)	24(5)
O(3)	64(6)	56(6)	148(11)	7(6)	28(7)	24(5)
O(4)	129(12)	132(12)	64(8)	21(7)	18(7)	-10(9)
O(5)	86(8)	108(9)	62(7)	-1(6)	10(6)	40(7)
O(6)	44(7)	300(30)	135(13)	-94(14)	8(7)	-38(11)
O(7)	76(7)	106(9)	64(6)	4(6)	-2(5)	33(7)
O(8)	73(6)	48(5)	93(7)	-18(5)	30(6)	-14(5)
O(9)	143(13)	64(8)	159(14)	-2(8)	34(11)	-6(8)
O(10)	73(8)	300(20)	85(9)	-50(12)	53(8)	-18(11)
O(11)	41(6)	102(9)	132(10)	5(8)	-4(6)	-1(6)
O(21)	138(11)	99(9)	120(10)	54(8)	80(9)	62(9)
O(22)	215(19)	97(10)	280(20)	19(12)	221(19)	22(11)
O(23)	154(14)	110(11)	103(10)	-18(8)	-9(9)	-26(10)
O(46)	72(9)	136(14)	74(9)	25(10)	4(9)	-6(9)
C(1)	67(9)	94(11)	52(8)	-21(8)	6(7)	35(9)
C(2)	75(10)	72(9)	71(10)	-9(8)	25(8)	10(8)
C(3)	60(9)	78(10)	75(10)	-16(8)	13(8)	42(8)
C(4)	41(7)	77(10)	85(10)	2(8)	19(7)	14(7)
C(5)	50(8)	101(12)	62(9)	2(8)	32(7)	11(8)
C(6)	46(7)	85(11)	57(8)	1(7)	20(6)	5(7)
C(7)	48(7)	40(6)	52(7)	4(5)	8(6)	12(5)
C(8)	47(7)	50(7)	69(8)	-1(6)	-4(6)	-3(6)
C(9)	79(10)	52(7)	66(9)	-1(7)	9(8)	-9(7)
C(10)	72(10)	62(8)	76(10)	-9(7)	21(8)	-12(8)
C(11)	47(8)	71(9)	87(11)	-20(8)	30(7)	-3(7)
C(12)	48(7)	53(7)	88(11)	-8(7)	20(7)	0(6)
C(13)	49(7)	44(7)	94(11)	7(7)	13(7)	16(6)
C(14)	69(10)	89(11)	72(11)	20(9)	18(9)	-4(9)
C(15)	119(14)	32(6)	75(10)	-8(7)	-11(10)	34(8)
C(16)	111(14)	51(8)	68(10)	-7(7)	-3(9)	28(9)
C(17)	86(13)	52(9)	170(20)	-60(11)	6(13)	-17(9)

C(18)	180(30)	53(11)	190(30)	-31(14)	90(20)	-30(13)
C(19)	240(30)	34(8)	89(13)	10(8)	60(18)	0(13)
C(20)	48(7)	82(10)	59(9)	11(7)	7(7)	9(7)
C(21)	46(9)	142(17)	85(12)	-39(11)	22(8)	-27(10)
C(22)	61(9)	93(11)	50(8)	10(7)	15(7)	-7(8)
C(23)	40(7)	62(8)	68(8)	4(7)	29(6)	10(6)
C(24)	33(6)	100(12)	71(9)	3(8)	22(6)	-3(7)
C(25)	74(10)	74(10)	81(11)	-13(8)	53(9)	-16(8)
C(26)	84(11)	74(10)	78(11)	38(9)	41(10)	1(9)
C(27)	44(7)	55(7)	55(8)	-3(6)	13(6)	18(6)
C(28)	55(8)	57(8)	59(8)	-16(6)	29(6)	2(7)
C(29)	41(7)	124(15)	60(9)	12(9)	16(7)	29(9)
C(30)	62(9)	121(14)	59(9)	-21(9)	-8(8)	32(10)
C(31)	61(11)	260(30)	34(9)	-4(14)	21(8)	0(17)
C(32)	95(16)	190(30)	74(14)	66(16)	-6(12)	-38(18)
C(33)	86(13)	131(18)	81(13)	20(12)	-8(11)	56(13)
C(34)	74(11)	80(11)	86(11)	12(9)	6(9)	18(9)
C(35)	58(10)	190(20)	61(10)	-21(12)	30(9)	-6(12)
C(36)	53(9)	74(10)	120(14)	3(10)	5(9)	-9(8)
C(37)	91(12)	88(12)	94(13)	40(10)	57(11)	60(11)
C(41)	48(10)	70(11)	160(20)	-9(12)	14(11)	14(9)
C(42)	72(14)	76(13)	150(30)	10(20)	30(20)	27(12)
C(43)	60(8)	97(11)	111(12)	-42(10)	23(8)	15(8)
C(44)	60(8)	97(11)	111(12)	-42(10)	23(8)	15(8)
C(45)	60(8)	97(11)	111(12)	-42(10)	23(8)	15(8)
C(46)	72(9)	136(14)	74(9)	25(10)	4(9)	-6(9)
C(47)	48(10)	70(11)	160(20)	-9(12)	14(11)	14(9)
C(48)	72(14)	76(13)	150(30)	10(20)	30(20)	27(12)
C(49)	44(12)	44(12)	77(17)	-2(11)	9(11)	6(10)
C(50)	44(12)	44(12)	77(17)	-2(11)	9(11)	6(10)
C(51)	44(12)	44(12)	77(17)	-2(11)	9(11)	6(10)
C(52)	64(15)	71(15)	53(13)	-18(13)	1(13)	21(12)
O(52)	64(15)	71(15)	53(13)	-18(13)	1(13)	21(12)
S(2)	132(4)	79(3)	59(2)	10(2)	15(2)	-28(3)
F(4)	226(16)	90(8)	126(10)	2(7)	-43(10)	25(10)
F(5)	148(13)	230(19)	115(11)	31(12)	17(9)	43(12)
F(6)	177(13)	118(10)	130(10)	24(8)	-50(10)	-31(10)
O(24)	203(19)	188(18)	105(11)	55(12)	39(12)	-62(15)
O(25)	140(12)	72(7)	88(8)	0(6)	25(8)	-5(7)
O(26)	155(13)	87(8)	88(8)	-13(7)	-15(8)	-32(9)
C(38)	170(20)	83(12)	61(11)	28(9)	-17(13)	-37(14)

Table 6.3.19.	**31** $*$ $2(C_2H_3N)$ $*$ $4(CH_2Cl_2)$
Empirical Formula	$C_{56}H_{40}Ag_2O_{16}P_8W_8(F_6P)_2(C_2H_3N)_2(CH_2Cl_2)_4$
Formula weight	3614.85 g/mole
Crystal size	0.433 x 0.286 x 0.181 mm
Crystal description	prism
Crystal color	red
Crystal system	triclinic

Space group	$P\bar{1}$	
Unit cell dimensions	a = 12.1812(3) Å	α = 112.356(2)°
	b = 13.2571(3) Å	β = 99.679(2)°
	c = 15.2390(3) Å	γ = 94.471(2)°
Volume	2216.20(10) Å^3	
Z, Calculated density	1, 2.708 Mg/m^3	
Absorption coefficient	11.271 mm^{-1}	
F(000)	1660	
Measurement device type	Oxford Diffraction Gemini Ultra	
Measurement method	omega-scan	
Temperature	123 K	
Wavelength	0.71073 Å	
Monochromator	graphite	
θ range for data collection	3.04 to 31.54°	
Index ranges	$-13 \leq h \leq 17$, $-19 \leq k \leq 19$, $-22 \leq l \leq 22$	
Reflections collected / unique	29481 / 14299 [R(int) = 0.0302]	
Reflections greater I>2\s(I)	11781	
Absorption correction	analytical	
Max. and min. transmission	0.221 and 0.021	
Refinement method	Full-matrix least-squares on F^2	
Data / restraints / parameters	14299 / 0 / 551	
Goodness of fit on F^2	1.069	
Final R indices [I>2sigma(I)]	R1 = 0.0350, wR2 = 0.0914	
R indices (all data)	R1 = 0.0441, wR2 = 0.0937	
Largest diff. peak and hole	2.939 and -2.616 e.Å^{-3}	

Table 6.3.19-a. Atomic coordinates (x 10^4) and equivalent isotropic displacement parameters (Å^2 x 10^3) for **31**. U_{eq} is defined as one third of the trace of the orthogonalized U_{ij} tensor.

Atom	**x**	**y**	**z**	U_{eq}
W(1)	2142(1)	-4511(1)	4073(1)	14(1)
W(2)	2373(1)	-4016(1)	2327(1)	16(1)
W(3)	-2393(1)	-1372(1)	2499(1)	16(1)
W(4)	-655(1)	281(1)	2349(1)	14(1)
Ag(1)	994(1)	-1399(1)	4386(1)	26(1)
P(1)	879(1)	-3547(1)	3255(1)	18(1)
P(2)	2539(1)	-2673(1)	4072(1)	18(1)
P(3)	-324(1)	-834(1)	3301(1)	18(1)
P(4)	-1376(1)	345(1)	3828(1)	17(1)
O(6)	217(4)	-6427(3)	2646(3)	30(1)
O(7)	477(4)	-3693(4)	5467(4)	37(2)
O(16)	2566(4)	-1740(4)	2159(3)	37(1)
O(17)	4970(4)	-3549(4)	3202(4)	34(2)
O(26)	-2298(4)	-2571(4)	3928(4)	41(2)
O(27)	-1192(4)	-3252(4)	1252(3)	35(1)
O(36)	1157(4)	2155(4)	3967(3)	33(1)
O(37)	-2344(4)	1994(4)	2620(3)	34(1)
C(1)	4048(5)	-4209(5)	4831(5)	26(2)
C(2)	3856(5)	-5223(5)	4029(4)	25(2)
C(3)	3059(6)	-5973(5)	4141(4)	27(2)
C(4)	2750(6)	-5421(5)	5043(4)	27(2)

C(5)	3370(6)	-4302(5)	5477(4)	29(2)
C(6)	906(5)	-5710(4)	3161(4)	20(2)
C(7)	1090(5)	-3979(5)	4943(4)	24(2)
C(11)	1902(6)	-5931(4)	1330(4)	26(2)
C(12)	2847(6)	-5490(5)	1095(4)	31(2)
C(13)	2528(6)	-4692(5)	732(4)	31(2)
C(14)	1381(6)	-4649(5)	748(4)	29(2)
C(15)	979(6)	-5409(5)	1109(4)	27(2)
C(16)	2484(5)	-2566(5)	2247(4)	27(2)
C(17)	4014(5)	-3707(5)	2904(4)	23(2)
C(21)	-3685(5)	-811(5)	1498(4)	26(2)
C(22)	-3969(5)	-455(5)	2417(5)	28(2)
C(23)	-4278(5)	-1408(6)	2599(5)	30(2)
C(24)	-4173(5)	-2363(5)	1782(4)	28(2)
C(25)	-3798(5)	-1981(5)	1102(4)	25(2)
C(26)	-2309(5)	-2121(5)	3412(4)	25(2)
C(27)	-1611(5)	-2545(5)	1714(4)	24(2)
C(31)	760(6)	110(6)	1501(5)	32(2)
C(32)	170(5)	-959(5)	1163(4)	27(2)
C(33)	-946(5)	-955(5)	695(4)	22(2)
C(34)	-1026(5)	130(5)	750(4)	25(2)
C(35)	52(6)	807(5)	1255(4)	29(2)
C(36)	489(5)	1478(5)	3399(4)	22(2)
C(37)	-1736(5)	1366(4)	2544(4)	20(1)
P(5)	4039(1)	1736(1)	1739(1)	24(1)
F(1)	5136(4)	1278(4)	1430(4)	56(2)
F(2)	3667(4)	667(3)	1907(4)	48(2)
F(3)	3359(5)	1164(5)	647(3)	68(2)
F(4)	4391(5)	2807(5)	1564(5)	84(3)
F(5)	4699(5)	2319(5)	2841(4)	74(2)
F(6)	2914(4)	2181(4)	2051(3)	52(2)
N(1)	1471(6)	7229(6)	-372(5)	48(2)
C(44)	2356(6)	7671(5)	-182(4)	29(2)
C(45)	3500(6)	8263(7)	89(6)	48(3)
Cl(1)	7987(5)	4855(5)	2461(4)	169(3)
Cl(2)	5924(4)	4665(3)	1117(3)	110(2)
C(41)	6694(11)	4535(11)	2154(9)	94(5)
Cl(3)	5100(4)	1151(4)	4635(3)	133(2)
Cl(4)	2790(5)	321(6)	4365(4)	186(3)
C(42)	3796(17)	880(30)	4147(19)	270(20)

Table 6.3.19-b. Anisotropic displacement parameters ($Å^2$ x 10^3) for **31**. The anisotropic displacement factor exponent takes the form: $-2\pi^2[h^2a^{*2}U_{11} + ... + 2hka^*b^*U_{12}]$.

Atom	U_{11}	U_{22}	U_{33}	U_{23}	U_{13}	U_{12}
W(1)	15(1)	16(1)	12(1)	6(1)	2(1)	3(1)
W(2)	20(1)	16(1)	12(1)	5(1)	5(1)	3(1)
W(3)	19(1)	16(1)	12(1)	6(1)	3(1)	1(1)
W(4)	16(1)	16(1)	10(1)	5(1)	3(1)	2(1)
Ag(1)	36(1)	29(1)	13(1)	5(1)	4(1)	19(1)
P(1)	17(1)	22(1)	19(1)	9(1)	5(1)	8(1)

P(2)	23(1)	16(1)	15(1)	4(1)	6(1)	3(1)
P(3)	21(1)	19(1)	14(1)	7(1)	1(1)	5(1)
P(4)	23(1)	18(1)	11(1)	4(1)	5(1)	2(1)
O(6)	32(2)	28(2)	26(2)	10(2)	1(2)	-7(2)
O(7)	47(3)	37(3)	37(3)	15(2)	31(2)	11(2)
O(16)	59(3)	23(2)	34(2)	17(2)	13(2)	4(2)
O(17)	20(2)	49(3)	42(3)	26(2)	10(2)	2(2)
O(26)	49(3)	46(3)	39(3)	30(2)	9(2)	1(2)
O(27)	44(3)	27(2)	25(2)	0(2)	6(2)	11(2)
O(36)	35(3)	28(2)	27(2)	8(2)	-3(2)	-9(2)
O(37)	29(2)	31(2)	42(3)	14(2)	5(2)	11(2)
C(1)	14(3)	27(3)	36(3)	17(2)	-5(2)	2(2)
C(2)	17(3)	32(3)	29(3)	18(2)	1(2)	5(2)
C(3)	37(4)	21(3)	25(3)	12(2)	5(2)	10(2)
C(4)	33(3)	34(3)	24(3)	20(2)	7(2)	9(2)
C(5)	35(4)	34(3)	16(3)	11(2)	-3(2)	7(3)
C(6)	22(3)	19(2)	21(3)	11(2)	2(2)	1(2)
C(7)	32(3)	22(3)	20(3)	9(2)	6(2)	4(2)
C(11)	42(4)	16(2)	14(2)	1(2)	6(2)	-1(2)
C(12)	31(3)	30(3)	22(3)	-2(2)	12(2)	8(2)
C(13)	45(4)	32(3)	14(3)	5(2)	13(3)	-1(3)
C(14)	40(4)	29(3)	13(2)	7(2)	-2(2)	5(2)
C(15)	36(3)	24(3)	13(2)	1(2)	4(2)	2(2)
C(16)	34(3)	31(3)	18(3)	12(2)	7(2)	10(2)
C(17)	24(3)	22(3)	24(3)	11(2)	8(2)	3(2)
C(21)	23(3)	30(3)	24(3)	15(2)	-1(2)	-4(2)
C(22)	19(3)	31(3)	36(3)	15(3)	7(2)	4(2)
C(23)	20(3)	44(4)	34(3)	22(3)	8(2)	5(3)
C(24)	27(3)	26(3)	28(3)	12(2)	-1(2)	-5(2)
C(25)	16(3)	35(3)	20(3)	13(2)	-7(2)	-4(2)
C(26)	32(3)	24(3)	19(3)	10(2)	6(2)	0(2)
C(27)	28(3)	29(3)	14(2)	10(2)	0(2)	3(2)
C(31)	22(3)	48(4)	25(3)	13(3)	11(2)	0(3)
C(32)	29(3)	35(3)	19(3)	8(2)	16(2)	14(2)
C(33)	28(3)	30(3)	8(2)	6(2)	6(2)	6(2)
C(34)	34(3)	30(3)	15(2)	11(2)	8(2)	6(2)
C(35)	43(4)	30(3)	16(3)	10(2)	16(2)	-3(3)
C(36)	18(3)	26(3)	21(3)	8(2)	5(2)	0(2)
C(37)	21(3)	21(2)	19(2)	9(2)	2(2)	2(2)
P(5)	24(1)	24(1)	25(1)	10(1)	3(1)	4(1)
F(1)	34(2)	83(4)	71(3)	43(3)	27(2)	24(2)
F(2)	53(3)	37(2)	67(3)	30(2)	24(2)	12(2)
F(3)	61(3)	110(5)	23(2)	21(2)	-2(2)	16(3)
F(4)	71(4)	59(3)	153(6)	75(4)	29(4)	5(3)
F(5)	63(4)	86(4)	36(3)	-1(3)	-17(2)	-4(3)
F(6)	49(3)	53(3)	57(3)	18(2)	25(2)	25(2)
N(1)	39(4)	57(4)	46(4)	21(3)	8(3)	-2(3)
C(44)	31(3)	31(3)	21(3)	8(2)	2(2)	8(2)
C(45)	29(4)	44(4)	59(5)	10(4)	8(3)	-1(3)
Cl(1)	127(4)	217(6)	138(4)	44(4)	22(3)	41(4)
Cl(2)	125(3)	82(2)	140(3)	38(2)	90(3)	20(2)

C(41)	84(9)	80(8)	83(8)	9(6)	-18(7)	13(7)
Cl(3)	115(3)	144(4)	110(3)	35(3)	3(2)	-27(3)
Cl(4)	130(4)	225(7)	136(4)	0(4)	25(3)	26(4)
C(42)	84(14)	570(60)	190(20)	200(30)	28(15)	-60(20)

Table 6.3.20.	**32**	
Empirical Formula	$C_{28}H_{20}Ag_2O_8P_{12}W_4(F_6P)_2$	
Formula weight	2097.12 g/mole	
Crystal size	0.244 x 0.081 x 0.017 mm	
Crystal description	plate	
Crystal color	yellow	
Crystal system	triclinic	
Space group	$P\bar{1}$	
Unit cell dimensions	a = 13.8337(6) Å	α = 96.950(4)°
	b = 14.2258(6) Å	β = 116.511(5)°
	c = 14.7877(7) Å	γ = 102.597(4)°
Volume	2460.7(2) A^3	
Z, Calculated density	2, 2.830 Mg/m^3	
Absorption coefficient	28.192 mm^{-1}	
F(000)	1920	
Measurement device type	Oxford Diffraction Gemini Ultra	
Measurement method	omega-scan	
Temperature	123.0(1) K	
Wavelength	1.54178 Å	
Monochromator	graphite	
θ range for data collection	3.29 to 66.70°	
Index ranges	$-16 \le h \le 15$, $-16 \le k \le 16$, $-11 \le l \le 17$	
Reflections collected / unique	16988 / 8299 [R(int) = 0.0359]	
Reflections greater I>2\s(I)	6830	
Absorption correction	analytical	
Max. and min. transmission	1.00000 and 0.12599	
Refinement method	Full-matrix least-squares on F^2	
Data / restraints / parameters	8299 / 0 / 613	
Goodness of fit on F^2	0.989	
Final R indices [I>2sigma(I)]	R1 = 0.0311, wR2 = 0.0762	
R indices (all data)	R1 = 0.0211, wR2 = 0.0472	
Largest diff. peak and hole	1.352 and -1.203 e. $Å^{-3}$	

Table 6.3.20-a. Atomic coordinates (x 10^4) and equivalent isotropic displacement parameters ($Å^2$ x 10^3) for **32**. U_{eq} is defined as one third of the trace of the orthogonalized U_{ij} tensor.

Atom	**x**	**y**	**z**	U_{eq}
W(1)	3666(1)	2324(1)	-450(1)	18(1)
W(2)	9039(1)	2245(1)	-528(1)	19(1)
W(3)	8276(1)	-2255(1)	-4293(1)	22(1)
W(4)	2967(1)	-2248(1)	-4248(1)	20(1)
Ag(1)	5691(1)	287(1)	-1020(1)	29(1)
Ag(2)	6190(1)	-231(1)	-3892(1)	33(1)
P(1)	4855(1)	1246(1)	293(1)	24(1)

P(2)	3004(1)	453(1)	-627(1)	24(1)
P(3)	3908(2)	908(1)	-1435(1)	28(1)
P(4)	6926(1)	1811(1)	-1267(1)	24(1)
P(5)	7620(1)	527(1)	-1254(1)	24(1)
P(6)	7476(2)	1413(1)	-2369(1)	31(1)
P(7)	8193(2)	-536(1)	-3695(1)	29(1)
P(8)	6797(2)	-1836(1)	-3944(2)	36(1)
P(9)	8446(2)	-1428(1)	-2581(2)	38(1)
P(10)	4744(1)	-834(1)	-3107(1)	25(1)
P(11)	6060(2)	976(1)	-5176(1)	28(1)
P(12)	3277(2)	-364(1)	-3901(2)	31(1)
O(1)	3000(5)	2275(4)	1336(5)	49(2)
O(2)	1098(4)	1690(4)	-2192(4)	43(2)
O(3)	10529(4)	853(4)	-497(4)	39(2)
O(4)	9072(4)	1802(4)	1528(4)	38(2)
O(5)	10711(5)	-849(4)	-3600(6)	60(2)
O(6)	7393(8)	-1730(5)	-6454(5)	83(3)
O(7)	2396(5)	-1893(4)	-2415(5)	45(2)
O(8)	586(5)	-2082(4)	-5794(5)	61(2)
C(1)	3212(6)	2287(4)	665(6)	32(2)
C(2)	2023(6)	1903(5)	-1555(6)	29(2)
C(3)	9969(6)	1346(5)	-517(5)	28(2)
C(4)	9081(5)	1939(5)	783(6)	31(2)
C(5)	9822(6)	-1340(5)	-3848(6)	36(2)
C(6)	7717(8)	-1879(6)	-5638(6)	49(3)
C(7)	2578(6)	-2015(5)	-3097(6)	34(2)
C(8)	1456(6)	-2133(5)	-5250(6)	39(2)
C(9)	3766(6)	3618(4)	-1231(6)	30(2)
C(10)	3773(6)	3962(4)	-282(6)	34(2)
C(11)	4769(6)	3905(4)	534(6)	29(2)
C(12)	5390(6)	3537(4)	106(6)	34(2)
C(13)	4756(6)	3372(5)	-992(6)	30(2)
C(14)	9038(6)	3895(4)	-398(7)	40(3)
C(15)	9292(7)	3624(5)	-1191(6)	35(2)
C(16)	10321(7)	3402(5)	-727(7)	43(3)
C(17)	10699(6)	3537(5)	345(7)	39(2)
C(18)	9886(7)	3836(5)	542(6)	40(3)
C(19)	8336(7)	-3664(5)	-3624(6)	36(2)
C(20)	7272(7)	-3902(5)	-4521(7)	40(3)
C(21)	7465(7)	-3835(5)	-5381(6)	43(3)
C(22)	8642(6)	-3554(5)	-5019(6)	33(2)
C(23)	9182(6)	-3447(4)	-3916(6)	35(2)
C(24)	4096(6)	-3315(5)	-3916(6)	33(2)
C(25)	3231(7)	-3640(5)	-3653(6)	38(3)
C(26)	2167(6)	-3919(4)	-4589(7)	41(3)
C(27)	2392(7)	-3743(5)	-5405(7)	41(3)
C(28)	3572(7)	-3372(5)	-4980(6)	37(3)
P(13)	1268(1)	5001(1)	7578(1)	24(1)
F(1)	2464(4)	5110(5)	7640(4)	63(2)
F(2)	685(4)	4909(4)	6354(3)	54(2)
F(3)	1529(5)	6165(3)	7789(5)	67(2)

F(4)	67(4)	4888(4)	7509(4)	51(2)
F(5)	1839(4)	5098(3)	8806(3)	41(1)
F(6)	1030(5)	3843(3)	7386(4)	73(2)
P(14)	6127(2)	4654(1)	7376(1)	29(1)
F(7)	5519(4)	4587(4)	6163(3)	49(2)
F(8)	5024(5)	4776(6)	7410(4)	87(3)
F(9)	7227(5)	4552(5)	7357(4)	70(2)
F(10)	5633(7)	3501(4)	7150(6)	102(3)
F(11)	6728(4)	4738(5)	8602(4)	63(2)
F(12)	6624(6)	5811(4)	7589(6)	92(3)

Table 6.3.20-b. Anisotropic displacement parameters ($Å^2$ x 10^3) for **32**. The anisotropic displacement factor exponent takes the form: $-2\pi^2[h^2a^{*2}U_{11} + ... + 2hka^*b^*U_{12}]$.

Atom	U_{11}	U_{22}	U_{33}	U_{23}	U_{13}	U_{12}
W(1)	21(1)	16(1)	22(1)	7(1)	13(1)	10(1)
W(2)	19(1)	17(1)	20(1)	3(1)	11(1)	4(1)
W(3)	25(1)	21(1)	22(1)	5(1)	12(1)	11(1)
W(4)	20(1)	17(1)	21(1)	3(1)	9(1)	5(1)
Ag(1)	29(1)	29(1)	38(1)	16(1)	20(1)	11(1)
Ag(2)	34(1)	29(1)	40(1)	8(1)	22(1)	11(1)
P(1)	25(1)	23(1)	31(1)	12(1)	14(1)	13(1)
P(2)	26(1)	20(1)	30(1)	8(1)	16(1)	8(1)
P(3)	40(1)	24(1)	33(1)	9(1)	25(1)	17(1)
P(4)	22(1)	22(1)	29(1)	6(1)	12(1)	7(1)
P(5)	23(1)	19(1)	30(1)	4(1)	12(1)	5(1)
P(6)	30(1)	37(1)	20(1)	5(1)	11(1)	5(1)
P(7)	32(1)	25(1)	32(1)	3(1)	17(1)	12(1)
P(8)	33(1)	33(1)	49(1)	9(1)	24(1)	15(1)
P(9)	48(1)	48(1)	26(1)	10(1)	19(1)	27(1)
P(10)	24(1)	25(1)	20(1)	2(1)	10(1)	4(1)
P(11)	33(1)	25(1)	22(1)	6(1)	11(1)	3(1)
P(12)	30(1)	20(1)	42(1)	5(1)	17(1)	11(1)
O(1)	70(4)	44(3)	46(4)	8(3)	44(3)	10(3)
O(2)	26(3)	54(3)	43(3)	14(3)	11(3)	14(2)
O(3)	30(3)	40(2)	52(3)	13(2)	22(3)	17(2)
O(4)	38(3)	59(3)	19(3)	10(2)	16(2)	13(2)
O(5)	36(3)	46(3)	104(5)	11(3)	43(4)	8(3)
O(6)	164(8)	74(4)	37(4)	24(3)	47(5)	83(5)
O(7)	50(3)	47(3)	50(4)	4(3)	40(3)	9(2)
O(8)	34(3)	53(3)	65(4)	15(3)	-2(3)	12(3)
C(1)	35(4)	24(3)	31(4)	-2(3)	13(3)	9(3)
C(2)	30(4)	33(3)	31(4)	11(3)	18(3)	17(3)
C(3)	25(3)	30(3)	30(4)	8(3)	15(3)	5(3)
C(4)	21(3)	30(3)	28(4)	-4(3)	5(3)	6(3)
C(5)	34(4)	35(3)	54(5)	12(3)	33(4)	15(3)
C(6)	88(7)	42(4)	24(4)	11(3)	23(4)	41(4)
C(7)	27(4)	26(3)	48(5)	4(3)	20(4)	5(3)
C(8)	25(4)	30(3)	44(5)	7(3)	3(4)	6(3)
C(9)	41(4)	26(3)	37(4)	19(3)	25(3)	15(3)
C(10)	44(4)	16(2)	59(5)	17(3)	33(4)	19(3)

C(11)	33(4)	14(2)	33(4)	1(2)	16(3)	0(2)
C(12)	31(4)	16(2)	57(5)	8(3)	25(4)	6(2)
C(13)	44(4)	29(3)	43(5)	22(3)	38(4)	13(3)
C(14)	36(4)	14(3)	73(6)	11(3)	30(4)	8(3)
C(15)	48(4)	25(3)	35(4)	14(3)	25(4)	1(3)
C(16)	47(5)	29(3)	74(6)	17(4)	51(5)	3(3)
C(17)	22(4)	26(3)	52(5)	6(3)	9(3)	-3(3)
C(18)	48(5)	23(3)	39(5)	-2(3)	19(4)	2(3)
C(19)	52(5)	26(3)	41(4)	19(3)	27(4)	19(3)
C(20)	38(4)	24(3)	60(6)	5(3)	25(4)	12(3)
C(21)	48(5)	23(3)	36(5)	-1(3)	5(4)	11(3)
C(22)	42(4)	25(3)	41(4)	3(3)	27(4)	17(3)
C(23)	27(4)	21(3)	44(5)	6(3)	5(3)	15(3)
C(24)	29(4)	27(3)	43(5)	7(3)	16(3)	13(3)
C(25)	50(5)	25(3)	44(5)	14(3)	24(4)	18(3)
C(26)	34(4)	19(3)	71(6)	7(3)	30(4)	5(3)
C(27)	45(5)	25(3)	48(5)	1(3)	20(4)	13(3)
C(28)	50(5)	26(3)	41(5)	-4(3)	31(4)	11(3)
P(13)	27(1)	23(1)	25(1)	9(1)	14(1)	11(1)
F(1)	49(3)	115(4)	67(4)	56(3)	44(3)	50(3)
F(2)	59(3)	95(4)	27(2)	21(2)	24(2)	47(3)
F(3)	64(3)	26(2)	82(4)	13(2)	12(3)	13(2)
F(4)	25(2)	88(3)	33(3)	16(2)	12(2)	11(2)
F(5)	34(2)	58(2)	24(2)	10(2)	10(2)	11(2)
F(6)	92(4)	24(2)	68(4)	4(2)	13(3)	16(2)
P(14)	29(1)	36(1)	24(1)	3(1)	14(1)	10(1)
F(7)	51(3)	79(3)	25(2)	13(2)	19(2)	32(2)
F(8)	41(3)	183(7)	39(3)	2(4)	21(3)	50(4)
F(9)	51(3)	133(5)	47(3)	27(3)	31(3)	51(3)
F(10)	143(7)	45(3)	89(5)	16(3)	46(5)	0(3)
F(11)	49(3)	123(5)	22(2)	15(3)	20(2)	31(3)
F(12)	100(5)	37(3)	92(5)	1(3)	19(4)	6(3)

Table 6.3.21.	**33** $*$ $3(SbCl_3)$	
Empirical Formula	$C_{10}H_{15}Cl_5W(SbCl_3)_3$	
Formula weight	1180.64 g/mole	
Crystal size	0.220 x 0.170 x 0.100 mm	
Crystal description	prism	
Crystal color	red to brown	
Crystal system	monoclinic	
Space group	$P2_1/n$	
Unit cell dimensions	a = 10.3662(2) Å	α = 90°
	b = 17.7874(3) Å	β = 97.349(2)°
	c = 16.0841(2) Å	γ = 90°
Volume	2941.35(8) $Å^3$	
Z, Calculated density	4, 2.666 Mg/m^3	
Absorption coefficient	7.898 mm^{-1}	
F(000)	2160	
Measurement device type	Oxford Diffraction Gemini Ultra	

Measurement method	omega-scan
Temperature	123 K
Wavelength	0.71073 Å
Monochromator	graphite
θ range for data collection	3.43 to 37.70°
Index ranges	$-16 \leq h \leq 17$, $-30 \leq k \leq 30$, $-27 \leq l \leq 26$
Reflections collected / unique	42416 / 15009 [R(int) = 0.0395]
Reflections greater I>2\s(I)	9070
Absorption correction	?
Max. and min. transmission	1.00000 and 0.43466
Refinement method	Full-matrix least-squares on F^2
Data / restraints / parameters	15009 / 0 / 258
Goodness of fit on F^2	0.883
Final R indices [I>2sigma(I)]	R1 = 0.0300, wR2 = 0.0543
R indices (all data)	R1 = 0.0592, wR2 = 0.0588
Largest diff. peak and hole	2.064 and -1.318 e.Å^{-3}

Table 6.3.21-a. Atomic coordinates (x 10^4) and equivalent isotropic displacement parameters (Å^2 x 10^3) for **33**. U_{eq} is defined as one third of the trace of the orthogonalized U_{ij} tensor.

Atom	**x**	**y**	**z**	$\boldsymbol{U_{eq}}$
W(1)	9863(1)	657(1)	1953(1)	12(1)
Cl(1)	10927(1)	369(1)	3304(1)	18(1)
Cl(2)	10629(1)	-470(1)	1461(1)	18(1)
Cl(3)	9693(1)	1137(1)	587(1)	21(1)
Cl(4)	9999(1)	1930(1)	2400(1)	19(1)
Cl(5)	12151(1)	978(1)	1800(1)	18(1)
C(1)	7763(3)	211(2)	1342(2)	17(1)
C(2)	8125(3)	-278(2)	2032(2)	17(1)
C(3)	8181(3)	150(2)	2780(2)	16(1)
C(4)	7837(3)	903(2)	2556(2)	15(1)
C(5)	7572(3)	945(2)	1665(2)	16(1)
C(6)	7454(3)	-41(2)	453(2)	25(1)
C(7)	8175(3)	-1111(2)	1994(2)	27(1)
C(8)	8310(3)	-167(2)	3644(2)	25(1)
C(9)	7595(3)	1503(2)	3163(2)	28(1)
C(10)	7002(3)	1615(2)	1204(2)	25(1)
Sb(1)	1402(1)	4624(1)	2333(1)	18(1)
Cl(11)	153(1)	4961(1)	3403(1)	28(1)
Cl(12)	-167(1)	3704(1)	1796(1)	25(1)
Cl(13)	438(1)	5529(1)	1364(1)	27(1)
Sb(2)	2754(1)	2042(1)	3694(1)	17(1)
Cl(21)	4919(1)	2479(1)	4112(1)	24(1)
Cl(22)	1790(1)	3237(1)	3849(1)	23(1)
Cl(23)	2394(1)	1648(1)	5037(1)	37(1)
Sb(3)	1931(1)	2664(1)	859(1)	20(1)
Cl(31)	3541(1)	2883(1)	2032(1)	31(1)
Cl(32)	2198(1)	3910(1)	387(1)	30(1)
Cl(33)	3404(1)	2144(1)	25(1)	31(1)

Table 6.3.21-b. Anisotropic displacement parameters ($Å^2$ x 10^3) for **33**. The anisotropic displacement factor exponent takes the form: $-2\pi^2[h^2a^{*2}U_{11} + ... + 2hka^*b^*U_{12}]$.

Atom	U_{11}	U_{22}	U_{33}	U_{23}	U_{13}	U_{12}
W(1)	13(1)	12(1)	12(1)	0(1)	2(1)	-1(1)
Cl(1)	17(1)	21(1)	15(1)	2(1)	0(1)	0(1)
Cl(2)	18(1)	16(1)	22(1)	-5(1)	5(1)	1(1)
Cl(3)	23(1)	25(1)	15(1)	5(1)	2(1)	-4(1)
Cl(4)	20(1)	12(1)	24(1)	-2(1)	2(1)	-1(1)
Cl(5)	15(1)	19(1)	21(1)	1(1)	4(1)	-2(1)
C(1)	9(1)	20(1)	20(1)	-6(1)	1(1)	-3(1)
C(2)	14(1)	14(1)	23(1)	2(1)	1(1)	-2(1)
C(3)	12(1)	20(1)	16(1)	2(1)	3(1)	-5(1)
C(4)	11(1)	16(1)	19(1)	-1(1)	4(1)	-1(1)
C(5)	12(1)	15(1)	21(1)	3(1)	4(1)	0(1)
C(6)	23(2)	34(2)	19(1)	-5(1)	3(1)	-6(2)
C(7)	22(2)	17(1)	43(2)	1(1)	11(1)	-3(1)
C(8)	25(2)	31(2)	21(1)	6(1)	4(1)	-6(2)
C(9)	35(2)	26(2)	27(2)	-10(1)	19(1)	-7(2)
C(10)	24(2)	23(2)	29(2)	5(1)	5(1)	6(1)
Sb(1)	14(1)	14(1)	25(1)	2(1)	1(1)	1(1)
Cl(11)	19(1)	30(1)	35(1)	-3(1)	8(1)	2(1)
Cl(12)	21(1)	18(1)	33(1)	2(1)	-2(1)	-3(1)
Cl(13)	23(1)	19(1)	38(1)	8(1)	-5(1)	0(1)
Sb(2)	21(1)	14(1)	14(1)	0(1)	-1(1)	-1(1)
Cl(21)	23(1)	21(1)	26(1)	-4(1)	-5(1)	0(1)
Cl(22)	28(1)	18(1)	22(1)	0(1)	1(1)	4(1)
Cl(23)	66(1)	26(1)	21(1)	6(1)	11(1)	-2(1)
Sb(3)	27(1)	19(1)	15(1)	-1(1)	1(1)	-6(1)
Cl(31)	38(1)	37(1)	17(1)	1(1)	-4(1)	-16(1)
Cl(32)	49(1)	20(1)	23(1)	2(1)	7(1)	-6(1)
Cl(33)	33(1)	32(1)	28(1)	-2(1)	6(1)	0(1)

Table 6.3.22.	**34**
Empirical Formula	$C_{13}H_{15}Cl_3O_3SnW$
Formula weight	628.14
Crystal size	0.125 x 0.105 x 0.026 mm^3
Crystal description	?
Crystal color	colorless
Crystal system	orthorhombic
Space group	$Pca2_1$
Unit cell dimensions	a = 16.84470(10) Å α= 90°
	b = 12.30850(10) Å β= 90°
	c = 17.32710(10) Å γ = 90°
Volume	3592.48(4) $Å^3$
Z, Calculated density	8, 2.323 Mg/m^3
Absorption coefficient	26.881 mm^{-1}
F(000)	2336
Measurement device type	Oxford Diffraction Gemini Ultra
Measurement method	omega-scan

Temperature	123(2) K
Wavelength	1.54178 Å
Monochromator	graphite
θ range for data collection	3.59 to 56.25°
Index ranges	$-18 \leq h \leq 18$, $-13 \leq k \leq 13$, $-18 \leq l \leq 18$
Reflections collected / unique	49907 / 4695 [R(int) = 0.0626]
Reflections greater I>2\s(I)	?
Absorption correction	semi-empirical from equivalents
Max. and min. transmission	0.497 and 0.003
Refinement method	Full-matrix least-squares on F^2
Data / restraints / parameters	4695 / 1 / 389
Goodness of fit on F^2	1.022
Final R indices [I>2sigma(I)]	R1 = 0.0199, wR2 = 0.0462
R indices (all data)	R1 = 0.0213, wR2 = 0.0465
Largest diff. peak and hole	0.693 and -0.764 e.Å^{-3}

Table 6.3.22-a. Atomic coordinates (x 10^4) and equivalent isotropic displacement parameters (Å^2 x 10^3) for **34**. U_{eq} is defined as one third of the trace of the orthogonalized U_{ij} tensor.

Atom	**x**	**y**	**z**	$\boldsymbol{U_{eq}}$
W(1)	6748(1)	-129(1)	3985(1)	12(1)
W(2)	1247(1)	4351(1)	1100(1)	13(1)
Sn(1)	5739(1)	-286(1)	5198(1)	17(1)
Sn(2)	332(1)	4732(1)	2354(1)	13(1)
Cl(1)	6033(1)	-1615(1)	6126(1)	30(1)
Cl(2)	5570(1)	1203(1)	6031(1)	33(1)
Cl(3)	4400(1)	-687(2)	4940(1)	35(1)
Cl(4)	-635(1)	6112(1)	2323(1)	24(1)
Cl(5)	-462(1)	3297(1)	2810(1)	23(1)
Cl(6)	989(1)	5253(1)	3494(1)	25(1)
C(1)	7749(4)	-969(5)	3826(4)	22(2)
C(2)	7340(4)	322(6)	4946(4)	24(2)
C(3)	6352(4)	-1652(6)	3972(4)	19(2)
C(4)	129(4)	3931(5)	797(4)	20(2)
C(5)	1814(4)	3585(5)	1976(4)	21(2)
C(6)	1433(4)	2869(6)	666(4)	24(2)
O(1)	8305(3)	-1472(4)	3698(3)	34(1)
O(2)	7657(3)	652(4)	5473(3)	39(1)
O(3)	6119(3)	-2530(4)	3929(3)	32(1)
O(4)	-500(3)	3773(4)	581(3)	28(1)
O(5)	2177(3)	3189(4)	2455(3)	33(1)
O(6)	1556(3)	2039(4)	395(3)	35(1)
C(11)	7168(4)	931(5)	2963(4)	21(2)
C(12)	6558(4)	243(5)	2685(4)	17(2)
C(13)	5839(4)	521(5)	3067(4)	16(2)
C(14)	6012(4)	1407(5)	3594(4)	19(2)
C(111)	8010(4)	981(6)	2660(5)	40(2)
C(15)	6842(4)	1660(5)	3523(4)	22(2)
C(21)	2333(4)	4993(5)	460(4)	16(2)
C(22)	2222(3)	5694(5)	1105(5)	15(1)
C(23)	1463(3)	6244(5)	1013(4)	13(1)

C(24)	1132(4)	5882(5)	296(4)	17(2)
C(25)	1658(4)	5110(5)	-41(4)	19(2)
C(121)	6624(5)	-559(6)	2033(4)	30(2)
C(131)	5038(4)	89(6)	2894(4)	25(2)
C(141)	5398(4)	2053(5)	4016(4)	23(2)
C(151)	7278(4)	2547(5)	3925(5)	32(2)
C(211)	3079(4)	4346(5)	302(4)	23(2)
C(221)	2806(4)	5934(6)	1728(4)	25(2)
C(231)	1192(4)	7178(5)	1481(4)	20(2)
C(241)	370(4)	6311(6)	-52(4)	23(2)
C(251)	1554(5)	4602(6)	-821(4)	28(2)

Table 6.3.22-b. Anisotropic displacement parameters ($Å^2$ x 10^3) for **34**. The anisotropic displacement factor exponent takes the form: $-2\pi^2[h^2a^{*2}U_{11} + ... + 2hka^*b^*U_{12}]$.

Atom	U_{11}	U_{22}	U_{33}	U_{23}	U_{13}	U_{12}
W(1)	13(1)	9(1)	14(1)	3(1)	0(1)	0(1)
W(2)	19(1)	7(1)	13(1)	0(1)	1(1)	0(1)
Sn(1)	22(1)	11(1)	16(1)	3(1)	4(1)	0(1)
Sn(2)	19(1)	9(1)	11(1)	0(1)	0(1)	-1(1)
Cl(1)	46(1)	18(1)	25(1)	11(1)	7(1)	5(1)
Cl(2)	59(1)	18(1)	22(1)	-2(1)	7(1)	8(1)
Cl(3)	20(1)	33(1)	52(1)	9(1)	6(1)	-2(1)
Cl(4)	26(1)	17(1)	28(1)	3(1)	3(1)	6(1)
Cl(5)	31(1)	16(1)	23(1)	3(1)	1(1)	-8(1)
Cl(6)	39(1)	18(1)	17(1)	-3(1)	-6(1)	-5(1)
C(1)	27(4)	14(3)	24(4)	3(3)	-1(3)	5(3)
C(2)	30(4)	19(4)	23(4)	0(4)	8(4)	-2(3)
C(3)	19(4)	22(4)	17(4)	0(3)	-1(3)	9(3)
C(4)	35(5)	7(4)	17(4)	-1(3)	-4(3)	1(3)
C(5)	29(4)	10(3)	26(4)	-1(3)	8(4)	-1(3)
C(6)	29(4)	25(5)	17(4)	13(4)	18(3)	3(3)
O(1)	25(3)	30(3)	47(3)	12(3)	8(3)	13(2)
O(2)	35(3)	52(4)	28(3)	-11(3)	-8(3)	-8(3)
O(3)	46(3)	14(3)	35(3)	-4(2)	2(3)	-3(2)
O(4)	29(3)	26(3)	28(3)	-7(2)	-5(2)	-7(2)
O(5)	44(3)	30(3)	25(3)	13(3)	-12(3)	11(2)
O(6)	58(4)	9(3)	36(3)	-11(2)	14(3)	5(2)
C(11)	29(4)	9(3)	25(4)	8(3)	9(3)	3(3)
C(12)	28(4)	12(4)	11(4)	6(3)	5(3)	7(3)
C(13)	19(4)	13(4)	17(4)	10(3)	2(3)	-1(3)
C(14)	21(4)	12(4)	23(4)	-3(3)	-7(3)	3(3)
C(111)	40(5)	28(5)	54(5)	21(4)	14(4)	-6(4)
C(15)	20(4)	9(4)	36(4)	10(3)	-6(3)	1(3)
C(21)	19(4)	13(4)	17(4)	-2(3)	1(3)	-1(3)
C(22)	11(3)	20(4)	14(3)	3(3)	3(4)	-10(3)
C(23)	19(3)	15(3)	4(3)	-5(3)	-5(3)	0(3)
C(24)	21(4)	16(4)	16(4)	8(3)	-1(3)	-2(3)
C(25)	34(4)	11(4)	12(4)	1(3)	6(4)	-8(3)
C(121)	47(5)	28(4)	15(4)	2(3)	8(4)	5(4)
C(131)	22(4)	29(4)	24(4)	1(3)	-8(3)	5(3)

C(141)	32(4)	8(3)	28(4)	3(4)	-1(4)	9(3)
C(151)	35(4)	13(3)	49(5)	4(4)	-10(4)	4(3)
C(211)	16(4)	18(4)	33(4)	-8(3)	4(3)	3(3)
C(221)	25(4)	30(4)	21(4)	-5(3)	-3(3)	3(3)
C(231)	17(4)	9(4)	35(4)	3(3)	0(3)	-7(3)
C(241)	29(4)	15(4)	23(4)	-2(3)	-10(3)	2(3)
C(251)	46(5)	22(4)	16(4)	1(3)	-1(4)	-4(4)

Table 6.3.23.	**35**	
Empirical Formula	$C_{26}H_{30}Cl_2O_6W_2$	
Formula weight	877.10 g/mole	
Crystal size	?	
Crystal description	?	
Crystal color	colorless	
Crystal system	?	
Space group	?	
Unit cell dimensions	*a* = 6.742(3) Å	α = 82.12(3)°
	b = 8.124(2) Å	β = 85.96(3)°
	c = 14.350(5) Å	γ = 67.41(3)°
Volume	718.7(4) $Å^3$	
Z, Calculated density	1, 2.027 Mg/m^3	
Absorption coefficient	16.594 mm^{-1}	
F(000)	416	
Measurement device type	Oxford Diffraction Gemini Ultra	
Measurement method	omega-scan	
Temperature	293(2) K	
Wavelength	1.54178 Å	
Monochromator	graphite	
θ range for data collection	3.11 to 56.06°	
Index ranges	$-7 \le h \le 7$, $-8 \le k \le 8$, $-15 \le l \le 15$	
Reflections collected / unique	4374 / 1856 [R(int) = 0.0315]	
Reflections greater I>2\s(I)	?	
Absorption correction	?	
Max. and min. transmission	?	
Refinement method	Full-matrix least-squares on F^2	
Data / restraints / parameters	1856 / 0 / 163	
Goodness of fit on F^2	0.941	
Final R indices [I>2sigma(I)]	R1 = 0.0231, wR2 = 0.0397	
R indices (all data)	R1 = 0.0320, wR2 = 0.0416	
Largest diff. peak and hole	1.106 and -0.725 e.Å-3	

Table 6.3.23-a. Atomic coordinates (x 10^4) and equivalent isotropic displacement parameters ($Å^2$ x 10^3) for **35**. U_{eq} is defined as one third of the trace of the orthogonalized U_{ij} tensor.

Atom	**x**	**y**	**z**	$\boldsymbol{U_{eq}}$
W(1)	10294(1)	8570(1)	7615(1)	21(1)
Cl(1)	11032(2)	11005(2)	6570(1)	38(1)
C(1)	13009(10)	7097(8)	6903(4)	27(2)

C(2)	11883(11)	6673(9)	8663(4)	33(2)
C(3)	10640(9)	10067(8)	8561(4)	26(2)
O(1)	14378(8)	6258(6)	6531(3)	47(1)
O(2)	12716(7)	5671(6)	9229(3)	50(1)
O(3)	10760(7)	10907(6)	9101(3)	43(1)
C(11)	6566(8)	10005(7)	7597(4)	20(1)
C(12)	7143(8)	8346(7)	8207(4)	21(1)
C(13)	8189(8)	6902(7)	7654(3)	17(1)
C(14)	8214(8)	7660(8)	6690(4)	20(1)
C(15)	7162(9)	9577(8)	6656(4)	22(1)
C(111)	5291(9)	11844(8)	7856(4)	28(2)
C(121)	6587(9)	8141(8)	9240(4)	27(2)
C(131)	8787(9)	4962(8)	7993(4)	29(2)
C(141)	9002(9)	6647(8)	5850(4)	32(2)
C(151)	6681(9)	10903(8)	5789(4)	30(2)

Table 6.3.23-b. Anisotropic displacement parameters ($Å^2$ x 10^3) for **35**. The anisotropic displacement factor exponent takes the form: $-2\pi^2[h^2a^{*2}U_{11} + ... + 2hka^*b^*U_{12}]$.

Atom	U_{11}	U_{22}	U_{33}	U_{23}	U_{13}	U_{12}
W(1)	22(1)	21(1)	20(1)	0(1)	-2(1)	-10(1)
Cl(1)	44(1)	42(1)	31(1)	-3(1)	0(1)	-21(1)
C(1)	21(4)	17(4)	39(4)	16(3)	-6(3)	-8(3)
C(2)	44(5)	39(5)	28(4)	-4(3)	-9(3)	-26(4)
C(3)	32(4)	27(4)	22(4)	11(3)	-13(3)	-18(3)
O(1)	47(3)	41(3)	53(3)	-13(3)	11(3)	-15(3)
O(2)	52(3)	39(3)	57(3)	15(3)	-23(3)	-16(3)
O(3)	74(4)	42(3)	27(3)	-6(2)	-12(2)	-34(3)
C(11)	21(3)	21(4)	22(3)	-2(3)	-3(3)	-12(3)
C(12)	19(3)	25(4)	23(3)	0(3)	1(3)	-15(3)
C(13)	24(3)	18(4)	15(3)	-3(3)	2(3)	-13(3)
C(14)	12(3)	30(4)	22(3)	-5(3)	-3(3)	-11(3)
C(15)	18(3)	28(4)	24(4)	0(3)	-4(3)	-15(3)
C(111)	17(3)	27(4)	38(4)	-2(3)	-7(3)	-6(3)
C(121)	27(4)	34(4)	22(3)	-3(3)	-2(3)	-13(3)
C(131)	33(4)	28(4)	30(4)	-2(3)	-1(3)	-16(3)
C(141)	32(4)	37(4)	26(4)	-6(3)	4(3)	-14(3)
C(151)	26(4)	31(4)	35(4)	5(3)	-8(3)	-14(3)

Table 6.3.24.	**36**	
Empirical Formula	$C_{13}H_{15}O_3W$	
Formula weight	403.10	
Crystal size	0.11 x 0.08 x 0.08 mm^3	
Crystal description	?	
Crystal color	colorless	
Crystal system	?	
Space group	?	
Unit cell dimensions	a = 9.28930(10) Å	α = 90°
	b = 9.01100(10) Å	β = 97.4176(10)°

	c = 15.4632(2) Å γ = 90°
Volume	1283.53(3) Å^3
Z, Calculated density	4, 2.086 Mg/m^3
Absorption coefficient	16.639 mm^{-1}
F(000)	764
Measurement device type	Oxford Diffraction Gemini Ultra
Measurement method	omega-scan
Temperature	123(2) K
Wavelength	1.54184 Å
Monochromator	graphite
θ range for data collection	5.27 to 62.23°
Index ranges	-10≤h≤10, -10≤k≤10, -17≤l≤17
Reflections collected / unique	23529 / 2023 [R(int) = 0.0367]
Reflections greater I>2\s(I)	?
Absorption correction	?
Max. and min. transmission	0.3495 and 0.2619
Refinement method	Full-matrix least-squares on F^2
Data / restraints / parameters	2023 / 0 / 159
Goodness of fit on F^2	1.042
Final R indices [I>2sigma(I)]	R1 = 0.0184, wR2 = 0.0507
R indices (all data)	R1 = 0.0284, wR2 = 0.0524
Largest diff. peak and hole	0.448 and -1.178 e.Å^{-3}

Table 6.3.24-a. Atomic coordinates (x 10^4) and equivalent isotropic displacement parameters (Å^2 x 10^3) for **36**. U_{eq} is defined as one third of the trace of the orthogonalized U_{ij} tensor.

Atom	**x**	**y**	**z**	U_{eq}
C(1)	3702(5)	-2476(5)	948(3)	13(1)
C(2)	4943(5)	-2426(5)	1584(3)	13(1)
C(3)	4642(5)	-1404(5)	2253(3)	15(1)
C(4)	3217(5)	-832(5)	2012(3)	13(1)
C(5)	2628(5)	-1492(5)	1204(3)	15(1)
C(6)	3474(5)	-3542(5)	188(3)	19(1)
C(7)	6248(5)	-3451(5)	1644(3)	20(1)
C(8)	5593(5)	-1175(5)	3108(3)	24(1)
C(9)	2402(5)	140(5)	2572(3)	23(1)
C(10)	1081(5)	-1342(5)	790(3)	22(1)
C(11)	5107(5)	1713(5)	1781(3)	17(1)
C(12)	3441(5)	1600(5)	403(3)	18(1)
C(13)	6779(6)	300(5)	965(3)	19(1)
O(1)	5376(4)	2708(4)	2255(2)	26(1)
O(2)	2642(4)	2515(4)	135(2)	27(1)
O(3)	8021(3)	436(4)	1059(2)	23(1)
W(1)	4666(1)	12(1)	1010(1)	9(1)

Table 6.3.24-b. Anisotropic displacement parameters (Å^2 x 10^3) for **36**. The anisotropic displacement factor exponent takes the form: $-2\pi^2[h^2a^{*2}U_{11} + ... + 2hka^*b^*U_{12}]$.

Atom	U_{11}	U_{22}	U_{33}	U_{23}	U_{13}	U_{12}
C(1)	16(2)	12(2)	13(3)	2(2)	3(2)	-2(2)

C(2)	19(2)	10(2)	11(3)	6(2)	5(2)	1(2)
C(3)	24(3)	9(2)	12(3)	5(2)	4(2)	-2(2)
C(4)	18(2)	10(3)	13(3)	1(2)	11(2)	-4(2)
C(5)	16(2)	13(2)	18(3)	6(2)	8(2)	-4(2)
C(6)	24(3)	16(3)	18(3)	1(2)	3(2)	2(2)
C(7)	19(3)	18(3)	22(3)	2(2)	3(2)	4(2)
C(8)	29(3)	20(3)	22(3)	3(2)	-2(2)	-2(2)
C(9)	26(2)	21(3)	24(3)	1(2)	14(2)	0(2)
C(10)	14(2)	26(3)	27(3)	5(2)	6(2)	2(2)
C(11)	13(2)	21(3)	17(3)	3(2)	4(2)	4(2)
C(12)	25(3)	13(3)	18(3)	-4(2)	8(2)	-3(2)
C(13)	27(3)	18(3)	13(3)	-2(2)	8(2)	3(2)
O(1)	27(2)	20(2)	30(2)	-11(2)	4(2)	-4(2)
O(2)	32(2)	20(2)	29(2)	5(2)	1(2)	9(2)
O(3)	12(2)	34(2)	22(2)	-2(2)	4(2)	-1(1)
W(1)	11(1)	7(1)	9(1)	0(1)	3(1)	0(1)

VI. Acknowledgements

I am thankful to Professor Doctor Manfred Scheer giving me the chance to study chemistry in Germany, Brian P. Johnson for convincing Professor Doctor Manfred Scheer to hire me and for helping me with the proposal to the DAAD, Dr. Laurence John Gregoriades for so many things. He introduced me to the group, and helped me get started on my project by showing me the equipment and the locations of most of the things that I needed. I would also like to thank Dr. Christian Eisenhut (Ironhat) for his generous assistance, and I hope I have also been helpful to him.

I thank my former lab mates Dr. Shining Deng for the good company while working and the similar taste in music. Anton Blokheen and I had good times biking, swimming, and hanging out together. Nikolay Pushkarevskiy always had a smile on his face and was very helpful and patient. Sergey Konchenko was mild mannered and quiet, which is good for writing a thesis around. Mike Butofski had a great sense of humor and outlook on life.

I am thankful to the Secretary (Karin Kilgert), the Central Analytical Department, the glassblowers, and the technicians associated with the Scheer Group for all the behind the scenes work as well as former and current members of the Scheer Group.

Finally I thank Professor Doctor Henri Brunner, Professor Doctor Albrecht Mannschreck and Dr. Joachim Wachter, for their acquaintance.